Lucie Strub-Klein

Field Measurements and Analysis of the Morphological, Physical and Mechanical Properties of Level Ice and Sea Ice Ridges

Thesis for the degree of Philosophiae Doctor

Trondheim, April 2012

Norwegian University of Science and Technology
Faculty of Engineering Science and Technology
Department of Civil and Transport Engineering

NTNU – Trondheim
Norwegian University of
Science and Technology

NTNU
Norwegian University of Science and Technology

Thesis for the degree of Philosophiae Doctor

Faculty of Engineering Science and Technology
Department of Civil and Transport Engineering

ISBN 978-82-471-3549-5 (printed ver.)
ISBN 978-82-471-3550-1 (electronic ver.)
ISSN 1503-8181

Doctoral theses at NTNU, 2012:133

Printed by NTNU-trykk

Abstract

Sea ice is a major obstacle for developing oil and gas industries in Arctic regions. To ensure safe and efficient exploration and exploitation of resources in the Arctic Basin, knowledge of the type, thickness, strength and concentration of sea ice is required, especially in areas in which developments are planned. In addition, data on the physical properties (e.g., the temperature, salinity and density) would greatly facilitate the prediction of ice loads because these properties influence ice strength. A special feature of the ice cover is the sea ice ridges, which are considered to be the design loads for offshore structures in ice-infested waters in the absence of icebergs. This thesis consists of 6 papers and is composed of 2 separate but nevertheless very close parts. The first part presents and analyzes field measurements of different properties of level ice, whereas the second part covers the spatial and temporal evolution of the morphology as well as the physical and mechanical properties of sea ice ridges.

Fieldwork investigating the mechanical and physical properties of land-fast level ice in the frozen fjords of Spitsbergen commenced in 2003. With the design of a transportable uniaxial compressive rig in 2005, uniaxial compressive strength tests were performed directly on-site. An intensive field campaign was performed in the winter of 2010 on Van Mijenfjorden, Spitsbergen, to study the spatial and temporal distribution of the properties of level ice, namely, uniaxial compressive strength, temperature and salinity. Sampling matrices were established, and 310 samples were extracted for immediate compression, considering the load direction. Additional samples were collected in the vicinity of these boreholes to measure the temperature, density and salinity profiles and to produce a structural profile using thin sections. The variability in strength correlated with the variability in salinity, the brine fraction and possibly the sample spacing. The drainage and the localization of the brine channels may have been important for the spatial variability of the strength.

Because uniaxial compressive tests were performed on site with the same rig from 2005 to 2011, the data were sufficient for a statistical analysis of the uniaxial compressive strength of sea ice. Over 7 years, 1237 samples were collected and used to determine a statistical distribution that explained the uniaxial compressive strength of sea ice. Seven groups were defined: “horizontal”, “vertical”, “early”, “late”, “horizontal early/late”, “vertical early/late” and “ridge”, to determine the impact of the loading direction and the season on the best fitting statistical distribution. Key statistics were calculated. The vertical samples were stronger than the horizontal samples with an average value of the strength of 4.2 MPa and 2 MPa, respectively. The early or “cold” samples were stronger than the late or “warm” samples, with an average value of the strength of 3.7 MPa and 2.1 MPa, respectively. The key statistics were visualized using box plots. The gamma, Weibull and lognormal distributions were examined. The least squares combined with QQ-Plots enabled the observation and the quantification of the fit between the data distribution and the hypothesized theoretical distribution. The Weibull parameters (scale and shape) were estimated using the maximum likelihood method, the method of the moments and the least squares method. The optimum pair (scale and shape) was obtained through a combination of the least squares method (for

the scale parameter) and the maximum likelihood method or the method of the moments (for the shape parameter). The fit between the data distribution and the theoretical distribution was good. Neither the sample orientation nor the season influenced the statistical distribution determination, even though the defining parameters varied between the groups. The gamma distribution was the best candidate for the statistical distribution of the field data with a coefficient of correlation of 0.986.

Finally, a new experimental setup was established in May 2008 to measure the propagation of stresses in the ice. This setup consisted of freezing 6 stress sensors in the ice. The sensors were placed at a depth of 0.2 m and every 0.6 m along a line. A borehole jack was used to trigger the stresses that propagated to the sensors. The borehole jack was placed along the same line at 8, 5, 2, 1 and 0.6 m from the first stress sensor. A 98% decreased pressure was recorded by the sensors within the first 60 cm, and the pressure was 0 after 4 m. The stresses decreased for increasing distances between the triggering source and the measurement point, following an inverse exponential law.

The second focus of this thesis was on sea ice ridges. For a better understanding and overview of the current knowledge of ridges, an extensive analysis of their morphological properties was performed. Over 300 full-scale, floating first-year ridges were examined from the Bering and Chukchi Seas, Beaufort Sea, Svalbard waters, Barents Sea and the Russian Arctic Ocean for the Arctic regions; from the Canadian east coasts, the Baltic Sea and Gulf of Bothnia, Sea of Azov, Caspian Sea and Offshore Sakhalin for the Subarctic regions. A catalogue of all the available dimensions of the ridges, their macroporosities and the dimensions of the blocks constituting the sail was also provided. The maximum sail height was 8 m (offshore Sakhalin), and the mean peak sail height was 2.0 m based on 356 profiles. The mean peak keel depth was 8.0 m based on 321 profiles. The correlation between the internal dimensions such as the sail height and the keel depth as well as or the sail width and the keel depth were $h_k = 5.11 h_s^{0.69}$ and $w_k = 7.19 h_k^{0.72}$. The statistical distribution of keel-to-sail ratios is best represented by a lognormal distribution. Ridge cross-sectional geometry can vary greatly along the length of a ridge, even over a short distance. The block thicknesses were very different from the surrounding level ice thicknesses and they correlate well with the sail height with a square root model: $h_s = 3.73 h_b^{0.5}$. The consolidated layer tended to grow evenly with time over the width of the ridge cross section. A statistical analysis based on 377 measurements of the consolidated layer of ridges in the Barents Sea showed that the gamma distribution well described the distribution of the consolidated layer thickness in that area.

When prospecting for sea ice ridges in Van Mijenfjorden in February 2009, only a small first-year ridge feature was found. The ridge was visited 6 times between February 14 and May 14. The thickness of the consolidated layer was measured by drilling along two lines across the ridge. It grew as fast as the surrounding level ice (approximately 25 cm in 3 months). The block thickness of the sail was relatively constant until May, after which the block thickness decreased rapidly due to solar radiation. In addition, temperature, density and salinity profiles were constructed. The salinity of the consolidated layer was relatively constant for increasing porosities, mostly because of increasing air temperatures. Samples were extracted for in field compressive tests during two visits. The average strength, porosity

and temperature for the first date was 3.0 MPa, 11% and -11.3°C, respectively, and for the second date 2.6 MPa, 11% and -10.6°C, respectively. The data fit reasonably well with the empirical formulae established for level ice. The rubble was soft and eroded, even more than in previous ridge studies in Van Mijenfjorden because of the small size of the ridge and the increased contribution of oceanic fluxes.

In early September 2009, six medium-sized sea ice ridges were investigated in the Fram Strait as part of the fourth year of a field study of multi-year ice ridges. The geometry and macroporosity were examined by cross-sectional drillings. The largest depth recorded was 7.8 m, and the highest sail measured was 1.9 m. In addition, a profile of the physical properties of each ridge was established. The average density, salinity and porosity of the keel were respectively 945 kg/m^3, 2.05 psu and 14%, respectively. For the first time in that area, uniaxial compression tests were performed at three stations, and the average strength of the keel was 1.8 MPa.

Preface

"*Adventure is just bad planning*", the famous Norwegian polar explorer Roald Amundsen once said. Well, I guess I really planned my life poorly when I decided to move to Svalbard in January 2007 because everything I had experienced before, all the knowledge I had gained, were almost all in vain. I was supposed to write my Master's thesis on sea ice rheology. Of course, I did write it, but I also discovered a new world, a new culture, and a new way of thinking - sea ice research. This was something I had never really thought about before: where in the northeast of France would I find sea ice anyway? Strangely enough for my family, friends and professors in France, I found myself very comfortable driving snowmobiles and extracting ice at -25ºC. I found it even more interesting to manage my own time and project. I simply fell in love with ice research and Svalbard.
I could not believe how lucky I was when a PhD position became available just as I was finishing my Master's thesis, and I was so grateful that I was selected for this position. "Four more years like that! I am the luckiest person on Earth!" Of course, I did not know what I was about to begin. Writing this thesis was certainly an interesting experience.

The first important part of this thesis was the fieldwork. It is a much greater task than you imagine. According to the topic of my project, being the spatial and temporal development of sea ice ridges, I was definitely supposed to find and examine an ice ridge. However, for my first fieldwork as a PhD candidate, the ridges were not very obliging, and I did not find a suitable one to study. We therefore decided to build one! That is how the "Fellowship of the Ridge" was born in 2008. Thanks to the good will, strength and tremendous endurance, at -40ºC, of Jomar Finseth, Christian Lønøy, Graeme Davies and Annelie Bergstrøm, we managed to create our first mini-ridge and equip it with instruments. The first season, although the project felt like a complete disaster at that time, taught me a lot: organization, risk prevention (what could go wrong next time?) and people management. The next season, I found a ridge that I could study and everything went really well. For my last field season in 2010, ridges were definitely not cooperating, and we did not spot any ridge in Van Mijenfjorden. Thus, I decided to study level ice instead. Thanks to all of my precious colleagues, I collected a large amount of data that I could use for good publications.

The publications are the second important part of the thesis. You collect data, but what should you do with them? Easy answer; publish them! How many hours did I not spend frustrated with my computer, knowing that I had good material to write? However, the words would not come together to describe my findings. I am so grateful that my supervisor Professor Knut Høyland was always there to support me and improve articles when improvement was needed. I learnt to be rigorous, to read and edit, to try to clearly express my thoughts. I discovered the frustration of stagnation: some days, I could produce only a few lines. However, on some other days, everything was unblocked, and suddenly the paper was finished. That is how I also discovered the satisfaction of having achieved something: the paper is reviewed and accepted for publication. This may be very basic for many people, but not for one who has struggled so much to write it. I should also say that I was not alone to write most of my papers, and I am grateful that some of my peers and colleagues accepted to

be co-authors in five of the six papers included in this thesis. They helped me to see clearly and improved considerably the quality of the article we were writing together. I was the first author in the paper of Chapter 3.2 as I collected the data, analyzed them and wrote most of the article. Professor Knut Høyland improved some sections and the analysis by examining closer the brine effect. The paper of Chapter 3.4 has been written by Sébastien Barrault and I stand as a second author as I helped him to collect the data and participated to the analysis. In the paper of Chapter 4.2, I am the first author as I took the initiative to write the paper in collaboration with the Canadian Hydraulic Centre, organized the work and did 75% of the analysis and writing. The second author, Denise Sudom, wrote some sections and did some of the analysis, and helped in the search of grey literature. She also edited the paper in good scientific English. In Chapter 4.3, I am first author as I collected the data and wrote the paper. Professor Knut Høyland, the second author of this article, added a few important points and improved the quality of the paper by helping me reformulating some sections where I found difficult to state clearly and concisely my findings. Finally, the last paper, included in Chapter 4.3, is the result of my collaboration with Dr. Nicolas Serré and Professor Knut Høyland. Dr Nicolas Serré and I collected the data, but I wrote most of the paper, and therefore I am the first author, while my two co-authors reviewed it and improved the formulation of some sections. Dr. Nicolas Serré also brought an important input in the introduction and the analysis of the data.

It is difficult for uninitiated people to understand how hard it can be sometimes to be a PhD candidate. Yes, I had some really good moments and a lot of fun during fieldwork, but I also went through very difficult times, including -30ºC temperatures and 20 m/s winds. The instruments, engines or tools I was using were not always cooperative, especially when it was very cold. I spent 3 months repairing the most important equipment for my fieldwork; the portable, uniaxial compressive rig, KOMPIS (which also means “friend” in Norwegian). The time spent is not in any published paper. Being so happy when a paper is accepted seems almost inadequate or exaggerated to people who do not understand how much effort, energy and sweat are required, although all that is required is sitting in a chair in front of a computer.
In these times, it is essential to have other activities to clear your mind and to keep your sanity. I was told that having dogs was almost suicidal when you are a PhD candidate because dogs are so time consuming. My dogs helped me stay positive and clear my mind when I was frustrated. My friends and family have also been of great support when I was tired and irritated.

“*The difficult is what takes a little time; the impossible is what takes a little longer*”, another famous Norwegian polar explorer Fridtjof Nansen declared. Why did I choose to quote Amundsen and Nansen? Because for me, writing this thesis on Svalbard has been like a polar exploration. You feel excitement and optimism during the preparation and early experimentation. Progressively, disappointment and frustration become your companions; you will feel like the goal is impossible to achieve, but you still hang in. However, after going through difficult times and succeeding, you dare hope that you will see the end of the journey. Finally, it happens; you cross the finish line! Thus, when you think your thesis is impossible to finish, just be a bit more patient.

Acknowledgements

I would like to thank all of the people who contributed, from near and far, to the success of my PhD work.

My supervisor, Professor Sveinung Løset, made it possible for me to do this work and thereafter provided me with great materials and financial support. His energy and enthusiasm inspired me to do my best.

My co-supervisor, Professor Knut V.Høyland, is sincerely acknowledged for his constant help and support through all phases of my work. He taught me to be rigorous and to think differently. His knowledge, patience and availability are precious to me. I am still amazed by how cleverly he can find order in chaos (and for this, I refer to two of the papers we co-wrote).

My co-supervisor, Professor Aleksey V. Marchenko, first introduced me to the ice sciences when he supervised me during my Master's thesis. Discussions with him felt like sitting in front of a fireplace and listening to fairy tales. His knowledge and experience are invaluable.

A major part of my work occurred in the field, and I would not have managed that by myself. Therefore, I would like to thank my fellow PhD candidate, Sébastien Barrault, who brought me out into the wild and taught me all I needed to know about fieldwork on ice. I would also like to thank Dr. Nicolas Serré for his help during the fieldwork in the Fram Strait, which made it so efficient. I never had so much fun while working!

Serguey Sukhorukov, Anatoly Sinitsyn and Christian Lønøy helped me during two field seasons. They encountered tough situations, everything from extreme weather conditions to meetings with polar bears, and I am very thankful that they still signed up to join me! My PhD colleague, Aleksey Shestov, was also of great help in the field. His strength and unbending will to continue no matter what happened were valuable. My good friend Jomar Finseth, also stepped up the very first year when we decided to build our mini ridge. I appreciated his help and the good moments we had teaching in the lab.

I also should acknowledge the students from courses AT208 and AT307, and in particular, Claire Chenot and Graeme Davies, who helped considerably to increase the amount of data collected.

Last but not least, I get to the help in the field, the logistics department. I sincerely thank Monica Votvik for her good will and help. The first year she joined me, she watched me drifting out in an aluminum boat and then swam in a survival suit to desperately try to reach out for my thermistor strings that were drifting away on a mini ice floe. Despite this, she joined me the second year, and she and Simon Løvås (I thank him too) volunteered to be covered with glucose and play "pull the string out of the tube" so that I could get all of my equipment returned. Kåre Johansen, the busiest mechanic I have ever met, always found some time to help and assist me in my fieldwork. His good mood and positive attitude always cheer me up.

Fieldwork was not all of the PhD work; scientific discussions and a good working environment are important, too. Therefore, I would like to thank Dr. Rolf Lande from DNV

for his great help with statistics. Thanks to him, I learned (and I was really eager to learn) more about statistics than I could ever have thought possible. His interest, enthusiasm and constructive comments helped me to considerably improve the final paper of this thesis.

I would also like to thank Dr. Ada Repetto for our interesting discussions (research-related or not). I enjoyed sharing experiences. Dr. Alex Klein-Paste always took her time to listen to my problems (related to the PhD work) and read my papers. He provided valuable advice, and thanks to him, I learned a lot about how to succeed (or survive?) as a PhD candidate. Dr. Raed Lubbad was also of valuable help reading my papers and providing good advice, when we were not too busy flooding the "basement" at NTNU.

I would also like to acknowledge all of my colleagues at NTNU for good times in the "basement", particularly Marion Beentjes for her kindness, energy, humor and great support.

Berit Jacobsen, the UNIS librarian, was of tremendous help when I needed special literature (which was almost all the time). She was so efficient and thoughtful that she sometimes found relevant papers that I had never come across.

My colleagues at the technology department, in particular, Pernilla Carlsson, Monika Trümper and Dr. Nataly Marchenko, as well as my other colleagues at UNIS, greatly contributed to a friendly working environment.

My friends (the list would be too long to write but I am pretty sure they will recognize themselves) have greatly helped cheering me up, and they show me that there is a life besides the PhD.

In addition, I would like to acknowledge Louis Delmas, who opened my eyes to the world of research, and without whom I would ever have heard about Svalbard. He has been a constant support in the good times and the bad. Louis also volunteered for fieldwork when no one else could.

I would like to thank my parents, Patrick and Monique, for always supporting my decisions, even the most bizarre ones. They are my support, and it is thanks to them that I have succeeded this far. My brother Adrien pulled me back to Earth when I needed it. Finally, Magne supported me the last two years (the worst ones!) with great courage, and I thank him for that.

Contents

Chapter 1 – Introduction

1.1 General

It is now well established that there are vast hydrocarbon resources in the Arctic regions. The oil and gas industries have developed greatly there in the past decade, and thus far, the main challenge to the exploitation of these resources is sea ice. The regions of interest are Sakhalin, Barents Sea, Pechora Sea, the Alaska North Slope and large areas of the Beaufort Sea. In addition, surveys have shown that Greenland may contain some of the world's largest remaining oil resources in the East Greenland Riff basin (especially in Kronprins Christian Basin) and in Baffin Bay.

A major part of the oil development in the Arctic consists of designing safe structures and ships to ensure efficient exploration. Sea ice must be considered in the design process because its concentration, thickness and strength are the main direct factors that influence ice action against Arctic offshore structures. More data must be collected on ice properties (physical and mechanical properties as well as the thickness and the concentration of the ice) in regions where developments are planned. These field data would greatly help improve existing codes because an overestimate of the ice load could lead to significantly increased construction costs; an underestimate of the ice load could lead to catastrophic events, including human loss. In the absence of icebergs in a specific area, sea ice ridges are the governing factor in Arctic marine design. The force induced by the ridges is not yet accurately defined because their properties and consolidation are still not well understood in some regions (e.g., the Fram Strait).

Climate change and the melting sea ice stimulate the race for Arctic exploitation because new routes and resources become available. While engineers are concerned that sea ice endangers the exploitation of hydrocarbons, geophysicists are concerned about the consequences of the disappearing sea ice.

Sea ice is an important component in the fragile equilibrium between the atmosphere and the ocean. Sea ice acts as a lid that controls (and is controlled by) the heat flux and moisture exchange between the ocean and the atmosphere. Small perturbations in the ocean or the atmosphere can have dramatic consequences for sea ice thickness and concentration, which in turn will affect the ocean and the atmosphere (Thomas and Dieckmann, Chapter 1). The albedo, or reflection coefficient α, is important for the breaking of sea ice. The albedo is a non-dimensional quantity that indicates how well a surface reflects solar energy. In general, the ocean albedo α_{ocean} is 0.06, which means that the surface (= the ocean) is almost a perfect absorber. Therefore, the absorbed solar energy heats and melts sea ice. For bare sea ice, $0.5 \leq \alpha_{sea\ ice} \leq 0.7$; however, if the ice is thick and covered with snow, the albedo can reach 0.9. Hence, snow insulates the sea ice, maintains cooler temperatures and delays the ice melt in the summer. However, with increasing air temperatures, the snow cover diminishes, thus decreasing the surface albedo. Melt ponds form on the ice, and existing cracks (leads) break the ice. The more the ice melts, the lower the albedo, the more energy is absorbed and the warmer the water becomes.

In addition, small-scale formation (or decay) of sea ice has global implications on ocean circulation: the brine released when the ice forms increases the density of the water. This causes convection and mixing of water columns, and the properties of water change. In contrast, when ice melts, freshwater is added to the upper water column, stabilizes the column and thus limiting vertical mixing (Thomas and Dieckmann, Chapter 3).

From a geophysical viewpoint, the sea ice thickness included in climate models must be studied in more detail because the processes of sea ice growth and melting as well as ice deformation and motion are not well understood. Thus, sea ice ridges are regarded as "much thicker level ice" (Thomas and Dieckmann, Chapter 4). Ridges act as sinks, sucking in the surrounding level ice as they form, leaving an area of open water. This process has many different consequences, whether it happens in summer or in winter: if ridges are formed in winter, the open water refreezes rapidly, thus increasing the extent of the ice cover. If ridges are formed in summer, the water will not refreeze, and the openings will increase the heat exchange between the air and the water, retarding or inhibiting ice formation and growth, or even accelerating the melting of the existing ice.

1.2 Objectives, scope and organization of the thesis

This thesis is intended to increase the knowledge of the spatial and temporal evolution of morphological, physical and mechanical properties of level ice and ice ridges. Full-scale field-measurements of the thickness, temperature, density, salinity, and uniaxial compressive strength of both level ice and ridges were crucial in this work. The measurements aimed at increasing the data available for predicting ice actions relevant to the design of offshore structures in Arctic regions. The main objectives of this thesis are the following:

1. To perform field experiments in order to study:
   - the evolution of the morphology of first- and second-year ridges by drilling and establishing morphological profiles. The evolution of the keel (development of the consolidated layer and rubble erosion) was of particular interest.
   - the evolution of salinity, temperature and density as well as the uniaxial compressive strength (when possible) of first- and second-year ridges.
   - the spatial and temporal heterogeneity of the salinity, temperature, density (and therefore air and brine volumes) and over all uniaxial compressive strength of first-year landfast ice.
2. To use analytical and statistical models to determine:
   - a reliable probability distribution for level ice strength.
   - a probability distribution for the keel-to-sail ratio of first-year ice ridges.
   - a reliable relationship between the different dimensions of first-year sea ice ridges.

The work presented in this thesis follows the investigations started by Dr. Knut Høyland and Dr. Svetlana Shafrova on the consolidation and morphology of first-year sea ice ridges. Høyland (2000) focused mainly on the measurement and numerical modeling of the

consolidation of first-year ice ridges, whereas Shafrova (2007) analyzed the mechanical behavior and cohesion of the rubble. The research on level ice strength heterogeneity and statistical modeling partly follows the research project of Shafrova (2007).

This thesis consists of 6 papers: 1 paper is published in a scientific journal, 2 papers are submitted to different scientific journals and 3 have been reviewed and published in international conference proceedings. Two additional papers reviewed and published in conference proceedings were written during this PhD work, but were not included in the final version. This thesis addresses sea ice features (level ice and ridges) and is organized as follows:

- Chapter 2 introduces the reader to sea ice and ridges by presenting basic sea ice physics, mechanics and thermodynamics. The locations of the fieldwork are described at the end of the chapter.
- Chapter 3 analyzes field measurements of level ice properties. This chapter consists of three papers. The first paper describes the variability of level ice physical properties and strength. This paper also presents some aspects of level ice growth. The results were based on fieldwork conducted during the winter season of 2010. The subsequent paper sought to determine a statistical analysis for the uniaxial compressive strength of level ice. This paper included samples from 2005 to 2011. The third paper presents a new method for measuring the propagation of in situ stresses on level ice.
- Chapter 4 presents morphological, physical and mechanical characteristics of sea ice ridges. This chapter consists of 3 papers. The first paper is a review and analysis of the morphological properties and shapes of first-year sea ice ridges. This paper also analyzes the variation of the consolidated layer and identifies gaps in the knowledge of first-year ice ridges. The second paper analyzes the temporal development of a first-year ice ridge in 2009 (growth/consolidation, temperature, salinity, density and strength), and the final paper presents the results of a series of second-year ridges investigations in the Fram Strait in the late summer of 2009.
- Chapter 5 provides the main conclusions and proposes further work.

1.3 Readership

This thesis aimed at increasing and improving our knowledge of the variability of level ice properties (in particular the uniaxial compressive strength), and morphological, physical and mechanical properties (and their temporal evolution) of first- and second-year ridges. Therefore, this thesis is addressed to engineers and scientists working with:

- offshore development of structures in the Arctic regions related to ice–structure interactions.
- studies and research on sea ice features, physics and mechanics.
- geophysical research on ice-covered waters.
- field activities in Arctic regions.

This thesis is also for anyone who is interested in this topic.

1.4 References

Høyland, K.V. (2000). Measurements and simulations of consolidation in first-year sea ice ridges, and some aspects of mechanical behavior. Thesis for the degree of philosophiae doctor 2000:94. Department of Structural Engineering of the Norwegian University of Technology (NTNU), Trondheim, Norway. September 2000. ISBN 82-7984-121-0. ISSN 0809-103X, 172p.

Shafrova, S. (2007). First-year sea ice features: investigation of ice field strength heterogeneity and modeling of ice rubble behavior. Thesis for the degree of philosophiae doctor 2007:176. Faculty of Engineering Science and Technology, Department of Civil and Transport Engineering of the Norwegian University of Technology (NTNU), Trondheim, Norway, and Department of Arctic Technology of the University Centre on Svalbard (UNIS), Longyearbyen, Norway, August 2007. ISBN 978-82-471-3859-5 (printed ver.). ISBN 878-82-471-3862-5 (electronic ver.). ISSN 1503-8181, 181p.

Thomas, D.N. and Dieckmann, G.S (2010). Sea ice. Second Edition. Edited by David N. Thomas and Gerhard S. Dieckmann. Wiley-Blackwell. ISBN 978-1-4051-8580-6 (hard cover).

Chapter 2 – Sea ice

2.1 Introduction

The goal of this chapter is not to provide an exhaustive review of sea ice. The interested reader can refer to Weeks (2010), Løset et al. (2006), Thomas and Dieckmann (2010) and Schulson and Duval (2009) for a more detailed description. The intent of this chapter is to provide the reader basic knowledge of sea ice to ease the understanding of the papers.

Sea ice forms from the freezing of seawater at the surface of seas and oceans, and sea ice covers a wide area north of the Arctic Circle and in Antarctica. Sea ice can be classified according to its age. The World Meteorological Organization (WMO) defines first-year sea ice as that which will form during the winter season but not survive the subsequent summer's melt. Old ice has survived at least one summer's melt (second-year ice) or several summer's melt (multi-year ice).

2.2 Sea ice physics

2.2.1 Microstructure of ice

The water molecule consists of one oxygen atom and two hydrogen atoms that are arranged in a tetrahedral orientation. The most common form of sea ice has a hexagonal crystal arrangement and is therefore called hexagonal ice, *Ih*. The Bernal-Fowler rules (Bernal and Fowler, 1933) describe the atomic structure of ice:

- two hydrogen atoms must be located near each oxygen atom and
- only one hydrogen must lie on each O-O bond.

The crystallographic arrangement is characterized by four axes: three a-axes in the same plane (the basal plane), separated by 120º, and the c-axis (or optical axis), perpendicular to the basal planes (see Figure 1 for an illustration of an ice crystal). Each oxygen atom has three hydrogen bonds in the basal plane and one hydrogen bond out of this plane; thus, a fracture along the basal plane requires the rupture of three bonds, whereas a rupture in any plan normal to the basal plane requires the rupture of four hydrogen bonds (Løset et al, 2006). This difference explains the mechanical properties of ice. Breaking of the Bernal-Fowler rules may result in defects in the ice: point defects, line defects or plane defects.

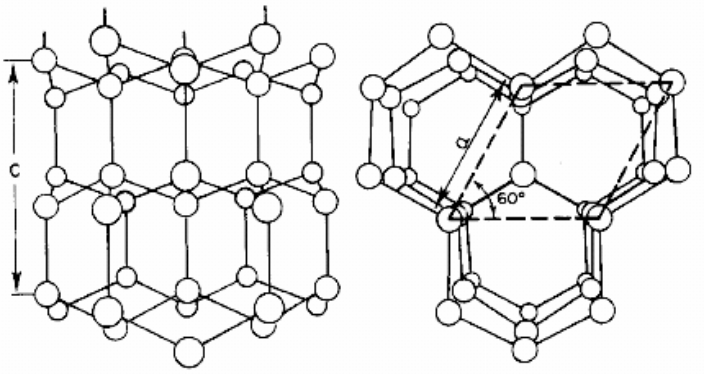

a) b)

Figure 1. Molecular structure of ice. From Michel (1978)

a) View perpendicular to the c-axis. b) View along the c-axis

2.2.2 Sea ice growth

The nucleation of ice occurs in general at the air/water interface. The salts in the sea lower the temperature at which water freezes to -1.9ºC (for a sea water salinity of 34.5 ppt). Once nucleation commences, crystals grow at the water surface until a skim forms. This skim is composed of platelets of ice called frazil. Ice rarely grows under quiet conditions, and swells, waves and winds turn the frazil ice into grease ice, which is no more consistent than slush. This thin frazil layer develops into dark nilas (<5 cm) that are converted into light nilas upon thickening (between 5 and 10 cm). The salts are progressively expelled from the thin platelets. As the platelets thicken and grow, brine is trapped, causing the ice to be salty. At first, ice crystals are randomly orientated; however, when the initial layer has covered the sea surface, favorably orientated crystals will expand along the basal plane. Weeks (1994) provides the following two reasons for this occurrence:

- There is no significant kinetic border that would limit the growth in the basal plane, whereas a growth in the perpendicular direction (parallel to the c-axis) requires re-nucleation;
- The sea ice crystals' laminar structure (brine and ice layers) and the thermal conductivity of brine makes this layer weaker than pure ice and allows the layered components to have a greater thermal conductivity when they are perpendicular to the c-axis rather than when they are parallel to it.

Consequently, ice crystals with vertical c-axes will be wedged out in favor of those that have a vertical basal plane. A new form of ice, pancake ice, appears at this stage. Pancake ice consists of nearly circular ice plates, typically 10 cm thick. With the swell and the wind, the plates constantly hit each other, and a rim forms at the edges. With constant negative air and water temperatures, the pancake ice will agglomerate until the entire surface is covered. The ice will then start to grow vertically.

2.3 Sea ice mechanics

Ice is a polycrystalline material. Thus, it is somewhat more complicated to apply classical engineering approaches to ice because of its different structure and stronger dependence on its own natural state compared with other materials. The grains are larger than those of other materials are, and as explained earlier, sea ice is composed of water, brine and air. However, continuum mechanics is still valid and sea ice behaves following an elastic-visco-plastic model where creep and relaxation are no different from any other material. It was chosen not to develop long-term loading further because it was not relevant for the rest of the study. However, the reader can refer to Løset et al. (2006), Ramseier (1971), Palathingal (1989), Sinha (1983) or Glen (1955) for more details concerning creep and Dowling (1999) and Gabrielsen et al. (2008) for relaxation.

Short-term loading is of more interest. The visco-plastic and visco-elastic strains are neglected because these strains are assumed not to have time to develop during short-term loading. The strength (i.e., the failure force) of a material is the most common parameter used to characterize the mechanical behavior of ice. Although ice fails rarely one-dimensional, the uniaxial compressive strength of level ice and ridges is easy to test and has been studied in this thesis. The uniaxial compressive strength characterizes the elastic-plastic behavior of the ice, and under ideal conditions, the stress-strain curve resembles the one given in Figure 2.

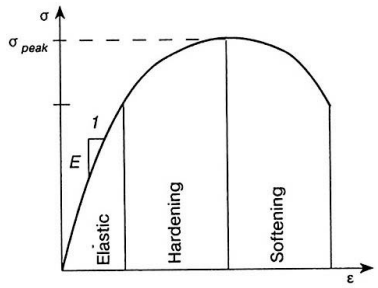

Figure 2. Typical stress strain diagram for a perfect linear-elastic-plastic material. From Løset et al. (2006)

The uniaxial compressive strength σ_c is defined by the maximal force F_{max} to the nominal area A_{nom} ratio:

$$\sigma_c = \frac{F_{max}}{A_{nom}} \tag{1}$$

Many parameters influence the uniaxial compressive strength of sea ice. These parameters can be related to physical properties (temperature T, density D, salinity S and by extension, the air and brine volumes η_a and η_b, respectively), structural properties (defects, grain size d, grain orientation), mechanical properties, testing conditions (failure mode, strain rate $\dot{\varepsilon}$, stiffness, in the field or in the laboratory) and other external causes (e.g., accuracy of

the measurement, stiffness of the machine). Peyton (1966, 1968) was the first to show a strong dependence of the strength to the square root of the brine volume. Timco and Frederking (1990) and Moslet (2007) simplified this relation to the square root of the porosity, whereas Kovacs (1996) developed a model with both the strain rate and the brine volume as parameters. By analyzing our data from 2010, we found that Peyton (1966, 1968) was correct to consider only the brine volume. These models will be presented in more detail in this section. The uniaxial compressive strength is commonly associated with the failure of ice against vertical structures and is therefore used in the Khorzavin formula (Khorzavin, 1983):

$$F=IKm\sigma_c Dh_i \tag{2}$$

where σ_c is the uniaxial compressive strength, D is the structure diameter, h_i is the ice thickness, I is an indentation factor, K is a contact factor and m is a shape factor. The ISO codes (ISO/FDIS 2010) recommend that the ice pressure p_G is calculated according to the following equation:

$$p_G = C_R \left(\frac{h}{h^*}\right)^n \left(\frac{w}{h}\right)^m \tag{3}$$

where h is the ice thickness (in m), h^* is a reference thickness (h^*=1 m), w is the projected width of the structure (in m), m and n are empirical coefficients (m=-0.16 and n=-0.5 if h<1.0 m; n=-0.3 if $h\geq$1.0 m) and C_R is the ice strength coefficient. This coefficient has been estimated using a deterministic analysis of first- and second-year ice samples from the Beaufort Sea and is estimated as C_R=2.8 MPa. For more temperate areas, such as the Baltic Sea, this coefficient was estimated as C_R=1.8 MPa. Because sea ice is anisotropic, the vertical uniaxial compressive strength is generally greater than the horizontal uniaxial compressive strength, and the ratio σ_v/σ_h is approximately 3 but can vary between 1.5 and 5 (Moslet, 2007).

Ice under compression is either ductile or brittle. The failure mode depends mainly on the loading speed. In addition, the strength increases with increasing strain rates in the ductile domain, until a specific transition after which the strength decreases as the strain rate increases. According to Schulson (1997), the peak strength is obtained at a loading speed of $\dot{\varepsilon}=10^{-3}$ s^{-1}, although this value is under debate (Løset et al., 2006).

Recent developments have established a functional relationship between the uniaxial compressive strength and the porosity (or the brine volume); this relationship was based on a large data set.

Timco and Frederking (1990) and Moslet (2007) separated granular from columnar ice and vertical samples from horizontal samples. Both studies are based on small-scale test results. Timco and Frederking (1990) expressed the uniaxial compressive strength as a function of the total porosity and the strain rate, using strain rates from 10^{-7} to 10^{-1} s^{-1}. Moslet (2007) decreased the number of parameters to only the total porosity. He based his models on samples tested at a strain rate of 10^{-3} s^{-1}. The proposed models are compared in Table 1.

Table 1. Analytical model for uniaxial compressive strength

	Timco and Frederking (1990)	Moslet (2007)
Horizontal samples	$\sigma_c^H = 37\dot{\varepsilon}^{0.22}\left[1-\sqrt{\frac{\nu_t}{270}}\right]$	$\sigma_c^H = 8\left[1-\sqrt{\frac{\nu_t}{0.7}}\right]$
Vertical samples	$\sigma_c^V = 160\dot{\varepsilon}^{0.22}\left[1-\sqrt{\frac{\nu_t}{200}}\right]$	$\sigma_c^V = 24\left[1-\sqrt{\frac{\nu_t}{0.7}}\right]$
Granular samples	$\sigma_c^G = 49\dot{\varepsilon}^{0.22}\left[1-\sqrt{\frac{\nu_t}{280}}\right]$	--

Although these relationships were in good agreement with the experimental data, the strength and behavior of the ice at failure could not be predicted. Weeks (2010) suggested that the sample history is also a factor to consider in the modeling.

Kovacs (1996) discussed the models proposed by Timco and Frederking (1990), arguing that bulk salinity is important. Kovacs then reanalyzed the data by adapting the creep law of Norton (1929) and Glen (1955, 1958):

$$\sigma_C = B_2\dot{\varepsilon}^{\frac{1}{n}}\varphi^m \tag{4}$$

where B_2, m and n are 2.7×10^3, 3 and -1, respectively. B is a parameter that includes the ice structure, temperature and activation energy, and n and m are empirically determined. φ is the bulk porosity and is expressed in ‰. Notably, Kovacs (1996) presented this law so that it would better fit the Exxon data already analyzed by Timco and Frederking (1990). Kovacs then expanded the analysis by developing an equation for the uniaxial compressive strength of the ice sheet:

$$\sigma_C = 1970\dot{\varepsilon}^{0.32}\varphi_B^{-0.95} \tag{5}$$

where φ_B is the bulk salinity expressed in ‰.

2.4 Sea ice thermodynamics

This paragraph focuses on a thermodynamic model to predict sea ice growth. At low air temperatures and reasonably low water temperatures, a thin cover of ice appears, and the ice starts to grow at the water/ice interface. During this process, the released latent heat is transported through the ice to the air. The ice growth rate is controlled by the energy balance at the bottom of the ice sheet. The flux from the air to the ice Q_i the oceanic flux Q_{ocean} and the latent heat of fusion l_f must be considered.

The model developed by Stefan (1891) proved to be a simple and rather efficient equation to predict ice growth. This equation assumes that there is no thermal inertia, no heat transfer from the ocean (Q_{ocean}=0), no internal heat source and that the temperature profile is

linear through the ice sheet. In addition, the simplest model presented in Eq. (9) neglects snow and solar radiation. The simple illustration in Figure 3 helps understanding the system of equations that enables the calculation of the ice thickness.

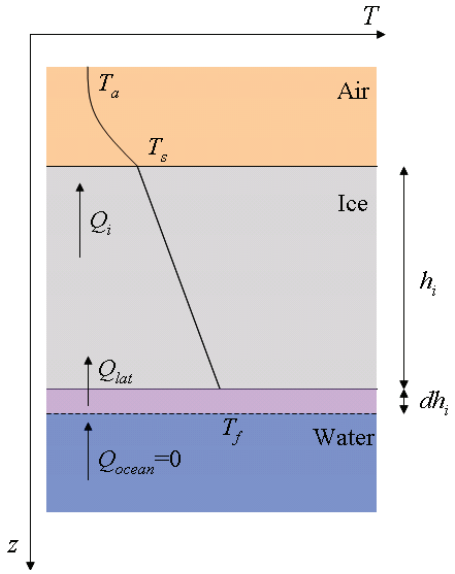

Figure 3. One layer model for sea ice growth using Stefan's assumptions

The flux Q_i is expressed using Fourier's law:

$$F_i = -k_i \frac{\Delta T}{\Delta x} \tag{6}$$

where k is the thermal conductivity (in W/mºC).
The latent heat Q_{lat} is expressed by the following equation:

$$Q_{lat} = \rho_i l_f \frac{dh}{dt} \tag{7}$$

where ρ_i is the density (in kg/m^3) and l_f is the latent heat of fusion (in J/kg). The surface heat flux Q_i is balanced by the release of latent heat: Q_i=Q_{lat}. The latter equation can then be reformulated as follows:

$$-k_i \frac{\Delta T}{h} = \rho_i l_f \frac{dh}{dt} \tag{8}$$

After solving this differential equation, the ice thickness h is expressed as follows:

$$h^2(t) - h_0^2 = \frac{2k_i}{\rho_i l_f} \int_0^t (T_f - T_S) d\tau \tag{9}$$

T_s is the temperature at the ice surface; however, this value is difficult to measure accurately. The air temperature is often more accessible for measurement, and it is reasonable to assume that T_s=T_a. Therefore, we can express Stefan's law as follows:

$$h^2(t) - h_0^2 = \frac{2k_i}{\rho_i l_f}\int_0^t (T_f - T_a)d\tau \quad (10)$$

Including the days of frost, $DD = \int_0^t (T_f - T_a)d\tau$, Stefans's law becomes the following:

$$h^2(t) - h_0^2 = \frac{2k_i}{\rho_i l_f} FDD \quad (11)$$

Stefan's model overestimates the ice thickness, and this model can therefore be used as an upper boundary for favorable ice growth conditions (Leppäranta, 1993). Stefan's model can be used with an extra layer of snow on top of the ice:

$$\int_0^t (T_f - T_a)d\tau = \int_0^{h_i} l_f \rho_i \left(\frac{k_i h_s + k_s h_i}{k_i k_s}\right) dh_i \quad (12)$$

Eq.(11) can be simplified if we consider a layer of snow with a constant thickness:

$$\int_0^t (T_f - T_a)d\tau = \frac{l_f \rho_i}{2k_i} h_i^2 + \frac{l_f \rho_i h_s}{k_s} h_i \quad (13)$$

The top conditions (air/ice interface) are not well understood. In addition, assuming no oceanic flux and no thermal inertia could lead to errors in the ice thickness prediction. Therefore, Leppäranta (1993) introduced an empirical factor a_* such that $0.5 \leq \frac{a_*}{a} \leq 1$. Høyland (2009) described the thermodynamic principles for level ice growth-predictions in Van Mijenfjorden and determined this factor (which he calls ω) using the measured ice growth from 2004 to 2005. He found values between 0.25 and 0.83 depending on snow precipitation. For sea ice, the thermal conductivity k_i and the latent heat of fusion l_f are usually assumed equal to 2.2 W/mºC and 333400 J/kg, respectively. The density should be determined by measuring the ice under consideration. Otherwise, a reasonable estimate of the sea ice density is ρ_i=916 kg/m^3. Notably, Schwerdtfeger (1963) derived tables for the thermal conductivity and the latent heat of fusion as a function of the temperature, density and salinity of the ice.

2.5 Sea ice ridges

Sea ice that remains attached to the shore is called landfast ice. Ice that is not attached to land is called floating ice. For floating ice, the ice drifts and can deform due to collisions between ice plates. Thus, rafts, ridges and hummocks are created. This thesis focuses on sea ice ridges. Ice ridges form when the ice is forced upward by the wind or the current. Ridges consist of a sail (above a waterline) and a keel (below the waterline). For young ice ridges

(first- and sometimes second-year ridges), the keel consists of a consolidated layer and a rubble. Older ridges present a consistent, smooth keel. Ridges are long, non-symmetrical, curvilinear, 3D features that are often represented (and modeled) as 2D triangular features; however, this 2D representation is limited. Figure 4 shows typical examples of cross-sections of first- and multi-year ridges, and Figure 5 shows two photos of first-year ridges in Barents Sea and the Fram Strait.

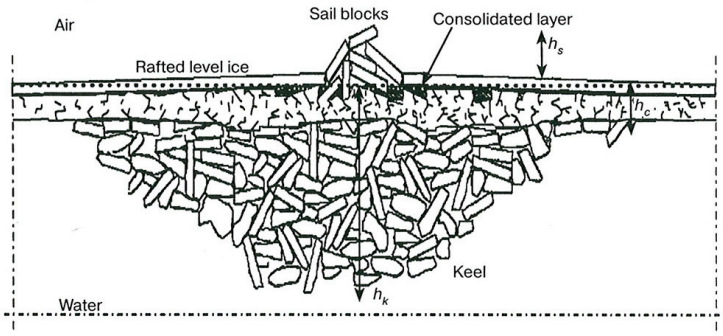

a. Typical cross section of a 1st year ridge (from Løset et al.,2006)

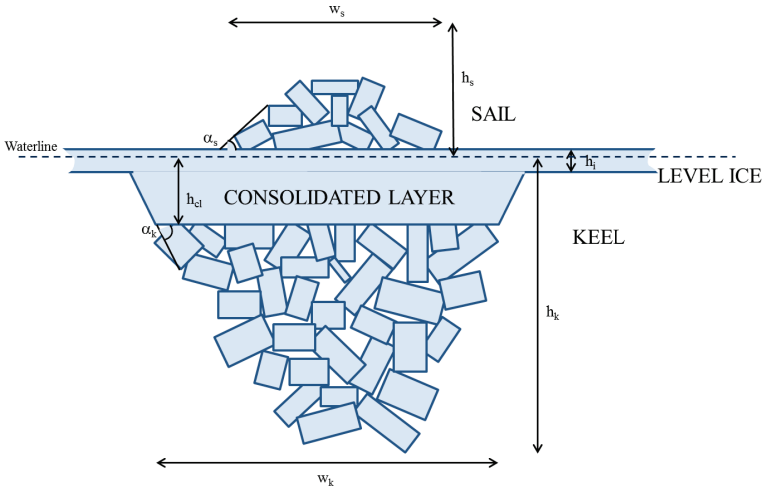

b. Key dimensions in 1st year ridges (from Strub-Klein and Sudom, 2012)

Figure 4. Cross-sections of a first-year ice ridge.

Figure 5. Left: first-year ice ridge in the Barents Sea, May 2008. Right: First-year ice ridge (in transition to becoming second-year) in the Fram Strait, September 2008.

The key dimensions of the ridges (Figure 4b) are the sail height (h_s), the consolidated layer thickness (h_c), the keel depth (h_k), the level ice thickness (h_i), the width of the sail (w_s) and the keel (w_k), as well as the angles of inclination of the sail (α_s) and the keel (α_k). Timco and Burden (1997) and Kankaanpää (1997) defined the keel depth as a function of the sail height of first- and multi-year ridges. In addition, Timco and Burden (1997) related the keel width with the keel depth, the keel width with the sail height as and the keel angle with the sail angle. They also examined the keel-to-sail ratio. A paper included in this thesis (Chapter 4) presents an extension of this work by adding 13 years of data. The morphology and the consolidation of first-year ridges is described and analyzed by Leppärantä et al. (1995), Høyland and Løset (1999), Høyland (2000b), Høyland (2002), Høyland and Liferov (2004), Høyland (2007) and Shafrova and Høyland (2008) and others.

2.6 Fieldwork locations

The data presented and analyzed in this thesis were collected in three frozen fjords of the Svalbard archipelago, in the Barents Sea and in the Fram Strait (see Figure 6 for a detailed map). The Svalbard archipelago is located between 76 and 81ºN and is covered with ice from November to July. Some coasts and fjords in the northern islands are covered by ice all year around. The city of Longyearbyen is developed; in 1993, the University Center on Svalbard (UNIS) opened its doors to scientists interested in polar-region research. The current technology and the transportation systems enable scientists to conduct good research under difficult conditions. The mining settlement of Svea, 60 km south of Longyearbyen, is accessible with snowmobile in winter and with small planes all year. Svea is located next to Van Mijenfjorden, a fjord frozen from December to June. From 1998 to 2000, Høyland (2000a) spotted and investigated first-year sea ice ridges further out in the same fjord. In addition, the facilities in Svea (barracks and storage) simplified the conditions for working on the ice.

The artificial ridge (in 2008), the mini ridge (in 2009) and the sampling matrices from level ice (in 2010) were all conducted in Van Mijenfjorden. In addition, the "Thermo-mechanical properties of materials" course at the UNIS performs a cruise in the Barents Sea every year in late April and early May. The purpose of this cruise is to study a first-year ice ridge during 5 days (depending on the floe and sea conditions). Data on the ridge morphology and physico-mechanical properties were collected in 2008. In 2009, the floes kept breaking; thus, no complete and useful data set could be collected that year. In 2010, the floes broke even more than in 2009; thus, we returned to Svalbard and settled in the outer part of Van Mijenfjorden, close to the island Akseløya. We established 2 sampling matrices, similar to those established earlier in the season further inside the fjord. In Chapter 3, a paper is presented that describes level ice data collected from 2005 to 2011. In addition to the locations mentioned above, the ice was sampled in the small fjord near Longyearbyen, Adventfjorden, as well as a fjord situated south of Van Mijenfjorden, Van Keulenfjorden (see Figure 6 for the location of all of these fjords). Chapter 4 describes sea ice ridges and presents data collected in Van Mijenfjorden, the Barents Sea and the Fram Strait.

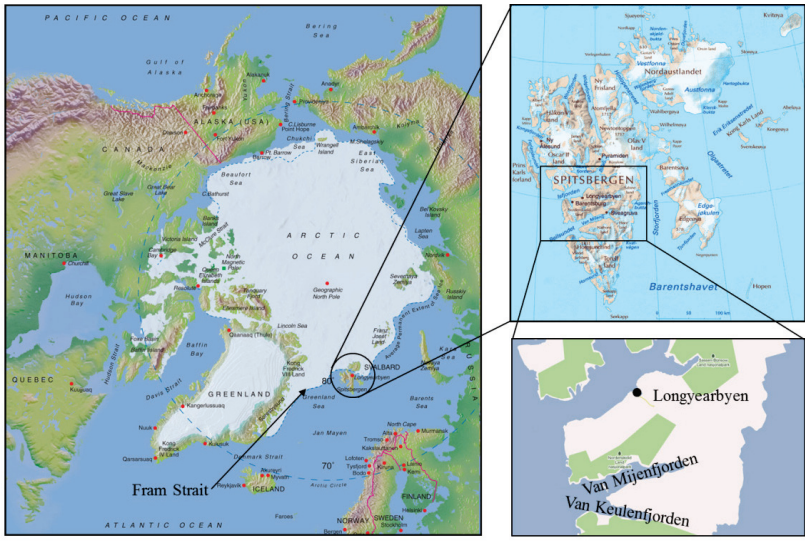

Figure 6. Location of the Svalbard archipelago in the Arctic Ocean, showing the average ice coverage. Zooms of the archipelago and the fjords in which the fieldwork was performed.

2.7 References

Bernal, J.D. and Fowler, R.H. (1933). A theory of water and ionic solution, with particular reference to hydrogen and hydroxyl ions. Journal of Chemistry and Physics, Vol.1, pp-515-548l.

Dowling, N. E. (1999). Mechanical behavior of materials. Engineering methods for deformation fracture, fatigue. 1999, Upper Saddle River, New Jersey: Prentice Hall. 830p.

Gabrielsen, M. et al. (2008). Comparison of physical and mechanical properties of coastal ice and level ice. Proceedings of the 19th International Symposium on Ice (IAHR), Vancouver, Canada, pp. 965-974.
Glen, J.W. (1955). The Creep of Polycrystalline Ice. in Proceedings of the Royal Society of London.1955.
Glen, J.W. (1958). The flow law of ice. Proceedings of the Chamonix Symposium. IASJ Publication 47, pp.171-183. Gentbrugge, Belgium.
Høyland, K.V. (2000a). Measurements and simulations of consolidation in first-year sea ice ridges, and some aspects of mechanical behaviour. Thesis for the degree of philosophiae doctor 2000:94. Department of Structural Engineering of the Norwegian University of Technology (NTNU), Trondheim, Norway. September 2000. ISBN 82-7984-121-0. ISSN 0809-103X. 172 pp.
Høyland, K.V. (2000b). Consolidation of first-year sea ice ridges. Journal of Geophysical Research. Oceans; 107 (6): 16 p.
Høyland, K.V. (2002). Simulations of the consolidation process in first-year sea ice ridges. Cold Regions Science and Technology **34**(2002), pp. 143-158.
Høyland, K.V. (2007). Morphology and small-scale strength of ridges in the North-western Barents Sea. Cold Regions Science and Technology **48**(2007), pp.169-187.
Høyland, K.V. (2009). Ice thickness, growth and salinity in Van Mijenfjorden, Svalbard, Norway. Submitted for publication in Polar Research. (2009).
Høyland, K.V. and Løset, S. (1999). Measurements of temperature distribution, consolidation and morphology of a first-year sea ice ridge. Cold Regions Science and Technology **29**(1999), pp.59-74.
Høyland, K.V. and Liferov, P. (2004). On the initial phase of consolidation. Cold Regions Science and Technology **41**(2005), pp.49-60.
ISO/FDIS 19906:2010 (E): Petroleum and natural gas industries – Arctic Offshore Structures.
Kankaanpää, P. (1997). Distribution, morphology and structure of sea ice pressure ridges in the Baltic Sea. Fennia, Internal Journal of Geography. Vol.175, pp.139-240. Geographical Society of Finland. Helsinki, Finland.
Khorzavin, K.N. (1983). Action of Ice Engineering Structures. Books for Business. New York – Hong Kong. ISBN 0-89499-171-X.
Kovacs, A. (1996). Sea ice part II. Estimating the Full-Scale Tensile, Flexural, and Compressive Strength of First-Year Ice. CRREL Report 96-11, September 1996.
Leppäranta, M. (1993) A review of analytical models of sea-ice growth. Atmosphere Ocean, Vol. 31 (1), pp. 123-138.
Leppäranta, M. et al. (1995). The life story of a first-year sea ice ridge. Cold Region Science and Technology **23**(1995), pp.279.290.
Løset , S., et al. (2006). Actions from ice on Arctic Offshore and Coastal Structures. Student's Book for Institutes of Higher Education. St Petersburg: Publisher "LAN", 2006. 272pp. ISBN S-8114-0703-3.
Michel, B. (1958). Ice mechanics. Les presses de l'université de Laval. 499p.

Moslet, P.O. (2007). Field testing of uniaxial compression strength of columnar sea ice. Cold Regions Science and Technology **48** (2007), pp. 1-14.
Norton, H.F. (1929). Creep of steel at high temperatures. New York:McGraw-Hill.
Ramseier, R.O. (1971). Mechanical Properties of Snow Ice. Proceedings of the 1st International Conference on Port and Ocean Engineering under Arctic Conditions (1971). Trondheim, Norway, pp.192-210
Palathingal, P. (1989). Some Laboratory Test Results on the Creep Behaviour of Fresh Water Ice. Proceedings of the 10th International Conference on Port and Ocean Engineering under Arctic Conditions. 1989. Luleå, Sweden.
Peyton, H. R. (1966). Sea ice strength. University of Alaska Report UAG-182. Fairbanks: Geophysical Institute.
Peyton, H. R. (1968). Sea ice strength effects of load rates and salt reinforcement. Arctic drifting stations, ed. J.E. Sater, pp. 197-217. AINA.
Schulson, E.M. (1997). The brittle failure of ice under compression. Journal of Physical Chemistry B (101), pp-6254-6258.
Schulson, E.M. and Duval, P. (2009). Creep and fracture of ice. Cambridge University Press, New York. ISBN 978-0-521-80620-6.
Schwerdtfeger, P. (1963). The thermal properties of ice. Journal of Glaciology **4**(1963):pp. 789-807
Shafrova, S. and Høyland, K.V. (2008). Morphology and 2D spatial strength distribution in two Arctic first-year sea ice ridges. Cold Regions Science and Technology **51**(2008). Pp. 38-55.
Strub-Klein, L. and Sudom, D. (2012). A comprehensive analysis of the morphology of first-year sea ice ridges. Article submitted to Cold Regions Science and Technology on 21 January 2012.
Sinha, N.K. (1983). Creep Model of Ice for Monotonically Increasing Stress. Cold Regions Science and Technology, **8**(1983). pp. 25 33.
Stefan, J. (1891). Über die Theorie der Eisbildung, insbesondere über Eisbildung im Polarmeere. Annals of Physics **42**(1891), 3rd Ser. pp 269-286.
Thomas, D.N. and Dieckmann, G.S (2010). Sea ice. Second Edition. Edited by David N. Thomas and Gerhard S. Dieckmann. Wiley-Blackwell. ISBN 978-1-4051-8580-6 (hard cover).
Timco, G.W. and Frederking, R.M.W (1990). Compressive strength of sea ice sheets. Cold Regions Science and Technology **17**(1990). Pp. 227-240.
Timco, G.W. and Burden, R.P. (1997). An analysis of the shape of sea ice ridges. Cold Regions Science and Technology **25**(1997) pp. 65-77.
Weeks W.F. (1994). Growth Conditions and the Structure and Properties of Sea Ice. Summer School, 1994. Savonlinna, Finland.
Weeks, W.F. (2010). On sea ice. University of Alaska Press. ISBN 978-1-60223-079-8.
World Meteorological Organization (1970). WMO sea ice nomenclature (supplement No 5. 1989). Technical Report MO No. 259.TP.145. World Meteorological Organization. Geneva. Switzerland.

Chapter 3 – Field measurements and analysis of level ice properties

3.1 Introduction

This chapter describes and analyzes uniaxial compressive tests performed mainly in Van Mijenfjorden but also in Adventfjorden, Van Keulenfjorden and Barents Sea.
This chapter consists of 3 papers. The first article, published in Cold Regions Science and Technology, analyzes the field season of 2010 with respect to the ice strength variability. Large amounts of uniaxial compressive test data were collected between 2005 and 2011. The second paper determined a probabilistic model for the fitting of sea ice uniaxial compressive strength data from 1237 samples. This work has been submitted for publication in the Journal of Offshore Mechanics and Arctic Engineering.

The final paper presents an experimental setup based on stress sensors and a borehole jack to measure the stress propagation in sea ice; this paper has been published and presented at the International Conference on Port and Ocean Engineering under Arctic Conditions (POAC) in 2009.

This chapter aimed at

- improving the existing knowledge of strength variability.
- improving the knowledge of the link between the mechanical and physical properties of ice by considering variability.
- improving models that predict sea ice growth.
- determining a statistical model for uniaxial compressive strength of level ice.
- enhancing our understanding of how stresses propagate in sea ice.

Publications:

(3.2)

Strub-Klein, L. and Høyland, K.V. (2012). Spatial and Temporal Distributions of Level Ice Properties. Experiment and thermo-mechanical analysis. Cold Regions Science and Technology **71**(2012), pp.11-22.

(3.3)

Strub-Klein, L. (2012). A statistical analysis for first-year level ice strength. Journal of Offshore Mechanics and Engineering (submitted).

(3.4)

Barrault, S. and Strub-Klein, L. (2009). An experimental set-up for measuring stress propagation in sea ice. Proceedings of the 20th International Conference on Port and Ocean Engineering under Arctic Conditions (POAC). Luleå, Sweden.

3.2 Spatial and temporal distribution of level ice properties. Experiments and thermo-mechanical analysis.

Cold Regions Science and Technology 71 (2012) 11–22

Contents lists available at SciVerse ScienceDirect

Cold Regions Science and Technology

journal homepage: www.elsevier.com/locate/coldregions

Spatial and temporal distributions of level ice properties Experiments and thermo-mechanical analysis

Lucie Strub-Klein *, Knut Vilhelm Høyland

The University Centre on Svalbard (UNIS), Arctic Technology Department, P.O. Box 156, 9170 Longyearbyen, Norway
The Norwegian University of Technology (NTNU), Department of Civil and Transport Engineering, Høgskoleringen 7a, 7034 Trondheim, Norway

ARTICLE INFO

Article history:
Received 15 June 2011
Accepted 9 October 2011

Keywords:
Uniaxial compressive strength
Brine volume
Variability
Coefficient of variation

ABSTRACT

Sampling matrices were established at three different sites of Van Mijenfjorden, Svalbard. In total, 193 horizontal and 117 vertical sea ice samples were tested in uniaxial compression from early March to early May 2010. Temperature, density and salinity (TDS) were also measured on every core. Additional samples were taken for TDS profiles as well as for thin sections. The variability in strength seemed to be correlated with the salinity variability, the mean value of the brine fraction and possibly the sampling spacing. Both the variability in strength and salinity increased when the brine fraction increased above 0.05, but for a further increase in the mean brine fraction, only the salinity variability increased (not the strength variability). This means that the drainage and localization of brine becomes a key factor for ice strength variability. The variability of the salinity of the horizontal samples was higher than for the vertical samples at the third site and suggests that one level of a typical brine channel spacing was between the diameter of the vertical samples (72 mm) and the length of the horizontal ones (175 mm). The ice growth predicted by Stefan's law fitted the measurements well with a correction factor $\omega = 0.40$. The thin sections revealed that the ice taken on the first two sites was granular up to 30 cm and then columnar. The transition from S2 to S3 ice may have occurred between 45 and 54 cm.

1. Introduction

Physical and mechanical properties of sea ice have been the main topic of a large number of publications the past decades. As the oil industry develops in the Arctic marine areas, accurate data are needed to improve existing models for the design of structures and ships in ice infested waters. Thus, understanding the ice action is of crucial importance, and it requires knowledge of both the ice features (level, rafted, ridge, rubble field or iceberg) and the ice properties (crystallography, temperature, salinity, porosity, strength, and surface tension). These, combined with the failure mode (crushing, bending, splitting, buckling, spalling and creep), the structure geometry and the scenario of interaction (limit stress, limit momentum, limit force and splitting) define the ice action. In the case of a limit stress scenario where the level ice fails by crushing against a vertical structure, the uniaxial compression strength is related to the load the ice generates against that structure. The Korzhavin's formula is commonly used to estimate the ice force F:

$$F = I \cdot K \cdot m \cdot \sigma_c \cdot D \cdot h_i \quad (1)$$

where σ_c is the uniaxial compressive strength, D is the structure diameter, h_i is the ice thickness, I is an indentation factor, K is a contact factor and m is a shape factor. However, this formula has shown to overestimate the loads for wide structures probably because of a scale effect, a non-homogeneous ice field and a non-simultaneous ice failure (Løset et al., 2006).

The uniaxial compressive test is a relatively simple way to characterize ice strength. However, it is not straightforward to determine this property, because it is governed by numerous parameters (see Fig. 1). Amongst them, the temperature, the porosity, the grain size and orientation as well as the strain rate have been long considered to be the most important.

Extensive work has been performed in the past decades on the uniaxial strength of sea ice. Timco and Weeks (2010) and Weeks (2010) published a large overview and review of the properties of sea ice, and in particular the uniaxial compressive strength of ice. They discuss the sampling and testing techniques and provide a list of authors presenting results on that topic as well as a summary of the existing analytical models for uniaxial compressive strength. Amongst them are Timco and Frederking (1990), who proposed an analytical model for horizontal and vertical samples. In these equations, the strain rate and the total porosity were the varying parameters. More recently, Moslet (2007) modified these models so that they would only depend on one parameter, the porosity.

But what about the variability of sea ice strength? The brine volume, the temperature, and the porosity are strongly related to the state of the ice and do not have an even distribution across and through the ice

* Corresponding author. Tel.: +47 79023374; fax: +47 79023301.
E-mail address: Lucie.Strub-Klein@unis.no (L. Strub-Klein).

0165-232X/$ – see front matter © 2011 Elsevier B.V. All rights reserved.
doi:10.1016/j.coldregions.2011.10.001

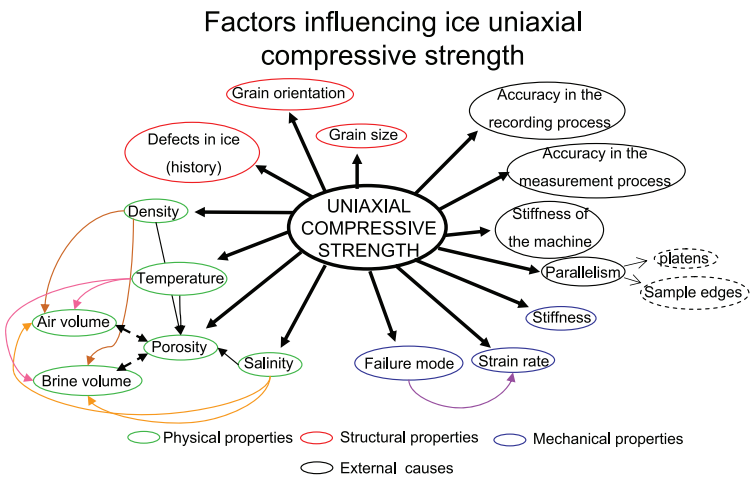

Fig. 1. Factors influencing ice strength.

sheet. Hence, the uniaxial compressive strength presents also variations within the ice sheet. Sanderson (1991) presented a statistical analysis of ice forces. When a large area of ice is in contact in the structure, the ice will fail non-simultaneously, more sporadically and more locally. In this sense, the total ice force against the structure would be the statistical sum of the localized failure events. According to Sanderson (1991), these events are not correlated in time or space. Hence, we believe that knowing more about the strength variability would help in forming a proper opinion on the distribution of ice loads against a structure and thus improve the existing statistical models, as it would give an additional indication on the occurrence and the conditions of occurrence of more extreme values. And yet, very little literature is available on that topic. Shafrova and Moslet (2006a,b) showed the importance of studying the ice strength heterogeneity, since it varies not only temporally but also spatially. The variability is often expressed with the standard deviation. However, for distributions with a large difference in mean values, this may not be a good way of expressing the variability. Cold and warm sea ice may differ in mean strength within an order of magnitude so an alternative is to express the global variability with the coefficient of variation (k_v) which is the ratio of the standard deviation to the mean. It measures the spread of a set of data as a proportion to its mean, and was used by Surkov and Truskov (1993) to characterize the ice strength. An advantage of the coefficient of variation is that it is a dimensionless number, although it cannot be used to construct intervals of confidence.

Probabilistic models are commonly used for the forces on, and the response of, structures exposed to wind and waves. A central idea in probabilistic modeling is the use of a statistical and not a deterministic description of the variables. Onishchenko (2009) gives a recent description of this method for the determination of ice actions. The use of this method means that the ice properties have to be described in a statistical way, which is through distributions. Shkhinek et al. (2008) collected data on ice strength heterogeneity and developed analytical models that predict:

- the probability of the structure contacting the strongest part of the ice (probabilistic factor influencing the ice load)
- if contact, the dependence of the load on the structure dimension and ice strength spatial heterogeneity (deterministic load).

They based their analysis on 5 field studies and it is believed that the models would be even more accurate with more field data and more insight on the causes for this strength heterogeneity.

In this study, 193 horizontal and 117 vertical sea ice samples have been compressed with a portable uniaxial compression rig from early March to early May 2010 on Van Mijenfjorden, Svalbard to study the variability of the ice strength and other physical properties in relation to the sampling depth and sampling spacing as well as to the temporal evolution. Some considerations on the ice structure and ice growth will also be discussed.

2. Location and experimental set up

The investigations took place in Van Mijenfjorden, Svalbard, Norway (Fig. 2). The Svalbard archipelago is located between 76 and 82°N and Van Mijenfjorden has a stable landfast ice cover from December/January to June/July every year. The ice conditions and the hydrography are explained in Høyland (2009), Kangas (2000) and Marchenko et al. (2010). This fjord is located 60 km south from the university and is easily accessible by snowmobile from December to May or by plane the whole year long. In addition, the mining settlement Svea provides facilities such as storage and housing. The sites were chosen firstly for convenience but the ice actions can be problematic against the coal quays and therefore this study could also help in improving the reinforcement of these structures (more information on the coal quays and ice related problems in this area can be found in Marchenko et al., 2011).

Several stations were established at three different sites in the fjord. Site 1 (77°52′497″N, 16°43′546″E, coordinates for one point of the matrix) was visited during four weeks and one sampling matrix per week was established. Site 2 (77°53′631″N, 16°45′064″E, coordinates of the common point between matrices 1 and 4) was visited two times during two weeks (1 visit per week). Samples were taken either along a line (first visit) or in a simple square (second visit). Site 3 was visited only once but two sampling matrices were established (77°43′657″N, 14°46′57″E, coordinates of the boat).

Level ice investigations were performed seven times from 3 March to 6 May. We defined sampling matrices at every visit (see Table 1 for a detailed description). These matrices were actually forming a mesh with two perpendicular sets of lines. One point was the ice in the vicinity (less than 1 m) of the intersection between the two sets of lines. In this way, several cores could be defined originating from one point. Fig. 3 shows the square matrices at site 1 and the intersections. Both matrices at site 3 were established following the same

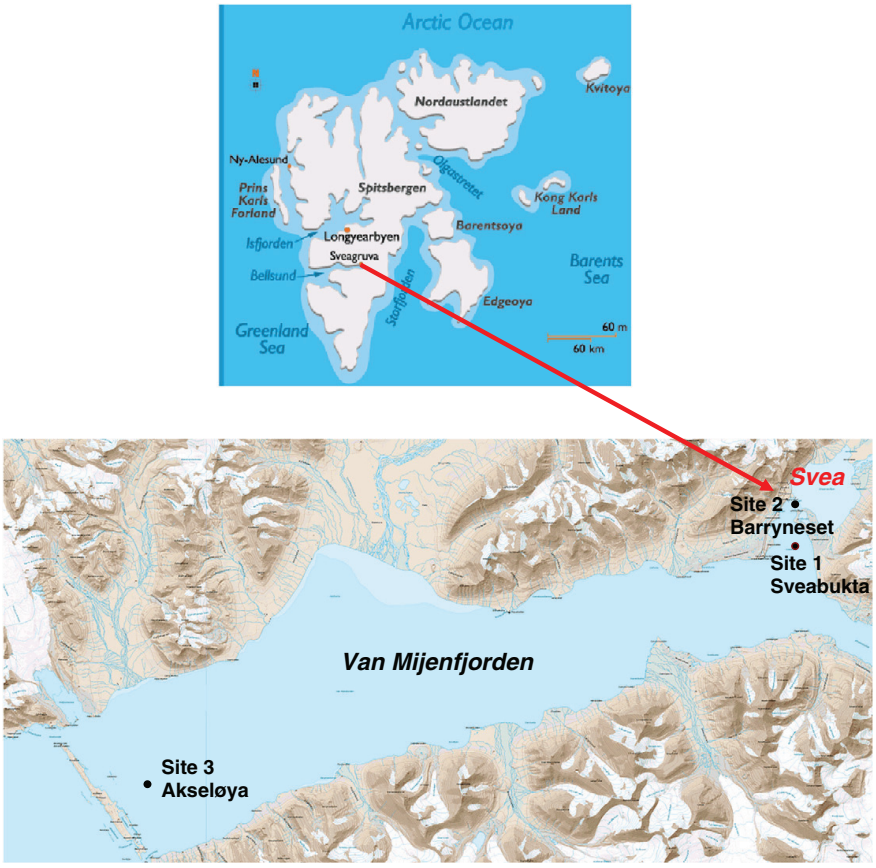

Fig. 2. Map of the three different matrix locations.

pattern. In the two visits at site 2 we used points along a one line (week 15) and in a simple square (week 16).

At all points of sites 1 and 3 we measured the ice and snow thicknesses and the freeboard in addition to sampling for uniaxial compression tests, whereas at site 2 we did not measure the ice thickness systematically. The compression tests were done on site almost immediately after the sample was extracted and we determined the temperature, density and salinity (TDS) for every sample. The density was measured by assuming a perfect cylindrical sample shape ($l=0.175$ m and $D=0.072$ m) and measuring the mass. The mechanical tests were done with the UNIS' field compression rig KOMPIS (see Moslet, 2007 for a description of the rig). All the samples were compressed at a nominal strain-rate of 10^{-3} s^{-1} (kept constant during the whole test) which, according to Schulson (1997), corresponds to the ductile-to-brittle transition and thus give the highest compressive strength. The ice was taken at different depths and the given depths in Table 1 refer to the center of the sample. At sites 1 and 2, all horizontal samples were taken in the same direction, which is 65°CN (Compass North). The ice in Van Mijenfjorden goes from S2 to S3 as it grows and Gabrielsen (2007) found that for the ice at his site on Van Mijenfjorden (close to our site 1), the c-axis was oriented 155°CN so that 65°CN should give the peak horizontal strength. No measurements of the under-ice currents have been made on a regular basis. It is believed that the currents entering the fjord are similar from year to year, but we do not know in a microscopic scale how the turbulences are exactly under the ice. We do know that there are bigger perturbations of the currents at site 2 due to the formation of an ice foot 15 m away from our sampling areas. We are aware that assuming that the c-axis has kept the same orientation since 2007 may increase the scatter in our results. One or two vertical TDS profiles were measured during every visit: The ice temperature was measured every 5 cm, starting from the bottom of the core. For that, we used a small electrical drill to make a hole in which we inserted a thermometer straight after. The same core was cut with a saw adjusted to produce 10 cm long pieces which were weighed with a spring scale. The density was calculated later (knowing that all the dimensions were constant). Each piece was melted and the conductivity of the water was measured. Air and brine fractions were calculated as suggested by Cox and Weeks (1983) for $T_i<-2$ °C and by Leppäranta and Manninen (1988) for $T_i>-2$ °C.

During the first three visits at site 1 (see Table 1) the matrices were equal (30×30 m and 16 points), but at the 4th visit we had the manpower to increase the size to 150×150 m and include 49 points. The depth of all the cores was 30 cm. At the second site (visits in April) we were more devoted to studying the effect of depth and sample orientation. Samples were taken along a line (3 points and 25 m spacing) in week 15, while in week 16 we used a simple square (10×10 m) and sampled in 5 points (corners and center). At site 3 two matrices were defined, one in ice with smooth surface (level

Table 1
Summary of the different locations, matrices and activities.

Week	Location	Size of matrix	Activities
9 (01.03–07.03) *Matrix* 1	Svea Bukta Site 1	30×30 m	Thermistor strings installed
		10 m spacing	h_i, h_s, *FB*
		16 points	σ_h
		16 horizontal samples	TDS
		Depth approximately 30 cm	TS
10 (08.03–14.03) *Matrix* 2	Svea Bukta Site 1	30×30 m	h_i, h_s, *FB*
		10 m spacing	σ_h*
		17 points	TDS
		17 horizontal samples	TS
		Depth approximately 30 cm	Beam tests
11 (15.03–21.03) *Matrix* 3	Svea Bukta Site 1	30×30 m	h_i, h_s, *FB*
		10 m spacing	σ_h*
		16 points	
		16 horizontal samples	
		Depth approximately 30 cm	
12 (22.03–28.03) *Matrix* 4	Svea Bukta Site 1	150×150 m	h_i, h_s, *FB*
		25 m spacing	σ_h, σ_v
		49 points	
		49 horizontal samples + 7 vertical samples	
		Depth approximately 30 cm	TDS
15 (12.04–18.04) *Matrix* 5	Barrynesset Site 2	3 points on line spaced by 25 m	h_i, h_s, *FB*
		2–3 cores per point	σ_h, σ_v
		10 horizontal + 10 vertical samples	
		Depths approximately 20 and 50 cm	
16 (19.04–25.04) *Matrix* 6	Barrynesset Site 2	10×10 m	Thermistor string removed
		5 points (corners + center)	h_i, h_s, *FB*
		2–3 cores per point	σ_h, σ_v
		22 horizontal + 29 vertical samples	TDS
		Depths approximately 20 and 50 cm	TS
18 (03.05–09.05) *Matrices* 7 and 8	Akseløya Site 3	2 matrices	h_i, h_s, *FB*
		7. level ice: 40×40 m, 25 points, 10 m spacing	σ_h, σ_v
		42 horizontal samples + 37 vertical samples	
		8. rough ice: 30×30 m, 16 points, 10 m spacing	
		21 horizontal samples + 34 vertical samples	TDS
		Depths approximately 15 and 40 cm	Beam tests

h_i: ice thickness, h_s: snow thickness, *FB*: free board.
σ_h: strength tests on horizontal samples σ_v: strength tests on horizontal samples, *: samples compressed 30 to 60 min after coring.
TDS: temperature, density and salinity profile.
TS: sample taken for thin section.

ice) and one in ice with rougher surface (rough ice). Table 1 is giving a more complete description of the experimental set-up, while some illustrations can be seen in Fig. 4.

Two thermistor strings were installed close to the common corner of matrices 1 and 4 (see Fig. 3). They measured the vertical temperature profile every 5 cm from the water below the ice, up through the ice and snow, and into the air from 4 March to 20 April. Finally, some cores were sampled and brought back to Longyearbyen where thin sections were made in a cold laboratory.

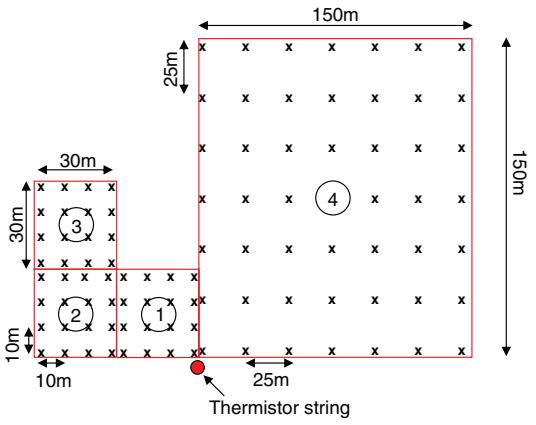

Fig. 3. Display of the four matrices established for set 1.

This paper presents the spatial and temporal variations of the physico-mechanical properties of sea ice. The temporal variations are studied when comparing the data week after week. However, when we deal with the spatial variations, we mean within each matrix and not between the three sites. Therefore, to avoid any further confusion, all the data collected at site 1 will be grouped as “set 1”, all the data collected at site 2 will be grouped as “set 2” and all the data collected at site 3 will be grouped as “set 3”.

3. Theory — ice growth and Stefan's law

A simple way to verify the growth of the ice is to confront the experimental data with the analytical model for ice growth described by Stefan's law:

$$h_i^2 - h_0^2 = \frac{2k_i}{l_f \rho_i} \mathrm{FDD} \tag{2}$$

$$\text{And FDD} = \int_0^t \left(T_f - T_a\right) dt \tag{3}$$

where $l_f = 333{,}400$ J/kg is the latent heat of fusion for sea ice, k_i (W/m °C) is the thermal conductivity, ρ_i (kg/m^3) is the density of the

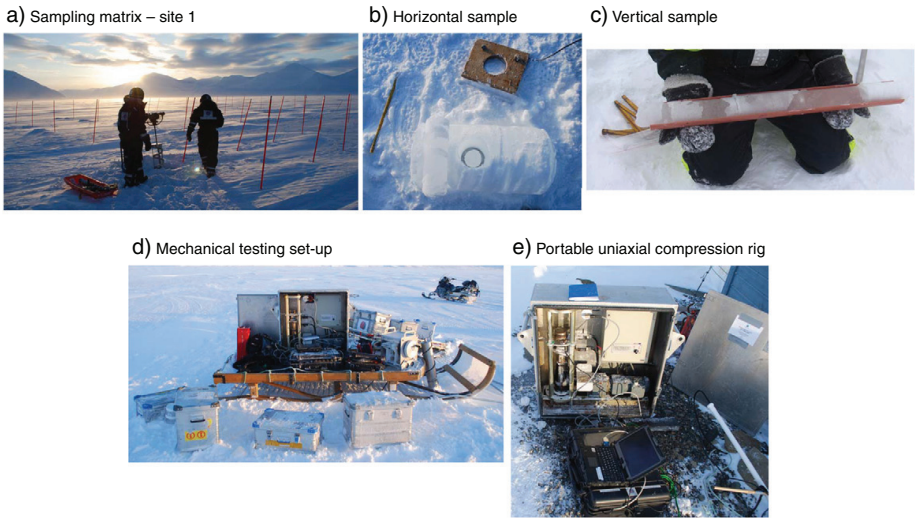

Fig. 4. Experimental set-up. a. Sampling matrix — site 1. b. Horizontal sample. c. Vertical sample. d. Mechanical testing set-up. d. Portable uniaxial compression rig.

ice, h_i (m) is the ice thickness, h_0 (m) is the initial ice thickness, T_a (°C) is the air temperature and T_f (°C) is the freezing point of the surrounding water. This formula is based on the assumptions that the temperature gradient throughout the ice sheet is linear, that the air temperature equals that of the ice surface, that there is no snow, no heat transfer from the ocean, no thermal inertia, no internal heat source and no solar radiation. Some of these assumptions (no oceanic flux and no snow cover) are oversimplifications that can be accounted for by using a correction factor ω introduced by Leppäranta (1993). The Stefan's law is then expressed by:

$$h_i^2 = h_0^2 + \omega \frac{2k_i}{l_f \rho_i} \mathrm{FDD}. \quad (4)$$

The thermal conductivity and the latent heat of fusion for sea ice depend on the size, concentration and distribution of brine, so they are not constant. Therefore three unknowns have to be considered

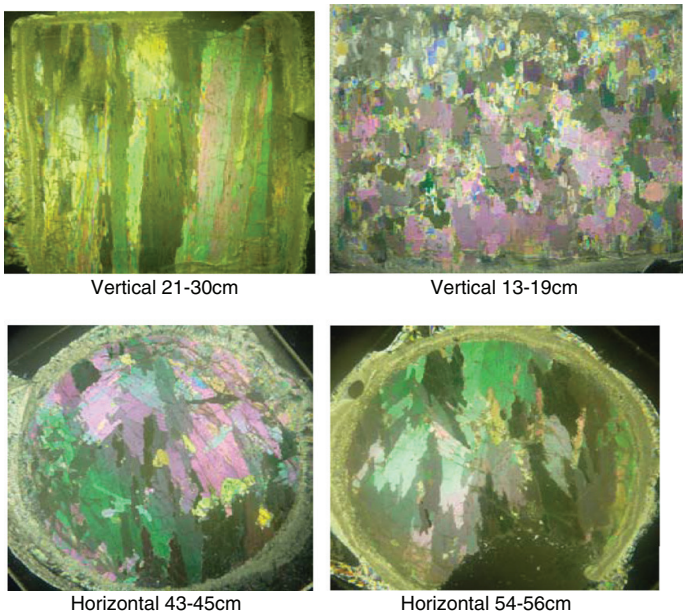

Fig. 5. Thin sections made on a sample of set 1, taken on 4 March.

in Eq. (4): ω, l_f and k_i. Høyland (2009) discussed the level ice growth in Van Mijenfjorden whereas Strub-Klein and Høyland (2011) compared it to the growth of a small first-year ice ridge. They used $k_i = 2.1$ W/m°C and $l_f = 333{,}400$ J/kg and these values will also be used in this paper for comparison.

4. Field data

4.1. Ice thickness, ice- and air temperatures, ice texture and TDS profiles

A few samples were taken on 4 March at site 1 and thin sections were made later in a cold laboratory. Fig. 5 shows that the transition from granular to columnar ice was complete at about 20 cm so that we assume all samples at 30 cm depth were columnar ice. Although the orientation was not measured, the crystals seemed to have a preferred azimuthal arrangement at a depth of 55 cm, so it seems reasonable to assume that the transition between S2 and S3 ice occurred between 45 and 54 cm depth. Site 2 is close to site 1 so we will suppose a similar texture for the samples of set 2. But site 3 was more than 40 km west of the two other sites, and we cannot expect that the columnar ice was developed at the same depth for the samples of set 3.

Table 2 gives an overview of the ice thicknesses estimated from the thermistor string (h_i^T) and from drillings (h_i^D). The average ice thickness from drilling grew from 0.63 m to 0.75 m in site 1 from week 9 to 12, whereas the thickness as indicated by the thermistor strings grew in average from 0.67 to 0.87 m. Neither the thermistor string nor the thickness of the TDS cores at site 2 (April) indicate much further ice growth. A thermistor string usually gives lower ice thickness than drilling (Høyland, 2002), but as h_i^D was an average value, the opposite is also reasonable. The freeboard was all the time positive and varied from 2.7 to 5 cm, and the snow depth varied between 10 and 16 cm. The thermistor strings gave no indication of warm water below the ice in weeks 12–16. The ice thicknesses in the two matrices of set 3 were respectively 0.44 and 0.72 m for the level ice and the rough ice so that either the level ice was formed later, or (more probably) the rough ice consisted of deformed ice.

The air temperatures given in Fig. 6 come from the weather station at Svea airport.

Fig. 7 shows the temperature and salinity profiles of sets 1 and 2 and Table 3 gives the average salinity values from the TDS profiles.

The density is an important property, but hard to measure accurately. Timco and Frederking (1996) and Weeks (2010) discuss the different approaches to density measurements. The method we used during this fieldwork is the most common technique for measuring sea ice density. Although it is rapid and easy to do, the samples rarely have a perfect cylindrical shape (refrozen slush on the surface and very rarely perfectly smooth and flat bases). In addition, the air temperature is not always low enough to prevent the samples from draining from the moment they are extracted to the moment the mass is measured. With the circular manual saw we had at our disposal, the edges were parallel and all our samples had the same dimensions. They were brushed carefully to remove the slush. Our main concern in these measurements was the spring scale. It was hung in a still

Table 2
Ice thickness evolution from the thermistor string (h_i^T) and from drillings (h_i^D) (cm).

Week	h_i^T (min)	h_i^T (max)	h_i^T (mean)	h_i^D
9	65	70	67.5	63.1 Site 1
10	75	80	77.5	72.3 Site 1
11	85	90	87.5	75.8 Site 1
12	85	90	87.5	75.1 Site 1
15	85	90	87.5	75 (from 3 TDS cores)
16	85	90	87.5	77 (from 2 TDS cores)
18 l	–	–	–	44.0 Site 3
18 r	–	–	–	71.5 Site 3

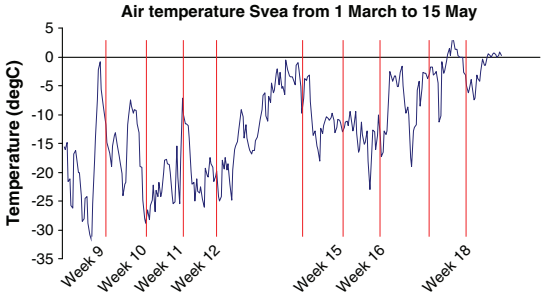

Fig. 6. Air temperature of Svea, winter 2010.

place protected from the wind and calibrated, but the cold could have modified the elastic properties of the metal spring. That could also be one of the reasons why it is difficult to evaluate the differences in densities between weeks 9 and 12 on one hand and 10 and 16 on the other. There could be inaccuracies in measurements or natural variations in the ice cover, both are reasonable conclusions. Further discussion on this matter is given in Section 5.2.1. We chose not to present the results we obtained, because some seemed so suspicious that a potential use of them in the future could lead to wrong predictions.

4.2. Compression tests

The sets were defined by the location (site 1, site 2, site 3) where the samples were taken. It was noticed that within each set, the mean values and the standard deviations of the measured properties were in the same order of magnitude. These 3 sets then delimit 3 steps that we will develop later in this section. Sometimes significant differences between these values within one set were also observed, inducing several levels (or steps) in the temporal evolution of these properties.

Fig. 8 displays the average values for the porosities (including air and brine fractions) and ice temperatures for the compressed samples as the season goes. It shows three levels of temperature and brine fractions corresponding to the three sets. The average salinity, on the other hand, was more or less constant.

Tables 4 and 5 give statistical key values of respectively the salinity and the temperature on one hand and the porosities of the compressed samples on the other hand. The variability of the salinity (either standard deviation, $S_{st.dev}$ or coefficient of variation, k_v^S) was also on three levels corresponding to the three sets, but week 15 belonged to the first level (together with set 1). Within set 1 the variability of the horizontal samples ($S_{st.dev}$ and k_v^S) increased between weeks 9 to 11 and week 12. There were some differences related to length-scale between these sub-sets as explained later in this section. When it comes to the variability of the brine fraction we can find 4 levels both for the standard deviation (see Table 5 and Appendix A.5) and the coefficient of variation: set 1 ($S_{st.dev} = 0.3\%$; $k_v^S = 16$), week 15 ($S_{st.dev} = 1.1\%$; $k_v^S = 22$), week 16 ($S_{st.dev} = 1.6\%$; $k_v^S = 35$) and set 3 ($S_{st.dev} = 8\%$; $k_v^S = 63$). As we see k_v^S in week 15 was closer to set 1 than to week 16, but $S_{st.dev}$ was closer to week 16.

Fig. 9 and Table 6 sum up the key results from the compression tests. The average strength (σ_{mean}) decreased gradually in three steps corresponding to the three sets, whether the ice was horizontal or vertical: set 1 ($\sigma_{mean\ hor} = 2.7$ MPa; $\sigma_{mean\ ver} = 5.2$ MPa), set 2 ($\sigma_{mean\ hor} = 2.1$ MPa; $\sigma_{mean\ ver} = 3.3$ MPa), set 3 ($\sigma_{mean\ hor} = 1.36$ MPa; $\sigma_{mean\ ver} = 1.68$ MPa). In addition the vertical strength was as expected higher than the horizontal one. But our prime concern in this paper is the variability in the strength and as Fig. 9 shows k_v^σ increased substantially between set 1 on the one hand and sets 2 and 3 on the other.

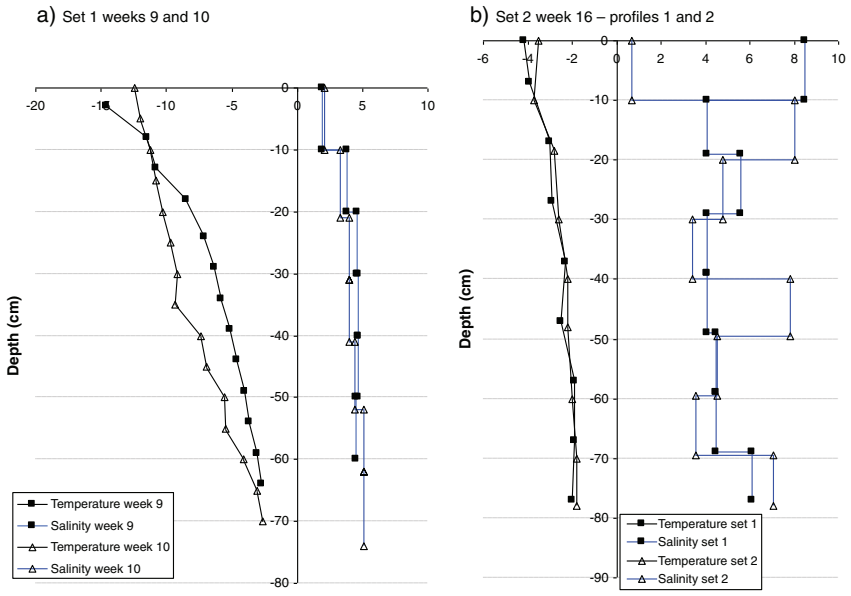

Fig. 7. Temperature and salinity plots from the TDS profiles for sets 1 and 2.

If we consider only horizontal samples within set 1 we see that both the coefficient of variation (k_v^{σ}) and the standard deviation ($\sigma_{st.dev}$) increased between weeks 9 to 11 and week 12, and there were very few brittle samples. Both the minimum and maximum values were more extreme in week 12, and this week was also special in three ways as it had: a) a higher number of samples, b) a larger spacing between the points and c) higher variability in salinity.

Table 7 shows horizontal and vertical strengths for different depths (or assumed ice texture) for both sets 2 and 3. We can see that in addition to the loading direction, the brine fraction seems to govern the strength, which is in good agreement with previous studies.

5. Discussion

5.1. Ice thickness, ice- and air temperatures, ice texture and TDS profiles

The ice growth can be modeled with Stefan's law (Eq. (4)) and when considering the ice growth from week 9 (4 March) to week 12 (23 March), we get FDD = 349. The ice as measured by drilling was 63 cm on week 9 (3 March) and 75 cm on week 12 (23 March). However, the calculation of the ice thickness could only start from week 10 as we needed an initial thickness, given by the drilling on week 9. The average air temperature in Svea in that period was −18.5 °C so an empirical factor of 0.40 was found. This factor was calculated using $h_0 = 0.63$ m and $h_i = 0.75$ m (found by drilling for respectively weeks 9 and 12) and therefore the variations of temperature and ice growth in between were not taken into consideration. This could be a possible explanation for the underestimation of the ice thickness in weeks 10 and 11 (Fig. 10). However, the modeling and the drilling match for week 12. In addition, this value is

Table 3
Average (bulk) salinities from the TDS profiles.

Week	9	10	12	16	18
S_{avg} (psu)	4	4	3.3	5.1	3.9

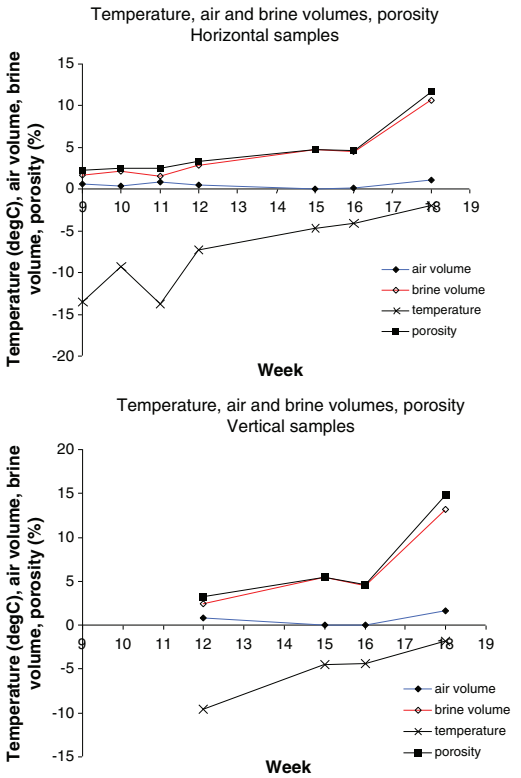

Fig. 8. The average ice temperature (in °C), brine and air fractions and porosity (all in %) of the compressed samples (set 1: weeks 9–12, set 2: weeks 15 and 16, set 3: week 18).

Table 4
Salinities and temperatures of the compressed samples.

		# Samples	Salinity (psu)		Temperature (°C)	
			Average	St dev	Average	St dev
Set 1	Week 9	16	3.7	0.3	−13.5	4.7
	Week 10	17	3.6	0.1	−9.2	1
	Week 11	16	3.7	0.3	−13.8	2.6
	Week 12 H	49	3.9	0.5	−7.3	0.9
	Week 12 V	7	4.1	0.4	−9.6	2.3
Set 2	Week 15 H	10	4.2	0.3	−4.7	0.8
	Week 15 V	10	4.4	0.3	−4.1	0.9
	Week 16 H	22	3.5	0.9	−4.5	1.4
	Week 16 V	29	3.5	0.6	−4.4	1.4
Set 3	Week 18 H	63	3.8	1.4	−1.9	0.6
	Week 18 V	71	4	1.5	−1.8	0.5

comparable to earlier years of level ice growth (Høyland, 2009) and to a small ridge (Strub-Klein and Høyland, 2011), both on Van Mijenfjorden.

5.2. Compression tests

5.2.1. Physical properties

The air and ice temperatures gradually increased through our three sets as they usually do throughout the spring. There was little air in the ice and since the salinity was rather constant the brine fraction was mostly governed by the ice temperature, so the average brine fraction naturally followed the same trend as the average ice temperature. However, the variability in the brine fraction depended more on the variability in the salinity as explained in Section 4.2. In addition, we would like to stress two points:

- The reported ice temperatures were the temperatures just after testing which were not necessarily equal to the in-situ temperature. In some cases the samples were somewhat affected by the air temperature before and after testing;
- The TDS values are from the compressed samples. This means that in this paper we do not report bulk values for the ice cover.

As stated earlier, S_{mean} did not change very much. However, there was one exception, where it decreased by 0.84 psu between weeks 15 and 16. In the same time interval the variability as expressed by the standard deviation ($S_{st.dev}$) clearly increased, basically because the minimum values decreased. This may be due to a flushing event caused by the warm weather in the preceding weeks (Fig. 6). The brine volume reached about 5% in week 15 and this is a level quoted to be the critical level for brine drainage (see Petrich et al., 2011 for a recent summary). The variability in salinity continued to increase in week 18, both because the maximum values increased and because the minimum values decreased, which suggests that the brine was

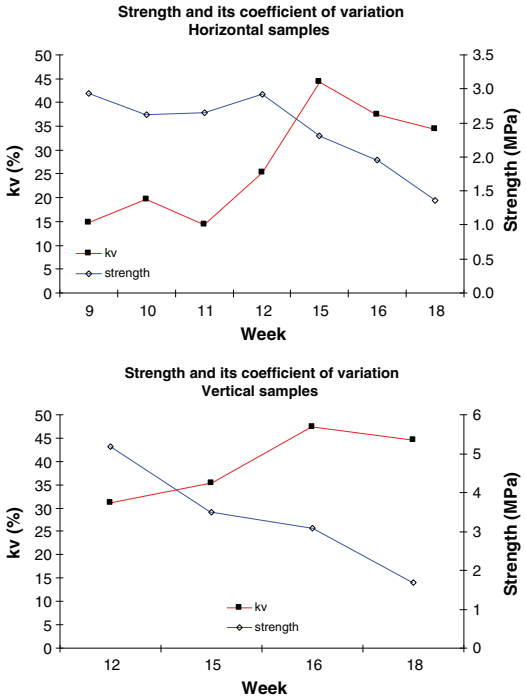

Fig. 9. The average strength and its corresponding coefficient of variation for horizontal and vertical samples (set 1: weeks 9–12, set 2: weeks 15 and 16, set 3: week 18).

even more localized here, and that means that instead of being randomly dispersed in the ice sheet, it was evenly distributed in the channels. It is interesting to notice the big difference between the coefficients of variation for brine fraction for vertical ($k_v{}^{\eta}{}_b^{v}$) and horizontal ($k_v{}^{\eta}{}_b^{h}$) samples in week 18. This may be due to the spatial distribution of one typical level of brine channels. If we then assume an even distribution of the brine channels in the horizontal plane, one level of characteristic spacing between them should be between the diameter of the vertical samples (72 mm) and the length of the horizontal ones (175 mm).

The samples from the three sets were not taken from the same depth in the ice cover so it is reasonable to expect certain differences, especially if top-ice growth occurred. The three sets had different air fractions, but there is no reason to believe that this is a seasonal development. As long as not much brine drains (S_{mean} was roughly

Table 5
Porosity, air and brine fractions (%) of the compressed samples.

		# Samples	Air fraction		Brine fraction		Porosity	
			Average	St dev	Average	St dev	Average	St dev
Set 1	Week 9	16	0.6	1.3	1.7	0.4	2.3	1.2
	Week 10	17	0.4	1.2	2.2	0.2	2.5	1.2
	Week 11	16	0.9	1.2	1.6	0.2	2.5	1.3
	Week 12 H	49	0.5	0.8	2.8	0.4	3.4	0.9
	Week 12 V	7	0.8	0.8	2.5	0.4	3.2	0.8
Set 2	Week 15 H	10	0	0	4.7	1	4.7	1
	Week 15 V	10	0	0	5.4	1.2	5.4	1.2
	Week 16 H	22	0.2	0.8	4.5	1.4	4.6	1.8
	Week 16 V	29	0	0.3	4.5	1.7	4.6	1.8
Set 3	Week 18 H	63	1.1	1.8	10.6	4.3	11.7	5
	Week 18 V	71	1.6	2.5	13.2	11.2	14.8	12.4

Table 6
Summary of the evolution of the ice strength.

		# Samples	Average (MPa)	Min (MPa)	Max (MPa)	St dev (MPa)	k_v (%)	FM
Set 1	Week 9	16	2.9	2.2	3.5	0.4	15	1B–15D
	Week 10	17	2.6	1.9	3.8	0.5	20	17D
	Week 11	16	2.6	1.7	3.1	0.4	14	1B–15D
	Week 12 H	49	2.9	1.4	4.5	0.7	25	49D
	Week 12 V	7	5.2	3.3	8	1.6	31	7B
Set 2	Week 15 H	10	2.3	1	3.7	1	44	2B–8D
	Week 15 V	10	3.5	2.4	5.7	1.2	35	10B
	Week 16 H	22	2	0.8	3.3	0.7	37	2B–1T–19D
	Week 16 V	29	3.1	1.1	7.3	1.5	47	9B–3T–17D
Set 3	Week 18 H	63	1.4	0.4	2.7	0.5	34	4T–59D
	Week 18 V	71	1.7	0.4	3.8	0.7	45	5T–66D

FM: failure mode — B: brittle — T: transitional — D: ductile.

Table 7
Horizontal and vertical strengths and brine fractions for different depths on sites 2 and 3.

Set	2		3	
Depth (cm)	20	50	15	40
Assumed ice texture	Granular	Columnar	Granular	Columnar
n^h	14	18	31	32
σ^h (MPa)	2.5	1.7	1.3	1.4
k_v^h (%)	25	46	39	30
η_b^h (%)	3.9	5.0	10.2	11.0
n^v	14	25	32	39
σ^v (MPa)	3.7	2.9	1.3	2.0
k_v^v (%)	45	41	48	36
η_b^v (%)	4.0	5.2	13.6	12.6

n^h: number of horizontal samples.
σ^h: uniaxial compressive strength for horizontal sample.
k_v^h: coefficient of variation for horizontal samples.
η_b^h: brine volume for horizontal samples.
n^v: number of vertical samples.
σ^v: uniaxial compressive strength for vertical samples.
k_v^v: coefficient of variation for vertical samples.
η_b^v: brine volume for vertical samples.

constant in the three sets), the air fraction should not increase. When the ice heats up, more brine is created and provided that little brine drains, the density should increase. This means that a higher density could be expected for sets 2 and 3. However, as the air fraction became close to 0 in weeks 15 and 16, we suggest that there were some problems with the estimations of average density values, at least in weeks 15 and 16. However, the variability may not have been affected, so the lower variability in week 15 compared to 16 supports the flushing hypothesis.

5.2.2. Strength

The decrease in σ_{mean} with the increase in η_b was expected, and both Moslet (2007) and Timco and Frederking (1990) showed that the porosity is a main factor in determining the mean compressive strength of sea ice. But let us move to analyzing the variability. As shown above, k_v^σ was higher for sets 2 and 3 than for set 1, and there was no difference between sets 2 and 3 in spite of substantial changes in ice temperature and the corresponding brine fraction. However, as the brine fraction was above 5%, (often quoted criterion for efficient brine drainage, Petrich et al., 2011) in sets 2 and 3, we suggest that the strength variability (for our sample size) is closely related to the localization of brine in the sea ice. In other words, young sea ice with many small brine pockets should give a lower coefficient of variability in strength than older sea ice with bigger and fewer brine channels. A question mark remains in relation to week 15 which we earlier assumed to belong to younger ice (as a flushing event may have occurred between weeks 15 and 16). If we examine Fig. 9 more closely we see that the coefficient of variation for the vertical samples ($k_v^{\sigma v}$) in week 15 was closer to set 1 than to sets 2 and 3, whereas that for the horizontal samples ($k_v^{\sigma h}$) was closer to sets 2 and 3 than to set 1 in week 15.

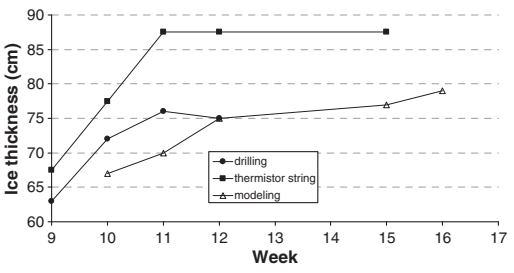

Fig. 10. Comparison between modeled and measured ice thicknesses.

Shafrova and Moslet (2006a,b) analyzed tests done from late March and as late as June and found coefficients of variation from about 10% to 40%, in general a bit less than what we found. They neither report variability in salinity nor brine fraction so it is not straightforward to compare with our results. They mostly compressed vertical samples, but in one of their test series they also did horizontal tests and found a lower variability. Surkov and Truskov (1993) also analyzed compression tests on vertical samples taken from a point (130 tests), a line (125 tests — 10 m spacing between each point) and a test area (191 tests — 20 m spacing between each point). They report $k_v^{\sigma v}$ of respectively 42%, 45% and 56%. No details were given concerning the time of the year the samples were taken and they did not study the variability in brine volume either. However, they noted that the heterogeneity of ice increased strongly from a point to a test area, but it did not vary much from a point to a line. The coefficients of variation for a point and a line are comparable to our results for the tests made in sets 2 and 3. Finally, Takeuchi et al. (2008) also report results from uniaxial compressive tests performed on horizontal samples taken on a line every 15 cm. They took a first series of 133 samples in March 1994 and a second series of 256 samples in February 1995. They immersed the samples in sea water so that they would all be at the same temperature (−1.7 °C in 1994 and −1.8 °C in 1995). They observed that the coefficient of variation for strength of the first series (29%) was higher than that of the second series (26%) because of a higher structural variation of the ice specimen in 1994. They explained this variation by an increase in the number and/or size of the brine drainage channels. This is in good agreement with our results.

Within set 1 we defined two subsets (weeks 9 to 11 and week 12) to examine the difference in ice strength variability. Let us examine the number of samples firstly. We split the matrix of week 12 (which has 49 points) into 4 smaller matrices with 16 points in each and calculated the key statistics. In this case 12 samples were used in two matrices and 1 sample was used in all four. Fig. 11 illustrates the division into the four sub-matrices.

Table 8 shows that the coefficient of variation k_v of the 4 submatrices created from the matrix of week 12 (matrix 12) was higher than those of weeks 9 to 11, but that it was lower than that of matrix 12, even though the values were rather close. This argues that the number of samples could have been important, but should not be the only explanation for the observed increase in variability.

What about the spacing? Another matrix, with 50 m spacing (see Fig. 11b) was studied. As Table 8 shows, the variability increased compared to the total of week 12, and indicates that a larger spacing contributed to increasing the variability. Shafrova and Moslet (2006a,b) examined the effect of spacing but their data are not conclusive. For one test series they found increasing $k_v^{\sigma v}$ (spanned from about 10% to about 40%) for spacing from 0.25 m to 8 m, in another they found decreasing $k_v^{\sigma h}$ (spanned from about 40% and down to about 25%) for spacing from 0.39 m to 50 m. For horizontal samples they found an increasing coefficient of variation from 10 to about 20% for spacing range of 6.25 m to 50 m. Surkov and Truskov (1993) noticed a consequent increase in the coefficient of variation between a line sampling and a test area sampling. During this transition, both the spacing between the points and the number of tests increased. On the other hand, Takeuchi et al. (2008) observed that $k_v^{\sigma h}$ decreased for an increase in testing samples, so there is a possibility that a larger spacing induced a larger variability, as we also observed in set 1.

Finally, one should also consider the data scatter that originates from the sampling and the testing methods. The samples were all collected the same way and cut with a saw that had two parallel rotary blades so all the samples would have the exact same length. However, it happened sometimes that a little piece of ice was cut off the edge

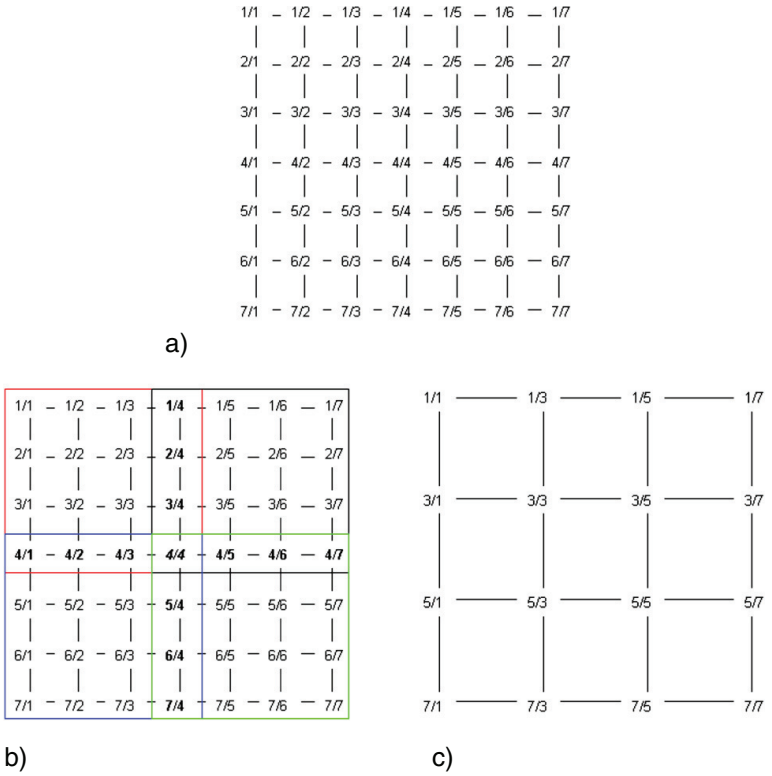

Fig. 11. Division of the matrix on week 12. a. Original grid with 49 points spaced by 25 m-week 12. b. Division of matrix 12 into 4 sub matrices (red, black, green and blue). 12 points (in bold) have been used twice. 1 point (in italic bold) has been used four times 1 point (in italic bold) has been used four times. c. Division of matrix 12 into a large submatrix. 16 points with 50 m spacing.

(or both) when finishing the cutting process so that the surfaces on which the load was applied were not entirely circular. The samples were compressed as fast as possible after their extraction (except in week 11 where there was a waiting time of 30 to 60 min). The same compressive rig was used for all the samples and as mentioned in Section 2 the strain rate was kept constant for all of them. So the scatter would most likely be coming from the sample preparation. It is however impossible to quantify how much scatter originates from this.

In general, the variation in spacing and sample number does not seem to be enough to explain the differences within set 1, so we still believe that the distribution of brine within the sea ice is a key factor but suggests further investigations on how the number of samples and the spacing may affect the ice strength variability.

Table 9 shows that as expected, the deeper samples had a bigger strength ratio than the samples taken closer to the surface. The assumed granular ice in set 2 was sampled about 0.05 m deeper than in set 3 and the wedge out effect had probably started. In general our values for vertical-to-horizontal strength ratios were quite low. Moslet (2007) measured down to 1.3 for cold and up to 4–5 for warm ice. Timco and Frederking (1990) suggest about 2–4. For ridged ice, Høyland (2007) measured a ratio of about 1.1, and refers to a span in reported values in the literature from 0.92 to 3.2. As explained earlier, the rough ice in set 3 could have been older, rafted, ridged or a combination of these. As the surface was rough it indicates the ice cover had been broken so that it was not ordinary S2 ice. As the vertical/horizontal ratio of the level ice in set 3 was similar, it is an indication that this ice was not fully developed S2 ice. The ice conditions in the vicinity of site 3 are in general more dynamic than further into the fjord and several rafting events could have disturbed the development of S2 ice. Set 2 gave a higher ratio, but still well below those of Moslet (2007) and Timco and Frederking (1990), and this indicates that neither here the ice was ordinary S2 ice, but we cannot quantify anything about this. Anyway, Table 9 shows that the ratio increased with increasing depth as expected.

Table 8
Week 12 matrices and sub-matrices.

	# Samples	Spacing (m)	Average (MPa)	Min (MPa)	Max (MPa)	St dev (MPa)	k_v (%)
Week 12 H	49	25	2.9	1.4	4.5	0.7	25
Submatrix 1	16	25	2.7	1.6	4.3	0.6	23
Submatrix 2	16	25	3.4	2.6	4.0	0.5	14
Submatrix 3	16	25	3.0	1.4	4.5	0.9	28
Submatrix 4	16	25	2.6	1.6	3.9	0.5	20
Submatrix large	16	50	2.9	1.4	4.3	0.8	27

Table 9
Vertical-to-horizontal strength ratios (σ^v/σ^h) for different depths in Sites 2 and 3.

Depth (cm)	15/20	40/50	All
Assumed ice texture	Granular	Columnar	
Set 2	1.6	1.9	1.8
Set 3	1.2	1.6	1.4
Set 2 + Set 3	1.3	1.7	1.6

Neither the failure mode nor the brine volume seems to be an influencing factor for the vertical to horizontal strength ratio (see Figs. 12 and 13).

6. Conclusions

This paper examined the results of a field campaign that took place from early March to early May 2010 on a frozen fjord of Svalbard, Norway. The ice was sampled in 8 matrices of different sizes and spacings. The main conclusion is that the variability in uniaxial compression strength correlated with the variability in sample salinity and with the mean brine fraction, so that evenly distributed brine pockets (young sea ice) gave low strength variability. Both the variabilities in strength and the salinity decreased when the brine fraction increased above 0.05, but for a further increase in the mean brine fraction, only the salinity variability increased. Other conclusions are:

6.1. General comments

- The ice grew until late March, and the growth as predicted by Stefan's law with a coefficient $\omega = 0.40$ is in good agreement with our measurements and what Høyland (2009) reported;
- A flushing event could be observed with the variation of the salinity;
- The density was calculated for every compressed sample by systematically measuring the mass of each sample with a spring scale. This method is the most practical in the field, but can result in a great imprecision in the data, leading to wrong calculations of the air volume and the total porosity. Therefore no density values were presented in this paper;
- As expected, the uniaxial compressive strength of sea ice decreased with an increasing brine volume.
- The vertical-to-horizontal strength ratios were quite low compared to previous results, and this could potentially be due to a disturbance in the development of the S2 ice.

6.2. Spatial evolution

- The variability of the uniaxial compressive strength is related to the localization of the brine (pockets and channels) in the sea ice: the coefficient of variation is lower for a young ice that has many small brine pockets than for an older ice with bigger and fewer brine channels;
- The spatial variation of the strength also depends on the distance between the samples and the number of samples;

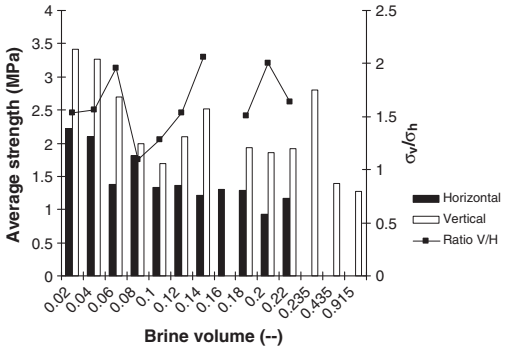

Fig. 12. Horizontal and vertical strengths as functions of the brine volume.

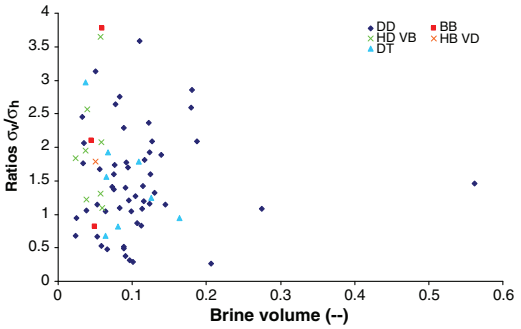

Fig. 13. Vertical-to-horizontal strength ratios as a function of the brine volume. *DD*: both vertical and horizontal samples; *BB*: both vertical and horizontal samples; *HD-VB*: ductile horizontal samples–brittle vertical samples; *HB-VD*: brittle horizontal samples–ductile vertical samples; *DT*: ductile and transitional samples.

6.3. Temporal evolution

- The air and the ice temperatures gradually increased with time. As the salinity was constant, the brine volume followed almost the exact same trend as that of the temperature;
- The uniaxial compressive strength decreased while its spatial variation increased as the season progressed (e.g. with increasing air temperature);
- The increase in the spatial variation of the strength with time suggests that the brine channels became more and more evenly distributed in the ice sheet. In other words, the strength became more variable because the brine pockets in the early season grew into brine channels and became more evenly distributed with the warming up of the ice.

Acknowledgments

The authors would like to thank Prof. Aleksey Marchenko and Prof. Sveinung Løset for their support and help in the field, Dr. Per Olav Moslet, Dr. Alex Klein-Paste and Dr Erland Schulson for their advice, Aleksey Shestov, Christian Lønøy, Serguiy Sukhorukov, Espen Særtre Østerås, Claire Chenot and the AT208 and AT307F students from UNIS for their help in the field. The financing help of the Norwegian National Research Council through the PetroArctic and the PetroRisk projects and DNV Research is also highly appreciated.

Appendix A. Supplementary data

Supplementary data to this article can be found online at doi:10.1016/j.coldregions.2011.10.001.

References

Cox, G.F.N., Weeks, W.F., 1983. Equations for determining the gas and brine volume in sea ice samples. Journal of Glaciology 29 (102), 306316.
Gabrielsen, M. (2007) Laboratory investigation of sea ice relaxation. Master thesis, The Norwegian University of Technology (NTNU) and The University Centre on Svalbard (UNIS).
Høyland, K.V., 2002. Consolidation of first-year sea ice ridges. Journal of Geophysical Research 107 (C6).
Høyland, K.V., 2007. Morphology and small-scale strength of ridges in the Northwestern Barents Sea. Cold Regions Science and Technology 48, 169–187.
Høyland, K.V., 2009. Ice thickness, growth and salinity in Van Mijenfjorden, Svalbard, Norway. Polar Research 28 (3), 339–352. doi:10.1111/j.1751-8369.2009.00133.x.
Kangas, T.V. (2000). Termohaline sesongvariasjoner i Van. Master thesis, University of Bergen (UiB) and The University Centre on Svalbard (UNIS).
Leppäranta, M., 1993. A review of analytical models of sea-ice growth. Atmosphere-Ocean 31 (1), 123–138.
Leppäranta, M., Manninen, T., 1988. The brine and gas content of sea ice with attention to low salinities and high temperatures. Finnish Institute of Marine Research: Internal Report, 2.

Løset, S., Shkhinek, K.N., Gudmestad, O.T., Høyland, K.V., 2006. Actions from ice on Arctic Offshore and Coastal Structures. Student's Book for Institutes of Higher Education. Publisher, "LAN", St Petersburg. 2006. 272 pp. ISBN S-8114-0703-3.

Marchenko, A.V., Morzov, E.G., Muzylev, S.V., Shestov, A.S., 2010. Interaction of short internal waves with the ice cover in an Arctic fjord. Oceanology 50 (1), 18–27 ISSN 0001-4370.

Marchenko, A., et al., 2011. Water-ice actions on the coal quay at Kapp Amsterdam in Svalbard. Proceedings of the 21st International Conference on Port and Ocean Engineering under Arctic Conditions. Montreal, Canada.

Moslet, P.O., 2007. Field testing of uniaxial compression test of columnar ice. Cold Regions Science and Technology 48, 1–14.

Onishchenko, D., 2009. Analytical approach to the calculation of the design values of the loads associated with the discrete ice features. Proceedings of the 20th International Conference on Port and Ocean Engineering (POAC). Luleå, Sweden (2009). paper # 126, 12 pages.

Petrich, C., Langhorne, P., Eicken, H., 2011. Modelled bulk salinity of growing first-year sea ice and implications for ice properties in spring. Proceedings of the 21st International Conference on Port and Ocean Engineering (POAC). Montreal, Canada (2011).

Sanderson, T.J.O., 1991. Statistical analysis of ice forces. Ice structure interaction. In: Jones, S.J.J., Mc Kenna, R.F., Tillotson, J., Jordaan, I.J. (Eds.), IUATM/IAHR Symposium St John's Newfoundland Canada 1989. Springer-Verlag, Berlin Heidelberg New York. ISBN: 3-540-52192-5.

Schulson, E., 1997. The brittle failure of ice under compression. The Journal of Physical Chemistry. B (101), 6254–6258.

Shafrova, S., Moslet, P.O., 2006a. In-situ uniaxial compression tests of the level ice. Part I: ice strength variability versus length scale. Proceedings of the 25th International Conference on Offshore Mechanics and Arctic Engineering (OMAE), Paper No. OMAE-92450.

Shafrova, S., Moslet, P.O., 2006b. In-situ uniaxial compression tests of the level ice. Part II: ice strength spatial distribution. Proceedings of the 25th International Conference on Offshore Mechanics and Arctic Engineering (OMAE), Paper No. OMAE-92451.

Shkhinek, K., et al., 2008. Causes and influence of the ice heterogeneity on loads on offshore structures. Proceedings of the ASME 27th International Conference on Offshore Mechanics and Arctic Engineering (OMAE). OMAE-2008-57736.

Strub-Klein, L., Høyland, K.V., 2011. One season of a first year sea ice ridge investigation — Winter 2009. Proceedings of the 21st International Conference on Port and Ocean Engineering (POAC). Montreal, Canada (2011).

Surkov, G.A., Truskov, P.A., 1993. Analysis of spatial heterogeneity of ultimate ice compressive strength. Proceedings of the 3rd International Offshore and Polar Engineering Conference (ISOPE), Singapore, pp. 596–599.

Takeuchi, T., et al., 2008. Randomness of strength on natural sea ice. Proceedings of the 19th International Symposium on Ice (IAHR), Vancouver, Canada, pp. 1185–1193.

Timco, G.W., Frederking, R.M.W., 1990. Compressive strength of sea ice sheets. Cold Regions Science and Technology 17, 227–240.

Timco, G.W., Frederking, R.M.W., 1996. A review of sea ice density. Cold Regions Science and Technology 24, 1–6.

Timco, G.W., Weeks, W.F., 2010. A review of the engineering properties of ice. Cold Regions Science and Technology 60, 107–129.

Weeks, W.F., 2010. On Sea Ice. University of Alaska Press, Fairbanks, Alaska ISBN: 978-1-60223-079-8.

Appendices

A.1 Temperature data

	# samples	Average (ºC)	Min (ºC)	Max (ºC)	St. dev. (ºC)	k_v (%)
week 9	16	-13.47	-20.30	-6.40	4.66	34.63
week 10	7	-9.22	-10.80	-7.00	0.98	10.65
week 11	16	-13.79	-21.70	-9.00	2.65	19.20
week 12 H	49	-7.31	-10.10	-5.50	0.91	12.44
week 12 V	7	-9.57	-11.90	-6.70	2.31	24.14
week 15H	10	-4.68	-5.80	-3.50	0.78	16.64
week 15 V	10	-4.54	-7.50	-3.10	1.43	31.45
week 16 H	22	-4.10	-5.70	-2.80	0.88	21.37
week 16 V	29	-4.40	-8.40	-2.10	1.38	31.43
week 18 H	63	-1.93	-5.80	-1.20	0.60	31.20
week 18 V	71	-1.81	-2.70	-0.50	0.46	25.48

A.2 Salinity data

	# samples	Average (psu)	Min (psu)	Max (psu)	St. dev. (psu)	k_v (%)
week 9	16	3.71	3.10	4.30	0.36	10
week 10	7	3.65	3.50	3.90	0.14	4
week 11	16	3.68	3.10	4.20	0.33	9
week 12 H	49	3.94	1.10	4.50	0.47	12
week 12 V	7	4.14	3.80	4.80	0.36	9
week 15H	10	4.20	3.84	4.70	0.30	7
week 15 V	10	4.43	4.02	5.07	0.29	7
week 16 H	22	3.47	1.10	5.40	0.91	26
week 16 V	29	3.48	1.90	4.40	0.59	17
week 18 H	63	3.81	0.50	7.60	1.43	37
week 18 V	71	3.96	1.10	8.30	1.46	37

A.3 Air volume data

	# samples	Average (--)	Min (--)	Max (--)	St. dev. (--)	k_v (%)
week 9	16	0.006	0	0.050	0.013	233
week 10	7	0.004	0	0.049	0.012	317
week 11	16	0.009	0	0.035	0.012	136
week 12 H	49	0.005	0	0.050	0.008	150
week 12 V	7	0.008	0	0.020	0.008	101
week 15H	10	0.000	0	0.000	0.000	--
week 15 V	10	0.000	0	0.000	0.000	--
week 16 H	22	0.002	0	0.037	0.008	469
week 16 V	29	0.000	0	0.014	0.003	538
week 18 H	63	0.011	0	0.086	0.018	169
week 18 V	71	0.016	0	0.081	0.025	155

A.4 Brine volume data

	# samples	Average (--)	Min (--)	Max (--)	St. dev. (--)	k_v (%)
week 9	16	0.017	0.012	0.025	0.004	25
week 10	7	0.022	0.019	0.027	0.002	11
week 11	16	0.016	0.013	0.022	0.002	13
week 12 H	49	0.028	0.008	0.037	0.004	15
week 12 V	7	0.025	0.019	0.030	0.004	17
week 15H	10	0.047	0.034	0.067	0.010	21
week 15 V	10	0.054	0.032	0.070	0.013	23
week 16 H	22	0.045	0.012	0.069	0.014	32
week 16 V	29	0.045	0.020	0.092	0.017	38
week 18 H	63	0.106	0.019	0.224	0.043	41
week 18 V	71	0.132	0.023	0.912	0.113	85

A.5 Porosity data

	# samples	Average (--)	Min (--)	Max (--)	St. dev. (--)	k_v (%)
week 9	16	0.023	0.012	0.062	0.012	53
week 10	7	0.026	0.019	0.070	0.012	45
week 11	16	0.025	0.013	0.051	0.013	51
week 12 H	49	0.034	0.009	0.077	0.009	28
week 12 V	7	0.032	0.021	0.044	0.008	26
week 15H	10	0.047	0.034	0.067	0.010	21
week 15 V	10	0.054	0.032	0.070	0.013	23
week 16 H	22	0.046	0.012	0.096	0.018	38
week 16 V	29	0.046	0.020	0.092	0.018	39
week 18 H	63	0.117	0.030	0.261	0.050	43
week 18 V	71	0.148	0.023	0.987	0.124	84

A.6 Strength data

A6.1 Week 9

σ (MPa)	T (°C)	S (psu)	η_a (--)	η_b (--)	η_t (--)	Sampling depth (cm)	FM	Orientation
2.9	-17.8	3.9	0	0.0143	0.0143	42	B	H
2.4	-18.6	3.6	0.0496	0.0121	0.0618	30	D	H
3.4	-17.6	3.3	0.0112	0.012	0.0232	17	D	H
3.4	-17.7	3.1	0	0.0117	0.0117	19	D	H
2.6	-10.5	3.8	0	0.0207	0.0207	27	D	H
3.5	-15.4	3.9	0	0.016	0.016	30	D	H
3.4	-20.3	4.3	0.0049	0.0143	0.0192	40	D	H
3.4	-19.6	4.2	0	0.0144	0.0144	30	D	H
3	-9.2	3.6	0.011	0.021	0.0321	30	D	H
2.5	-8.4	3.9	0	0.0255	0.0255	30	D	H
2.6	-8.4	3.3	0	0.0212	0.0212	19	D	H
3	-9.8	3.8	0	0.0216	0.0216	30	D	H
2.9	-13.6	--	--	--	--	30	D	H
3.4	-9.5	3.3	0.0031	0.019	0.022	17	D	H
2.2	-6.4	--	--	--	--	30	D	H
2.6	-12.7	3.9	0	0.0185	0.0185	30	D	H

FM: failure mode
B: brittle
D: ductile
T: transitional

H:horizontal
V: vertical

A6.2 Week 10

σ (MPa)	T (°C)	S (psu)	η_a (--)	η_b (--)	η_t (--)	Sampling depth (cm)	FM	Orientation
1.9	-8.2	3.9	0	0.0256	0.0256	41	D	H
3.2	-10	3.9	0	0.0217	0.0217	30	D	H
3	-10.2	3.5	0	0.0192	0.0192	30	D	H
2.2	-10.8	3.7	0.0036	0.0193	0.0228	30	D	H
2.7	-9.9	3.5	0	0.0198	0.0198	30	D	H
2.8	-9.1	3.6	0	0.0216	0.0216	30	D	H
1.9	-10.2	3.7	0.0036	0.0201	0.0237	30	D	H
2.8	-10.3	3.5	0	0.019	0.019	30	D	H
2.5	-9	3.5	0.0033	0.021	0.0243	30	D	H
2.2	-8.5	3.7	0	0.0234	0.0234	30	D	H
2.7	-9	3.8	0.0037	0.0228	0.0265	30	D	H
3.3	-9.6	3.5	0	0.0202	0.0202	30	D	H
3.8	-7	3.6	0	0.0271	0.0271	30	D	H
2.2	-8.5	3.8	0	0.0242	0.0242	17	D	H
2.4	-9.4	3.7	0.0492	0.0205	0.0696	30	D	H
2.2	-9.1	3.7	0	0.0222	0.0222	30	D	H
2.7	-8	3.5	0	0.0233	0.0233	30	D	H

FM: failure mode
B: brittle
D: ductile
T: transitional

H:horizontal
V: vertical

A6.3 Week 11

σ (MPa)	T (°C)	S (psu)	η_a (--)	η_b (--)	η_t (--)	Sampling depth (cm)	FM	Orientation
2.7	-13	3.6	0.0035	0.0163	0.0199	30	D	H
3.2	-13.2	3.7	0.0037	0.0166	0.0203	30	D	H
2.7	-14.6	3.1	0	0.013	0.013	30	D	H
2.9	-14.3	3.9	0	0.0169	0.0169	30	B	H
2.7	-13	3.7	0.0037	0.0168	0.0204	30	D	H
2.3	-13.6	3.6	0	0.0159	0.0159	30	D	H
2.3	-13	3.1	0.003	0.0141	0.017	30	D	H
2.8	-12.8	3.5	0	0.0162	0.0162	30	D	H
3	-12	3.6	0	0.0174	0.0174	30	D	H
3	-12.3	3.6	0.0339	0.0165	0.0504	30	D	H
2.8	-21.7	4.2	0.005	0.0133	0.0182	30	D	H
1.7	-15	4.2	0.0347	0.0167	0.0514	30	D	H
2.8	-14.5	3.5	0.0111	0.0146	0.0257	30	D	H
2.9	--	4.2	--	--	--	30	D	H
2.3	-9	3.7	0.0112	0.022	0.0332	30	D	H
2.3	-14.8	3.7	0.0266	0.015	0.0416	30	D	H

FM: failure mode
B: brittle
D: ductile
T: transitional

H:horizontal
V: vertical

A6.4 Week 12

σ (MPa)	T (°C)	S (psu)	η_a (--)	η_b (--)	η_t (--)	Sampling depth (cm)	FM	Orientation
4.3	-9.3	3.5	0	0.0211	0.0211	30	D	H
2.6	-6.8	4	0.0118	0.03	0.0418	30	D	H
2.5	-7.8	4	0.0116	0.0267	0.0384	40	D	H
1.6	-7	3.7	0.0114	0.0271	0.0384	40	D	H
1.9	-5.8	4	0.0045	0.0347	0.0391	40	D	H
2.3	-6.9	4.1	0	0.0308	0.0308	30	D	H
2.9	-7.3	3.8	0	0.0272	0.0272	30	D	H
2.2	-5.7	3.7	0.004	0.0326	0.0366	45	D	H
2.6	-7	4.3	0	0.0319	0.0319	30	D	H
2.3	-6.1	4.3	0.0048	0.0357	0.0405	45	D	H
2.6	-6.9	3.9	0.0497	0.0278	0.0774	30	D	H
2.5	-7.3	3.8	0.0114	0.0268	0.0383	30	D	H
2.4	-6.9	3.8	0	0.0288	0.0288	30	D	H
2.8	-6.8	4.3	0.0122	0.0322	0.0445	16	D	H
2.4	-6.7	1.1	0.0001	0.0084	0.0085	40	D	H
2.3	-6.4	3.9	0.0118	0.0308	0.0425	40	D	H
2.3	-6.6	3.8	0.004	0.0294	0.0334	42	D	H
2.3	-6.7	4	0	0.0308	0.0308	40	D	H
2.3	-5.5	4.1	0.0047	0.0373	0.042	42	D	H
2.9	-7	4.2	0.0044	0.0309	0.0354	30	D	H
2.8	-6.7	3.7	0.0114	0.0281	0.0395	30	D	H
2.2	-6.7	4.1	0.0044	0.0314	0.0357	30	D	H
2.3	-8.5	4	0.0116	0.0249	0.0365	30	D	H
2.2	-5.8	4	0.0045	0.0347	0.0391	43	D	H
2.7	-7.3	3.9	0.0192	0.0273	0.0465	17	D	H
2.6	-7.8	4.4	0.0122	0.0294	0.0416	30	D	H
3.9	-7	4	0.0042	0.0295	0.0336	30	D	H
3.3	-7.8	3.5	0.011	0.0234	0.0344	16	D	H
1.4	-7.1	3.8	0	0.0279	0.0279	30	D	H
1.9	-7.7	4.2	0.0119	0.0284	0.0403	30	D	H
3.6	-7.1	4.3	0.0046	0.0313	0.0359	30	D	H
2.7	-7	4.3	0	0.0322	0.0322	30	D	H
2.7	-8.1	4.2	0	0.0276	0.0276	30	D	H
4	-10.1	4	0	0.0222	0.0222	30	D	H
3.4	-7.4	3.8	0	0.0271	0.0271	30	D	H
4.5	-6.9	3.7	0	0.0278	0.0278	40	D	H
3.9	-8.4	4.1	0	0.0262	0.0262	30	D	H
3.4	-8	4	0	0.0266	0.0266	30	D	H
3.6	-8.6	4	0	0.0251	0.0251	30	D	H
3.7	-9	4.4	0	0.0266	0.0266	30	D	H
3.9	-8.2	3.8	0	0.0247	0.0247	30	D	H
3.7	-7.1	4.1	0	0.0301	0.0301	30	D	H
3.3	-7.5	4	0.0041	0.0278	0.0319	30	D	H
3.1	-7.4	4	0.0041	0.0281	0.0322	30	D	H
4	-7.7	3.7	0.0037	0.0252	0.0288	30	D	H
3.6	-8.1	4.2	0	0.0278	0.0278	30	D	H
3.5	-7.1	3.8	0.0039	0.0277	0.0315	30	D	H

3.5	-7.5	4.5	0.0048	0.0313	0.0361	30	D	H
3.7	-8.1	4.1	0.0041	0.0268	0.0309	30	D	H
8	-11.3	3.9	0.0114	0.0195	0.0309	35	B	V
6.2	-10.8	4.4	0	0.0236	0.0236	28	B	V
4.7	-11.9	4.2	0	0.0209	0.0209	35	B	V
5.5	-6.7	3.9	0.0117	0.0296	0.0413	30	B	V
3.3	-8	3.8	0.0114	0.0249	0.0362	29	B	V
4.8	-6.8	4	0	0.0304	0.0304	31	B	V
3.6	-11.5	4.8	0.0201	0.0235	0.0435	25	B	V

FM: failure mode
B: brittle
D: ductile
T: transitional

H:horizontal
V: vertical

A6.5 Week 15

σ (MPa)	T (°C)	S (psu)	η_a (--)	η_b (--)	η_t (--)	Sampling depth (cm)	FM	Orientation
3.7	-4.1	4.12	0	0.0509	0.0509	20	D	H
2.4	-3.8	3.94	0	0.0527	0.0527	50	D	H
1.3	-4.5	4.39	0	0.0497	0.0497	50	D	H
3.2	-5.4	3.97	0	0.0381	0.0381	20	D	H
1.8	-3.5	4.7	0	0.067	0.067	45	D	H
3.5	-5.3	4.02	0	0.0389	0.0389	30	D	H
1.3	-4.8	4.62	0	0.0491	0.0491	50	B	H
1	-5.8	3.84	0	0.0343	0.0343	45	D	H
1.6	-4.2	4.37	0	0.0527	0.0527	20	D	H
3.2	-5.4	4.03	0	0.0386	0.0386	50	B	H
2.6	-3.6	4.78	0	0.0673	0.0673	50	B	V
4.8	-3.5	4.34	0	0.0637	0.0637	50	B	V
4.6	-3.5	4.22	0	0.061	0.061	50	B	V
5.7	-7.5	4.29	0	0.0321	0.0321	50	B	V
4.4	-4.4	4.46	0	0.0515	0.0515	20	B	V
2.4	-4.7	4.41	0	0.0476	0.0476	50	B	V
2.8	-5.2	4.02	0	0.0408	0.0408	50	B	V
2.6	-6.3	5.07	0	0.0446	0.0446	50	B	V
2.6	-3.6	4.36	0	0.0609	0.0609	50	B	V
2.5	-3.1	4.36	0	0.07	0.07	45	B	V

FM: failure mode
B: brittle
D: ductile
T: transitional

H:horizontal
V: vertical

A6.6 Week 16

σ (MPa)	T (°C)	S (psu)	η_a (--)	η_b (--)	η_t (--)	Sampling depth (cm)	FM	Orientation
2.2	-3.2	3.2	0	0.0498	0.0498	30	B	H
0.9	-3.1	3.9	0.0368	0.0589	0.0956	50	D	H
1.9	-3.8	3.1	0	0.0411	0.0411	20	D	H
2.1	-2.8	3.1	0	0.055	0.055	35	D	H
2.1	-4.8	4.1	0	0.0437	0.0437	20	D	H
1.2	-3.6	4.2	0	0.0583	0.0583	35	D	H
2	-4	4.07	0	0.0511	0.0511	20	D	H
1.1	-3.1	3.2	0	0.0517	0.0517	50	D	H
2.4	-4.9	3.2	0	0.0342	0.0342	25	D	H
1.7	-4.3	2	0	0.0236	0.0236	35	D	H
3.3	-5.1	2.9	0	0.0293	0.0293	10	D	H
2.7	-4.5	3.9	0	0.0441	0.0441	20	D	H
1.6	-3.1	3.5	0	0.0562	0.0562	50	D	H
2.4	-5.2	3.1	0	0.0307	0.0307	20	D	H
1.2	-4	4.4	0	0.0564	0.0564	50	T	H
2.5	-5.2	4.2	0	0.0417	0.0417	20	D	H
0.8	-3.1	4.3	0	0.069	0.069	50	B	H
2.8	-4.9	2.5	0	0.0264	0.0264	20	D	H
0.9	-3.2	3.9	0	0.0616	0.0616	50	D	H
3.3	-4.8	1.1	0	0.0117	0.0117	20	D	H
2.3	-3.9	3	0	0.0391	0.0391	42	D	H
1.9	-5.7	5.4	0	0.049	0.049	20	D	H
3.9	-3.6	3.6	0	0.0503	0.0503	30	D	V
1.5	-2.1	3.7	0	0.0916	0.0916	50	D	V
1.3	-3.1	4.1	0	0.0634	0.0778	20	D	V
1.1	-2.9	3.5	0	0.0609	0.0609	50	D	V
1.8	-3.5	3.7	0	0.0531	0.0531	20	D	V
1.7	-3.6	3.9	0	0.0565	0.0565	50	D	V
2.4	-3.5	4.1	0	0.061	0.061	20	D	V
1.9	-2.7	3.9	0	0.0745	0.0745	50	T	V
2.4	-2.9	4.2	0	0.0752	0.0752	35	T	V
2.5	-4	3	0	0.0393	0.0393	12	D	V
1.9	-4.1	3.2	0	0.0395	0.0395	50	D	V
4.2	-5	3.2	0	0.0326	0.0326	28	D	V
3.1	-8.4	3.5	0	0.0239	0.0239	50	B	V
3.1	-4.9	1.9	0	0.0197	0.0197	23	D	V
2.3	-4	3.6	0	0.0462	0.0462	50	B	V
5.3	-5.1	2.9	0	0.0293	0.0293	20	B	V
3.2	-3.5	4.1	0	0.061	0.061	54	B	V
5.8	-6.2	3.9	0	0.0333	0.0333	17	D	V
4.2	-5.7	3	0	0.0278	0.0278	46	B	V
7.3	-6.1	3.6	0	0.0321	0.0321	25	T	V
2.9	-4.7	4.4	0	0.0489	0.0489	50	B	V
4.1	-6.6	4.1	0	0.0332	0.0332	14	D	V
5	-5.6	3.7	0	0.0354	0.0354	50	B	V
3.4	-3.1	3	0	0.0492	0.0492	23	B	V
2.7	-3.8	2.9	0	0.0385	0.0385	50	D	V

2.2	-5.2	3.6	0	0.0362	0.0362	27	D	V
1.6	-4	3.2	0	0.0419	0.0419	50	B	V
3.8	-5.3	2.1	0	0.0206	0.0206	15	D	V
2.4	-4.3	3.2	0	0.0381	0.0381	50	D	V

FM: failure mode
B: brittle
D: ductile
T: transitional

H:horizontal
V: vertical

A6.7 Week 18

σ (MPa)	T (°C)	S (psu)	η_a (--)	η_b (--)	η_t (--)	Sampling depth (cm)	FM	Orientation
2.1	-2.1	3.19	0	0.0761	0.0761	40	D	H
1	-3.1	7	0	0.1132	0.1132	15	D	H
1.3	-1.8	2.2	0	0.0628	0.0628	40	D	H
1.9	-1.8	3.7	0	0.1072	0.1072	15	D	H
1.5	-1.8	2.2	0	0.0619	0.0619	35	D	H
1.5	-2.5	4.9	0	0.0976	0.0976	15	D	H
1.3	-1.9	4	0	0.1101	0.1101	40	D	H
2.5	-2.1	3.4	0	0.0824	0.0824	15	D	H
1.2	-1.6	6.7	0	0.224	0.224	40	D	H
1.5	-1.7	3.41	0	0.1036	0.1036	15	D	H
1.1	-1.8	4.09	0	0.1193	0.1193	5	D	H
1.3	-1.8	5.36	0	0.1564	0.1564	35	D	H
0.7	-2.1	2.37	0	0.057	0.057	15	D	H
1.6	-1.9	3.8	0	0.1024	0.1024	30	D	H
2.1	-1.6	2.7	0	0.0884	0.0884	40	D	H
0.9	-1.9	2.8	0	0.0754	0.0754	15	D	H
0.9	-1.7	7.07	0	0.2117	0.2117	15	D	H
1.1	-2.6	4.7	0	0.0933	0.0933	40	D	H
1.2	-1.6		--			40	D	H
1.4	-2.1	4.1	0	0.1015	0.1015	15	D	H
1.5	-1.5	3.5	0	0.1231	0.1231	15	D	H
1.5	-1.7	3.1	0	0.0928	0.0928	25	D	H
1.1	-1.6	3.4	0	0.1145	0.1145	40	D	H
1.1	-1.5	3.8	0	0.1356	0.1356	15	D	H
1.3	-1.7	2.3	0	0.0689	0.0689	40	D	H
0.9	-2.1	3.4	0.0076	0.0787	0.0863	15	T	H
1.7	-2	3.4	0	0.0873	0.0873	30	D	H
1.6	-2.1	3.5	0	0.0866	0.0866	15	D	H
0.9	-2	3.71	0	0.0953	0.0953	40	D	H
1.1	-2.2	4.3	0	0.0977	0.0977	15	D	H
0.9	-1.9	7.48	0	0.2059	0.2059	40	D	H
1.8	-2	--	--	--	--	15	D	H
1.1	-1.8	--	--	--	--	40	D	H
2.7	-1.9	1.9	0	0.0512	0.0512	40	D	H
1.4	-2	2.9	0	0.0734	0.0734	15	D	H
0.6	-1.4	2.7	0.0087	0.0974	0.1061	40	D	H
2.3	-1.8	2.6	0	0.0742	0.0742	15	T	H
1.9	-2	1.3	0.0093	0.0315	0.0408	15	D	H
0.4	-2.4	5.9	0.0131	0.1189	0.1321	15	D	H

1	-1.8	3.8	0	0.1109	0.1109	40	D	H
0.4	-2.2	4.2	0.0548	0.0884	0.1432	15	D	H
1.3	-5.8	3.2	0	0.0296	0.0296	40	D	H
0.9	-2.7	3.2	0	0.0576	0.0576	22	D	V
2.6	-2.1	3.7	0	0.0909	0.0909	46	D	V
1.7	-2.5	--	--	--		15	D	V
1	-2.3	3.3	0	0.0706	0.0706	11	D	V
1	-1.7	2.3	0	0.0694	0.0694	34	D	V
0.7	-1.9	3.22	0.0457	0.0798	0.1255	12.5	D	V
2.5	-1.7	4.6	0	0.1377	0.1377	39	D	V
0.9	-2.6	5.03	0	0.0991	0.0991	15	D	V
3.8	-2.2	5.7	0	0.1363	0.1363	40	D	V
0.9	-2.3	4.94	0.0337	0.1017	0.1354	9.5	T	V
1.8	-1.8	3.64	0	0.1039	0.1039	19.5	D	V
0.6	-2.5	6	0.0356	0.1133	0.1489	11	D	V
1.5	-1.6	3.2	0	0.104	0.104	36	D	V
1.5	-1.6	3.7	0	0.1193	0.1193	11	D	V
2.4	-1.3	3.17	0	0.1303	0.1303	35	D	V
1.9	-2	7.63	0	0.2017	0.2017	31	D	V
1.9	-1.7	4	0	0.1251	0.1251	27.5	D	V
1.3	-0.5	5.8	0.0026	0.9124	0.915	12	D	V
2.1	-2	3.84	0	0.1037	0.1037	38	D	V
0.4	-1.4	2.9	0.0398	0.1015	0.1412	11	D	V
2.6	-1.7	3.9	0	0.122	0.122	36	D	V
1.6	-1.4	2.7	0	0.1041	0.1041	13	D	V
2.1	-1.7	3.7	0	0.1133	0.1133	11	D	V
1	-1.9	4.3	0.0187	0.1099	0.1286	35	D	V
1.3	-1.7	3.2	0	0.0972	0.0972	36.5	D	V
0.6	-2.5	2.6	0.012	0.0499	0.0619	10	D	V
2.2	-2	3.8	0	0.1005	0.1005	31	D	V
1.4	-2.1		--			27	D	V
0.5			--			35	D	V
2.2	-2.1		0	0.0958	0.0958	12	D	V
1.3	-2.1	3.9	0	0.0727	0.0727	37.5	D	V
1.2	-1.9	2.8	0	0.0838	0.0838	14	D	V
2.8	-1.9	3	0	0.057	0.057	35	D	V
1.9	-1.9	2	0	0.0866	0.0866	15	D	V
3.2	-2	3.3	0	0.0799	0.0799	15	D	V
0.7	-2.1	3.4	0.0365	0.0651	0.1016	13	D	V
0.6	-2.1	2.9	0.0582	0.0651	0.1233	15	D	V
1.7	-1.7	4.2	0	0.1258	0.1258	72	D	H
0.8	-1.7	4.9	0	0.1467	0.1467	40	D	H
1.9	-1.9	7.6	0	0.2077	0.2077	15	D	H
1.8	-1.2	3.3	0	0.1467	0.1467	15	D	H
1.3	-1.2	4	0	0.1805	0.1805	40	D	H
1.3	-1.7	3.7	0	0.1149	0.1149	40	D	H
1.3	-1.6	5	0	0.1601	0.1601	15	D	H
1.4	-1.9	4.6	0	0.131	0.131	40	D	H
2	-1.5	3.3	0	0.1219	0.1219	40	D	H
0.9	-1.8	1.5	0	0.0428	0.0428	15	D	H

1.7	-2.3	4.75	0	0.1039	0.1039	30	D	H
1	-1.3	0.5	0.0075	0.0195	0.027	15	D	H
1.7	--	2.8	--	--	--	40	D	H
1.3	-2.3	3.1	0.0061	0.0653	0.0714	15	T	H
1.4	-1.85	3.2	0	0.0907	0.0907	53	D	H
1.7	-1.5	3.6	0	0.1248	0.1248	15	D	H
1.7	--	--	--	--	--	40	D	H
0.7	-1.8	4.1	0	0.1179	0.1179	15	D	H
1.3	-1.8	3.5	0	0.1014	0.1014	40	D	H
0.9	-2.3	4.8	0.0182	0.1003	0.1186	15	T	H
1.3	-1.6	4.5	0	0.1419	0.1419	40	D	H
3	-1.3	3.8	0	0.1619	0.1619	39	D	V
2.2	-1.8	3.1	0	0.0937	0.0937	62	D	V
2	-1.9	3.8	0	0.0994	0.0994	41	D	V
1.5	-1.3	2.8	0	0.1134	0.1134	63	D	V
1.3	-1.9	3.7	0	0.1055	0.1055	29	D	V
0.9	-1.1	2.6	0	0.1273	0.1273	52	D	V
2.1	-1.1	4.2	0	0.2164	0.2164	75	D	V
1.3	-2	4.6	0	0.1216	0.1216	24	D	V
2.3	-1.2	3.1	0	0.1409	0.1409	45	D	V
1.7	-1	3.2	0	0.18	0.18	25	T	V
1.9	-1.3	4.2	0	0.1776	0.1776	46	D	V
0.8	-2	6.9	0	0.1747	0.1747	15	D	V
1.4	-0.8	5.8	0	0.4348	0.4348	35	D	V
2.4	-2.6	6.3	0.0058	0.1179	0.1236	15	D	V
1.3	-2.4	2.6	0	0.0556	0.0556	66	D	V
0.8	-1.5	4	0	0.1407	0.1407	10	D	V
2.5	-1.6	3.5	0	0.1154	0.1154	40	D	V
2	-1.2	3.9	0	0.1734	0.1734	12	D	V
1.7	-1.3	2.7	0	0.1101	0.1101	35	D	V
2.4	-1.3	3.2	0	0.1334	0.1334	58	T	V
1.9	-1.6	6.8	0.0222	0.2112	0.2335	12.5	D	V
2.1	-2.4	1.1	0	0.023	0.023	37.5	D	V
3.1	-1.7	2.5	0	0.0771	0.0771	52.5	T	V
1.4	-1.8	4.6	0	0.1304	0.1304	26	D	V
3.1	-2.1	4.4	0	0.1089	0.1089	50	T	V
0.9	-2.1	8.3	0	0.2025	0.2025	40	D	V
1.4	-2.3	5.6	0	0.1224	0.1224	62.5	D	V
0.5	-2.1	2.8	0	0.0683	0.0683	15	D	V
1.1	-1.1	2.4	0.0403	0.1114	0.1517	14	D	V
1.9	-1.7	2.6	0	0.0807	0.0807	38	D	V
1.2	-2	5.6	0	0.1512	0.1512	26	D	V
2	-2.4	3.6	0	0.0786	0.0786	46	D	V
2.2	-1.3	3.08	0	0.1275	0.1275	70	D	V
2.8	-1.8	8.25	0	0.2321	0.2321	40	D	V

FM: failure mode
B: brittle
D: ductile
T: transitional

H:horizontal
V: vertical

3.3 A statistical analysis for level ice strength

Is not included due to copyright

3.4 An experimental set-up for measuring stress propagation in sea ice

POAC 09
Luleå, Sweden
POAC09-16

Proceedings of the 20th International Conference on
Port and Ocean Engineering under Arctic Conditions
June 9-12, 2009
Luleå, Sweden

AN EXPERIMENTAL SET-UP FOR MEASURING STRESS PROPAGATION IN SEA ICE

Sébastien Barrault and Lucie Strub-Klein

University Centre in Svalbard (UNIS), Longyearbyen, Norway

Norwegian University of Science and Technology (NTNU), Trondheim, Norway

ABSTRACT

An experimental set-up has been tested in the Barents Sea in May 2008 to measure the propagation of stresses in the ice. Six stress sensors frozen in ridged ice at the depth of 20 cm and every 0.6 m in a row and parallel to each other recorded stresses triggered by a borehole jack placed at different locations. Tests were performed at 8, 5, 2, 1 and 0.6 m from the first sensor. The maximal strength generated by the borehole jack was up to 18.8 MPa and data shows the pressure dropped by 98% the first 0.6 m. The horizontal stresses propagated inversely proportional with distance and vanished after approximately 4 m.

INTRODUCTION

Since oil and gas industries have been showing a great interest in the Arctic regions, the need of understanding sea ice behaviour is a constant engineering challenge. Several investigations analysed the ice cover deformation due to swell and waves. Dynamical response on fast ice boundary using strain gauges was studied by Squire and Allan (1980) for instance. On the other hand, ice pressures have been surveyed and measured in many ways but little information is known about stress propagation in the ice cover.

The University Centre in Svalbard (UNIS) and the Norwegian University of Science and Technology (NTNU) acquired a borehole jack (BHJ) for determining in-situ the confined compressive strength of the ice. Significant contributions in that area were previously made by several authors both by measuring ice strength and by interpreting the measurement tests (Gold (1992), Masterson (1996), Johnston and Ferderking (2001), Timco and Johnston (2002), Shina (2005)).

The data presented here provide information about how stresses introduced by the borehole jack influence the surrounding ice. In-ice pressure sensors were used to detect the stress field up to four meters from where the borehole jack tests were conducted. This paper focuses on the experimental set-up and presents first results.

SITE AND EXPERIMENTAL SET-UP

The tests were performed during the annual UNIS cruise on R/V Lance in the Barents Sea. The sea ice station was located at 77°84'N and 28°26'E in early May 2008 (Figure 1a). The floe was about 40 m x 50 m, with a crossing ridge in the middle. Three transect measurements of the ridge done with a 2" drill (black dots in Figure 1b) depicted both dimensions of the keel and the sail. The keel varied between 4.6 to 11.27 m and the sail reached up to 4 m at some locations. For the following experiment, the most levelled part of the floe was chosen (along the white dots in Figure 1b). The snow thickness was about 0.2 m.

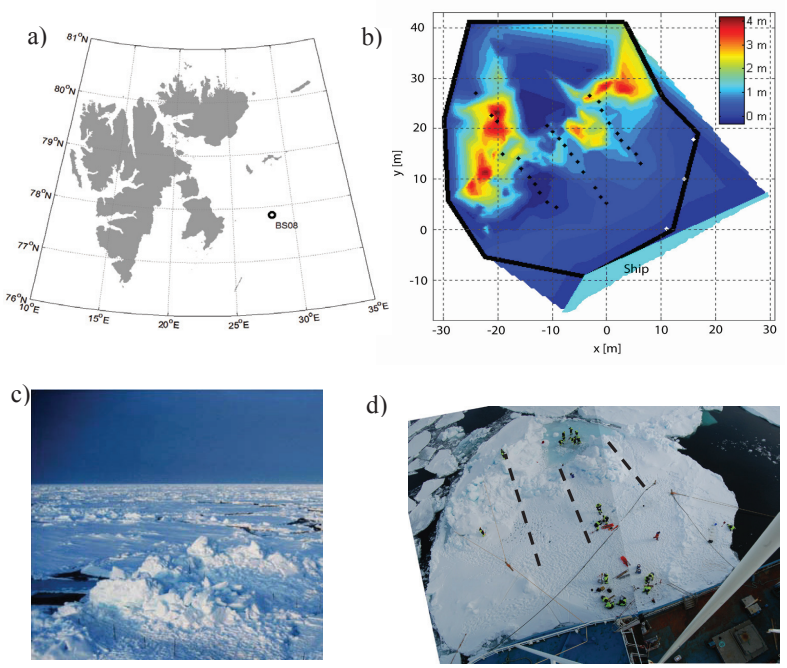

Figure 1. a) Location of R/V Lance in the drifting ice station in the Barents Sea in May 2008 (BS08) ; b) The ridge sail was reconstructed after topographic measurements with a theodolite. The black points show the positions of the drilling transects; c) ridge with drilling transects (bamboo sticks); d) top view of the floe with the 3 transects (dash lines) and the set-up site (solid line on the right side of the floe)

On May 8th, six Amplified Solid State Pressure Sensors 242PC100G were frozen in the ice in a row, parallel and distant of 0.6 m from each other (Figure 2). The sensors were placed at 20 cm from the ice surface and slightly laterally shifted from each other. To expedite the freezing process, the pressure sensors were frozen into the ice with freshwater, rather than seawater. On May 10th, after 40 hours at air temperature below zero (-3.6°C in average over that period), the instruments were well immobilized (the good contact with the sensors with the surrounding ice was confirmed when they were recovered after completion of the experiment). These sensors consisted of a disc of 10.5 cm in diameter filled with hydraulic oil and a transducer head

measuring the voltage difference. The instruments were calibrated in laboratory before the field campaign. They read compressive stresses with a resolution of ± 0.1 kPa.

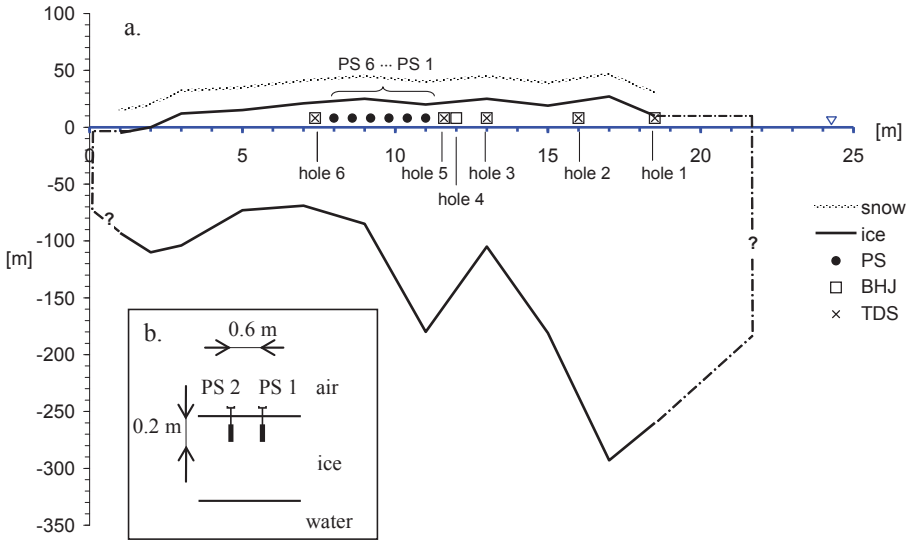

Figure 2: a) Floe profile with instruments set-up: six pressure sensors (PS), six tests performed with a borehole jack (BHJ) in six holes. Five measurements of temperature, density and salinity (TDS) were done along the testing line; b) Detailed close-up of two pressure sensors set-up. Note that the ice floe horizontal dimensions are correct. However no information is given for the keel shape at the edges of the floe.

The use of a Sandwell borehole jack (2007) was necessary to trigger the initial in-situ pressure. The unidirectional piston was hydraulically actuated and had a maximum opening of 25 mm. The tool fitted into a 150 mm diameter borehole. For operating the jack, an electric ENERPAC PUJ1400E pump was coupled to it. The model used was a double acting cylinder with advance, retract and neutral position. The maximum operating pressure of this model was 70 MPa. The output flow rate was 3.2 litre/min at first stage and reached 0.32 litre/min at maximal pressure.
The indenter of the borehole jack extended horizontally into the ice, perpendicular to the in-ice pressure sensors (Figure 3). Two synchronized CR1000 Campbell Scientific loggers recorded independently the data from the in-ice pressure sensors (PS, stress) and the borehole jack (BHJ, oil pressure and displacement). Note that from now the pressure read by the BHJ is reported in the text as ice pressure and no longer as oil pressure. The sampling rate of both loggers was 2 Hz.

A 30 to 40 cm long ice core was first taken out at 5 of the 6 locations and used for measuring temperature, density and salinity (see TDS in Figure 2a). The density was calculated from the dimensions of the core sample and the mass. The salinity was determined by melting the sample and by measuring the water conductivity.

Table 1: Distances given in [m] between BHJ and the pressure sensors. BHJ tests were performed at the depth of 20 cm. In addition temperature, density and salinity measurements are mentioned when they were done before the test

		Distance from hole (BHJ) to sensor					
	TDS	PS 1	PS 2	PS 3	PS 4	PS 5	PS 6
Hole 1	x	8.0	8.6	9.2	9.8	10.4	11.0
Hole 2	x	5.0	5.6	6.2	6.8	7.4	8.0
Hole 3	x	2.0	2.6	3.2	3.8	4.4	5.0
Hole 4	-	1.0	1.6	2.2	2.8	3.4	4.0
Hole 5[a]	x	0.6	1.2	1.8	2.4	3.0	3.6
Hole 6[a]	x	3.6	3.0	2.4	1.8	1.2	0.6

[a] tested at 25 cm

The borehole jack was then lowered down into the 150 mm diameter hole to the same depth as the sensors (20 cm). Six borehole jack tests were performed at 6 locations distant from 8.0 to 0.6 m distant from the sensors (see Table 1). During Test 1 for example, the BHJ was placed in hole 1 at 8.0 m distant from the first sensor (PS 1), 8.6 m distant from the second one (PS 2), 9.2 m distant from the third one (PS 3), etc. For Test 5 and 6, the BHJ was lowered to a depth of 25 cm.

Figure 3 : Left: The distance of first test (hole 1 at 8.0 m distant from PS1) was near by the walrus. Middle: The borehole jack was lowered down in hole 4 with the indenter directed to the sensors. Right: borehole jack after the test. Some cracks are visible on the surface

RESULTS

Temperature, density and salinity profiles down to the first 35 cm are plotted in Figure 4. If temperature gradient showed the same general trend, density and salinity revealed more scattered patterns. Table 2 focuses at the depth of the operating instruments. Temperatures are warmer in

holes 5 and 6. The salinity was more even along the testing line and its average value was 4.2 psu. Ice was less dense in holes 1 and 2. Porosity, computed from relations given in Cox and Weeks (1983), showed that air fraction was significant in those two holes, i.e. about half of the total porosity. However calculations enlightened that the presence of brine was clearly dominant in holes 3, 5 and 6.

Table 2 :. Summary of some of the physical and mechanical properties measured in ice covering the depth where the instruments were placed: T, temperature, S, salinity, ρ, density, η_{air}, air fraction, η_{brine}, brine fraction, η_{total}, the sum of the air and brine fraction, σ_{BHJ}, the maximal pressure of the BHJ and $\dot{u}_{BHJ}$, the displacement rate of the BHJ

hole	depth [cm]	T [°C]	S [psu]	ρ [g/cm^3]	η_{air} [-]	η_{brine} [-]	η_{total} [-]	σ_{BHJ} [MPa]	$\dot{u}_{BHJ}$ [mm/s]
hole 1	10	-3.7	5.4	0.8179	0.1179	0.0630	0.1809	9.72[a]	0.81[a]
	18	-3.6	4.1	0.8513	0.0795	0.0511	0.1306		
	22	-3.7	4.1	0.8513	0.0794	0.0498	0.1292		
hole 2	13	-3.3	4.4	0.8547	0.0769	0.0599	0.1368	12.69[a]	0.64[a]
	18	-3.0	4.2	0.8732	0.0570	0.0642	0.1212		
	23	-3.9	4.0	0.8818	0.0460	0.0478	0.0938		
hole 3	10	-3.2	4.0	0.9337	0	0.0613	0.0613	8.08[a]	0.87[a]
	20	-3.3	4.2	0.9058	0.0213	0.0606	0.0819		
	25	-3.5	4.2	0.9058	0.0210	0.0572	0.0782		
hole 4	20	-	-	-	-	-	-	14.08[a]	0.83[a]
hole 5	11	-2.6	-	0.9262	-	-	-	18.88[b]	0.71[b]
	16	-2.9	3.8	0.9266	0	0.0637	0.0637		
	21	-3.0	4.2	0.9237	0.0035	0.0678	0.0713		
	26	-3.1	4.0	0.9359	0	0.0634	0.0634		
hole 6	10	-1.8	4.6	0.9175	0.0145	0.1251	0.1396	16.17[b]	0.78[b]
	15	-2.4	4.5	-	-	-	-		
	20	-2.7	4.0	-	-	-	-		
	25	-2.8	-	-	-	-	-		

[a] tested at 20 cm; [b] tested at 25 cm

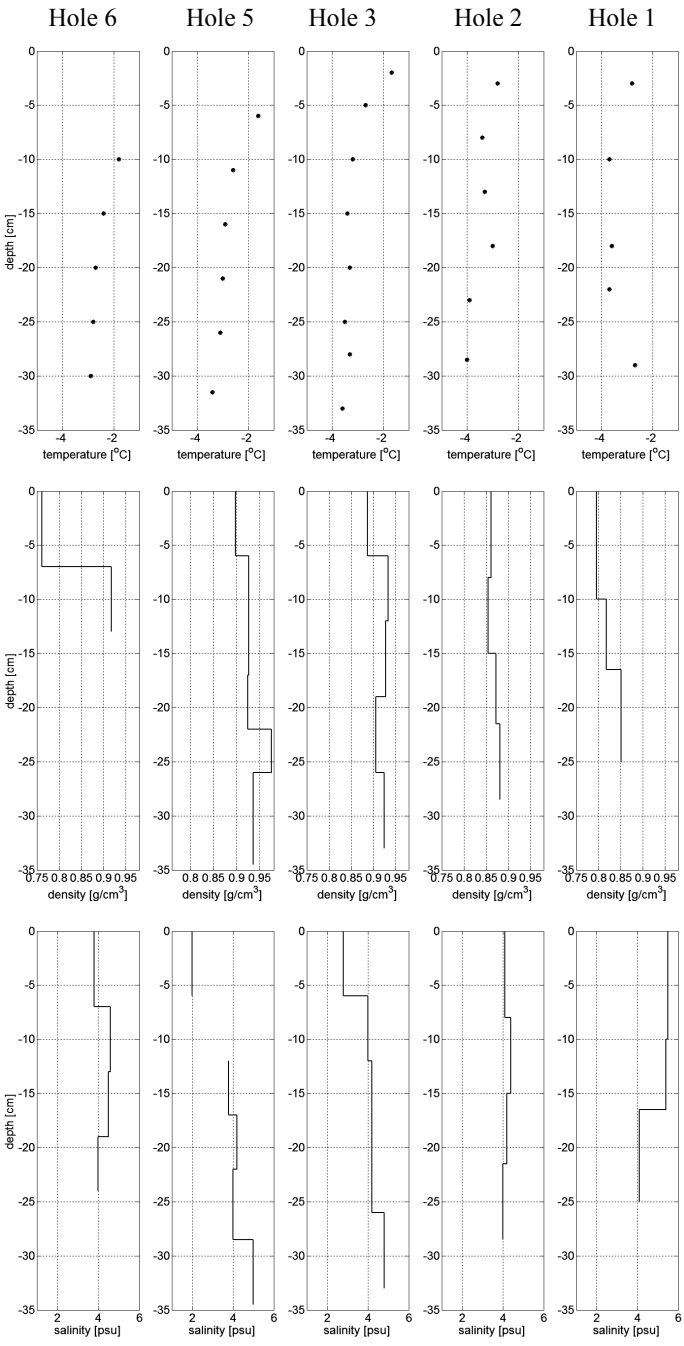

Figure 4: Temperature, density and salinity (TDS) resulted from measurements done from the core extracted

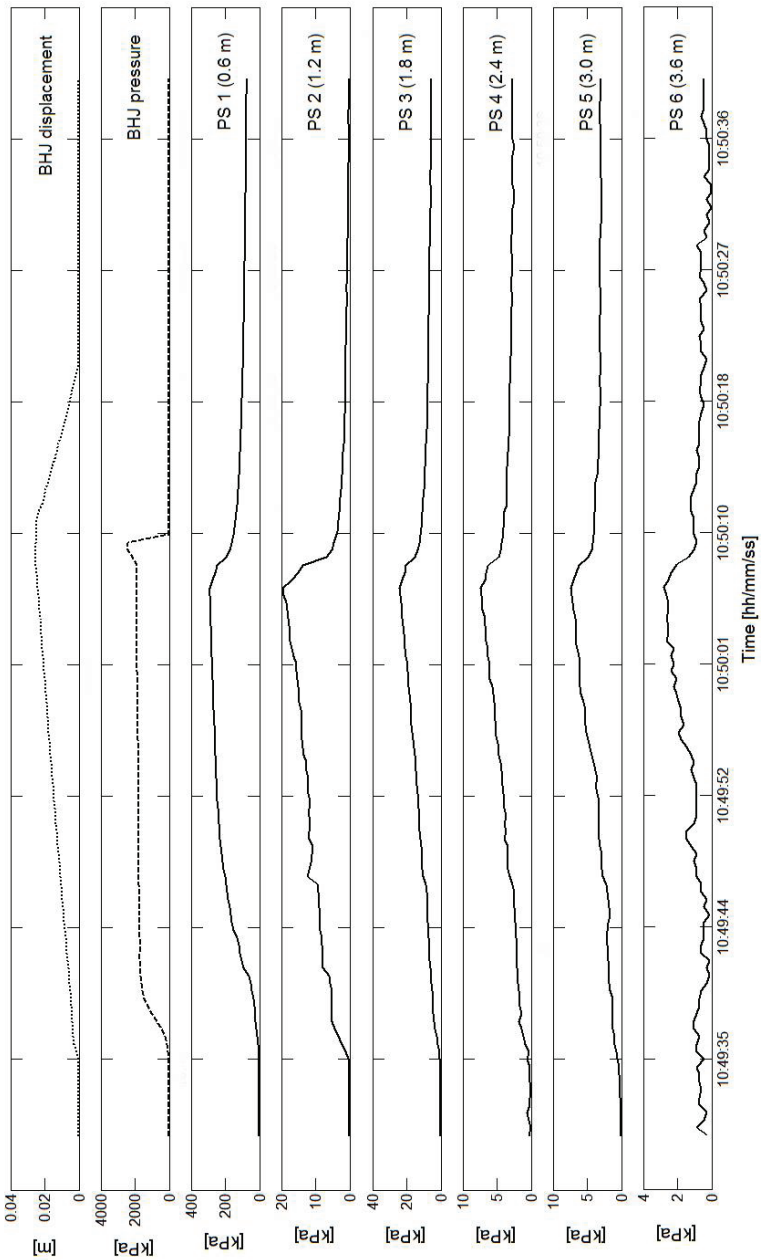

Figure 5 : Test in hole 5 with BHJ positioned at 0.6 m from the first sensor PS 1. Note the different scales on the pressure-axis

The maximal pressure, σ_{BHJ}, showed wide variability along the tested line: it varied with a factor from one to two according to the location. The average displacement rate, $\dot{u}_{BHJ}$, had range from 0.64 to 0.81 mm/s. The typical borehole jack tests were completed in less than 35 seconds. The rapidity of deformation of ice involved cracks in the direction of the indenter and up to the surface (Figure 3).

An example of the stress responses from the BHJ testing in hole 5 is presented in Figure 5. The abnormal pressure of the BHJ occurring at the end of test is due to the oil overpressure when the piston reached the full opening. It shall not be mistaken as the actual ice pressure. The maximum opening of the piston was 25 mm and for the current experiment, the pressure was not considered when it went over 24 mm.

The flow rate of the BHJ pump controlled the piston and was rather linear. The confined compressive ice strength measured by the BHJ (Figure 5) showed a quick increase over the first seconds of the test. Then the pressure stayed constant around 18 MPa. The pressure sensors reached their maximum stress before the BHJ "over-pressurized".

The response of the pressure sensors did not follow strictly the BHJ pressure pattern. In the other hand, the response was immediate at the beginning of the test. The sensors reacted in a synchronised way when the load was applied and when the ice yielded. The maximal pressure was read at the same time for all sensors.

The maximal stress read by PS1 reached 2% of the BHJ maximal pressure, indicating that the stress response decreased by 98% within the first 0.6 m. There was no stress recorded by the in-ice pressure sensors for borehole jack tests conducted in 8.0 m and 5.0 m distant: stresses induced by the borehole jack vanished around 4 meters.

DISCUSSION

The physical properties alone can not explain the variability of the maximal pressures measured by the BHJ. Holes 3 and 5, for instance, where it has been measured the lowest and the highest pressure, have indeed comparable porosity and density. However the latter point is subject to discussion since brine drainage occurred when taking out the ice core. Temperature difference may be an important factor as existing internal cracks or dislocation leading to local cracking process during the indentation test. But more significantly is the ice feature itself. The tests were conducted in ridged ice, highly deformed. Therefore the variability in ice structure may be major.

Values of the BHJ and PS maximal pressure at four locations (holes 3 to 6) are presented in Figure 6. The higher pressure from the BHJ was recorded, the higher the stress response was.

A power fit of four tests respectively done in holes 3 to 6 was calculated so that the stress decay was expressed as

$$\sigma = \frac{A}{r^{\lambda}} \qquad (1)$$

where r is the distance in [m], λ the power of the distance and A is an empirical constant expressed in [kPam$^{\lambda}$]. It was found that $\lambda = 2.76$ and $A = 67.5$.

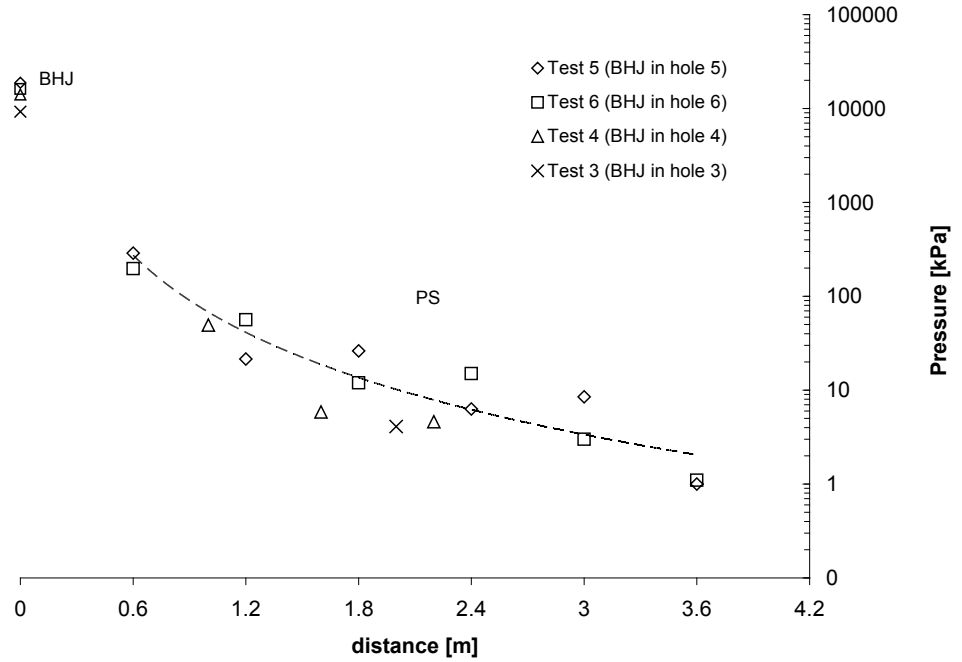

Figure 6. Maximal stresses read by the sensors corresponding to maximal pressure of BHJ for 4 tests respectively done in holes 3 to 6. The dashed line gives the best fit given in Equation 1.

Beside the main results, this experiment gave a good opportunity to estimate quantitatively one "side effect" of the borehole jack on the surrounding ice. The borehole jack affects ice significantly on the local scale. The present experiment recorded stresses up to 4 m distant from where the borehole jack tests were conducted. The influence was very strong within the first meters from the borehole jack. It is however not clear yet how far the ice was subject to plastic deformation.
The empirical data confirms that the borehole jack tests are to be conducted in holes made several meters apart.

CONCLUSION AND PERSPECTIVE

In early May 2008, six pressure sensors and a borehole jack were combined to quantify the stress propagation in ridged ice. An unidirectional load was applied in-situ and the stress response was recorded with distance. The results led to a main observation. The stresses travelled in the ice up to 4 meters, decreasing exponentially with radial distance from the source of stress (borehole jack). The decrease was considerable: 98% of the stress was dissipated within the first 0.6 m.
Penetration velocity, ice feature size and structure and ice temperature count as main factors in ice action. In that respect comparable experiments may be performed in colder, thinner, more

homogenous ice (level ice). If the data may be compared at different indenter speeds, it should also be compared for different depths (in granular and columnar ice).
The present experiment focused on the stress propagated along one axis. It did not give any information around the bulb generated by the indenter. In further work, sensors deployed with different angles and at different depths could give a 3D picture of the impact of the bulb on the surrounding ice. This will lead to further specific recommendations after finding out empirically how much damage the tests do induce, how does it affect successive tests in the same hole, what is the minimum vertical distance between two tests in the same hole.
The information about the deformation may be improved by additional strain gauges in order to depict the elastic/plastic deformation. In addition, the recording frequency of the loggers may be increase as well.

AKNOWLEDGEMENTS

The authors express their gratitude to MSc student Ole-Christian Ekeberg for his relevant help with both software and BHJ, the students from AT-208 at UNIS in particular Christopher Borsa, Marina Yurova and Jostein Jerkø for their contribution on ice as well as all crew members of R/V Lance for being always dedicated on the frozen seas. Mauri Määttänen and Prof. Jukka Tuhkuri from Helsinki University of Technology in Finland are also thanked for using their pressure sensors. Last but not least, the authors are very grateful to the anonymous reviewers for using their precious time amending this paper with valuable comments.

REFERENCES

Cox and Weeks, 1983. Equations for determining the gas and brine volume in sea ice samples. Journal of Glaciology, Vol. 29, No. 102, pp. 306-316
Gold, L. W., 1992. Interpretation of field measurements for ice engineering applications. In Proc. of the 11th Int. Symp. on Ice (IAHR), Banff, Albertia (2), pp. 856-869
Johnston, M., R. Frederking, et al. 2001. Seasonal decay of first-year sea ice. Technical Report HYD-TR-058, Canadian Hydraulics Centre.
Masterson, D., and Graham. W. 1996. Development of the original borehole jack. Can. J. Civ. Eng. (23), pp. 186-192
Sandwell, Borehole Jack Test Manual Sandwell (Alberta) Ltd, 2007
Sinha, N. 2005. NRCC borehole jack indentor: measuring ice strength. Proc. 18th Int. Conf. on Port and Ocean Eng. Under Arctic Condition. (1), pp. 153-164
Squire V.A. and. Allan, A.J, 1980. Propagation of flexural gravity waves in sea ice. Sea Ice Processes and Models, Proceedings of the Arctic Ice Dynamics Joint Experiment, University of Washington Press, Seattle, pp. 327--338
Timco, G.W. and Johnston, M.E, 2002. Sea ice strength during the melt season. Proceedings of the 16th IAHR International Symposium on Ice, Dunedin, New Zealand, pp. 187-193

Chapter 4 – Morphology and physical and mechanical properties of first- and second-year sea ice ridges

4.1 Introduction

This chapter comprises 3 papers. The first paper introduces the reader to first-year sea ice ridges by presenting a large review of the current knowledge of ridge morphology and by describing the block thickness and variation of the consolidated layer. The first paper also catalogues the morphological data of first-year ridges. This paper was published in Cold Regions Science and Technology. The second paper describes the spatial and temporal evolution of a first-year ridge in Spitsbergen and has been published and presented at the Port and Ocean Engineering under Arctic Conditions (POAC) Conference in 2011. The third paper presents and discusses the data collected for second-year ridges in the Fram Strait in 2009. This paper has been published and presented at the International Symposium on Ice (IAHR) in 2010. This chapter aimed at:

- increasing the existing database for the morphology of first-year sea ice ridges
- correlating the different dimensions of a first-year ice ridge
- examining the variation of the consolidated layer
- providing a better visualization of the constitution of a first-year ice ridge and the variation of its morphological properties
- improving the knowledge on the spatio-temporal evolution of physical and mechanical properties of first-year sea ice ridges
- providing data for ridges in the Fram Strait in late summer and a better understanding of the transition from a first- to second-year sea ice ridge.

Publications:

(4.2)

Strub-Klein, L. and Sudom, D. (2012). Analysis of the morphology of first-year sea ice ridges. Submitted on January 21st 2012 to Cold Regions Science and Technology.

(4.3)

Strub-Klein, L. and Høyland, K.V. (2011). One season of a first-year ice ridge investigation – Winter 2009. Proceedings of the 21st International conference on Port and Ocean Engineering under Arctic Conditions (POAC). Montreal, Canada.

(4.4)

Strub-Klein, L. et al. (2010). Physical and mechanical properties if sea ice ridges in the late summer in the Fram Strait. Proceedings of the 20th International Symposium on Ice (IAHR). Lahti, Finland.

4.2 A comprehensive analysis of the morphological properties of first-year sea ice ridges

A comprehensive analysis of the morphology of first-year sea ice ridges

Submitted to Cold Regions Science and Technology on January 21, 2012

Lucie Strub-Klein[1,2]
Denise Sudom[3]

[1]*The University Centre on Svalbard (UNIS), Arctic Technology Department, PO. Box.156, 9170 Longyearbyen, Norway*
[2]*The Norwegian University of Technology (NTNU), Department of Civil and Transport Engineering, Høgskoleringen 7a, 7034 Trondheim, Norway*
[3]*Canadian Hydraulics Centre, National Research Council Canada, 1200 Montreal Road, Ottawa Canada K1A 0R6*

Abstract

A review of the morphological properties of over 300 full-scale floating first-year sea ice ridges has been made, including measurements from 1971 until the present time. Ridges were examined from the Bering and Chukchi Seas, Beaufort Sea, Svalbard waters, Barents Sea and Russian Arctic Ocean for the Arctic regions; and from the Canadian East Coast, Baltic Sea and Gulf of Bothnia, Sea of Azov, Caspian Sea and Offshore Sakhalin for the Subarctic (or temperate) regions. Grounded ridges were excluded. A wide catalogue comprising the ridge thicknesses (sail, keel and consolidated layer), widths and angles as well as the macroporosity and the block dimensions is provided. The maximum sail height was found to be 8 m (offshore Sakhalin), and the mean peak sail height was 2.0 m, based on 356 profiles. The mean peak keel depth is 8.0 m, based on 321 profiles. The relationship between the maximum sail height, h_s, and the maximum keel depth, h_k, for all ridges is best described by the power equation $h_k = 5.11h_s^{0.69}$. The correlation differs depending on the region. For Arctic ridges a linear relationship was found to be the best fit ($h_k = 3.84h_s$), while for the Subarctic ridges a power relationship ($h_k = 6.14h_s^{0.53}$) best fit the data. The ratio of maximum keel to maximum sail is 5.17 on average (based on 308 values), and has also been calculated for each region mentioned above. Arctic ridges generally have a lower keel-to-sail ratio than those in Subarctic regions. The statistical distribution of keel-to-sail ratios is best represented by a lognormal distribution. The average sail and keel widths were 12 and 36 m, respectively. The relationships between the sail and keel widths and other geometrical parameters were also determined. Variation of sail and keel thicknesses within individual ridges has been compared with the variability of all ridges. Ridge cross-sectional geometry can vary greatly along the length of a ridge, even over a short distance. A study was made on sail block thicknesses, and it was found that they correlate well with the sail height with a square root model. The typical macroporosity for a first-year ice ridge is 22% (based on 58 values) with an average sail macroporosity of 18% (based on 49 values) and average keel rubble macroporosity of 20% (based on 44 values). The average ridge consolidated layer thickness was 1.36 m based on 118 values. The ratio of the consolidated layer to the level ice thickness was found to be 1.52. The variation of the consolidated layer was examined, and it was found that the layer tends to grow evenly with time over the width of the ridge cross section. A greater spacing between the measurements seemed to affect the variation, as it decreased with an increasing distance between each borehole. A statistical analysis based on 377 measurements of the consolidated layer of ridges in the Barents Sea showed that the gamma distribution well describes the distribution of the consolidated layer thicknesses in that area.

Key words: first-year ridges, ratios, block dimensions, macroporosity, consolidated layer

1. Introduction

Over large areas, sea ice is generally not flat and on average consists of 10-40% ridges by volume (Leppäranta, 2011). If the ice remains attached to the shore, it is called landfast ice. Floating ice is more dynamic and is often subjected to drift caused by winds and currents. Floating ice floes may collide, resulting in ice deformation by rafting, ridging or rubbling. A ridged ice feature may also become grounded (referred to as a stamukha). The World Meteorological Organization (WMO, 1970) defines an ice ridge as "a line or wall of broken ice forced up by pressure". These can be "fresh" or "first-year" features, or "weathered" and "old" (WMO, 1970). For the purposes of this paper, first-year ridges are defined as those which have not survived one summer's melt. First-year ridges may present very sharp sails with visible blocks, and their degree of consolidation is almost always much less advanced than the older multi-year ridges. Ridged multi-year ice may also reach greater thickness than first-year ridges – in the range of 40 to 50 m (Johnston et al., 2009). The present study concerns only first-year ridged ice features that are not grounded.

Ridges usually consist of three distinguishable parts:

- The sail, which is above the water line. It consists of blocks of ice piled up and frozen together by contact.
- The consolidated layer, which is below the water line. The blocks that initially pile up underwater form cavities which fill up with water. As the season progresses, the water freezes in these voids, contributing to the continuous consolidation of the ridge.
- The rubble, which is under the consolidated layer. It consists of loose blocks partially refrozen together, with water trapped in between.

The rubble and the consolidated layer form the keel. In general, the keel is wider than the sail and extends under the surrounding level ice.

Ridges are complex structures with a wide variability in shape and size. They are often modeled by triangles or trapezes (see Fig. 1) and characterized by their thicknesses, widths and angles. The base of the keel is often irregular and not represented by a triangle. Although we do not investigate detailed ridge shapes in this paper, the ISO code (ISO 19906, 2010) gives a range of values for the base or flat part of the keel (up to 5 times the sail height). Fig. 1 indicates the maximum dimensions for a typical ridge. However, not all the papers and reports present these dimensions the same way; for example, sometimes the sail and keel thicknesses are given as values averaged over a cross section.

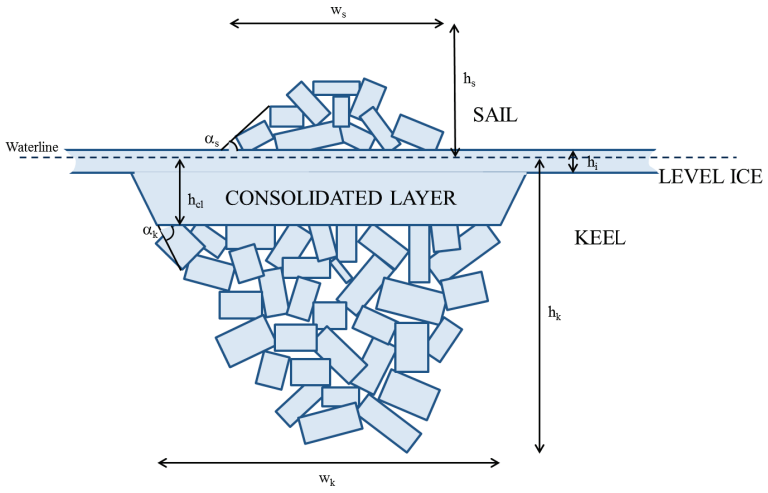

Fig. 1. Typical model of a first-year ice ridge

It has been common to establish ratios between the maximum keel depth h_k and the maximum sail height h_s, the keel width w_k and the sail height h_s, or the keel width w_k and the keel depth h_k (these are reported in Timco and Burden, 1997, Sudom et al. 2011, and Strub-Klein, 2011, amongst others). These relationships have their use in the design of offshore structures and ships.

Indeed, sea ice ridges are often used to calculate the design load in Arctic marine regions in the absence of icebergs (Blanchet, 1998). In this case (and in theory), the ridge dimensions, macroporosity, and physical and mechanical properties are the necessary inputs for accurate modeling and calculations. In practice, these data are difficult to collect all at once, due to the lack of time and the difficult fieldwork conditions in cold regions.

Burden and Timco (1995) and Timco and Burden (1997) have presented and analyzed data collected on first-year sea ice ridges and multi-year ice ridges with a special focus on the keel-to-sail ratios (h_k/h_s) and relationships between the sail height and the keel depth. More recently, Sudom et al. (2011) and Strub-Klein (2011) have extended this existing database and while Sudom et al. (2011) focused on a comparison of the morphological properties between first- and multi-year ice ridges, Strub-Klein (2011) developed the relationship between the sail and the keel for first-year ridges and attempted to find a suitable statistical relationship for the keel-to-sail ratios.

The idea came to gather all the data and previous analyses on floating first-year sea ice ridges in one paper. Therefore we will first present the various data sources, compiling available data on the ridge dimensions and morphological properties. Next, we go deeper into the ridge geometry and morphology to improve the existing relationships and statistical models for ridge dimensions. We will also analyze the block thicknesses and the consolidation of first-year ridges with some considerations on the macroporosity and the variation of the consolidated layer thickness. In the last section of this paper we identify what is still lacking in ridge investigations.

2. Data sources

In total, 45 sources were used to compile the available data about floating first-year sea ice ridges. These papers presented ridges from the Bering and Chukchi Seas, Beaufort Sea, Svalbard waters, Barents Sea, Arctic Ocean (considered Arctic regions); and from East

Coasts of Canada, Baltic Sea and Gulf of Bothnia, Sea of Azov, Caspian Sea and Offshore Sakhalin (considered Subarctic or temperate regions). These regions are shown in Fig. 2, except for the more southern Caspian Sea on the border of Europe and Asia, and the Sea of Azov to the south of Eastern Europe. The division for Arctic/Subarctic is at the Arctic Circle (generally defined as about 66°34'N). A precise location was not available for all ridges in the study – for example, profiles were available for some ridges in the Bering and Chukchi Seas without exact coordinates, so these ridges were grouped into "Bering and Chukchi" and considered to be Arctic. Most of the data sources for this study have been used by Burden and Timco (1995), Timco and Burden (1997), Sudom et al. (2011) or Strub-Klein (2011), with the addition of some data that was newly available or newly discovered by us. We aimed at presenting a catalogue that is as complete as possible. Diverse pieces of information were collected from at least 300 floating first-year ice ridges, and a summary of the data sources is given in Table 1. Raw data on keel and/or sail geometry was available for 251 distinct ridges, many having more than one profile. The 45 data sources are not the only ones existing on floating first-year sea ice ridges; other sources are discussed in Section 6. Some papers or reports which did not give precise enough data for us to use in the analysis are also listed in Table 1.

Fig. 2. Map of the Arctic and Subarctic regions where ridges were investigated (from Ahlenius, 2006)

The dimensions that are typically reported by the authors of the various papers include: sail height h_s, keel depth h_k, sail width w_s, keel width w_k, consolidated layer thickness h_{cl}, sail angle α_s, keel angle α_k, length of the ridge l_r and/or the total width w_r. As one might expect, data were not collected and presented the same way by each author. The column "type of available data" indicates if the data given in the paper were the average ("avg") or maximum ("max") dimensions, or if the whole cross section ("whole") was available.

The data sources were selected such that at least one of the ridge dimensions amongst h_s, h_k, h_{cl} and h_b is reported (maximum or average). In most of the papers, some additional information such as the surrounding level ice thickness h_i, the porosity η, etc, is also

presented. A summary of the additional properties (morphological, physical and mechanical) that each paper proposes as potentially useful to measure is given in Section 6 of this paper.

The ridge morphology can be investigated with the help of different techniques, which are: Drilling, Thermal Drilling, Diving, Survey, Sonar, or even Thermistor String. The techniques used in data collection for each source are given in Table 1. These methods are explained further in Section 3 of this paper.

Table 1
Data sources and available data

References	*Method**	*# ridges surveyed*	*Type of available data*	*Available ridge dimensions*
ARCTIC REGIONS				
Bering and Chukchi Seas				
Voelker et al. (1981a)	Su+So+Dr	40	max	$h_k\ h_s\ h_{cl}\ w_s\ w_k\ h_i$
Voelker et al. (1981b)	Su+So+Dr	3	max, avg	$h_k\ h_s\ h_{cl}\ w_s\ w_k\ h_i$
Voelker et al. (1982)	Su+So+Dr	26	whole	$h_k\ h_s\ h_{cl}\ w_s\ w_k\ h_i$
Voelker et al. (1983)	Su+So+Dr	4	whole	$h_k\ h_s\ h_{cl}\ w_s\ w_k\ h_i$
Voelker et al. (1984)	Su+So+Dr	11	whole	$h_k\ h_s\ h_{cl}\ w_s\ w_k\ h_i$
Beaufort Sea				
Barker et al. (2008)	Dr	1	whole	$h_k\ h_s\ w_k\ \alpha_s\ \alpha_k\ h_i$
Gladwell (1976)	Dr+So	5	max	$h_k\ h_s\ \alpha_s\ \alpha_k\ h_b$
Mc Gonigal (1978)	Su+So+Dr	10	max	$h_k\ h_s\ h_{cl}\ w_s\ w_k\ \alpha_s\ \alpha_k\ h_i\ h_b$
Vaudrey (1979)	Su+So+Dr	11	max	$h_k\ h_s$
Lowings and Banke (1981)	Thermistor chains+Su+ Dr	6	whole	$h_k\ h_s\ h_{cl}$
Bowen and Topham (1996)	Su+So+Dr	1	whole	$h_k\ h_s\ w_s\ w_k\ h_i\ h_b\ l_r$
Banke (1982)	Su+So+Dr	7	whole	$h_k\ h_s\ h_{cl}\ w_k\ h_i\ h_b$
Tucker and Govoni (1981)	Su	30	max	$h_s\ h_b$
Sayed and Frederking (1989)	Thermistor chains+ Su+ Dr	19	max, avg	$h_s, w_s\ h_b$
Melling et al. (1993)	Su+So+video	complex feature of intersecting ridges	whole	$h_k\ h_s\ w_s\ w_k\ \alpha_s\ \alpha_k\ h_i\ h_b$
Svalbard waters				
Høyland (2002a,b), Høyland and Løset (1999a), Høyland et al. (2000)	Dr+Th S	2	whole	$h_k\ h_s\ h_{cl}\ w_r\ l_r\ h_i\ h_b$
Høyland and Løset (1999b)	Dr+Su	1	whole	$h_k\ h_s\ h_{cl}\ h_i\ h_b$
Sharfrova and Høyland (2008)	Dr	1	whole	$h_k\ h_s\ h_{cl}\ h_i\ h_b$
Sand et al. (2011)	Dr	1	whole	$h_k\ h_s\ w_s\ w_k\ \alpha_s\ \alpha_k\ h_i\ h_b$
Barents Sea				
Høyland (2005, 2007), Bonnemaire et al.(2003),Shafrova and Høyland (2008)	Dr	4	max, avg	$h_k\ h_s\ h_cl\ w_s$ (1R) w_k (1R) α_s (1R) α_k(1R) h_i h_b
Krupina et al. (2009)	Dr	1	whole	$h_k\ h_s$
Strub-Klein et al. (2009)	Dr	1	whole	$h_s\ \ h_k\ h_{cl}\ h_i\ h_b$
UNIS, unpublished data (2007)	Dr	1	whole	$h_s\ \ h_k\ h_{cl}\ h_i\ h_b$
UNIS, unpublished data (2011)	Dr	1	whole	$h_s\ \ h_k\ h_cl\ h_i$
Sand et al. (2011)	Dr	1	whole	$h_k\ h_s\ \ w_s\ w_k\ \alpha_s\ \alpha_k\ h_b$

Kharitonov (2008)	Th Dr	13	max, avg	$h_k\ h_s\ h_{cl}\ h_i\ h_b$
*Mironov and Porubayev (2005)***	Th Dr	?	avg	$h_k\ h_s\ h_{cl}\ w_r\ h_i\ h_b$
Arctic Ocean (Russia)				
*Kharitonov and Morev (2005)***	Th Dr	1	avg	$h_k\ h_s\ h_{cl}\ h_i$
Kharitonov (2008)	Th Dr	3	avg	h_{cl}
SUBARCTIC REGIONS				
East Coast Canada				
Evers (1986)	Dr	4	whole	$h_k\ h_s\ w_s\ w_k\ \alpha_s\ \alpha_k$
Williams and Kirby (1994)	Dr	5	whole	$h_k\ h_s\ h_{cl}\ l_r\ w_r$
Croasdale et al. (1999)	Su+Dr+Th Dr	5	max	$h_k\ h_s\ h_{cl}\ h_b$
Obert and Brown (2011)	So	3199 (complete data for 10 ridges)	max, avg	$h_k\ w_k\ \alpha_k$
Baltic Sea and Gulf of Bothnia				
Høyland (2002a), Høyland et al. (2000)	Dr+Th S	1	whole	$h_k\ h_s\ h_{cl}\ h_i\ h_b$
Kankaanpää (1997)	Dr+Di	14	max	$h_k\ h_s\ w_s\ w_k\ h_i\ h_b$
Leppäranta and Hakala (1992)	Dr	6	max	$h_k\ h_s\ h_cl\ w_s\ w_k\ h_i\ h_b$
Leppäranta et al. (1995)	Dr	1	max, avg	$h_k\ h_s\ h_{cl}\ h_i$
Palosuo (1975)	Di	16	max	$h_s\ h_k\ h_b$
Veitch et al. (1991a)	Su+Dr	2	max	$h_k\ h_s$
Veitch et al. (1991b)	Dr	1	whole	$h_k\ h_s\ h_{cl}\ h_i\ h_b$
Sea of Azov				
Kharitonov (2008)	Th Dr	2	max, avg	$h_k\ h_s\ h_{cl}\ h_i\ h_b$
Caspian Sea				
Kharitonov (2008)	Th Dr	9	avg	$h_{cl}\ h_i\ h_b$
*Mironov and Porubayev (2005)***	Th Dr	?	avg	$h_k\ h_s\ h_{cl}\ w_r\ h_i\ h_b$
Offshore Sakhalin				
Beketsky et al. (1996)	Th Dr	3	max, avg	$h_k\ h_s\ h_{cl}$
*Mironov and Porubayev (2005)***	Th Dr	?	avg	$h_s\ h_k\ h_{cl}\ w_r\ h_i\ h_b$
Mironov et al. (1998)	Th Dr	2	max	$h_k\ h_s$
Surkov and Truskov (1995)	Th Dr	18	max	$h_s\ h_k$
Kharitonov (2008)	Th Dr	14	avg	$h_k\ h_s\ h_{cl}\ h_i$

* Dr: Drilling; Su: Survey; So: Upward Looking Sonar; Th Dr: Thermal Drilling; Th S: Thermistor Strings; Di: Diving
** Papers from which raw data could not be used for further analysis, but are catalogued in the Appendix

We would like to emphasize that we tried to give a summary of the existing data that was as precise and complete as possible. However, if one wishes to use these data for a deeper application, we would recommend reading the original paper they were taken from.

Additional literature such as Johnston and Barker (2000), Sisodyia and Vaudrey (1981), Kankaanpää (1989), Truscov (undated monograph), Tucker et al. (1984) or Bonnemaire and Bjerkås (2004) are not included in Table 1 because either we could not use the data, or the data had already been published in another paper (Johnston and Barker, 2000 in Croasdale et al., 1999, Sisodiya and Vaudrey, 1981 in Vaudrey, 1979 and Kankaanpää, 1989 in Kankaanpää, 1997).

For the reader's comprehension, we also provide further information on some of the papers: Tucker and Govoni (1981) and Tucker et al. (1984) present a deep analysis of the block thicknesses and how these related to the sail heights. No raw data could be obtained from Tucker et al. (1984) and therefore it does not appear in Table 1. Obert and Brown (2011) reported on 3199 ridge keel measurements in the Northumberland Strait, but provide raw data

on only several of these. The data obtained from Høyland (2002a,b), Høyland and Løset (1999a,b) and Høyland et al. (2000) were supplemented with internal reports and data provided by Prof. Knut Høyland. The results presented by Strub-Klein et al. (2009) have been used along with the data from an internal (and unpublished) report on the same ridge (UNIS Report, 2008). The data from Sand et al. (2011) is contained in an internal report held at Norut Northern Research Institute at Narvik provided by Prof. Peter Wide. Kankaanpää (1997) studied 14 ridges but sometimes several cross sections were drilled. One was complete and the others just reported the surface elevation of the ridge. The block dimensions were measured for all these cross sections, but we chose to present only the data for which all the measurements were made on the ridge (i.e. when the keel depth, sail width and keel width were also included). Kharitonov (2008), Kharitonov and Morev (2005), and Mironov and Porubayev (2005) also presented data for several areas, however, most data were given only as ranges of values and could not be used in further analysis. What was surveyed is shown in Table 1 and later in Section 6.1., and numerical results are found in the Appendices. The ridges presented by Kharitonov and Morev (2005) were apparently formed from second-year ice, but we have considered them as first-year ice ridges since they had not yet been subjected to a summer's melt and the consolidated layer was quite thin (with a macroporosity of 16% in the keel). Mironov et al. (1998) report more than 2500 hot drill measurements and more than 107 profiles on ridges. Unfortunately, none of these data are available in the paper they published, except for two cross sections with the maximum values for the keel depth and the sail height.

3. Ridge geometry

3.1 Methods of investigations

Ridge morphology can be surveyed by diverse techniques. They have partially been presented by Timco et al. (2000) and partially discussed by Strub-Klein (2011). In this section we will discuss discrete measurements of the ice ridges, which are generally performed when there are time and resources to measure the ridge geometry on site. These measurements give precise data about the ridge keel, depth, width and angles simultaneously.

- **Drilling**: This is the most common technique (because it is relatively easy and efficient) to determine the sail height, keel depth, the consolidated layer thickness or even the macroporosity. It consists of connecting an auger (often 2'') to an engine (running on fuel, electricity or battery) and drilling through and across the ridge (adding depth extensions). One cross section establishes a 2D profile of the ridge morphology. The bottom of the consolidated layer is often defined when the ice feels softer, when the auger reaches a gap or when water or slush is brought up by the drill. Practically, the macroporosity is defined by recording the vertical extension of each gap felt while drilling. However, this technique is subjective and operator dependent, so the consolidated layer thickness and morphology may be determined in an approximate way.
- **Survey**: A level, theodolite or differential GPS are used to measure the surface elevation. This method gives accurate results for the surface geometry, but does not give any information about the rest of the ridge.
- **Thermal drilling**: This method has been developed by the Arctic and Antarctic Research Institute and has been widely used in the Russian areas. It consists of a tube with an open end through which hot water or steam melts a hole in the ice. The penetration rate is recorded to determine the ice consistency. This method has the

advantage of higher precision for assessing the macroporosity and consolidated layer thickness. However, the apparatus can be large and heavy, it requires a power supply, and its deployment can be time-consuming.

- **Sonar**: An Upward Looking Sonar (ULS) is deployed on the sea bottom and points towards the surface of the sea. It enables the measurement of the sea ice thickness and concentration. It is a very common tool to use for continuous measurements including the frequency of ridges drifting. When used for discrete measurements, one has to be sure that the ridge is well positioned over the sonar to get the right keel depth. It will most likely not give any indication of the macroporosity, the consolidated thickness or the age of the ridge.
- **Diving**: This method gives a good overview of the ridge's shape underwater. It also enables the measurement of the deepest point of the keel, but neither the macroporosity nor the consolidated layer thickness can be estimated. This technique requires qualified manpower (as much on the ice as under water) and a lot of time (and therefore stable conditions on the ice).
- **Thermistor strings**: This method has been very little used. It enables the recording of ice growth and consolidation. If the ridge is monitored an entire season, this method can reliably model the thermodynamic behavior of the ridge.
- **Electromagnetic induction (EM)**: EM sensors can be used to determine ice thickness. EM instrumentation can be used from a helicopter or plane, mounted to a fixed structure, or deployed on the ice surface. The interpreted ice thickness is averaged over a certain area, and can therefore underestimate the peak thickness in a ridge. For airborne measurements this footprint diameter is approximately proportional to the distance of the sensor from the bottom surface of the ice (Prinsenberg and Holladay, 2009). Due to this averaging and uncertainty, EM measurements were not analyzed in this paper but are reviewed in Section 6.

3.2 Catalogue of available ridge data and key statistical figures

All available data on ridge geometries from the sources listed in Table 1 (except those noted as not analyzed in this study) are given in Appendix A. Data have been extracted from each ridge cross section from the original reports or papers. Researchers may have made several, or just one, cross sections of a ridge. Each cross section is given equal weight for the purposes of this analysis.

Table 2 shows the key statistical figures, with the corresponding number of data points, for ridge sail and keel geometry. For sail height and keel depth, the statistics are given for both the average and maximum values measured for each cross section. The definitions of maximum sail height, h_s, sail width, w_s, maximum keel depth, h_k, and keel width, w_k, are shown in Fig. 1. The average sail height is an average of the heights measured across a ridge cross section; the average keel depth is calculated in a similar manner. Ridge lengths were not analyzed as too few data were available. The data in Table 3 are divided into geographical regions as described in Section 2, and also summarized for all ridges, and for all ridges within the Arctic and Subarctic regions. The statistical figures are not summarized for the Russian Arctic Ocean or Sea of Azov, as too few data were available, but are included in their respective Arctic/Subarctic categories, and in the "all ridges" category. Also, no raw data were available for the Caspian Sea.

Table 3 shows the key statistics for the total overall ridge thickness (sail height plus keel depth). These data are meant to give an indication of the total size of ridges. The extent and thickness of ridges is related to wind and ocean dynamics – in areas where wind has a predominant direction, more dynamic effects are created, leading to more ridging (Mironov

and Porubayev, 2005). The most heavily ridged sea ice in the world (considering ridges of all ages) is said to exist in the northern Canadian Arctic (Melling, 2002) and the thickest ridges have been measured in the Beaufort Sea (Sudom et al., 2011). This study, which concerned only first-year ridges, also found the thickest overall ridge to be in the Beaufort Sea (thickness of 34 m measured by McGonigal, 1978), as shown in Table 3. However, first-year ridges of comparable thickness (over 30 m) have also been measured in both the Bering/Chukchi Seas (Voelker et al., 1983) and in the Baltic Sea (Palosuo, 1975). The Sakhalin region also has relatively heavily ridged ice at over 20 m thickness. It is important to note that in all these regions, only a very small proportion of measured ridges actually have such great thicknesses. For the Beaufort Sea, we found only 11 first-year ridge measurements with a total overall thickness of greater than 20 m. For other regions, even fewer ridges of greater than 20 m thickness were measured (four ridges in the Bering/Chukchi Seas, and two ridges in each of the Baltic and Sakhalin areas).

In this paper we do not focus on the overall thickness of the ridge, and instead examine the sail and keel as separate measurements. The keel is generally of more concern than the sail, since it often has higher strength due to consolidation. In Section 3.3.1, we examine the relationship between ridge sails and keels in detail.

Table 2
Key statistical figures for ridge geometries. Mean and maximum values are calculated by regions; *n* is the corresponding number of measurements.

		Bering and Chukchi Seas	Beaufort Sea	Svalbard waters	Barents Sea	East Coast Canada	Baltic Sea and Gulf of Bothnia	Offshore Sakhalin	**All ridges**	Arctic	Subarctic
Maximum sail height (m)	mean	1.7	2.7	1.2	2.1	1.7	1.1	3.3	**2**	2.1	1.6
	max	2.5	7.5	4.5	4.7	4.2	3.4	8	**8**	7.8	8
	n	91	96	21	19	32	69	23	**356**	230	126
Average sail height (m)	mean	1.1	1.6	0.3	0.5	0.6	0.3	2.3	**0.7**	0.8	0.6
	max	1.4	3.3	0.7	0.8	1.1	0.4	3.5	**3.5**	3.3	3.5
	n	3	12	19	6	18	14	3	**78**	43	35
Sail width (m)	mean	9.6	17.5	6.6	10.2	13.7	7.4	-	**12**	12.7	9.8
	max	37.5	73.2	8	-	30	24	-	**73.2**	73.2	30
	n	72	50	2	1	17	27	0	**169**	125	44
Maximum keel depth (m)	mean	5.9	12.6	4.8	8.5	6.5	7.3	12	**8**	8.2	7.8
	max	23.8	26.8	10.8	15	12.4	28	19	**28**	26.8	28
	n	85	58	21	19	42	68	23	**321**	186	135
Average keel depth (m)	mean	4.9	10.5	2.5	5.6	4.1	3.8	6.3	**4.5**	4.8	4.2
	max	6	12.4	3.5	9.3	6.7	4.9	8.5	**12.4**	12.4	8.5
	n	3	6	19	10	15	13	3	**72**	41	31
Keel width (m)	mean	24.6	55.9	13.8	37	52.1	29.9	-	**36**	33.6	41.2
	max	82	149.4	37.4	-	201.9	59.5	-	**201.9**	149.4	201.9
	n	57	37	16	1	26	25	0	**162**	111	51

Table 3
Key statistics for maximum and average total ridge thickness

		Bering and Chukchi Seas	Beaufort Sea	Svalbard waters	Barents Sea	East Coast Canada	Baltic Sea and Gulf of Bothnia	Offshore Sakhalin	**All ridges**	Arctic	Subarctic
Maximum keel depth + maximum sail height (m)	mean	7.5	15.5	6.1	10.3	9.1	8.4	15.3	**10**	10.2	9.8
	median	5.7	14.7	5.5	10.2	8.3	7	15.8	**9**	9.1	8.8
	max	31.7	34.3	14.1	19.7	15.2	31.4	23	**34.3**	34.3	31.4
	n	85	58	21	17	32	68	23	**309**	184	125
	stdev	5.6	6.4	2.3	3.4	3.6	5.1	3.4	**6**	6.5	5.2
Average keel depth + average sail height (m)	mean	6	13.4	2.8	4.4	4.5	4.1	8.6	**5**	5.3	4.7
	median	7	13.1	2.9	3.9	3.9	4.3	9.1	**3.8**	3.3	4.3
	max	8.2	15.7	3.7	7.5	7.3	5.2	10	**15.7**	15.7	10
	n	3	6	19	6	15	13	3	**68**	37	31
	stdev	2.8	1.5	0.6	1.6	1.5	0.9	1.7	**3.2**	4	1.8

3.3 Correlation between morphological parameters of ridges

Relationships between keel and sail morphological parameters have been presented using two methods: as lines or curves fitted to the data, and as ratios. The relationships based on curve fitting use a least-squares method. The coefficient of determination (R^2) is given as an indication of how well the regression line fits the data set. For the second method, ratios are calculated between several parameters, and statistics are evaluated for these ratios. Maximum sail height vs. maximum keel depth is investigated using both curve-fitting and ratios, as well as a probabilistic study to determine the best statistical distribution for the keel-to-sail ratio (using Q-Q plots). Averaged keel and sail thicknesses are examined using ratios only, since fewer data are available. The sail and keel widths are compared to each other as well as to the sail height and keel depth. Note that maximum keel depths used in this study are occasionally not actual "maximums" – sometimes researchers could not drill the entire depth of the ridge so the maximum keel depth was not reached.

Data have been analyzed from 9 selected geographical regions: Bering and Chukchi Seas, Beaufort Sea, Svalbard area, Barents Sea, Arctic Ocean (Russia), East Coast Canada, Baltic Sea and Gulf of Bothnia, Sea of Azov, and Sakhalin area. Where possible, statistics are given by region. These should be used with caution, noting that some regions have very few measurements available.

3.3.1 Sail height and keel depth relationships

3.3.1.1 Curve fitting

Fig. 3 shows the maximum sail plotted against maximum keel for all ridge cross sections (n = 308). A quadratic curve best fits the data (R^2 = 0.56), but is not logical since for very high sails it will predict a lower value of keep depth. The best fit curve is given by the power equation $h_k = 5.11h_s^{0.69}$. The best fit line $h_k = 3.82h_s$ is also shown.

These relationships may be compared to previous studies on first year ridges:

- $h_k = 4.5h_s$ (typical value given by ISO 19906, 2010)
- $h_k = 3.95h_s$ or $h_k = 4.60h_s^{0.88}$ (Timco and Burden, 1997); n = 97
- $h_k = 3.54h_s$ or $h_k = 4.43h_s^{0.82}$ (Sudom et al., 2011); n = 126
- $h_k = 5.38log(3.32h_s)$ (Strub-Klein, 2011); n = 204

The present study includes all relevant data from Timco and Burden (1997), Sudom et al. (2011) and Strub-Klein (2011). The main difference for the variation in the results is likely that the present study uses the methodology of Strub-Klein (2011) and includes multiple cross sectional profiles from some ridges, whereas the other studies used only one set of values per ridge (that of the maximum sail and keel).

Fig. 4 shows the maximum sail and keel data, but divided into 9 regions. This figure illustrates that the deepest first-year ridge keels have been measured in the Baltic, Beaufort, and Bering/Chukchi Seas. Fig. 5 shows the maximum sail vs. maximum keel for all ridge cross sections, grouped by Arctic and Subarctic regions. For Arctic regions, the data is best fit by the line $h_k = 3.84h_s$. For temperate or Subarctic regions, the data was better fit by a power relationship, $h_k = 6.14h_s^{0.53}$.

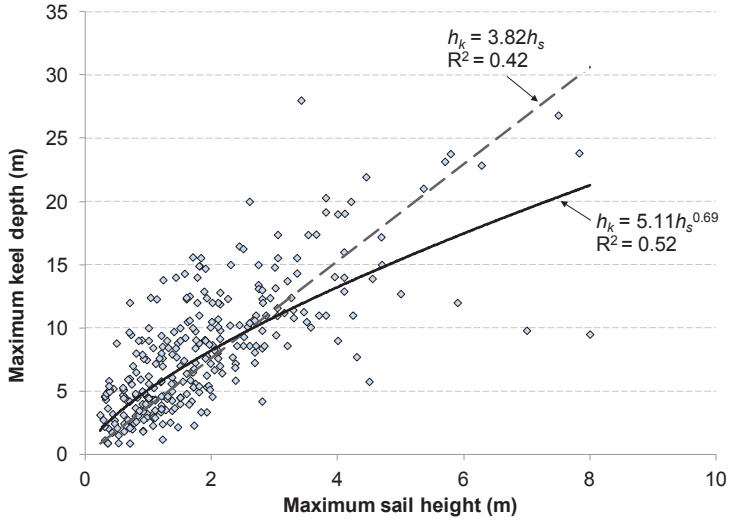

Fig. 3. Sail vs. keel, for all data (note that one outlying zero value of sail height was removed).

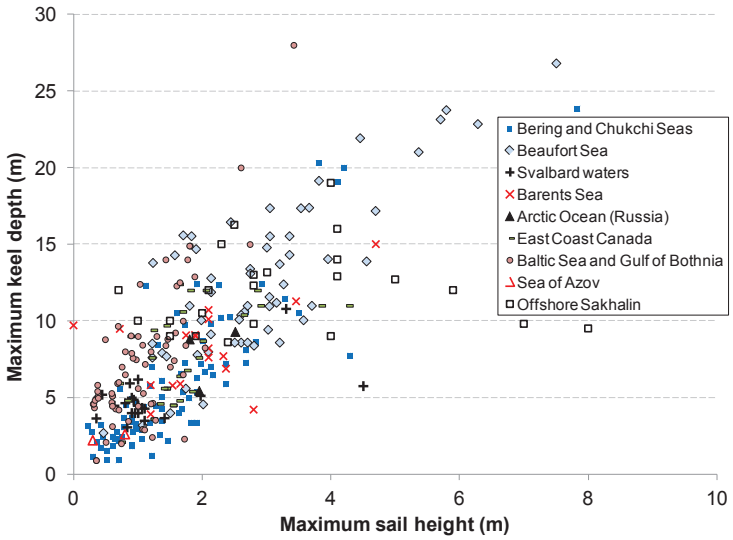

Fig. 4. Maximum sail vs. maximum keel for all ridge cross sections, by region

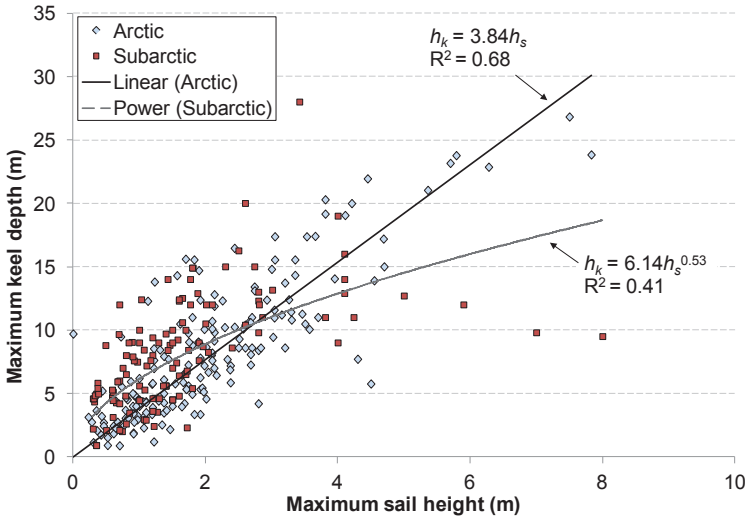

Fig. 5. Maximum sail vs. maximum keel for all ridge cross sections, for Arctic and Subarctic regions

3.3.1.2 Keel-to-sail ratios

The keel-to-sail ratios and key statistics were determined for 7 geographical regions, and then summarized for all ridges, and for all ridges falling within Arctic and Subarctic areas (Table 4). Statistics are not given for regions with only one available reference and very few data points. Some regions have few available data, especially for the ratios of average keel and sail thickness, therefore the values presented may not be typical for all regions. For all ridges, the mean keel-to-sail ratio is 5.17, and the median ratio is significantly lower at 4.21. As seen in the figures of Section 3.3.1.1, the data have quite a bit of scatter; the standard deviation of the data set is 2.96. The average ratio $h_k/h_s = 5.17$ may be compared to previous studies on first year ridges:

- $h_k/h_s = 4.5$ (typical value given by ISO 19906, 2010)
- $h_k/h_s = 4.46$ (Timco and Burden, 1997); $n = 97$
- $h_k/h_s = 4.35$ (Sudom et al., 2011); $n = 126$
- $h_k/h_s = 5.20$ (Strub-Klein, 2011); $n = 204$

Again, the present study includes all relevant data from Timco and Burden (1997), Sudom et al. (2011) and Strub-Klein (2011), but uses the methodology of Strub-Klein (2011) and includes all cross sections from ridges, whereas the other studies used only one ratio per ridge (that of the maximum sail and keel).

Arctic ridges generally have a lower keel-to-sail ratio than ridges in Subarctic/temperate regions. For the Arctic regions, the mean keel-to-sail ratio is 4.34 and the median is 3.92. The Arctic ratios are less scattered and have a standard deviation of 2.05. For Subarctic regions, the mean and median values are 6.39 and 5.84, respectively, with a standard deviation of 3.62. The maximum keel to maximum sail ratios for Arctic and Subarctic regions are summarized in the histogram in Fig. 6.

Table 4
Key statistical figures on the ratio of maximum keel depth to maximum sail height, and average keel depth to average sail height, by region.

		Bering and Chukchi Seas	Beaufort Sea	Svalbard waters	Barents Sea	East Coast Canada	Baltic Sea and Gulf of Bothnia	Offshore Sakhalin	All ridges	Arctic	Subarctic
Ratio of maximum keel depth to maximum sail height [m]	mean	3.94	4.72	5	4.4	4.73	7.69	4.94	5.17	4.34	6.39
	median	3.42	4.11	4.44	3.75	4	7.63	4.39	4.21	3.92	5.84
	max	13.61	11.22	11.82	13.15	10.71	17.94	17.14	17.94	13.61	17.94
	n	85	57	21	17	32	68	23	308	183	125
	stdev	1.99	1.78	2.51	2.45	2.04	3.84	3.33	2.96	2.05	3.62
Ratio of average keel depth to average sail height [m]	mean	6.08	3.71	11.08	8.19	9.2	16	3.22	9.96	8.7	11.47
	median	7.18	3.87	10.12	8.1	8.24	16	2.4	9.01	8.51	12.02
	max	8.06	4	23.17	10.52	16.73	19.91	5.67	23.17	23.17	19.91
	n	3	6	19	6	15	13	3	68	37	31
	stdev	2.7	0.39	6.3	2.12	3.03	1.8	2.15	5.36	5.45	4.92

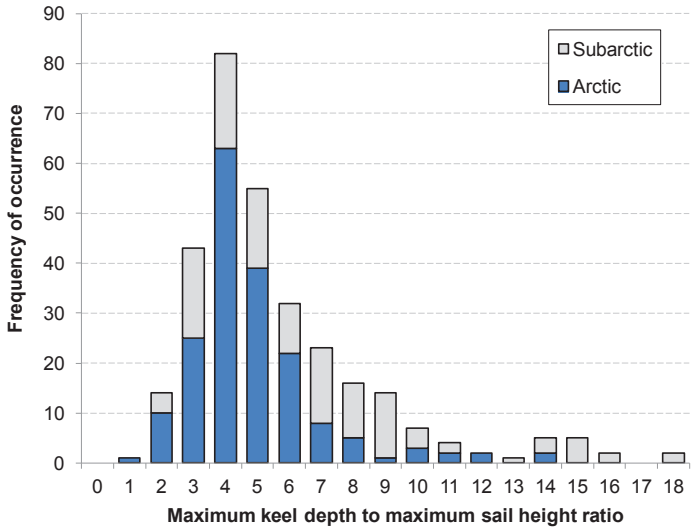

Fig. 6. Histogram of maximum keel to maximum sail ratios

A statistical analysis was made to determine the best fitting distribution to the 308 available keel-to-sail ratios. The method used is QQ-Plots, a graphical technique that compares the quantiles of the empirical data to the quantiles of the theoretical data (e.g. data calculated with the given statistical distribution). If the theoretical distribution and the field data distribution are in agreement, the quantiles should be the same and therefore would be plotted along a y=x line. If the distribution differs, some quantiles should lay off the y=x line. The normal, lognormal and gamma distributions were chosen as potential and relevant statistical distributions for the keel-to-sail ratios. They are defined respectively by the mean and the standard deviation; the logarithm of the mean and the standard deviation; the shape and the rate. The shape and the rate are also uniquely defined by the mean and the standard

deviation of the experimental data. These parameters are summarized in Table 5. The QQ-Plots for these three distributions are shown in Fig. 7.

The lognormal distribution best fits the empirical set of data. In Fig. 7, one observes very few outliers on the top right hand corner which means that the right tail of the empirical distribution is shorter than that predicted by the theory. Timco and Burden (1997) had found the same distribution for 97 keel-to-sail ratios using goodness-of-fits tests (chi-squared test). Strub-Klein (2011) used the QQ-Plots technique on 204 ratios and also found out that the lognormal distribution was the best match.

Table 5
Defining parameters for the normal, gamma and lognormal distributions

Normal		Gamma		Lognormal	
mean	St. dev.	shape	rate	meanlog	sdlog
5.17	2.96	4.11	0.80	0.71	0.47

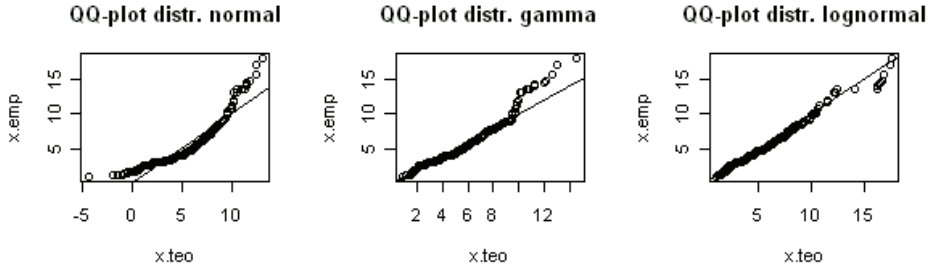

Fig. 7. Comparison of the normal, gamma and lognormal distributions for the keel-to-sail ratios (theoretical vs. empirical data).

3.3.2 Sail width and keel width relationships

Ratios of the sail and keel width to each other and to other geometrical parameters are shown in Table 6. All keel depths and sail heights are the maximums for a given cross section. The points at which the deformed ice begins to slope away from the level ice thickness, as shown in Fig. 1, define the sail and keel widths for a given cross section. The width of a ridge can be difficult to assess, especially when the ridge does not present an "idealized" sharply triangular cross section, or when ridges intersect or are in close proximity to each other.

For all comparisons of keel and sail widths to other parameters, the variation is relatively high, as shown in Table 6. On average, the keel width to sail width ratio is 6.75.

The sail width to height average ratio is 3.75, meaning that for a symmetrical ridge the average sail angle is 28°. The sail width and height are also plotted in Fig. 8, and the best-fit curve and line are given. The power relationship $w_s = 6.6h_s^{0.69}$ best fits the data.

The keel widths are compared to both sail height and keel depth. The average keel width to sail height ratio is approximately 20.9 with a standard deviation of 12.9, as given in Table 6. Sail height vs. keel width is plotted in Fig. 9. The best-fit line and curve are $w_k = 16.7h_s$ and $w_k = 19.2h_s^{0.76}$, respectively. This can be compared to $w_k = 14.85h_s$ and $w_k = 20.75h_s^{0.78}$ found by Timco and Burden (1997). As shown in Table 6, the keel width to keel depth average ratio is 4.85. The data are plotted in Fig. 10, and the best fit relationships given ($w_k = 4.28h_k$ or $w_k = 7.19h_k^{0.72}$). Timco and Burden (1997) found $w_k = 3.91h_k$ or $w_k = 5.67h_k^{0.87}$.

Table 6
Key statistical values for ratios of sail width to sail height, keel width to sail width, keel width to sail height, and keel width to keel depth

	w_k/w_s	w_s/h_s	w_k/h_s	w_k/h_k
mean	6.75	3.75	20.91	4.85
max	35.89	9.62	86.67	16.67
n	*165*	*130*	*152*	*149*
standard deviation	4.60	1.88	12.93	2.65
CoV	68%	50%	62%	55%

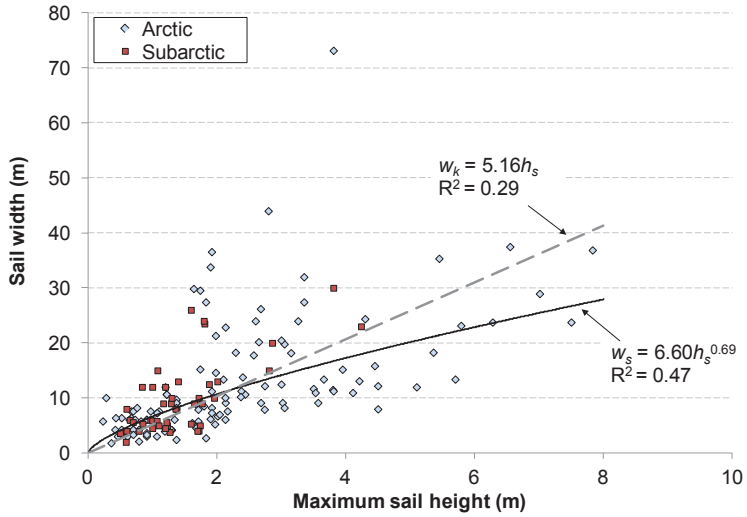

Fig. 8. Maximum sail height vs. sail width for Arctic and Subarctic regions. The linear and power relationships are shown for all data.

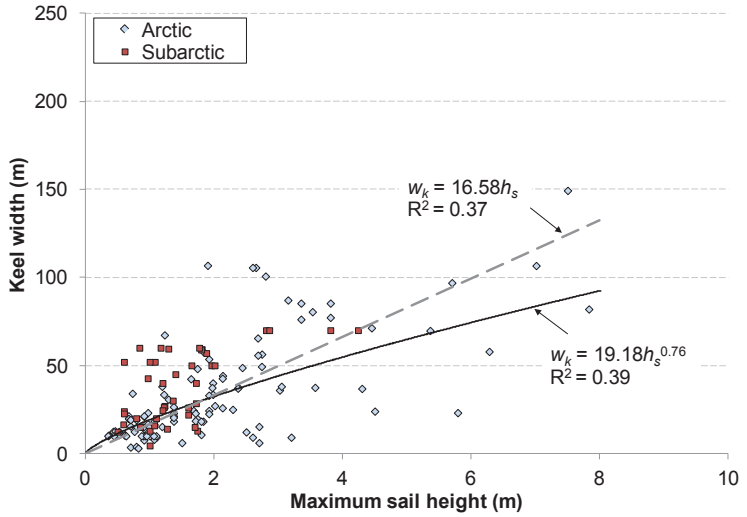

Fig. 9. Maximum sail height vs. keel width for Arctic and Subarctic regions. The linear and power relationships are shown for all data.

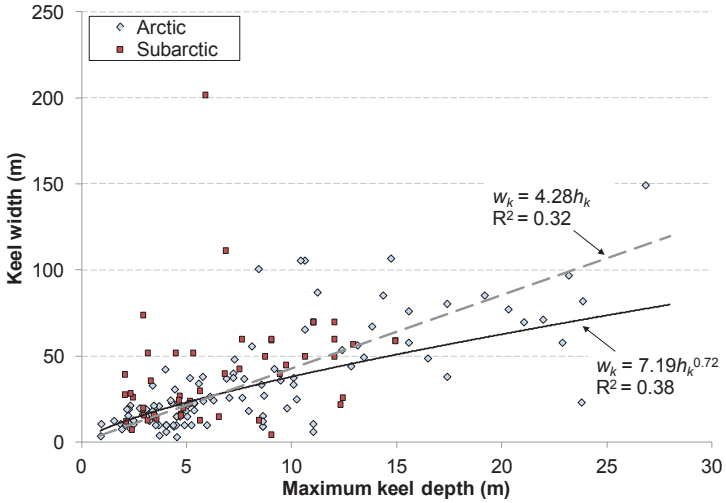

Fig. 10. Maximum keel depth vs. keel width for Arctic and Subarctic regions. The linear and power relationships are shown for all data.

3.4 Variation in sail and keel

Ridge cross-sectional geometry can vary greatly along the length of a ridge. The variation within individual ridges has been compared with the variability of all ridges. Ridges were selected for which several cross sections were profiled at approximately the same time, and compared to the variation of all cross sections, and of all cross sections in that geographical region.

UNIS drilled detailed profiles of two Barents Sea ridges, one in May 2007 (unpublished data), and the other in May 2008 (Strub-Klein et al., 2009). Four cross-sectional profiles were made for each of the two ridges (ridge measurements were all made within a maximum of 3 days, so no significant change in morphology occurred). The four cross sections were spaced at 1 m for each ridge.

Sayed and Frederking (1989) profiled three ridges – sails only – in the Beaufort Sea over a period of 10 days in April 1986, and reported on the range of sail height and width values. Cross-sectional profiles were made at 20 – 40 m intervals (a much greater spacing than the UNIS studies). For one 4 km long ridge in pack ice, 18 cross sectional profiles were made over a 2 km length. For the other two ridges, 9 or 10 profiles were made.

Fig. 11 shows the range of sail height values reported for the two Barents Sea ridges, the three Beaufort Sea ridges, along with the range of values for all Barents and Beaufort ridges, and ridges in all regions. It is interesting to note that the 2007 and 2008 UNIS ridge cross sections were made at only 1 m apart, but still display as much variability as the Sayed and Frederking (1989) ridges which had a much greater spacing. This variation in sail heights is often caused by irregular piling of rubble blocks.

Fig. 12 shows the variation of keel depth for the 2007 and 2008 UNIS ridges, compared to all ridges in the Barents Sea and to ridges in all regions. The keel depth for the individual UNIS ridges shows much less variation than the sail height, and less variation than the keel depth of ridges in either the Barents Sea or in all regions as a whole. For ridges in all regions, the sail heights display approximately the same degree of variation as the keel depths.

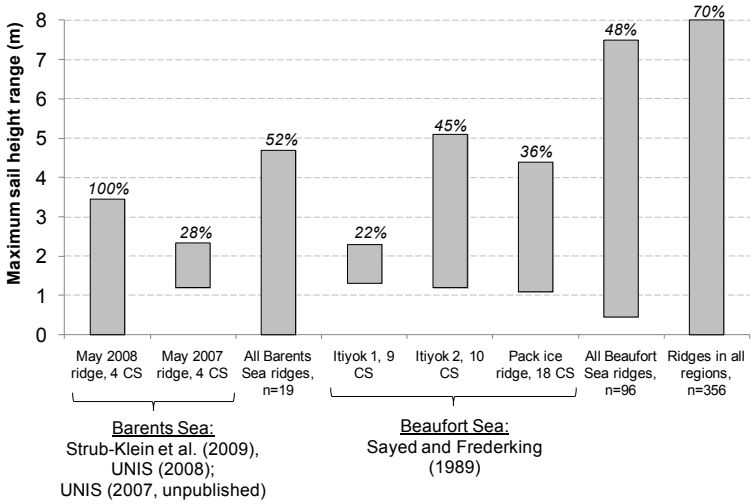

Fig. 11. Range of maximum sail height values for ridge cross sections, comparing variation within one ridge to variation of all ridges. The number of cross section (CS) profiles is indicated for each ridge or region. Coefficient of variation is given above the bars.

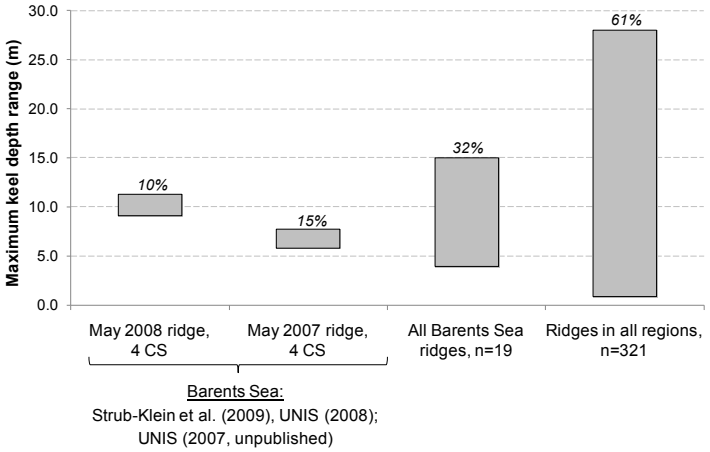

Fig. 12. Range of maximum keel depth values for two ridges in Barents Sea, compared to all Barents Sea ridges and ridges in all regions. Coefficient of variation is given above bars.

4. Block dimensions

All the data available on the blocks composing the sails of first-sea ridges are given in Appendix B. These data are actually mean values for the block dimensions measured on each ridge. A summary is given in Table 7. The thickness (h_b), width (w_b) and length (l_b) of the blocks are given per area. In addition, when the block orientation α_b was mentioned, the data were added to the same table.

Table 7.
Summary of the block dimensions and orientation.

	h_b [m]	w_b [m]	l_b [m]	α_b [°]
Beaufort Sea	0.71	1.12	1.21	
Svalbard	0.305	0.2-0.3, 0.68	0.2-0.3, 0.96	69[1]/47[2]
Barents Sea	0.67	0.88	9.47	38.58
East Coast Canada	0.26	1.08	1.35	30.75
Baltic Sea and Gulf of Bothnia	0.24	0.71	0.92	--
Sakhalin	0.15-0.7	--	--	--

1: 0 to 180°
2: 0 to 90°

The blocks from the Barents and Beaufort Seas seem to be much thicker than in other areas, with average values of 0.67 m and 0.71 m, respectively. These higher values are due to some large thicknesses (of 1.9 m in the Barents Sea and several thicknesses over 1 m in Canada). Some extreme values were also reported in Sakhalin. 58% of the measured blocks belonged to Arctic ridges and the rest belonged to the Subarctic ridges.

The block thicknesses were considered more relevant than the surrounding level ice thickness to relate to the sail height. Even though their thickness can decrease as the season progresses, the blocks are considered to be a better representation of the original level ice thickness than the actual ice surrounding the ridge at the time the measurements were done, unless they were done soon after the ridge forms. They also help modeling the formation of the ridge (see Parmeter and Coon, 1972). The dynamics around ridges can be such that the surrounding ice thickness changes with time; more rafting events can occur, or the existing surrounding ice can grow, melt or even disappear. The block thicknesses are plotted against the surrounding level ice thicknesses in Fig. 13. If the parent level ice was the same thickness as that which composed the ridge, then a y=x line should have appeared.

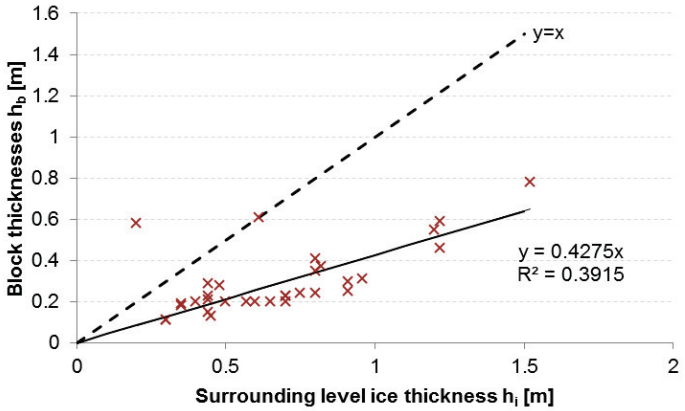

Fig. 13. Block thicknesses vs surrounding level ice thickness

A histogram of all block thicknesses is plotted in Fig. 14. The bars represent 0.1 m intervals. Blocks composed of thicknesses between 0.2 and 0.4 m are most commonly measured. In fact, 58% (22% in the Arctic and 90% in the Subarctic regions) of the average block thicknesses reported are under 0.4 m thick. This contrasts with the Tucker and Govoni (1981) findings that 50% of the measured ridges were composed of ice that was more than 1 m thick (even though these data are included in the present analysis). Fig. 14 shows the distribution of the block thicknesses in the Arctic and Subarctic regions.

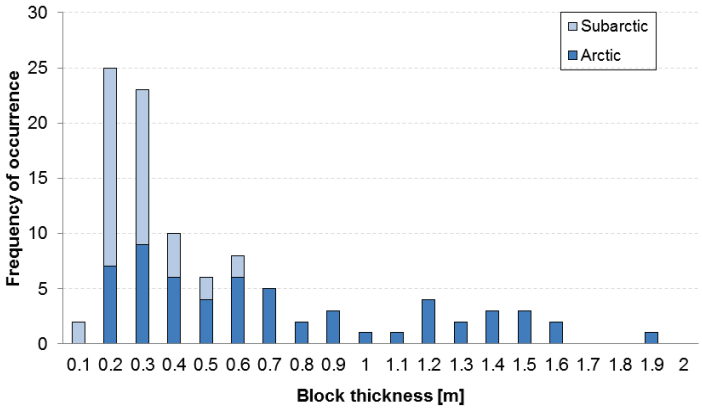

Fig. 14. Histogram of the block thicknesses

We also plotted in Fig. 15 the block thicknesses against the maximum sail height every time they were reported together. We used the average value for the block thicknesses and an average value of the corresponding maximum sail heights. Tucker and Govoni (1981) did a similar study on 30 ridges and developed a relationship between the sail height and the block thickness. They considered several analytical models, but explained that even though a linear or an exponential model would fit better in a statistical sense, they preferred the square root model "because it allows height to go to zero with thickness". They found out that the sail height h_s can be expressed as:

$$h_s = 3.69\sqrt{h_b} \quad (1)$$

Tucker et al. (1984) added data from a field campaign in 1981 to the 30 ridges from Tucker and Govoni (1981) and found a new relationship that was:

$$h_s = 3.71\sqrt{h_b} \quad (2)$$

The correlation coefficient for this model was 0.77 and determined by the least squares procedure. They noted that there was no variation in the morphological parameters of the ice ridges from season to season, which led them to think that the factors that may control the height of a ridge are relatively homogeneous year after year in the same area.

Truscov (undated monograph) repeated this study and added some data from Sakhalin. He reports a relationship such that:

$$h_s = 3.72\sqrt{h_b} \quad (3)$$

Approximately 60 more measurements (from the Baltic Sea, Barents Sea, Canada, Russian Arctic Ocean) were added to the 30 ridges examined by Tucker and Govoni (1981) and a similar study was made in the present paper. The new data did not include those of Truscov (undated monograph) and Tucker et al. (1984) because only the graphs were presented (without any numerical value). A linear, logarithmic and square root models were compared and it appeared that the square root model was the best fit to the data. The new relationship is:

$$h_s = 3.73\sqrt{h_b} \quad (4)$$

It is in excellent agreement with those found by Tucker and Govoni (1981) and Truscov (undated monograph), but the coefficient of determination for Eq.4 R^2=0.49 (and therefore a coefficient of correlation of R=0.70) is such that only 49% of the data can be explained by the present relationship. This low value indicates a consequent scatter in the data

as can be seen in Fig. 15. This model does not indicate whether the ridges have reached their maximum sail height or not.

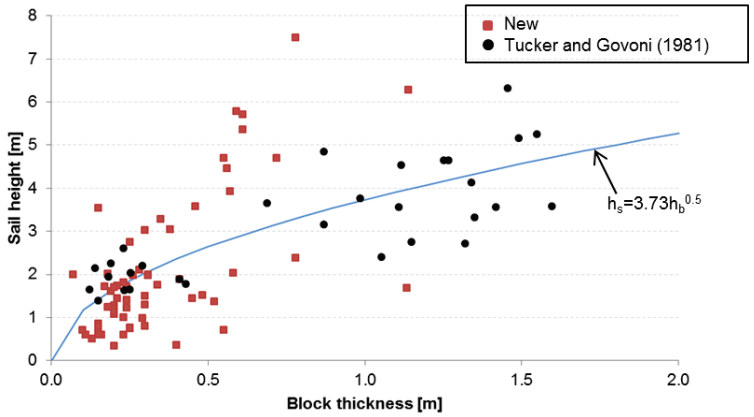

Fig. 15. Maximum sail heights as a function of the corresponding block thicknesses.

The scatter is quite important, but can be explained in several ways. First, as described in the paper of Tucker and Govoni (1981), the ridge building forces vary between ridging events, which means that the speed of the ice drift and the duration of the ridging process vary considerably due to the ocean dynamics and therefore the resulting sail heights may or may not reach their maximum. This could be confirmed by the fact that ridges come from different areas with different ocean regimes.

Note that the ridges were not investigated immediately after their formation, so the measured block thickness may differ from the ice thickness at the time of ridge formation. Strub-Klein and Høyland (2011) report a change of thickness in the blocks up to 5-6 cm within 2 months due to wind and solar erosion.

Parmeter and Coon (1972) have modeled the formation of first-year ridges including a kinematic aspect, which takes into account the continuous movement of the blocks during the ridge formation combined with the force balance and breaking stress calculations. They developed a program modeling the formation of the ridge as a function of many parameters including the ice thickness, stress and stress fracture of the ice, Young's modulus, and the density of sea water and ice. They actually found out that the sail height-to-ice thickness ratio is much greater for thin ice: from the simulations, the sails could indeed be 5 to 6 times thicker than the level ice when it was between 15 and 25 cm thick. On the other hand, the ridges could not possibly be that thick when the level ice was 1 to 4 m. We did not compare the sail height-to-level ice ratios since we had very little data available on the surrounding level ice and the sail height simultaneously, but we did calculate the sail height-to-block thickness ratio. We found that this ratio is decreasing with increasing block thicknesses up to 0.8 m but that it remains constant for block thicknesses h_b>0.8 m (see Fig. 16). For blocks between 15 and 25 cm thick, this ratio was on average 7.5, which is higher than that predicted by the simulations of Parmeter and Coon (1972). There was a poor correlation between the points, but an inverse exponential model could describe the data with a coefficient of determination R^2=0.23.

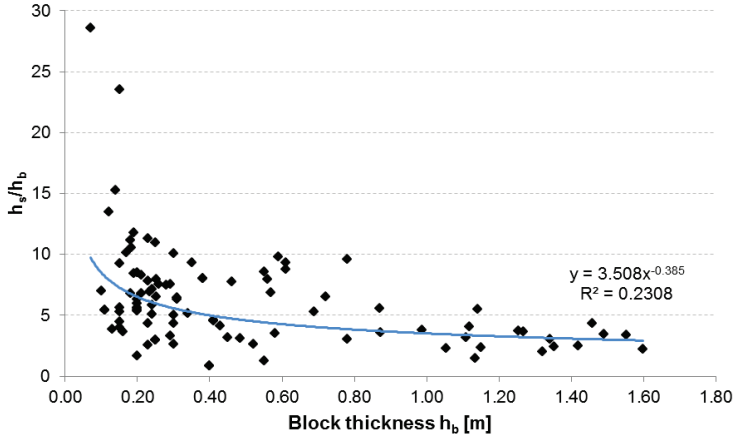

Fig. 16. Sail height-to-block thickness ratio as a function of the block thickness.

5. Consolidation of first-year ridges

5.1 Macroporosity

The macroporosity η_{macro} is an important property of a ridge as it indicates its degree of consolidation and therefore factors into a better estimation of the force a ridge can exert against a structure. It is the volume of any non sea ice material divided by the total volume, excluding the air volume.

$$\eta_{macro} = \frac{V_{sea\ water}}{V_{seawater} + V_{brine} + V_{pure\ ice}} \tag{5}$$

The total porosity η_{total} is the volume of ice divided by the total volume, including air and brine volume in the original sea ice:

$$\eta_{total} = \frac{V_{sea\ water} + V_{brine}}{V_{seawater} + V_{brine} + V_{pure\ ice}} \tag{6}$$

The porosity can be estimated for every part of the ridge and can vary as a function of depth and/or ice temperature. It is often estimated from one cross section, and these results might not be representative of the whole ridge macroporosity, since a single (or several) big void(s) could have been detected or missed when drilling.

A brief description of the various components of a ridge is given in the Introduction. The sail is composed of blocks that accumulate above the water level when ice floes fail against each other. Below the waterline is what we call the keel, which originally is composed of blocks that are pushed underwater during ridge formation. The keel consists of two entities: the consolidated layer and the rubble. The consolidated layer is a solid layer of ice which forms when the water trapped between the blocks freezes. The rubble is the part of the keel that has not yet consolidated, and consists of blocks that are either loose or partly refrozen together.

Appendix C displays the porosities that have been published along with other ridge geometrical parameters, and Table 8 summarizes the average values of the macroporosity for the ridge, the sail, and the keel rubble by region. Sometimes the measurements were given as an average for the ridge instead of an average value for each part of the ridge.

Table 8
Average macroporosities (in %) in the Arctic Basin; *n* is the corresponding number of measurements for each part of the ridge or the ridge itself.

	n	ridge	***n***	sail	***n***	keel rubble
Svalbard	**3**	23.2	**1**	14.0	**1**	7.0
Barents Sea	**9**	27.0	**13**	18.7	**14**	26.9
Russian Arctic Ocean	**3**	13.0	**3**	4.7	**3**	14.3
East Coast Canada	**0**	--	**6**	15.0	**0**	--
Baltic Sea/Gulf of Bothnia	**41**	30.8	**24**	20.0	**24**	29.5
Sakhalin	**3**	16.3	**3**	33.0	**3**	22.0
Total	**59**	22.1	**50**	17.6	**45**	19.9

The macroporosities vary widely from region to region and the values for each individual area differ much from the average value for all ridges. This shows that the geographical region should be considered when attributing a value for the macroporosity for a first-year ice ridge in a numerical model. The geographical location determines the speed of consolidation of the ridge as rafting processes can differ as a function of the ocean dynamics. Note that for most areas very few measurements were available, so one must be careful in applying these results.

5.2 The consolidated layer

The consolidated layer of sea ice ridges raises special interests as it plays an important role in the determination of actions caused by ridges. The ISO codes (ISO 19906, 2010) propose that the horizontal action caused by a first-year ridge F_r is the sum of the action component due to the consolidated layer F_{cl} and the keel action component F_k:

$$F_r=F_{cl}+F_k \quad (7)$$

The action component from the sail is neglected due the small volume of the sail compared to that of the keel (for first-year ridges). The determination of the action component for the consolidated layer is similar to that of level ice. Therefore it requires, amongst other parameters, knowledge on strength and thickness for that layer. The spatial variation of the consolidated layer thickness is an important input in the improvement of the ridge loads predictions.

However, the consolidated layer thickness is believed to depend on the geographical location, therefore the following studies will be divided by region, as each has a different regime. Highly dynamic seas will increase the frequency of rafting and therefore ridges will have thicker consolidated layers (ISO 2010).

5.2.1 Measurement of the consolidated layer thickness

5.2.1.1 Methods

The most common method to determine the thickness of the consolidated layer is by mechanical or thermal drilling. Mechanical drilling can be subjective, as it depends on how the operator feels the ice consistency. Thermal drilling is probably more precise because one can refer to the penetration rate recordings but the interpretation of the data can be difficult like Kharitonov (2008) stated. Another method to measure the consolidated layer consists in installing thermistor strings through the ridge. Sensors are placed along a string to record the temperature at a given frequency. In general, if $T_{recorded}<T_f$, where T_f is the freezing point of the water, the sensor is assumed to be in the consolidated layer. If $T_{recorded}=T_f$, the sensor is assumed to be in the rubble. Blanchet (1998) also mentions the use of the borehole jack as a tool to measure the consolidated thickness.

The interpretation of the data from thermal drilling raises the question: what is the critical value for the penetration rate? The determination of the consolidated layer boundary is also subjective. Finally, the thermistor strings will only give a span where the lower limit of the consolidated layer would be.

The variation of the consolidated layer is not only due to the natural formation of the ridge, but also to the methods used to investigate the ridge, and the interpretation of the data.

5.2.1.2 Data collection

Detailed data of the consolidated layer thicknesses can be found in Appendix A. In addition, for a better comparison between the sail and keel characteristics and the consolidated layer characteristics, Table 9 summarizes the key statistics for the sail, the consolidated layer and the keel by area.

Table 9
Maximum and average thickness for the level ice and the consolidated layer.

	h_i[m]				h_{cl}[m]			
	n	max	***n***	avg	***n***	max	***n***	avg
Bering and Chukchi Seas	**2**	0.61	**49**	0.82	**36**	12.07	**37**	2.09
Beaufort Sea	**6**	1.7	**19**	1.48	**25**	7.62	**10**	1.71
Svalbard waters	**0**	--	**16**	1.05	**20**	5.41	**19**	1.37
Barents Sea	**0**	--	**7**	0.76	**7**	4.53	**12**	1.47
Russian Arctic Ocean	**3**	2.9	**3**	2.13	**0**	--	**1**	0.38
East Coast Canada	**0**	--	**0**	--	**6**	12.4	**20**	1.62
Baltic Sea and Gulf of Bothnia	**0**	--	**37**	0.53	**10**	2.03	**19**	0.86
Offshore Sakhalin	**3**	8.5	**0**	--	**0**	--	**0**	--

One may notice that the maximum value for the Bering and Chukchi Seas is lower than the average value. This is because the maximum level ice thickness has been reported only two times, whereas 49 measurements were available for the average thickness.

The Bering and Chukchi Seas, the Beaufort Sea and the East Coast of Canada have the thickest consolidated layers on average, followed by the Barents Sea and Svalbard. Finally the Baltic Sea/Gulf of Bothnia and the Russian Arctic Ocean all have average consolidated layer thicknesses of less than 1 m. No measurements offshore Sakhalin were obtained.

Except for the East Coast of Canada, the thickest consolidated layers were found where there are strong currents. The observation of sea ice drift maps available from the National Snow and Ice Data Center (NSDIC) and the French ERS Processing and Archiving Facility (CERSAT) indicates the existence of a Beaufort Sea gyre where the ice is strongly drifting in circles and exits through the Fram Strait. The ridges examined in the Bering and Chukchi seas had the thickest consolidated layers. The Bering Sea is delimited in the South by the Aleutian Islands that isolate it from the Subarctic current. There are strong surface currents flowing from the Aleutian Islands to the Strait along the coast, but in the winter time, the currents are orientated towards Russia and down to the Pacific Ocean and can have speeds from 5 to 25 cm/s (Brower et al., 1988). The East Coast Canada showed an abnormally high maximum thickness, but this was from a shear ridge presented in Williams and Kirby (1994) where it seemed that the keel was completely consolidated, and that would be a good explanation for a higher average consolidated layer thickness.

One may think that fjords on Svalbard should be rather closed and therefore isolated from the Gulf Stream, but most of the ridges investigated in that area were located close to a zone of high currents. The Barents Sea is a very open area and therefore more ridging/rafting

events are likely to occur, but the average thickness is slightly lower than that of the Bering, Chukchi and Beaufort Seas, probably because the ridges are smaller in that area.

The Baltic Sea is enclosed by Sweden and Finland with an opening of only 50 km in the South, which limits the currents. Consequently, the ice is less subjected to movements, and rafting events occur less frequently. For the Russian Arctic Ocean, only one measurement was found and it may not be indicative of the typical consolidated layer thicknesses in the area.

5.3 Key ratios

It can be useful to know how the consolidated layer relates to the other ridge dimensions or even to the surrounding level ice, so as to make some predictions when complete measurements are not possible. Therefore the average consolidated layer-to sail, consolidated layer-to-keel, consolidated layer-to-level ice ratios were calculated for the Arctic Ocean, the Barents Sea, the Baltic Sea, Svalbard, the East Coasts in Canada, the Beaufort Sea and the Bering and Chukchi Seas. The maximum-to-average thicknesses were also calculated. However, there was not often many ridges (column "*n*" in Table 10) in each area that were measured so that all the ratios could be calculated. Average ratios were then calculated for all the ridges that were reported with the relevant information. They are summarized in Table 10.

Table 10
Summary of the key ratios for 7 regions

	h_{cl}/h_s			h_{cl}/h_k			h_{cl}/h_i			h_{clmax}/h_{clavg}		
	n	avg	stdev	***n***	avg	stdev	***n***	avg	stdev	***n***	avg	stdev
Bering and Chukchi Seas	**36**	2.48	1.86	**36**	0.6	0.28	**10**	2.55	1.84	**2**	1.31	0.55
Beaufort Sea	**25**	1	0.47	**25**	0.26	0.11	**0**	--	--	**6**	1.31	0.14
Svalbard waters	**20**	2.71	1.76	**20**	0.54	0,2	**15**	1.33	0.21	**19**	1.79	0.73
Barents Sea	**7**	2.02	0.53	**7**	0.53	0.19	**4**	1.83	0.36	**6**	2.21	0.35
Russian Arctic Ocean	**0**	--	--	**0**	--	--	**1**	0.18	--	**0**	--	--
East Coast Canada	**6**	4.23	2.07	**6**	0.74	0.18	**0**	--	--	**6**	2.15	0.79
Baltic Sea and Gulf of Bothnia	**10**	3.82	1.36	**10**	0.29	0.07	**18**	1.7	0.45	**10**	1.56	0.46
Total	**104**	2.71	1.18	**104**	0.49	0.19	**48**	1.52	0.87	**49**	1.72	0.4

The ratios were calculated using the maximum thicknesses for the sail, keel and consolidated layer when they belonged to the same ridge. However, the level ice thickness is more commonly given as an average value, and therefore the ratio h_{cl}/h_i is calculated using the average values for the consolidated layer and the level ice values.
Timco and Burden (1997) and Høyland (2007) reported respectively 1.68 and 2 for the h_{clmax}/h_{clavg} ratios for the consolidated layer. This is well in the range of what we found here: the average ratio is 1.72, the minimum 1.31 is found in the Bering, Chukchi and Beaufort Seas and the maximum 2.21 in the Barents Sea.

The h_{cl}/h_i ratio is also commonly used. Bonnemaire et al. (2003) assumed a ratio between 1.3 and 1.6 in the ridge they investigated in the Barents Sea, based on previous estimations of the level ice thickness in the same area and assuming that the level ice is undisturbed. Høyland (2005) reported a ratio of 2.0 for three ridges in the Barents Sea (including that of Bonnemaire et al., 2003), but also identified the difficulty of measuring an undisturbed level ice close the ridges. This is well in range with the ratio of 1.83 found in Table 10. The average ratio for all the areas is 1.52, which is lower than what was reported by Høyland (2002a) and Høyland (2005) for ridges in the Barents Sea, Svalbard and Baltic Sea. The ISO Codes (ISO 19906, 2010) recommend that in the absence of field data, to assume the consolidated layer is twice as thick as the surrounding level ice which has grown under the

same conditions as the ridge. This is somehow higher than the average ratio of 1.52, which could lead to an overestimation of the level ice thickness in most cases.

The h_{cl}/h_k ratio is interesting as it shows the fraction of consolidated part in the keel. This ratio is quite heterogeneous and the consolidated layer represents between 20 and 75% of the keel. This is probably due to the difference in age of the ridges that were examined as those with a high ratio indicated that the consolidation was advanced and therefore one may think they were older.

The h_{cl}/h_s ratio would be useful as it would enable the rough determination of the consolidated layer thickness by only surveying the sail. The average ratio is 2.71, but as shown in Table 10 the results have a wide range from 1 to 4.23.

5.4 Spatial variation of the consolidated layer.

None of the papers we collected gave the complete set of data for the ridge, and in particular the consolidated layer thickness is seldom mentioned (often because difficult to measure).

Some investigations in the Baltic Sea (Høyland 2002, Høyland et al. 2000), on Svalbard (Høyland and Løset, 1999a&b, Høyland, 2002 a&b, Høyland et al. 2000) and in the Barents Sea (Høyland 2005, 2007, Bonnemaire et al. 2003, Shafrova and Høyland, 2008 and Strub-Klein et al., 2009) included the systematic determination of the consolidated layer thickness. Table 11 summarizes the ridges and the number of cross sections and holes.

Table 11
Ridges with complete measurements of the consolidated layer thickness

Ridge	Location	References	# of cross sections	#holes
1	Svalbard - Van Mijenfjord	Høyland (2002a&b), Høyland et al. (2000), Høyland and Løset (1999a)	10	94
2	Svalbard - Tempelfjord	Høyland and Løset (1999b)	5	143
3	Finland - Marjaniemi	Høyland (2002 a&b), Høyland et al. (2000)	8	81
4	Svalbard - Van Mijenfjord	Høyland (2002a&b), Høyland et al. (2000)	4	37
5	Barents Sea	Bonnemaire et al. (2003), Høyland (2005, 2007)	1	34
6	Barents Sea	Høyland (2005, 2007)	2	40
7	Barents Sea	Høyland (2005, 2007)	3	63
8	Barents Sea	Høyland (2005, 2007)	1	50
9	Arctic Ocean	Shafrova and Høyland (2008)	1	29
10	Barents Sea	UNIS, unpublished data (2007)	4	91
11	Barents Sea	Strub-Klein et al. (2009)	4	80
12	Barents Sea	UNIS, unpublished data (2011)	1	19

Holes were drilled every meter across each ridge. The complete set of data for the cross sections that were made during these investigations has remained unpublished until now. The minimum, maximum and average values of the consolidated layer thickness h_{cl} were calculated for each cross section. These values were compared with the minimum, maximum and average values of the sail height h_s and the keel depth h_k. In addition, the coefficient of variation $CoV=\sigma/\mu$ was calculated for each cross section. This coefficient gives a good indication of the two-dimensional variability of the consolidated layer. Table 12 summarizes the maximum and average thicknesses (and their variation) for each ridge. Høyland (2007) provided the variation of the consolidated layer for ridges 5, 6, 7 and 8.

Table 12
Average, maximum and coefficient of variation of the consolidated layer, sail and keel thicknesses.

	h_{cl} [m]			h_s [m]			h_k [m]		
	mean	max	CoV [%]	mean	max	CoV [%]	mean	max	CoV [%]
Ridge 1	1.54	3.00	32	0.17	1.10	181	2.19	5.94	53
Ridge 2	1.17	5.41	59	0.26	4.50	163	2.32	6.19	51
Ridge 3	0.90	2.03	38	0.27	0.38	19	4.38	5.82	13
Ridge 4	1.19	1.60	12	0.19	1.00	178	3.07	5.00	31
Ridge 5	1.91	5.00	58	--	--	--	--	--	--
Ridge 6	1.73	3.20	30	--	--	--	--	--	--
Ridge 7	1.75	4.01	44	--	--	--	--	--	--
Ridge 8	1.05	2.22	50	--	---	--	--	--	--
Ridge 9	1.98	4.85	57	0.71	3.27	136	6.14	10.73	46
Ridge 10	1.59	4.53	58	0.40	2.33	144	3.21	7.69	64
Ridge 11	1.74	4.50	50	0.49	2.40	113	3.60	7.70	52
Ridge 12	1.52	3.35	45	0.75	1.75	83	6.74	9.05	31

Ridges 1, 2, 3 and 4 were examined throughout one season. Several-cross sections (2 to 6) were drilled at least two times. Ridges 5 to 10 were examined during 3 to 5 days and 1 to 4 cross sections were drilled per ridge. Fig. 17 shows the evolution of the coefficient of variation CoV of h_{cl} for each ridge.

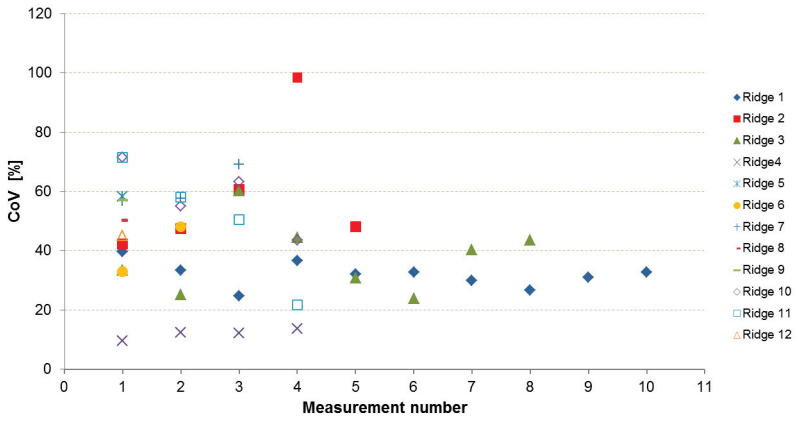

Fig. 17. Evolution of the coefficient of variation for consolidated layer thickness

It is difficult to assess variability for ridges 5, 8, 9 and 12 because there is only one value of the coefficient of variation, but Fig. 17 indicates that ridges 1, 3, 4, and 7 have a coefficient of variation that is quite constant. This means that in the case of ridges 1, 2 and 4, the consolidated layer grew in a very regular manner through the season and across the ridge. This is confirmed by the steadiness of the coefficient of variation of ridges 7 and 10, which was investigated only once in the season but where several cross sections were drilled. Ridge 2 shows a high irregularity on the fourth measurement. This is because this ridge was created from buckling due to a surging glacier. The ice could have been under pressure through the season, disturbing the growth of the consolidated layer. Ridge 11 has a coefficient of variation that is decreasing, but we have not found any reasonable explanation for this.

A study has been made to see if the spacing (or the number of holes) would affect the coefficient of variation for the consolidated layer. Fig. 18 and 19 show the influence of the

spacing/number of holes on the maximum and average values of the consolidated layer thickness within each cross section, and also on the variation.

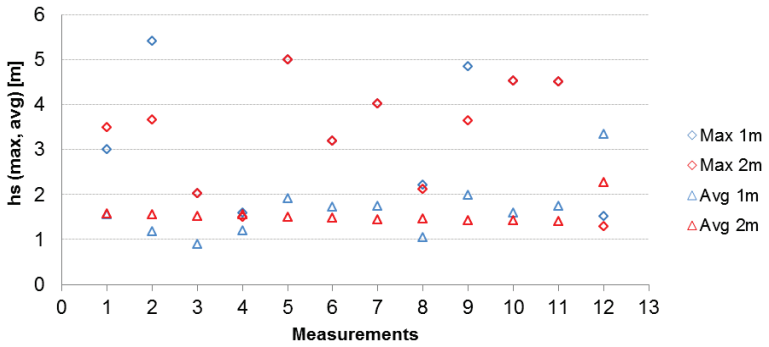

Fig. 18. Maximum and average values of the consolidated layer thickness for cross sections of 1 and 2m spacing.

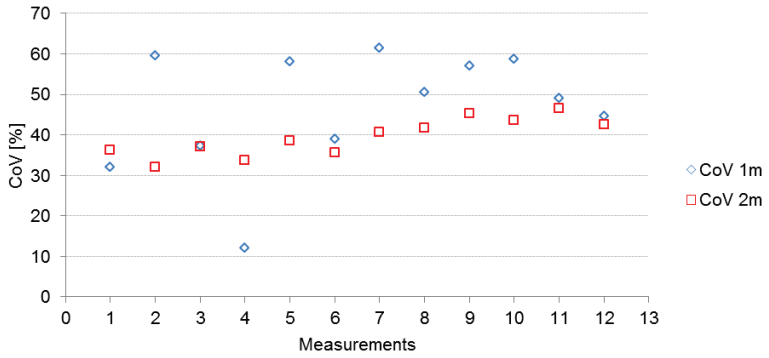

Fig. 19. Coefficient of variation for the consolidated layer thickness for cross sections of 1 and 2m spacing.

A larger spacing does not seem to greatly influence the maximum and average values for the consolidated layer thickness. However, it appears that its variation becomes lower with a higher spacing (see Fig. 19). Fewer measurements could lead to the appearance of less variation and a more homogeneous layer, since some singularities may not be detected. The coefficients of variation for the consolidated layer and the keel are within the same order of magnitude, and are much lower than that of the sail.

Kharitonov (2008) had a different approach of the spatial variation of the consolidated layer. He used the thermal drill to characterize the ridge morphology and more specifically the macroporosity and the consolidated layer thickness. A considerable amount of boreholes was drilled, but the estimation of the consolidated layer thickness is somehow difficult from the data obtained with the thermal drill. He estimated the lower and upper boundaries of the consolidated layer with a probability of accuracy, and also gave estimations of the average thicknesses with their standard deviations for the overall measurements.

4.5 Probability distribution for the consolidated layer thickness.

The ISO Codes (ISO 19906, 2010) state: "*The thickness h_c of the consolidated layer of an ice ridge is locally variable in the vicinity of the structure during an ice action. This can be*

considered if field data is available to create a probability distribution for the consolidated layer thickness." This probability distribution could then be used to determine an average value of h_c for each event, considering the thickness variability in an area defined by the thickness of the structure.

Field campaigns on first-year sea ice ridges in the Barents Sea have been performed by the University Centre on Svalbard from 2002 to 2011. Numerous data on ridge morphologies were collected and amongst them thicknesses of the consolidated layer. In total, 377 measurements were made on the consolidated layers and they were used in a statistical analysis.

Table 13 summarizes the key statistics for the consolidated layer thickness for the years 2002 to 2005, 2007, 2008 and 2011.

Table 13

Thickness of the consolidated layer statistics in the Barents Sea.

n	min [m]	avg [m]	max [m]	stdev [m]	k_v [%]	skewness	kurtosis
377	0.08	1.59	5	0.93	58	0.81	0.67

The histogram of the CL thickness is shown in Fig. 20.

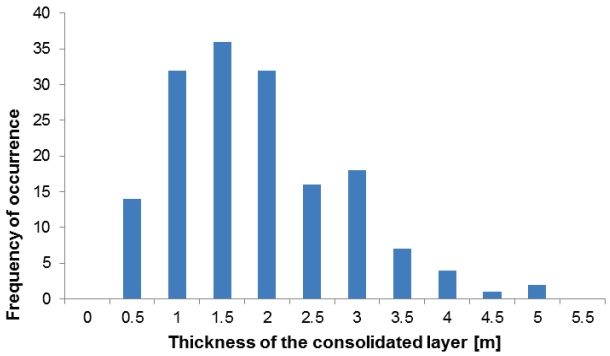

Fig. 20. Distribution of the consolidated layer thickness for first-year sea ice ridges in the Barents Sea.

The histogram of Fig. 20 reveals an asymmetrical distribution with a slight right tail, as indicated by the value of the skewness in Table 13. The value of the kurtosis shows that the distribution is more spread in the tails, and in our case especially the right.

A statistical analysis was made to determine which distribution was the most appropriate to describe the consolidated layer thickness. The normal, lognormal and gamma distributions were compared using QQ-Plots. The key statistical parameters are summarized in Table 14.

Table 14

Defining parameters for the normal, gamma and lognormal distribution

Normal		Gamma		Lognormal	
mean	St. dev.	shape	rate	meanlog	sdlog
1.59	0.93	2.55	1.6	0.26	0.72

The QQ-Plots were represented side by side in Fig.21.

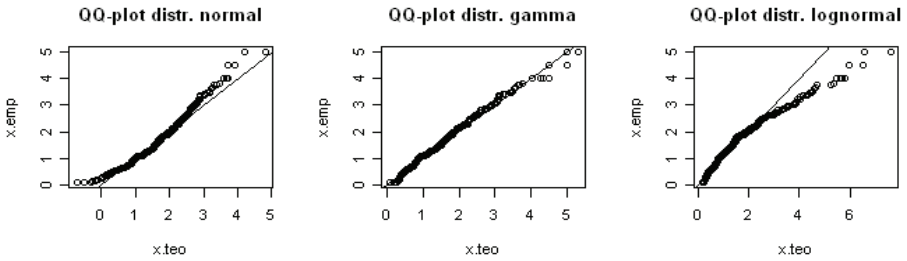

Fig. 21. Comparison of the QQ-Plots for the normal, gamma and lognormal distributions applied to the thickness of the consolidated layer of ridges in the Barents Sea.

There is no doubt from Fig. 21 that the gamma distribution is a very good match apart from the very few outliers in the top right corner, which correspond to right tail of the histogram in Fig. 20.

6. Complementary information

The present article tried to summarize and analyze as many papers related to first-year ridges dimensions as possible. While this catalogue may be incomplete, a large amount of data have been collected to produce a relevant and improved analysis of the shape of floating first-year sea ice ridges. We are aware of papers from the Russian scientists such as Surkov (2001) and Beketsky and Truscov (1995), but often the results are given in graphs with no numerical values so it is difficult to use them. Some papers are in Russian, Chinese or Japanese, and we did not translate these for the current work.

Continuous upward-looking sonar measurements of keel drafts are currently taken in the Beaufort Sea (Melling and Riedel, 2004, Pilkington and Wright, 1991), and at the Confederation Bridge in the Northumberland Strait (Obert and Brown, 2011) where the ice surface is also monitored by video. These keel measurements are very useful but time is required to process the vast quantities of data, and differentiating the type/age of the ice would be problematic in areas with both first- and multi-year ridges. Measurements of sails and keels simultaneously has been done at the Norströmsgrund lighthouse in the Gulf of Bothnia, but possible problems were noted in measuring keel depth with electromagnetic (EM) instrumentation (Bonnemaire and Bjerkås, 2004, and Haas and Jochmann, 2003). EM instrumentation has also been used in the Canadian Arctic but was found to underestimate ridges greater than about 10 m thick (Johnston and Haas, 2011). We examined some sources of continuous ULS and EM data, but for this paper we were only able to use 10 ridge profiles from the Northumberland Strait. Obert and Brown (2011) used ULS data along with surface video to identify ridges.

We had to make some decisions during our analysis, which we tried to keep as logical as possible: what to include, how to include the data, how to use them in the analysis, etc. Data have been collected with different techniques and presented in very many different ways. To analyze them we had to choose those which would be most relevant for industrial purposes. A typical example is the maximum sail and the maximum keel that we only considered if they were belonging to the same ridge cross section.

6.1 Summary of the literature

We also took note of all the other activities that were reported in all the papers we compiled (see Table 1). The tables can be found in Appendix D. Johnston and Barker (2000) published in essence the same results as Croasdale et al. (1999) without the analysis on block dimensions, but they presented the results of thin sections, which is not given in Croasdale et al. (1999) and will be added under their name in the following figures and the table in Appendix D, as they were made on the same ridges. Summarizing figures are presented below. They present the different activities that were performed as well as the dimensions that were measured per area. The total number of authors or groups of authors who have reported on ridge measurements in each area is given above each ensemble of bars as a "Total" value. These authors/groups are those whose work we analyzed, as listed in Table 1.

Fig. 22 shows the number of authors/groups that reported measurements on the sail (h_s), keel (h_k), consolidated layer (h_{cl}), level ice (h_i) and block thickness (h_b).

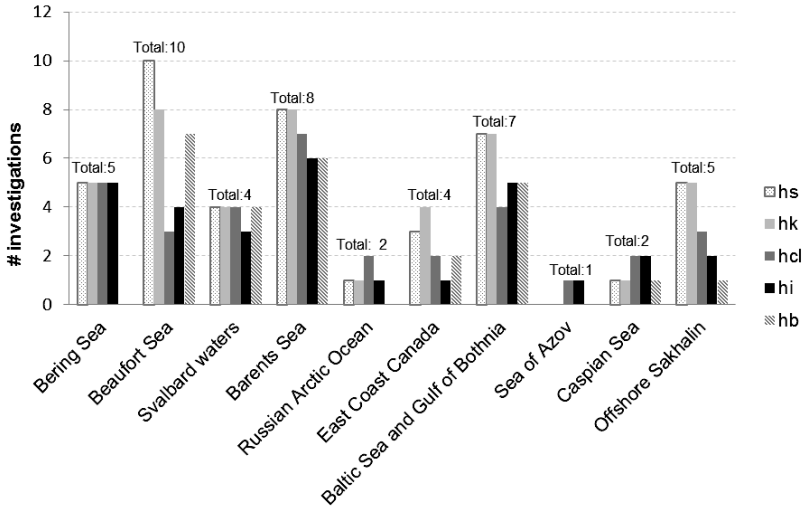

Fig. 22. Number of authors/groups of authors presenting the main ridge dimensions

The keel and sail heights are very commonly measured, except when the study was focusing on a specific part of the ridge, like the blocks (see Tucker and Govoni, 1981, Tucker et al. 1984, Sayed and Frederking, 1989). The consolidated layer is not systematically measured in every area, and especially in the Beaufort Sea, but there exist already a good number of measurements. The level ice data are scarcer in the Beaufort Sea, East Coast Canada and Offshore Sakhalin. There has been no measurement on the block thickness made in the Bering Sea and they are seldom measured in the East Coast Canada, the Russian Arctic Ocean and Offshore Sakhalin.

Fig. 23 shows the number of author/groups of authors that reported measurements on the sail (w_s), keel (w_k) and ridge (w_r) widths, sail (a_s) and keel (a_k) angles and/or the length of the ridge (l_r).

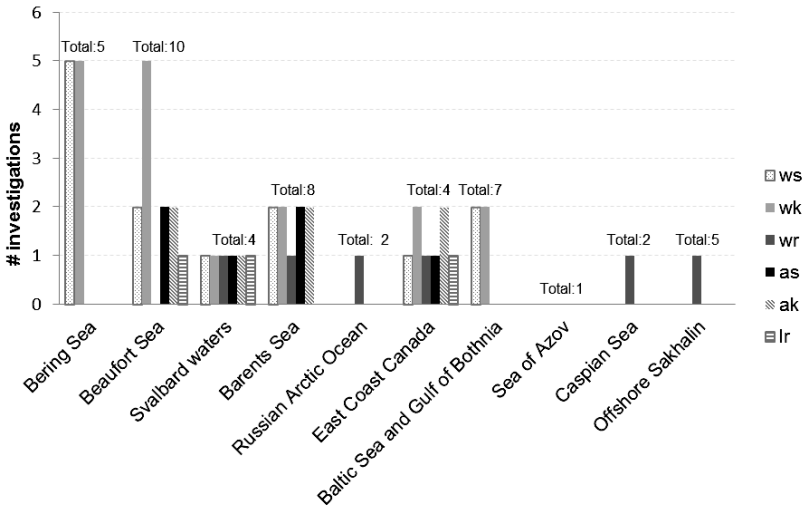

Fig. 23. Number of authors/groups of authors presenting widths, angles and/or length of ridges

The widths and angles of both the sail and keel (or the ridge in general) are not often measured, in any region. The length of the ridge is even more scarcely measured. All the measurements from the Bering and Chukchi Seas included the sail and the keel widths, but did not give any indication on the sail and keel angles, neither on the length of the ridges. In many cases, however, the ridge angles can be calculated from available plots of ridge cross sections (time did not allow for this during the present study). No data could be located for the Sea of Azov. Numerous ridges have been investigated Offshore Sakhalin, but only one paper reported measurements on the ridge widths. Data from Svalbard waters, the Barents Sea and the Baltic Sea/Gulf of Bothnia are lacking too.

Fig. 24 shows the number of author/groups of authors that reported measurements on the macroporosity, volume/area, mechanical testing and/or microstructure (thin sections) of ridges.

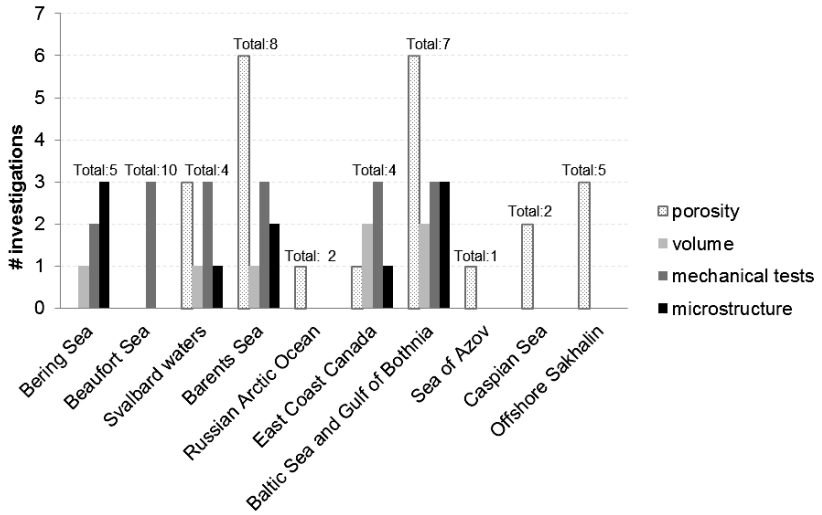

Fig. 24. Number of authors/groups of authors presenting macroporosity, volume, mechanical testings and/or microstructure of ridges

No measurement of the macroporosity has been presented in the papers related to the Bering and Chukchi Seas and the Beaufort Sea. However it is rather well documented on the other areas. The ridge area/or volume is often neglected as well, in all the regions. Mechanical tests were reported everywhere except the Russian Arctic Ocean, the Sea of Azov, the Caspian Sea and Offshore Sakhalin. Very little documentation on the microstructure of ice in ridges is given in the papers we collected.

Fig. 25 shows the number of author/groups of authors that reported measurements of the temperature, salinity and/or density of ridges.

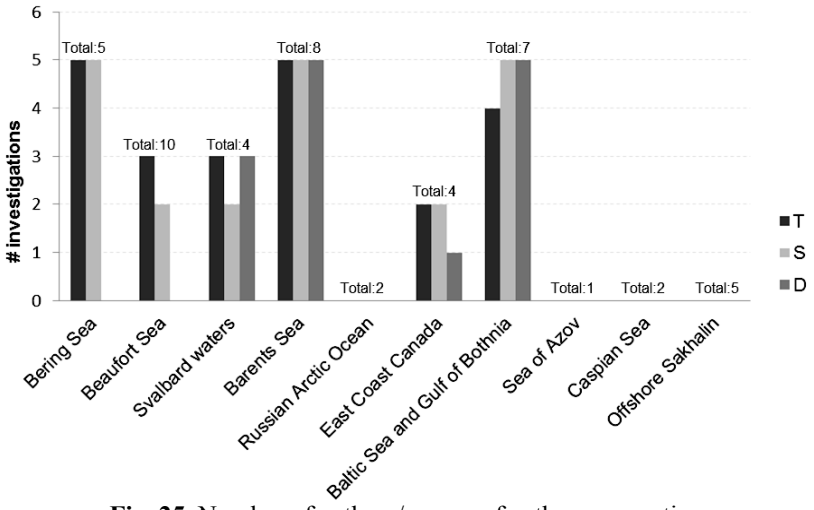

Fig. 25. Number of authors/groups of authors presenting temperature, density and/or salinity in ridges

The temperature and the salinity have been frequently measured for expeditions in the Bering and Chukchi Seas, Svalbard waters, the Barents Sea and the Baltic Sea/Gulf of Bothnia. The density has been seldom measured, but it is also a difficult property to measure accurately with current techniques.

The Russian regions in general are lacking in data concerning the physical properties of ridges.

6.2 Recommendations for further investigations

The figures in Section 6.1 and the tables in Appendix D showed that more measurements should be made on the block thicknesses, as it would help to relate block thickness to sail height, and enable more precise modeling of the formation of a ridge.

The ridge widths, in particular the keel widths, seem to be of high importance, as Obert and Brown (2011) showed that the widest keels produced higher loads on the piers of the Confederation Bridge in Canada. To that effect, ridge angles should be measured more systematically as well.

From the literature we collected, the Russian regions (Arctic Ocean, Sea of Azov, Caspian Sea and Offshore Sakhalin) lack data on the physical (temperature, density, salinity) and mechanical properties. Very little data is available on ridge widths and no precise measurement of the sail and keel widths and angles were given. As these areas are crucial for oil and gas development and navigation, it would be of high interest to investigate these properties to improve models for ridges.

The consolidated layer thickness is a crucial element in terms of ridge actions against Arctic offshore structures, yet it is not always reported. We examined the variation of the consolidated layer thickness, but what about its strength? Shafrova and Høyland (2008) presented a 2D map of ridge strength from uniaxial compressive tests. Blanchet (1998) and Yashima and Tabuchi (1999) performed borehole jack tests in the consolidated layer of ridges. This would be a good technique to estimate the spatial and temporal variation of the strength of the consolidated layer in a simpler and more accurate way than uniaxial tests.

We also noticed that ridges are generally drilled across their width (and most of the time only once), which gives only a two-dimensional picture. One could also try to establish both longitudinal and cross-sectional profiles for a better mapping of the keel, as the maximum keel could be missed if drilling only one cross section.

Continuous ice keel draft measurements, such as those carried out in the Beaufort Sea (Melling and Riedel, 2004 and Pilkington and Wright, 1991), the Confederation Bridge in Northumberland Strait (Obert and Brown, 2011), and the Norströmsgrund lighthouse in the Gulf of Bothnia (Bonnemaire and Bjerkås, 2004) can be used to calculate the concentration of ridges in a given area. Ideally, sails should be measured simultaneously, but it is difficult to install instruments far offshore. Monitoring of both sails and keels has been done at the Norströmsgrund lighthouse and Confederation Bridge.

Some work that is related only to mechanical tests performed on ridges has been done, such as Croasdale et al. (2001) in East Coast Canada, Heinonen (2004) in the Baltic Sea/Gulf of Bothnia, and Liferov and Høyland (2004) on Svalbard. There is a very wide variety of tests that can be done and that have been done, which makes it difficult to create a single database for ridge strength.

We know that the resources to investigate the ice and more particularly the ice ridges are limited regarding time, manpower and economic matters. In addition, weather conditions often change quickly, making the fieldwork even more difficult. It is almost impossible to measure everything at the same time for every expedition.

7. Conclusions

The dimensions of floating first-year ridges have been collected and analyzed. This study covered a very large area of ice infested waters; ridges were studied from the Bering and Chukchi Seas, Beaufort Sea, Svalbard waters, Barents Sea, Russian Arctic Ocean, temperate East Coasts of Canada, Baltic Sea and Gulf of Bothnia, Sea of Azov, Caspian Sea and Offshore Sakhalin. This analysis is an extension of previous reviews published by Sudom et al. (2011) and Strub-Klein (2011) and previously Timco and Burden (1997). In addition, we have presented the raw data are in Appendices for the convenience of future analyses. Data from 45 sources and over 300 ridges were extracted and they are summarized below:

- The maximum reported sail height was 8 m offshore Sakhalin, and the average peak sail height was 2.0 m based on 356 profiles.
- The overall average sail height (e.g. averaged over the width of the ridge) is 0.7 m, based on 78 profiles.
- The maximum reported keel depth was 28 m in the Baltic Sea, with comparable keel depths measured in the Beaufort and Bering/Chukchi Seas. The Beaufort Sea was found to have the greatest number of first-year ridge keel depths greater than 20 m (n=6).
- The overall average keel depth (e.g. averaged over the width of the ridge) was 4.51 m based on 72 profiles.
- The average sail width was 12 m and the average keel width was 36 m.
- The best fit correlation for keel depth and sail height depends on the region. For Arctic regions, a linear relationship fits best: $h_k = 3.84h_s$. For temperate or Subarctic regions, the data was better fit by a power relationship, $h_k = 6.14h_s^{0.53}$.
- The maximum keel-to-sail ratios were calculated; overall, h_k/h_s= 5.17 with a standard deviation of 2.96, based on 308 values; the ratios were governed by a lognormal distribution. The average ratio is higher for Subarctic regions: h_k/h_s= 6.39; for Arctic regions, h_k/h_s= 4.34.
- The ratios of average keel to average sail were calculated; $h_{k,avg}/h_{s,avg}$ = 9.96 with a standard deviation of 5.36, based on 68 values.
- On average, the keel width to sail width ratio is 6.75.
- The sail width to sail height ratio is 3.75 on average; the relationship can also be described by the power equation $w_s = 6.6h_s^{0.69}$.
- Keel width was compared to maximum sail and keel thickness, but the data are scattered. The keel width to keel depth ratio is 4.85 on average; the relationship can also be described by $w_k = 4.28h_k$ or $w_k = 7.19h_k^{0.72}$. The keel width to sail height ratio is on average 20.9; the relationship can also be described by $w_k = 16.7h_s$ or $w_k = 19.2h_s^{0.76}$.
- The variation within 5 individual ridges has been compared with the overall variability of all ridge cross sections. Ridge cross-sectional geometry can vary greatly along the length of a ridge, even over a short distance. The sail heights for individual ridges showed more variation than the keel depths. For ridges in all regions, the sail heights display approximately the same coefficient of variation as the keel depths.
- All the block dimensions (width, length, thickness and even angle of inclination) were compiled. The block thicknesses and the sail height correlated well with a square root model, which was in excellent agreement with previous studies.
- The average macroporosity for a first-year ridge was calculated to be 22 % based on 58 values. The average sail macroporosity was 18%, based on 49 values and the average rubble macroporosity was 20%, based on 44 values.

- The average consolidated layer for the ridge was 1.36 m based on 118 values, but this varies strongly from area to area. The average h_{cl}/h_i ratio was 1.52, which is lower than what was previously predicted.
- When several cross sections were drilled and the data were available, the spatial variation of the consolidated layer thickness was examined. It appeared that the variation did not change with time, which means that the ridges were developing evenly in width. A higher spacing between the measurements seemed to affect the variation as it decreased with an increasing distance between each borehole.
- Several ridges were investigated thoroughly in the Barents Sea by UNIS, which in the end provided 377 measurements of the consolidated layer thickness. A statistical analysis showed that the consolidated layer thickness was governed by a gamma distribution.

Gaps of knowledge were identified from the papers and reports we compiled. Although there has been quite a good collection of data in the Bering and Chukchi Seas, there exists no measurement of the blocks at all. In general, the block dimensions are not sufficiently reported. They correlate to the sail height with a square root model, which does not indicate whether the ridges have reached their maximum sail height or not. A model with an upper bound curve could be more relevant.

The widths are also seldom mentioned, which is important to note since keel widths can be crucial in the load determinations.

The Russian regions provide information on the main ridge dimensions but lack totally of data on the physical and mechanical properties.

The consolidated layer, which is a very important element of the load determinations, is not systematically reported. It is believed that the spatial variation of its thickness and strength is essential.

A better mapping of the keels would be to perform longitudinal and cross-sectional profiles of the same ridge.

Fieldwork in ice infested waters is difficult and requires time, manpower and sufficient economic resources, which are very hardly available for many complete investigations of ridges.

Acknowledgements

We would like to thank Dr. Robert Frederking and Professor Knut Høyland for their help and advice; Dr. Bjørnar Sand and Prof. Peter Wide at Norut Northern Research Institute, Professor Knut Høyland at the Norwgian University of Technology (NTNU) and the University Centre on Svalbard (UNIS), and the Canadian Hydraulics Centre (CHC) for providing private and valuable data; Berit Jakobsen, the UNIS librarian, for excellent help finding some grey literature; and of course all the ice researchers for their contribution to the knowledge on ice ridges that we have summarized in this work.

References

Ahlenius,. H. (2006). Arctic map, political. UNEP/GRID-Arendal.
http://maps.grida.no/go/graphic/arctic-map-political

Banke, E. (1982). First-year pressure ridges investigations near Booth Island, N.W.T. during Spring 1978. Prepared for Dome Petroleum Ltd. by Martec Ltd. (Held at NRC-CHC).

Barker A. et al. (2008). Surveying a four-week old first-year ridge. Proceedings of the 19th IAHR International Symposium on Ice, Vancouver, British Columbia, Canada 2008. pp1263-1272.

Beketsky, S.P., Truskov, P.A. (1995). Internal structure of ice pressure ridges in the sea of Okhotsk. Proc. of the 13th Int. Conference on Port and Ocean Engineering under Arctic Conditions (POAC), vol. 1. Peterburgkomstat, Murmansk, Russia, pp. 109-111.

Beketsky, S.P. et al. (1996). Structure of hummocks offshore of Northern Sakhalin. Proceedings of the 6th International offshore and Polar Engineering Conference (1996). Los Angeles, USA. Vol. 2 pp 398-400.

Blanchet, D. (1998). Ice loads from first-year ice ridges and rubble fields. Canadian Journal of Civil Engineering **25**(1998), pp. 206-219.

Bonnemaire, B. et al. (2003). An ice ridge in the Barents Sea, part I: morphology and physical parameters in-situ. Proceedings of the 17th International Conference on Port and Ocean Engineering under Arctic Conditions (POAC) 2003. Trondheim, Norway. Vol.2, pp. 559-568.

Bonnemaire, B. and Bjerkås, M. (2004). Ice ridge-structure interaction, Part I: Geometry and failure modes of ice ridges. Proceedings of the 17th International Symposium on Ice. St Petersburg, Russia.

Bowen, R.G. and Topham, D.R. (1996). A study of the morphology of a discontinuous section of a first-year arctic pressure ridge. Cold Region Science and Technology **24** (1996). Pp. 83-100.

Brower, W.A., et al.(1988). Climatic Atlas of the Outer Continental Shelf Waters and Coastal Regions of Alaska NCDC/NESDIS/NOAA, Arctic Environmental and Data Center, University of Alaska,Anchorage, AK.

Burden, R.P. and Timco, G.W. (1995). A catalogue for sea ice ridges. Technical report TR-1995-27. National Research Council Canada – Institute for marine dynamics. April 1995.

Croasdale, K.,R. et al. (1999). Field study of Ice Characteristics off the Western Coast of Newfoundland. Volume 1 .Public Data. PERD/CHC Report 2-70.

Croasdale, K. et al. (2001). In-situ measurements of the strength of first-year ice ridge keels. Proceedings of the 16th International Conference on Port and Ocean Engineering under Arctic Conditions (POAC) 2001. Ottawa, Ontario, Canada. Vol.3 pp. 1445-1454.

Evers, K.U. (1986). Erste Eisbrechtechnische Expedition mit FS Polarstern. Schlussbericht, Basnd III Kapittel 13: Geometrie und Konsolidierungsgrad der von “Polarstern” durchbrochenen Presseisrücken. Hamburgische Schiffbau Versuchanstalt. Hamburg.

Gladwell, R.W. (1976). Field studies of eight first-year se ice pressure ridges in the southern Beaufort Sea. APOA Project no.75. IPRT-8ME-76. Imperial Oil Limited. Production Department. Calgary, Alberta.

Haas, C. and Jochmann, P. (2003). Continuous EM and ULS Thickness Profiling in Support of Ice Force Measurements. Proceedings of the 17th International Conference on Port and Ocean Engineering under Arctic Conditions, June 16-19, 2003, Trondheim, Norway, Vol. 2, p. 849

Heinonen, J. (2004). Constitutive Modeling of Ice Rubble in First-Year Ridge Keel. Dissertation for the degree of Doctor of Technology. Espoo 2004. VTT Publications 536. 142p.

Høyland, K.V. (2002a). Consolidation of first-year sea ice ridges. Journal of Geophysical Research. Vol. 107, No. C6, pp. 15_1-15_7.

Høyland, K.V. (2002b). Simulations of the consolidation process in first-year sea ice ridges. Cold Regions Science and Technology **34**(2002), pp.143-158.

Høyland, K.V. (2005). Ridges in the Barents Sea. Proceedings of the 18th International Conference on Port and Ocean Engineering under Arctic Conditions (POAC) 2005. Potsdam, Germany. Vol.2, pp. 949-960.

Høyland, K.V. (2007). Morphology and small-scale strength of ridges in the North-western Barents Sea. Cold Regions Science and Technology. 48(2007), pp. 169-187.

Høyland, K.V. and Løset, S. (1999a). Monitoring and observation of the formation of a first-year sea ice ridge-field. Proceedings of the 15th International Conference on Port and Ocean Engineering under Arctic Conditions (POAC) 1999. Helsinki, Finland.

Høyland, KV and Løset, S (1999b). Measurements of temperature distribution, consolidation and morphology of a first-year sea ice ridge. Cold Region Science and Technology **29**(1999), pp. 59-74.

Høyland, K.V. et al. (2000). LOLEIF ridge experiments at Marjaniemi: the size and the strength of the consolidated layer. Proceedings of the 15th International IAHR Symposium on Ice (2000), Gdansk, Poland. Vol.1, pp. 45-52.

ISO 19906 TC 67(2010). Petroleum and natural gas industries - Arctic offshore structures. International Organization for Standardization.

Johnston, M. and Barker, A. (2000). Microstructure of first-year sea ice ridges. Technical Report HYD-TR-043. Canadian Hydraulic Centre, Ottawa, Canada.

Johnston, M.E., and Haas, C. (2011) Validating helicopter-based EM (HEM) thicknesses over very thick multi-year ice. Proceedings of the 21st International Conference on Port and Ocean Engineering under Arctic Conditions, July 10-14, 2011, Montreal, Canada, Paper POAC11-132.

Johnston, M., et al. (2009). Multi-year ice thickness: knowns and unknowns. Proceedings of the 20th International Conference on Port and Ocean Engineering under Arctic Conditions, June 9-12, 2009, Luleå, Sweden, Paper POAC09-120.

Kankaanpää, P. (1989). Structure of first-year pressure ridges in the Baltic Sea. Proceedings of the 10th International Conference on Port and Ocean Engineering under Arctic Conditions (POAC), 1989. Luleå, Sweden. Vol.1, pp.87-102.

Kankaanpää, P. (1997). Distribution, morphology and structure of sea ice pressure ridges in the Baltic Sea. Fennia, Internal Journal of Geography. Vol.175, pp. 139-240. Geographical Society of Finland. Helsinki, Finland.

Kharitnonov, V. V. (2008). Internal structure of ice ridges and stamukhas based on thermal drilling data. Cold Regions Science and Technology **52**(2008). Pp. 302-325.

Kharitonov, V. V. and Morev V.A. (2005). Research of the internal structure of ridges of the Central Arctic by electrothermal drilling method. Proceedings of the 18th International Conference on Port and Ocean Engineering under Arctic Conditions (POAC) 2005. Potsdam, New York. Vol.2, pp. 917-926.

Krupina, N.A. et al. (2009). Full-scale ice impact study of icebreaker Kapitan Nikolaev: General Descritpion. Proceedings of the 19th International Offshore and Polar Engineering Conference (2009), Osaka, Japan.

Leppäranta, M. (2011). The drift of sea ice, 2nd ed. Heidelberg: Springer-Verlag.

Leppäranta, M. and Hakala, R. (1992). The structure and strength of first-year sea ice ridges in the Baltic Sea. Cold Regions Science and Technology. 20(1992), pp. 295-311.

Leppäranta, M. et al. (1995). The life story of a first-year sea ice ridge. Cold Regions Science and Technology. 23(1995), pp. 279-290.

Liferov, P. and Høyland, K.V. (2004). In situ ice ridge scour tests: experimental set up and basic result. Cold Regions Science and Technology. **40(**2004), pp. 97-110.

Lowings, M.G. and Banke, E.G. (1983). Consolidation of Pressure Ridges in First Year Landfast Ice Eastern Beaufort Sea, Winter 1981-1982. Prepared for Gulf Canada by Martec Ltd. (Held at NRC-CHC).

McGonigal, D. (1978). First-year pressure ridge study Beaufort Sea, April-May 1978. Frontier Research Division, Gulf Canada, Calgary, Canada.

Melling, H. (2002). Sea ice of the northern Canadian Arctic Archipelago. Journal of Geophysical Research, Vol. 107, No. C11, 3181, doi:10.1029/2001JC001102.

Melling, H. et al. (1993). Topography of the upper and lower surfaces of 10 hectares of deformed sea ice. Cold Region Science and Technology **21**(1993), pp. 349-369.

Melling, H. and Riedel, D.A. (2004). Draft and Movement of Pack Ice in the Beaufort Sea: A Time-Series Presentation April 1990-August 1999. Can. Tech. Rep. Hydrogr. Oc. Sci. 238, v + 24 pp.

Mironov, Y. et al. (1998). Winter 1998 study of ice ridge geometry offshore Sakhalin Island. Proceedings of the 15th International Conference on Port and Ocean Engineering under Arctic Conditions (POAC) 1998, Helsinki, Finland.

Mironov, Y.U. and Porubayev, V.S. (2005). Structural peculiarities of ice features on the offshore of the Caspian Sea, the Sea of Okhotsk and the Pechora Sea. Proceedings of the 18th International Conference on Port and Ocean Engineering under Arctic Conditions (POAC), Potsdam, Germany, Vol.2 pp. 483-492.

Obert, K.M. and Brown, T.G. (2011). Ice ridge keel characteristics and distribution on the Northumberland Strait. Cold Regions Science and Technology **66**(2011), pp. 53-64.

Palosuo, E. (1975). The formation and structure of ice ridges in the Baltic. Winter Navigation Research Board. Report Nr 12. University of Helsinki, Department of Geophysics.

Parmerter, R. R. and Coon, M.D. (1972). Model of pressure ridge formation in sea ice. Journal of Geophysical Research. Vol. 77, No. 33, pp. 6565-6575.

Pilkington, G.R. and Wright, B.D. (1991). Beaufort Sea ice thickness measurements from an acoustic, under ice, upward looking ice keel profiler. Proceedings of the First International Offshore and Polar Engineering Conference, Edinburgh, August 11-16, 1991.

Prinsenberg, S., and Holladay, S. (2009). Ice thickness measurements with a miniature electromagnetic sensor sled. Proceedings of the Nineteenth (2009) International Offshore and Polar Engineering Conference, Osaka, Japan, June 21-26, 2009, pp. 666-671.

Sand, B. et al. (2011). ColdTech 2011 – Field studies and laboratory work. Norwegian Research Council Project no. 195153, Sustainable Cold Climate Technology Technical report rt2-o011-cc. Confidential report held at Norut Narvik.

Sayed, M. And Frederking, R.M.W. (1989). Measurement of ridge sails in the Beaufort Sea. Canadian Journal of Civil Engineering 16 (1989), pp. 16-21.

Shafrova, S. and Høyland, K.V. (2008). Morphology and 2D spatial strength distribution in two Arctic first-year sea ice ridges. Cold Regions Science and Technology **51**(2008), pp. 38-55.

Sisodiya, R.G. and Vaudrey, K.D. (1981). Beaufort Sea first-year ice features survey - 1979. Proceedings of the 6th International Conference on Port and Ocean Engineering under Arctic Conditions. Quebec, Canada. Vol.2, pp. 755-764.

Strub-Klein, L. (2011). A review of the morphological and mechanical properties of first-year ice ridges. Proceedings of the 21st International Conference on Port and Ocean Engineering under Arctic Conditions (POAC). Montreal, Canada. 2011. Paper no POAC11-042.

Strub-Klein, L. et al. (2009). Physical properties and comparison of first- and second-year sea ice ridges. Proceedings of the 20th International Conference on Port and Ocean Engineering under Arctic Conditions (POAC), 2009, Luleå, Sweden.

Strub-Klein, L. and Høyland, K.V. (2011). One season of a first-year sea ice ridge investigations. Winter 2009. Proceedings of the 21st International Conference on Port and Ocean Engineering under Arctic Conditions (POAC). Montreal, Canada. 2011. Paper No. POAC11-043.

Sudom, D. et al. (2011). Analysis of first-year and old ice ridge characteristics. Proceedings of the 21st International Conference on Port and Ocean Engineering under Arctic Conditions (POAC). Montreal, Canada. 2011. Paper No. POAC11-164.

Surkov, G.A. (2001). Thickness of the consolidated layer in first-year hummocks. Proceedings of the 16th International Conference on Port and Ocean Engineering under Arctic Conditions (POAC), Ottawa, Ontario, Canada, pp. 245-252.

Surkov, G. and Truskov, P. (1995). Ice pressure ridges and stamukhas offshore of Sakhalin. Proceedings of the International Conference on Port and Ocean Engineering under Arctic Conditions (1995). St Petersburg, Russia. Vol.2, pp. 140-142.

Timco, G.W. and Burden, R.P. (1997). An analysis of the shape of sea ice ridges. Cold Regions Science and Technology **25**(1997), pp. 65-77.

Timco, G.W. et al. (2000). An overview of first-year sea ice ridges. Technical Report HYD-TR-047. PERD/CHC Report 5-112. August 2000.

Truskov (no date). Monograph on ice formation, Sakhalin Island. Held at NRC-CHC.

Tucker. W.B.III and Govoni, J.W. (1981). Morphological investigations of first-year sea ice pressure ridge sails. Cold Regions Science and Technology 5(1981), pp.1-12

Tucker, W.B. III et al. (1984). Structure of first-year pressure ridge sails in the Prudhoe Bay Region. The Alaskan Beaufort Sea: Ecosystems and Environments. Edited by P.W. Barnes, D.M. Schell, E. Reimnitz. Academic Press, Inc. ISBN 0-12-079030-0.

UNIS Report (2008). Scientific cruise with R/V Lance May 5-15, 2008. Student report from the course AT 208: Thermo-mechanical properties of materials. The University Centre on Svalbard.

Vaudrey, K. D. (1979). Beaufort Sea First-year Ice Features Survey - 1979 Volume 1: Field Investigation. Held at NRC-CHC.

Veitch, B. et al. (1991a). Field observations of ridges in the northern Baltic Sea. Proceedings of International Conference on Port and Ocean Engineering under Arctic Conditions (1991), St. John's Newfoundland. Vol.1, pp.381-400.

Veitch, B. et al. (1991b). Field Measurements of the Thermodynamics of an ice ridge. Helsinki University of Technology, Laboratory of Naval Architecture and Marine Engineering, Report No. M-114.

Voelker, R.P. et al. (1981a). Assessment of ice conditions in the South Bering Sea Based on April 1980 USCG Polar Class Trafficability Test Data, Vols. I and II. Prepared by ARCTEC

Inc. Report MA-RD-920-80094, US Department of Commerce/Maritime Administration/Office of Commercial Development. Springfield, Virginia, USA.

Voelker, R.P. et a.l (1981b). Winter 1981 Trafficability tests of the USCGC Polar Sea. Vol. 2.. Prepared by ARCTEC Inc. for U.S. Department of Transportation/Maritime Administration, Springfield, Virginia, USA.

Voelker et al. (1982). Arctic Deployment of USCGC polar Star- Winter 1982 Volume 2 Environmental Data. ARCTEC Inc Report No. 730B for U.S. Department of Transportation/Maritime Administration, Springfield, Virginia, USA.

Voelker et al. (1983). Arctic Deployment of USCGC Polar Sea Winter 1983 Volume 2 Environmental Data. ARCTEC Inc Report No. 800C for U.S. Department of Transportation/Maritime Administration, Springfield, Virginia, USA.

Voelker et al. (1984). Bering Sea Data Collection February/March 1984 Volume 1 Environmental Data. ARCTEC Inc Report No. 1005C for U.S. Department of Transportation/Maritime Administration, Springfield, Virginia, USA.

Williams, F.M. and Kirby, C.S. (1994). Ice features in Northumberland Strait. National Research Council Canada Report TR-1994-08, St. John's Newfoundland.

World Meteorological Organization (1970). WMO sea ice nomenclature (supplement No 5.1989). Technical Report MO No. 259.TP.145. World Meteorological Organization. Geneva, Switzerland.

Yashima, N. and Tabuchi, H. (1999). Field survey of pressure ridges in offshore Sakhalin. Proceedings of the International Workshop on Rational Evaluation of Ice Forces on Structures, Mombetsu, Japan, pp 11-20.

APPENDICES

A. Ridge dimensions

A.1. Bering and Chukchi Seas

References	Ridges	CS/#holes	h_s [m]		h_k [m]		h_i [m]			h_{ci} [m]			w [m]	
			max	avg	max	avg	min	max	avg	min	max	avg	sail	keel
Voelker et al. (1981a)	Ridge 1		1.10		4.36				0.61, 0.36			2.59	7.62	9.14
	Ridge 2		1.07		2.89				0.40			2.89	7.31	16.46
	Ridge 3		0.61		1.83				0.3, 0.53			1.22	3.05	10.67
	Ridge 4		1.37		4.27				0.91, 0.46			2.89	9.75	22.86
	Ridge 5		1.74		9.75				1.58, 0.46			5.70	15.24	19.81
	Ridge 6		1.74		7.25				0.76, 0.43			--	29.56	48.16
	Ridge 7		0.36		2.07				0.76, 1.22			2.07	1.83	10.36
	Ridge 8		1.19		3.35				0.85, 0.73			1.46	4.57	15.24
	Ridge 9		0.67		2.29				1.07, 0.76			2.29	7.62	21.34
	Ridge 10		0.52		1.52				0.4, 0.46			1.52	6.40	12.50
	Ridge 11		0.70		2.19				0.67, 0.36			1.34	7.62	15.54
	Ridge 12		0.97		3.26				0.61			1.55	6.10	16.76
	Ridge 13		1.37		5.00				2.13, 2.29			3.81	2.44	21.34
	Ridge 14		0.91		1.89				1.07, 0.46			1.89	6.10	7.62
	Ridge 15		0.97		2.93				0.36			1.28		
	Ridge 16		1.37						1.07			3.35	9.14	
	Ridge 17		0.76		2.44				0.36,0.46			0.91	8.23	12.50
	Ridge 18		1.92		3.35				0.76,0.67			2.89	11.23	33.05
	Ridge 19		1.68		4.21				1.34,0.82			4.21	8.84	24.38
	Ridge 20		0.79		3.05				0.97,0.91			1.52	4.27	19.20
	Ridge 21		0.43		3.20				0.46,0.76			3.20	6.40	12.50
	Ridge 22		0.97		4.57				0.46,1.04			1.68	7.62	23.16
	Ridge 23		1.37		3.47				0.46,0.70			2.74	7.92	20.42
	Ridge 24		1.07						1.13			1.89	7.31	18.29
	Ridge 25		0.91						1.13			1.22	3.66	14.02
	Ridge 26		0.92		2.74				0.36,0.4			0.76		
	Ridge 27		2.13		7.00				0.7,0.4			--	10.07	25.91
	Ridge 28		1.92		6.25				--			--	8.23	24.38
	Ridge 29		1.71		5.33				0.36-0.61			--	7.92	18.59
	Ridge 30		1.92		5.33				0.61-0.43			1.52	7.31	22.55
	Ridge 31		1.71		5.33				0.76			--	5.79	22.86
	Ridge 32		0.52		0.91				0.46-0.76			0.91	4.27	10.67
	Ridge 33		0.61		2.44				0.91			0.91	3.05	10.36
	Ridge 34		0.91		3.66				0.61			1.07	6.10	21.03
	Ridge 35		0.67		2.74				1.37,0.36			1.52	6.40	19.81
	Ridge 36		0.70		2.22				0.61,0.3			0.91	4.27	19.20
	Ridge 37		1.83		3.35				0.61,0.36			2.13	2.74	18.29
	Ridge 38		0.46		2.44				0.3,0.61			1.46	3.05	12.80
	Ridge 39		0.91		3.41				0.91			1.34	3.05	21.34
	Ridge 40		0.70		2.13				0.75,0.61			1.58	4.27	19.20
Voelker et al. (1981b)	Ridge 1		1.64	0.31	3.96	2.50			0.64		2.22	1.31	29.87	42.37
	Ridge 10		2.29	0.85	10.21	6.10			0.61				18.29	25.00
	Ridge 12		4.30	2.04	7.71	6.13			2.29,5.18		5.52	6.00	24.38	36.88
Voelker et al (1982)	1		1.46		2.16				0.70		1.55			
	2		2.38		5.85				0.30		2.26			
	0304		2.83		8.60				0.91		3.26			

	5		1.80	4.94		0.43	1.34	8.53	18.29
	6		2.01	8.66		0.46		6.71	27.13
	7		2.16	6.43		0.46	1.58	7.62	
	8		0.70	0.88		0.55	0.76	3.35	3.60
	9		2.04	6.68		0.58		7.01	
	10		1.07	2.29		0.55	2.16	3.05	8.02
	11		0.30	1.13		0.76	1.13		
	13		0.91	4.88		0.49	1.65		
	14		2.44	10.24		0.46	7.86		
	15		2.68	7.25		0.46	4.36		
	16		3.51	10.49		0.52	6.25		
	17		1.31	8.44		0.46	7.92		
	18		1.98	7.19		1.01	2.50	14.63	40.02
	19		2.26	12.31		0.55	3.72		
	20		2.38	7.19		0.52		11.28	37.49
	21		1.62	10.49			2.77	5.49	
	22		2.68	8.08				9.14	55.78
	23		3.29	11.43					
	25		1.13	12.28					
	26		2.93	12.37					
	27		2.13	9.81		0.76			
	28		1.22	6.98		0.61	2.71		
	29		1.68	6.55				4.57	
	01-A	A	0.91	1.82		1.83	1.82	3.35	
	01-B	B	0.42	1.73		1.83	1.73	4.26	
	01-C	C	0.79	3.68		1.83	3.68	2.13	3.96
	2		0.82	4.51		1.83	4.51	5.79	3.05
Voelker et al (1983)	08-A	A	7.83	23.83		1.83		36.88	81.99
	08-B	B	6.55			1.83		37.49	
	08-C	C	5.45			1.83		35.35	
	17-A	A	2.68	10.60		1.37	8.77	26.21	65.53
	17-B	B	1.92	12.37		1.37	12.07	36.57	53.64
	1		0.28	2.74		0.61	1.59	10.05	
	2		0.23	3.13		0.76	1.81	5.79	
	6 - ridge 1		1.34	2.53		0.30	1.16	6.09	
	6 - ridge 2		1.22	1.19		0.30	1.19		
	7		0.64	2.28			0.60	6.09	
	8		1.37	6.09		0.30	1.37	8.22	26.52
Voelker et al (1984)	9		1.29	4.41	0.30 0.61	0.46	2.13	4.26	30.78
	10-Profile 1	1	0.73	5.55		0.61	2.45	6.09	34.14
	10-Profile 2	2	1.19	5.74	0.46 0.61	0.53	1.31	3.96	38.10
	11-Profile A	A	3.81	20.29			10.64	11.27	77.26
	11-Profile B	B	4.21	19.99			7.44	13.10	
	13		4.11	19.05				10.97	
	14		3.04						

A. 2 Beaufort Sea

References	Ridges	CS/#holes	h_s [m]		h_k [m]		h_i [m]			h_{cl} [m]			α [°]		w [m]			l [m]
			max	avg	max	avg	min	max	avg	min	max	avg	sail	keel	ridge	sail	keel	ridge
Barker et al. (2008)		1 CS -9 holes	3.70		11.00							1.30	32/12	22	42.60			
Sayed and Frederking	Itiyok ridge 2 -	CS 1	1.30													4.20		
		CS 2	3.80													11.50		

(1989)		CS 3	2.40									13.80	
		CS 4	1.90									6.20	
		CS 5	2.10									13.40	
		CS 6	3.00									12.50	
		CS 7	1.20									12.00	
		CS 8	3.50									11.70	
		CS 9	4.50									12.20	
		CS 10	5.10									12.00	
	Itiyok ridge 1 -	CS 1	1.16										
		CS 2	1.25										
		CS 3	1.59										
		CS 4	1.65										
		CS 5	1.76										
		CS 6	1.82										
		CS 7	2.20										
		CS 8	2.25										
		CS 9	2.37										
		CS ws max										21.50	
		CS ws min										6.70	
	Pack ice ridge -	CS 1	1.03										
		CS 2	1.47										
		CS 3	1.60										
		CS 4	1.71										
		CS 5	1.78										
		CS 6	2.09										
		CS 7	2.10										
		CS 8	2.13										
		CS 9	2.44										
		CS 10	2.47										
		CS 11	2.50										
		CS 12	2.70										
		CS 13	2.84										
		CS 14	2.87										
		CS 15	2.91										
		CS 16	3.03										
		CS 17	4.16										
		CS 18	4.39										
		CS ws max										17.90	
		CS ws min										3.60	
Gladwell (1976)	Ridge 2		4.69	17.19		2.43	3.35	2.43<hc<3.35	27/20	17/19			
	Ridge 3		3.20	13.72				3.04	20/59	7/23			
	Ridge 4		3.04	10.97		0.61	3.04	0.61<hc<3.04	23/39	13/22			
	Ridge 5		3.04	11.58				2.44	36/34	17/16			
	Ridge 7		2.01	4.57				4.57	23/41	13/13			
Mc Gonigal (1978)	Ridge 1		7.50	26.82	1.52		7.62		41/25	28.5/15		23.77	149.35
	Ridge 2		3.02	9.44	0.91		5.18		36/22	28/23		9.14	35.97
	Ridge 3		6.28	22.86			3.05		36/25.5	40/20.5	>57.91	23.77	57.91
	Ridge 4		3.57	10.06	1.22		2.44		42/36	18		9.14	37.49
	Ridge 5		5.70	23.16	1.52/0.61		6.1		41/23.5	26.5/24		13.41	96.93
	Ridge 6		5.36	21.03	0.61		7.01		31/27	70/23		18.29	69.80
	Ridge 7		2.74	13.41	0.91		1.52		32/19	59/29		7.92	49.38
	Ridge 8		3.53	17.37			3.05		49/40	37/22.5		10.97	80.47

	Ridge 11		4.45		21.94			0.91/1.52		5.18		44/18	30/23	15.85	71.32	
	Ridge 13		5.79		23.77			1.22		5.18		39.5/31	46/28	23.16	23.16	
Vaudrey et al. (1979)	F14B'	Ridge 2 Line 2	7.01						2.13					28.96	106.68	
	F15'	Ridge 2A	3.35		14.33				1.83					27.43	85.34	
	F17A	Ridge 3 Line 1	1.98		10.06				1.98					21.34	33.53	
	F17B	Ridge 3 Line 2	1.37		7.92				1.83					9.14	18.29	
	F18A	Ridge 4 Line 1	1.22		8.53				2.44					10.67	33.53	
	F18B	Ridge 4 Line 2	1.22		7.62				2.44					10.67	25.91	
	F19A	Ridge 5 Line 1	2.13		12.80				4.88					22.86	44.20	
	F19B	Ridge 5 Line 2	2.13		9.14				3.35					6.10	42.67	
	F20A	Ridge 6 Line 1	2.44		16.46				1.52					10.67	48.77	
	F20B	Ridge 6 Line 2	3.05		17.37				1.98					19.81	38.10	
	F21'	Ridge 7	3.66		17.40				1.22					13.41		
	F23A	Ridge 9 Line 1	3.35		15.54				1.22					32.00	76.20	
	F23B	Ridge 9 Line 2	3.05		15.54				1.83					8.23		
	F24'	Ridge 10	3.81		19.16				3.66					73.15	85.34	
	F25A	Ridge 10 Line 1	1.83		15.54				2.44					27.43	57.91	
	F25B	Ridge 10 Line 2	2.13		11.89				1.22					9.14		
	F26'	Ridge 12	2.74		13.11				1.68					12.19	56.39	
Lowings and Banke (1981)	ridge 1		0.46	0.16	2.70					1.27	1					
Burden Timco (1995)	ridge 2		1.44	0.27	7.70					1.53	1					
	ridge 3		1.92	0.40	7.80					1.21	1.1					
	ridge 4		1.07	0.23	3.20					0.4	0.3					
	ridge 5		1.74	0.42	5.60					1.51	1.2					
	ridge 6		2.09	0.43	8.00					1.5	1.1					
Banke (1982)	ridge 1		2.70		11.00					2.5					6.10	
	ridge 2		1.80		11.00					2.5					10.70	
	ridge 3		1.50		4.00					2					6.10	
	ridge 4		3.20		8.60					2.5					9.20	
	ridge 5		2.60		8.60					2.5					9.20	
	ridge 6		2.70		8.60					2.5					15.30	
	ridge 7		2.50		8.60					2.1					12.20	
Bowen and Topham (1996)	CS - Fig 9a		2.65	2.65	10.60	10.60	1.00	1.70	1.70					20.20	105.60	1500
	CS - Fig 9b		3.15	3.15	11.20	11.20	1.00	1.70	1.70					18.20	87.10	1500
	CS - Fig 9c		2.60	2.60	10.40	10.40	1.00	1.70	1.70					24.00	105.60	1500
	CS - Fig 9d		3.26	3.26	12.40	12.40	1.00	1.70	1.70					24.00		1500
	CS - Fig 9e		2.57	2.57	10.10	10.10	1.00	1.70	1.70					17.80		1500
	CS - Fig 9f		2.80	2.80	8.40	8.40	1.00	1.70	1.70					44.00	100.70	1500
Melling,Topham and Riedel (1993)	T2 - Fig 6a		3.00		14.80				1.65					20.50		
	B20 - Fig 6b		1.90		14.70				1.65					33.80	106.80	
	T3 - Fig 6c		3.95		14.05				1.65					15.20		
	B15 - Fig 6d		1.23		13.80				1.65						67.30	
	B09 - Fig 6e		1.57		14.30				1.65							

	T1 - Fig 6f	4.55	13.90	1.65
	T5 - Fig 6g	1.70	15.60	1.65
Tucker and Govoni (1981)	Site 1 - ridge 1	1.64		
	Site 1 - ridge 2	1.78		
	Site 1 - ridge 3	4.63		
	Site 1 - ridge 4	5.16		
	Site 1 - ridge 5	5.24		
	Site 1 - ridge 6	6.32		
	Site 2 - ridge 1	1.62		
	Site 2 - ridge 2	1.88		
	Site 2 - ridge 3	2.19		
	Site 2 - ridge 4	2.25		
	Site 2 - ridge 5	2.71		
	Site 2 - ridge 6	4.64		
	Site 3 - ridge 1	1.39		
	Site 3 - ridge 2	1.93		
	Site 3 - ridge 3	2.02		
	Site 3 - ridge 4	2.40		
	Site 3 - ridge 5	2.74		
	Site 3 - ridge 6	4.13		
	Site 4 - ridge 1	1.64		
	Site 4 - ridge 2	3.31		
	Site 4 - ridge 3	3.55		
	Site 4 - ridge 4	3.64		
	Site 4 - ridge 5	3.75		
	Site 4 - ridge 6	4.53		
	Site 5 - ridge 1	2.14		
	Site 5 - ridge 2	2.59		
	Site 5 - ridge 3	3.16		
	Site 5 - ridge 4	3.56		
	Site 5 - ridge 5	3.57		
	Site 5 - ridge 6	4.84		

A.3. Svalbard

References	Ridges	CS/#holes	h_s [m]		h_k [m]		h_i [m]	h_{cl} [m]			α [º]			w [m]		l [m]
			max	avg	max	avg	avg	min	max	avg	sail	keel	ridge	sail	keel	ridge
Høyland (2000), Høyland (2002a,b)	Svartodden 1998-1999	snitt 4 28.04	0.35	0.10	3.65	1.92	1.10	1.00	3.00	1.68					10	15
		snitt 5 25.03	0.44	0.13	5.20	2.90	1.07	0.97	2.59	1.67					10	15
		snitt 5 12.05	1.00	0.23	4.00	2.36	1.16	1.16	2.90	1.80					10	15
		snitt 5.5 19.03	0.63	0.16	4.48	2.11	0.93	0.85	2.22	1.41					10	15
		snitt 5.5 12.05	1.10	0.25	3.50	2.25	1.16	1.06	2.48	1.72					10	15
		snitt 6 02.03	1.06	0.22	4.34	2.14	0.95	0.66	1.94	1.16					10	15
		snitt 6,5 20.03	0.93	0.65	4.87	2.20	0.93	0.74	1.92	1.19					10	15
		snitt 6,5 12.05	0.90	0.68	4.00	2.44	1.16	1.15	2.80	1.87					10	15
		snitt 7 16.04	0.87	0.65	5.94	2.27	1.10	0.97	2.35	1.40					10	15
		snitt 7 12.05	0.95	0.68	4.00	2.19	1.16	1.06	2.85	1.59					10	15
	Camp Morton	CS 2 24.03.99	1.00	0.23	4.50	3.05		1.00	1.28	1.15					15	
		CS 2 21.04.99	0.80	0.13	4.65	3.00		1.00	1.45	1.25					15	
		CS 3 08.04.99	0.90	0.21	5.00	2.70		0.90	1.30	1.05					15	
		CS 3 23.04.99	0.99	0.19	4.50	3.51		1.00	1.60	1.31					15	
Høyland and Løset (1999b)	1998 ridge field	CS 1 (2 times) -55holes avg														
		CS1_May5	4.50	0.32	5.76	2.98	1.20	0.25	5.41	1.21			24	8	24	
		CS1_March11	1.41	0.29	3.67	1.32	0.85	0.41	2.18	1.05						
		CS 2(4 times) - 89holes avg														
		CS2_May5	1.00	0.31	6.19	3.35	1.20	0.05	3.20	1.35						
		CS2_April21	1.10	0.26	4.29	2.17	1.20	0.00	2.25	1.09						
		CS2_March12	0.83	0.16	3.07	1.80	0.85	0.35	2.46	1.16						
Shafrova and Høyland (2008)	North Spitsbergen	1 CS- 29 holes	3.30	--	10.80	--	0.80	0.23	4.11							
Sand et al (2011)	R1-2011		2.32		5.13						14.99	15.35		17.33	37.38	

A.4. Barents Sea

References	Ridges	CS/#holes	h_s [m]		h_k [m]		h_i [m]	h_{cl} [m]			α [°]			w [m]		
			max	avg	max	avg	avg	min	max	avg	eff	sail	keel	ridge	sail	keel
Høyland (2005,2007), Bonnemaire et al. (2003), Shafrova and Høyland (2008)	2002	1CS- 35 holes	4.70		15.00		1.20			1.90		22-30	17-29			
	2003	CS 1	2.10		10.10		0.96			2 (1.4T)						
		CS 2	1.90		9.00		0.96			1.40						
	2004	CS 1- 30	2.80		4.20		--			1.80						
		CS 2 -31	1.20		3.90		--	1.90	3.20	(1.9D/3.2D)						
		CS 3 -21	2.10		10.70		--			1.00						
	2005	1 CS- 28 holes	2.10		8.20		0.48	0.37	2.22	1.05	0.91					
Strub-Klein et al. (2009), UNIS report (2008)	2008	CS A -19	0.00		9.70	6.88										
		CS B -24	3.46		11.27	9.26										
		CS C -26	1.89		9.07	8.33	0.20									
		CS D -11	0.72		9.47	7.64	0.82									
Krupina et al (2009)		1 CS 17 holes	2.10	0.70	7.60	4.07										
UNIS, unpublished data (2007)	2007	CS A -19	2.33	0.51	7.69	3.68			4.53	1.78						
		CS B -24	1.20	0.29	5.80	3.05			2.85	1.31						
		CS C -31	1.66	0.50	5.88	3.04			4.03	1.56						
		CS D -17	1.54	0.29	5.77	3.05			2.73	1.69						
UNIS, unpublished data (2011)	2011	1CS- 19 holes	1.75	0.75	9.05	6.74			3.35	1.52						
Sand et al (2011)	R2-2011		2.37		6.87							24.86	20.35		10.23	37.04
Kharitonov (2008), Kharitonov and Morev (2005)	Pechora Sea	13 ridges	3.98	1.08	11.37	6.09	0.70			0.59						
Mironov and Porubayev (2005)	Pechora Sea	?		2-3		10-12	0.6-0.8			1.5-2				60-80		

A.5. Russian Arctic Ocean

References	Ridges	CS/#holes	h_s [m]		h_k [m]		h_i [m]			h_{cl} [m]	
			max	avg	max	avg	min	max	avg	max	avg
Kharitonov and Morev (2005)	1	14 ridges	1.95	1.43	5.44	3.82	1.87	2.86	2.15		0.38
	2	14 ridges	1.8	0.59	8.81	5.95	1.95	2.01	1.98		--
	3	40 ridges	2.51	0.57	9.3	4.98	1.66	2.9	2.27		--
Kharitonov (2008)										3.5	3

A.6. East Coast Canada

References	Ridges	CS/#holes	h_s [m]		h_k [m]		h_{cl} [m]			α [°]			w [m]		l [m]
			max	avg	max	avg	min	max	avg	sail	keel	ridge	sail	keel	ridge
Evers (1986)	Ridge 1	CS 1 – 30 holes	1.65	0.60	10.60	2.62				23/16	17/14	50	9	50	
		CS 2 – 27 holes	1.40	0.44	9.70	3.19				23/7	39/37	45	13	45	
		CS 3 – 34 holes	1.20	0.33	9.40	2.95				16/6	21/18	40	12	40	
	Ridge 2	CS 1 – 25 holes	1.17	0.33	7.60	4.25				45/11	10/14	>60	9	60	
		CS 2 – 33 holes	0.84	0.22	9.00	3.68				10/6	51/16	>60	12	60	
		CS 3 – 28 holes	1.96	0.56	8.70	4.30				17/27	20/21	50	10	50	
	Ridge 3	CS 1 – 33 holes	1.77	0.56	12.00	6.73				15/10	21/23	>60	9	60	
		CS 2 – 26 holes	2.81	0.91	12.00	6.30				17/21	17/20	>70	15	70	
		CS 3 – 27 holes	2.01	0.62	12.00	6.66				3/58	37/31	50	13	50	
	Ridge 4	CS 1 – 35 holes	4.24	1.07	11.00	--				20/32	24/?	>70	23	70	
		CS 2 – 31 holes	2.86	0.81	11.00	--				11/26	20/?	>70	20	70	
		CS 3 – 34 holes	3.81	1.14	11.00	--				20/10	42/?	>70	30	70	
Obert and Brown (2011)	2/20/2007 7:41:10				6.83									111.46	
	2/20/2007 7:25:33				3.11									12.97	
	39754.38				2.03									27.79	
	2/22/2007 12:13:21				2.03									39.52	
	39754.38				5.86									201.85	
	39510.62				2.36									7.47	
	3/23/2008 8:07:15				3.26									35.86	
	2/22/2007 12:17:57				2.90									73.99	
	2/22/2007 10:41:09				4.69									15.69	
	39754.38				3.41									15.97	
Croasdale & Associates (1999)	Site 4	line 1	1.40		5.60				1.30						
		line 2	1.40		5.60				1.30						
		line 3	1.40		5.60				1.30						
	Site 6	line 1	1.90		7.60				1.20						
		line 2	1.60		6.40				1.20						
	Site 7	line 1	1.60		4.80				1.08						
		line 2	1.50		4.50				1.08						
		line 3	1.20		3.60				1.08						
	Site 8	line 1	2.60		10.40				1.30						
		line 2	1.50		4.50				1.30						
		line 3	1.80		5.40				1.30						
	Site 9	line 1	1.20		3.60				1.70						
		line 2	1.50		4.50				1.70						
		line 3	0.70		2.10				1.70						
Williams and Kirby (1994)	Shear ridge	1CS 5 holes	1.60	0.54	12.40	4.06	1.07	12.40	3.64			26	26	26	100
	Ridge 1	1CS 7 holes	1.72	0.49	6.78	3.43	0.70	3.88	2.17			26	10	40	400
	Ridge 2	1CS 5 holes	0.67	0.36	5.93	3.25	1.04	3.73	2.18			--			--
	Ridge 3	1CS 6 holes	1.30	0.45	4.60	3.50	0.14	3.51	2.42			--	10		--

	Ridge 4	1CS 9 holes	0.79	0.33	4.81	2.72	0.29	2.75	1.63			4 to 20	4	20	90	
	Ridge 5	1CS 9 holes	1.36	0.31	5.60	3.39	0.00	4.92	1.73			8	8	30	100	

A.7. Baltic Sea and Gulf of Bothnia

References	Ridges	CS/#holes	h_s [m]		h_k [m]		h_{cl} [m]				α [°]					w [m]	
			max	avg	max	avg	avg	min	max	avg	Sail 1	sail 2	Keel 1	Keel 2	ridge	sail	keel
Høyland (2000), Høyland (2002a,b)	Marjaniemi	Å - 25.03.99	0.35	0.23	4.96	4.58	0.6	0.05	1.73	0.94							
		A - 10.03.99	0.32	0.27	4.34	3.94	0.57	0.45	0.88	1.84							
		B - 19.03.99	0.3	0.24	4.58	4.15	0.59	0.65	2.03	1.04							
		C - 02.03.99	0.31	0.24	4.59	4.28	0.55	0.45	1.13	0.79							
		D - 26.02.99	0.33	0.28	4.83	4.55	0.47	0.57	1.37	0.87							
		E - 04.03.99	0.38	0.29	5.12	3.96	0.55	0	1.59	0.78							
		F - 16.03.99	0.38	0.29	4.97	4.68	0.59	0.6	1.32	1.01							
		G - 10.03.99	0.37	0.31	5.82	4.86	0.57	0.51	1.41	0.91							
		H - 04.03.99					0.55										
Kankaanpää (1997), Kankaanpää (1989 POAC)	A	main cross section	1.6	0.43	12.29		0.35				8	12	45	38		5.3	22
	A1	10m north of main profile A	1.65		12.51		0.35										
	A2	10m south of main profile A	1.03		12.4		0.35										
	R1	1CS - 25holes - 3 ridges	0.59		4.69		0.44				31	30	38	27		2	16.5
	R2		1.74		8.41		0.44				35	38	64	37		5	12.9
	R3		0.97		7.48		0.44				26	14	8	64		6	42.7
	T	1CS-12holes	0.85		3.46		0.44				19	16	21	24		5.3	15
	S1	1CS-15 holes	1.23		4.64		0.35				26	32	17	25		5	27
	S2	2CS – 21 holes	0.6		5.13		0.3				17	17	27	12		4	24
	S3	1CS – 8 holes	0.65		4.27		--				9	12				6	
	Sampo 1N	1CS – 28 holes - 2ridges	1		5.6		0.7									5.9	12.9
	Sampo 1S		1.81		14.9											23.5	59.2
	Sampo 2	1CS-12 holes	1.88		12.89		0.8									12.5	57
	Sampo 3	1CS 8 holes	1		9		0.7									4.5	4.5
	Sampo 4	1CS 11 holes	1.29		9		0.75									9	59.5
	GA	1CS 12 holes	0.5		2.09		0.45									3.6	12.3
	GB	1CS 16 holes	1.27		3.53		0.6									3.8	14
	GC	1CS 13 holes	1.07		2.94		0.65									5.8	15.9
	GE	1CS 7 holes	1.22		2.41		0.8									5.6	26.3
	GF	1CS 15 holes	1.72		2.3		0.75									4.05	28.5
Leppäranta and Hakala	Ridge 1		1.1		2.9		0.7			1						5	20
	Ridge 2	1 CS –	1.7		6.5		0.5			1						4	15

(1992)		10 holes											
	Ridge 3		1.2		4.6		0.4		0.5			4.5	24.5
	Ridge 4		0.6		5.1		0.3		0.4			4	22.7
	Ridge 5		0.7		4.2		--		0.4			5.6	
	Ridge 6	1 CS-17 holes	1.8		14.9		0.7		0.8			24	59
Leppäranta et al. (1995)	Ridge 1 - Visit no. 1		1.08	0.21	5.28	3.13	0.31		0.52		52	15	52
	Ridge 1 - Visit no. 2		1	0.17	4.45	2.89	0.55		0.93		52	12	52
	Ridge 1 - Visit no. 3		0.6	0.14	3.12	2.19	0.58		1.02		52	8	52
Veitch et al. (1991a)	Ridge 1	Line 1	0.37		5.41								
		Line 2	0.68		5.93								
		Line 3	0.92		7.58								
		Line 4	0.49		8.79								
		Line 5	1.07		8.43								
		Line 6	0.9		7.9								
		Line 7	0.69		9.66								
		Line 8	0.89		9.04								
	Ridge 2	Line 1	1.46		8.81								
		Line 2	1.56		7.42								
		Line 3	1.58		9.23								
		Line 4	2.04		8.25								
		Line 5	1.43		8.4								
		Line 6	1.11		7.18								
Palosuo (1975)	Ridge 1		0.8		8								
	Ridge 2		0.35		0.9								
	Ridge 3		0.35		0.9								
	Ridge 4		0.7		6								
	Ridge 5		1.2		8								
	Ridge 6		2.6		20								
	Ridge 7		0.8		6.5								
	Ridge 8		0.75		7								
	Ridge 9		0.74		2								
	Ridge 10		1.77		14								
	Ridge 11		1.43		14								
	Ridge 12		1.5		7								
	Ridge 13		3.42		28								
	Ridge 14		2.74		15								
	Ridge 15		1.7		10								
	Ridge 16		2										
Veitch et al. (1991b)	ridge 1	line A	0.59	0.26	5.28	3.4	0.31	0.31	1.21	0.62			
	ridge 1	line B	0.6	0.2	4.45	3.2	0.57	0.57	1.44	0.97			

A.8. Sea of Azov

References	Ridges	h_s [m] max	h_k [m] max	h_{cl} [m] avg
Kharitonov (2008)	Ridge 1	0.8	2.6	0.29
	Ridge 2	0.3	2.2	0.29

A.9. Caspian Sea

References	Ridges	CS/#holes	h_s [m] avg	h_k [m] avg	h_i [m] avg	h_{cl} [m] avg	w [m] ridge
Kharitonov (2008)	2003	4 ridges				0.35	
	2005	5 ridges				0.55	
Mironov and Porubayev (2005)			1-2	3-4	0.15-0.35	0.3-0.7	15-20

A.10. Offshore Sakhalin

References	Ridges	CS/#holes	h_s [m]		h_k [m]		h_i [m]		h_{cl} [m]	
			max	avg	max	agv	min	max	avg	avg
Bekestsky et al. (1996)	Odoptu		5	1.5	12.7	8.5	2.9	7.2		
	Sakhalinsky Bay		7	2	9.8	4.8	4.1	8.5		
	Severny Bay		8	3.5	9.5	5.6	1.4	3.2		
Mironov et al. (1998)		CS 1- 54 holes	3.01		13.16					
		CS 2- 45 holes	2.5		16.26					
Surkov and Truskov (1995)	Ridge 1		5.9		12					
	Ridge 2		4		9					
	Ridge 3		4.1		12.9					
	Ridge 4		4.1		14					
	Ridge 5		4.1		16					
	Ridge 6		4		19					
	Ridge 7		2.8		9.8					
	Ridge 8		2.8		12.3					
	Ridge 9		2.8		13					
	Ridge 10		2.4		8.6					
	Ridge 11		2.3		15					
	Ridge 12		2.1		12					
	Ridge 13		2		10.5					
	Ridge 14		1.9		9					
	Ridge 15		1.5		9					
	Ridge 16		1.5		10					
	Ridge 17		1		10					
	Ridge 18		0.7		12					
Kharitonov (2008)	14 ridges			0.6		8			0.98	1-1.2

B. Block dimensions

B.1. Beaufort Sea

References	Ridge	# blocks	h_b [m]	w_b [m]	l_b [m]
Gladwell (1976)	Ridge 2		0.72		
	Ridge 3		--		
	Ridge 4		0.38		
	Ridge 5		0.38		
	Ridge 7		0.18		
Mc Gonigal (1978)	Ridge 1		0.78		1.71
	Ridge 2		0.3		0.91
	Ridge 3		1.14	0.61	1.83
	Ridge 4		0.46	1.01	1.22
	Ridge 5		0.61	0.91	1.22
	Ridge 6		0.61	1.22	0.91
	Ridge 7		0.25		0.61
	Ridge 8		0.15	0.91	0.61
	Ridge 11		0.56	1.22	1.83
	Ridge 13		0.59	2.13	1.22
	Ridge 14		0.61	0.91	1.22
Tucker and Govoni (1981)	Site 1 - ridge 1		0.25		
	Site 1 - ridge 2		0.43		
	Site 1 - ridge 3		1.27		
	Site 1 - ridge 4		1.49		
	Site 1 - ridge 5		1.55		
	Site 1 - ridge 6		1.46		
	Site 2 - ridge 1		0.23		
	Site 2 - ridge 2		0.41		
	Site 2 - ridge 3		0.29		
	Site 2 - ridge 4		0.19		
	Site 2 - ridge 5		1.32		
	Site 2 - ridge 6		1.25		
	Site 3 - ridge 1		0.15		
	Site 3 - ridge 2		0.18		
	Site 3 - ridge 3		0.25		
	Site 3 - ridge 4		1.05		
	Site 3 - ridge 5		1.15		
	Site 3 - ridge 6		1.34		
	Site 4 - ridge 1		0.12		
	Site 4 - ridge 2		1.35		
	Site 4 - ridge 3		1.11		
	Site 4 - ridge 4		0.69		
	Site 4 - ridge 5		0.99		
	Site 4 - ridge 6		1.12		
	Site 5 - ridge 1		0.14		
	Site 5 - ridge 2		0.23		
	Site 5 - ridge 3		0.87		
	Site 5 - ridge 4		1.42		
	Site 5 - ridge 5		1.60		
	Site 5 - ridge 6		0.87		
Bowen and Topham (1996)		9 blocks	0.38		
Sayed and Frederking (1989)			0.57		

Banke (1982)	0.3-0.35	1	1
Melling et al. (1993)	1.50	3.5	

B.2. Offshore Svalbard

References	Ridge	# blocks	h_b [m]	w_b [m]	l_b [m]	α_b[°]
Shafrova and Høyland (2008)		50	0.35	0.68	0.96	69[1]/47[2]
Høyland (2000), Høyland (2002a,b), Høyland and Løset (1999a)	Svartodden		0.2-0.25			
	Camp Morton		0.10-0.15			
Høyland and Løset (1999b)			0.2-0.3	2-3	2-3	
Sand et al. (2011)	RS 1		0.26			

B.3. Barents Sea

References	Ridge	# blocks	h_b [m]	w_b [m]	l_b [m]	α_b[°]
Høyland (2007)	2005	210	0.28	0.58	0.83	38
	2004	40	0.58	1.3	2.1	26
	2003	70	0.31	0.52	0.72	38
	2002	110	0.55	1.5	2.2	40
Strub-Klein et al (2009), UNIS report (2008)	zone 1	4	0.5	0.71	>3	
	zone 2	4	0.58	1.15	1.1	
	zone 3	26	0.37	0.74	1.04	
UNIS, unpublished data (2007)	zone 1	40	0.9	0.6	36.5	44.9
	zone 2	28	1.9	1.1	40.5	33.9
	zone 3	37	0.7	0.5	0.3	49.3
Mironov and Porubayev (2005)			0.2-0.5			
Sand et al. (2011)	RS 2		0.78			

B.4. East Coast Canada

References	Ridge	# blocks	h_b [m]	w_b [m]	l_b [m]	α_b[°]
Croasdale & Associates (1999)	Site 4	31	0.24	1	1.35	24.5
	Site 6		0.34	1.51	2.15	37
	Site 7		0.21	0.73	1.03	
	Site 8		0.31	1.06	1.5	
	Site 9		0.2	0.87	1.32	
Williams and Kirby (1994)	Ridge 1		0.17	0.83	0.9	
	Ridge 2		0.15	0.7	0.62	
	Ridge 3		0.3	1.25	1.57	
	Ridge 4		0.15	0.8	0.8	
	Ridge 5		0.52	2	2.28	

B.5. Baltic Sea and Gulf of Bothnia

References	Ridge	# blocks	h_b [m]	w_b [m]	l_b [m]
Høyland (2000), Høyland (2002a,b)			0.2		
Kankaanpää (1997)	A	12	0.19	0.58	0.92
	R1	7	0.23	0.68	0.96
	R2	13	0.21	0.8	1.07
	R3	2	0.29	1.16	1.67
	T	5	0.15	0.76	1.03
	S1	11	0.18	0.54	0.75
	S2	10	0.11	0.5	0.71
	S3				
	Sampo 1N	7	0.23	0.6	0.6
	Sampo 1S	1 (max)			
	Sampo 2	1(max)	0.41	0.96	1.2
	Sampo 3	10	--	--	--
	Sampo 4	10	--	--	--
	GA	10	0.13	0.52	0.78
	GB	10	0.2	0.61	0.83
	GC	10	0.2	0.42	0.71
	GE	10	0.24	0.73	1.01
	GF	10	0.24	1.01	1.33
Leppäranta and Hakala (1992)	Ridge 1		0.2		0.9
	Ridge 2		0.2		--
	Ridge 3		0.2		0.75
	Ridge 4		0.11		0.6
	Ridge 5		0.1		--
	Ridge 6		0.23		0.7
Palosuo (1975)	Ridge 1		0.3		
	Ridge 2		0.4		
	Ridge 3		0.4		
	Ridge 4		0.55		
	Ridge 5		0.15-0.5		
	Ridge 6		0.4-0.8		
	Ridge 7		0.2-0.3		
	Ridge 8		0.25		
	Ridge 9		0.25		
	Ridge 10		0.45-0.5		
	Ridge 11		0.45		
	Ridge 12		0.3		
	Ridge 13		0.8-1.2		
	Ridge 14		0.7-0.8		
	Ridge 15		0.4-0.6		
	Ridge 16		0.07		
Veitch et al. (1991b)	site 1		0.16		
	site 2		0.15		

B.6. Caspian Sea

References	Ridge	h_b [m]
Mironov and Porubayev (2005)	Northwestern Caspian Sea	0-15-0.3

B.7. Offshore Sakhalin

References	Ridge	h_b [m]
Mironov and Porubayev (2005)	Eastern Shelf of Sakhalin Island	0.3-0.7

C. Macroporosity

C.1. Offshore Svalbard

References	Ridge	Based on	Macroporosity [%]		
			Ridge	Sail	Rubble
Høyland (2002), Høyland and Løset (1999a), Høyland et al. (2000)	Svartodden	10 CS 105 holes	32.5		
	Camp Morton	4 CS 37 holes	35 (uncertain)		
Høyland and Løset (1999b)		CS 1 54 holes	18		
		CS 2 87 holes	19		
Sand et al. (2011)	RS 1			14	7

C.2. Barents Sea

References	Ridge	Based on	Macroporosity [%]		
			Ridge	Sail	Rubble
Høyland (2005, 2007), Bonnemaire et al. (2003), Shafrova and Høyland (2008)	2002	1 CS -35 holes		15.3	29.7
	2003	CS 1		35	10
		CS 2		10	11
	2004	CS 1- 30		26	36
		CS 2 -31		12	38
		CS 3 -21		12	32
	2005	1 CS- 28 holes		29	45
Strub-Klein et al. (2009), UNIS report (2008)		CS A -17	34	--	48
		CS B- 9	19	14.3	20
		CS C - 9	22	23	25
		CS D - 9	16	10	17
UNIS, unpublished data (2007)	2007	CS A -19 holes	36		
		CS B -24 holes	37		
		CS C -31 holes	34		
		CS D -17 holes	28		
UNIS, unpublished data (2011)	--	1CS 19 holes	--	19	22
Sand et al. (2011)	RS 2	--	--	24	5
Kharitonov (2008)	--	13 ridges	17	13	38
Mirnonov and Porubayev (2005)	?		28-30		

C. 3. Russian Arctic Ocean

References	Ridge	Based on	Macroporosity [%]		
			Ridge	Sail	Rubble
Kharitonov and Morev (2005)	Ridge 1	1CS 14 holes	12	12	12
	Ridge 2	1CS 14 holes	14	1	16
	Ridge 3	1CS 40 holes	13	1	15

C.4. East Coast Canada

References	Ridge	Based on	Macroporosity [%]		
			Ridge	Sail	Rubble
Williams and Kirby (1994)	Shear ridge	1CS 5 holes		0	
	Ridge 1	1CS 7 holes		10	
	Ridge 2	1CS 5 holes		20	
	Ridge 3	1CS 6 holes		20	
	Ridge 4	1CS 9 holes		15	
	Ridge 5	1CS 9 holes		25	

C. 5. Baltic Sea and Gulf of Bothnia

References	Ridge	Based on	Macroporosity [%]		
			Ridge	Sail	Rubble
Høyland (2000), Høyland (2002a,b)		1CS	38		
Kankaanpää (1997)	A	2 CS -20 holes	23	13	24
	R1	1CS - 25holes - 3 ridges	20	5	22
	R2		38	41	37
	R3		33	20	34
	T	1CS- 12holes	29	20	29
	S1	1CS- 15 holes	27	17	28
	S2	2CS - 21 holes	32	19	32
	S3	1CS - 8 holes	33	23	33
	Sampo 1N	1CS - 28 holes -2ridges	33	15	35
		Sampo 1S	28	9	28
	Sampo 2	1CS- 12 holes	30	30	30
	Sampo 3	1CS 8 holes	32	30	32
	Sampo 4	1CS 11 holes	29	14	30
	GA	1CS 12 holes	22	0	24
	GB	1CS 1 6 holes	32	32	33
	GC	1CS 13 holes	30	31	30
	GE	1CS 7 holes	30	24	31
	GF	1CS 15 hole	23	25	21
Leppäranta and Hakala (1992)	Ridge 1		30	31	30
	Ridge 2	1 CS - 10 holes	23	14	23
	Ridge 3		27	17	29
	Ridge 4		32	19	32
	Ridge 5		33	23	33
	Ridge 6	1 CS- 17 holes	28	9	28
Leppäranta et al (1995)		3 CS -73 holes	22		
Veitch et al. (1991a)	Ridge 1	Line 1	22		
		Line 2	30		
		Line 3	32		
		Line 4	31		
		Line 5	35		
		Line 6	35		
		Line 7	31		
		Line 8	34		
	Ridge 2	Line 1	35		
		Line 2	37		
		Line 3	30		
		Line 4	30		

	Line 5	30	
	Line 6	38	
Veitch et al. (1991b)		55	

C.6 Sea of Azov

References	Ridge	Based on	Macroporosity [%]		
			Ridge	Sail	Rubble
Kharitonov (2008)		2 ridges	28	30	27

C.7 Caspian Sea

References	Ridge	Based on	Macroporosity [%]		
			Ridge	Sail	Rubble
Kharitonov (2008)	2003	5 ridges	17	11	18
	2005	4 ridges	14	17	13
Mironov and Porubayev (2005)			16-18		18-20

C.8 Offshore Sakhalin

References	Ridge	Based on	Macroporosity [%]		
			Ridge	Sail	Rubble
Beketsky et al. (1996)	Odoptu		16	43	23
	Sakhalinsky Bay		10	30	15
	Severny Bay		23	26	28
Mironov and Porubayev (2005)			18-20		19-21
Kharitonov (2008)		14 ridges		6-8	22-24

D. Summary of the literature

D.1. Bering and Chukchi Seas

References	Method	# ridges surveyed	Type of available data	Available dimensions	Block size	η	V	TDS	Mechanical tests	Micro structure
Voelker et al. (1981a)	Su+So+Dr	40	max	$h_k\ h_s\ h_{cl}\ w_s\ w_k$	N	N	Y (area)	TS (2 ridges)	Y (flexural strength on 2 ridges)	N
Voelker et al. (1981b)	Su+So+Dr	2	max, avg	$h_k\ h_s\ h_{cl}\ w_s\ w_k$	N	N	N	T S	calculated	N
Voelker et al. (1982)	Su+So+Dr	26 ridges, 1 CS each	whole	$h_k\ h_s\ h_{cl}\ w_s\ w_k$	N	N	N	T S	N	Y
Voelker et al. (1983)	Su+So+Dr	4 ridges, 1 to 3 CS each	whole	$h_k\ h_s\ h_{cl}\ w_s\ w_k$	N	N	N	TS	N	Y
Voelker et al. (1984)	Su+So+Dr	11 ridges, 1 or 2 CS each	whole	$h_k\ h_s\ h_{cl}\ w_s\ w_k$	N	N	N	TS	N	Y

η: Macroporosity
V:Volume
T: Temperature; D: Density; S: Salinity
Y: Yes
N: No

D.2. Beaufort Sea

References	Method	# ridges surveyed	Type of available data	Available dimensions	Block size	η	V	TDS	Mechanical tests	Micro structure	Comment
Barker et al. (2008)	Dr	1	whole	$h_k\ h_s\ w_k\ \alpha_s\ \alpha_k\ h_i$	N	N	N	N	N	N	
Gladwell (1976)	Dr+So	5	max	$h_k\ h_s\ \alpha_s\ \alpha_k$	Y	N	N	T, S	Y (BHJ)	N	ratios
Mc Gonigal (1978)	Dr+Su+So	10	max	$h_k\ h_s\ h_{cl}\ w_s\ w_k\ \alpha_s\ \alpha_k\ h_i$	Y	N	N	T, S	Y (BHJ)	N	
Vaudrey et al. (1979)	Su+So+Dr	10 ridges, 1 or 2 CS each	max	$h_k\ h_s$	N	N	N	N	N	N	
Lowings and Banke (1981)	Su+Dr+ThS	6 ridges, 1 CS each	whole	$h_k\ h_s\ h_{cl}$	N	N	N	N	N	N	
Banke (1982)	Su+Dr+So	7 ridges, 1 CS each	whole	$h_k\ h_s\ h_{cl}\ w_k\ h_i$	Y	N	N	T	Y (BHJ)	N	
Bowen and Topham (1996)	Su+So	1 ridge, 6 profiles	whole	$h_k\ h_s\ w_s\ w_k\ h_i\ l_r$	Y	N	N	N	N	N	Aerial stereography
Melling et al. (1993)	Su+So	7 CS	whole	$h_k\ h_s\ w_s\ w_k\ \alpha_s\ \alpha_k\ h_i$	Y	N	N	N	N	N	Complex ridge structure
Tucker and Govoni (1981)	Su (?)	30	max	h_s	Y	N	N	N	N	N	
Sayed and Frederking (1989)	ThS, Su, Dr	19	max, avg	$h_s\ w_s$	Y	N	N	N	N	N	

η: Macroporosity
V:Volume
T: Temperature; D: Density; S: Salinity
Y: Yes
N: No

D.3. Offshore Svalbard

References	Method	# ridges surveyed	Type of available data	Available dimensions	Block size	η	V	TDS	Mechanical tests	Micro structure	Comment
Høyland (2002) Høyland and Løset (1999a) Høyland et al. (2000)	Dr+ TS	2	whole	h_k h_s h_{cl} w_r l_r h_i	Y	Y	N	TDS	Y (1 ridge) compression tests	N	
Høyland and Løset (1999b)	Dr + Su	1	whole	h_k h_s h_{cl} h_i	Y	Y	N	S	N	N	ridge examined several times
Sharfrova and Høyland (2008)	Dr	1	whole	h_k h_s h_{cl} h_i	Y	N	N	TDS	Y (uniaxial compressive tests)	N	width, length and inclination of the FB
Sand et al (2011)	Su+Dr	1 ridge 1 CS	whole	h_k h_s w_s w_k α_s α_k h_i	Y	Y	Y (area)	TDS	Y (uniaxial compression, uniaxial tension)	Y	

η: Macroporosity
V:Volume
T: Temperature; D: Density; S: Salinity
Y: Yes
N: No

D.4. Barents Sea

References	Method	# ridges surveyed	Type of available data	Available dimensions	Block size	η	V	TDS	Mechanical tests	Micro structure	Comment
Høyland (2005, 2007), Bonnemaire et al. (2003), Shafrova and Høyland (2008)	Dr	4	max, avg	h_k h_s $h_c l$ w_s (1R) w_k (1R) α_s (1R) α_k(1R) h_i	Y	Y	N	TDS	Y (drop ball test, laboratory uniaxial compressive tests)	Y (1 ridge)	angle of inclination of the blocks
Strub-Klein et al. (2009)	Dr	1	whole	h_k h_s	Y	Y	N	TDS	N	N	
Krupina et al (2009)	Dr	1	whole	h_s h_k h_{cl} h_i	N	N	N	N	N	N	
UNIS unpublished (2007)	Dr	1	whole	h_s h_k h_{cl} h_i	Y	Y	N	TDS	N	N	
UNIS unpublished (2011)	Dr	1	whole	h_s h_k $h_c l$ h_i	N	Y	N	TDS	Y (uniaxial compression, BHJ)	N	
Sand et al (2011)	Su+Dr	1 ridge, 1 CS	whole	h_k h_s w_s w_k α_s α_k	Y	Y	Y (area)	TDS	Y (uniaxial compression, uniaxial tension)	Y	
Kharitonov (2008)	Th Dr	13	max, avg	h_k h_s h_{cl} h_i	Y	N	N	N	N	N	summary of several investigations already published
Mironov and Porubayev (2005)	Th Dr	?	avg	h_k h_s h_{cl} w_r h_i	Y	Y	N	N	N	N	

η: Macroporosity
V:Volume
T: Temperature; D: Density; S: Salinity
Y: Yes
N: No

D.5. Russian Arctic Ocean

References	Method	# ridges surveyed	Type of available data	Available dimensions	Block size	η	V	TDS	Mechanical tests	Micro structure	Comment
Kharitonov and Morev (2005)	Th Dr	1	avg	$h_k\ h_s\ h_{cl}\ h_i$	N	Y	N	N	N	N	
Kharitonov (2008)	Th Dr	3	avg	$h_k\ h_s\ h_{cl}\ w_r\ h_i$	N	N	N	N	N	N	summary of several investigations already published

η: Macroporosity
V:Volume
T: Temperature; D: Density; S: Salinity
Y: Yes
N: No

D.6. East Coast Canada

References	Method	# ridges surveyed	Type of available data	Available dimensions	Block size	η	V	TDS	Mechanical tests	Micro structure	Comment
Evers (1986)	Dr	4	whole	$h_k\ h_s\ w_s\ w_k\ \alpha_s\ \alpha_k$	N	N	Y (area)	N	Y (BHJ)	N	
Croasdale &Associates (1999)	Su + Dr+ Th Dr	5	max	$h_k\ h_s\ h_{cl}\ l_r\ w_r$	Y	N	N	TDS	Y (BHJ)	Y	Microstructure from Johnston and Barker (2000)
Williams and Kirby (1994)	Dr	5	whole	$h_k\ h_s\ h_{cl}\ h_b$	Y	sail only	N	TS (1 ridge)	N	N	
Obert and Brown (2011)	So	3199	max, avg	$h_k\ w_k\ \alpha_k$	N	N	Y (keel area)	N	load panels	N	

η: Macroporosity
V:Volume
T: Temperature; D: Density; S: Salinity
Y: Yes
N: No

D.7. Baltic Sea and Gulf of Bothnia

References	Method	# ridges surveyed	Type of available data	Available dimensions	Block size	η	V	TDS	Mechanical tests	Micro structure	Comment
Høyland (2002), Høyland et al. (2000)	Dr+TS	1	whole	$h_k\ h_s\ h_{cl}\ h_i\ h_b$	Y	Y	N	TDS	Y (1 ridge) compression tests	N	
Kankaanpää (1997)	Dr+Di	14	max	$h_k\ h_s\ w_s\ w_k\ h_i\ h_b$	Y	Y	Y	TDS	N	Y	orientation of the blocks
Leppäranta and Hakala (1992)	Dr	6	max	$h_k\ h_s\ h_c l\ w_s\ w_k\ h_i\ h_b$	Y	Y	Y	SD	Y - shear load test	N	
Leppäranta et al (1995)	Dr	1 1CS/visit	max, avg	$h_k\ h_s\ h_{cl}\ h_i$	N	Y	N	TDS	N	Y	ridge examined several times
Palosuo (1975)	Di	16	max	$h_s\ h_k\ h_b$	Y	N	N	N	N	N	repose angle and block in the sail
Veitch et al. (1991a)	Dr	2	max	$h_k\ h_s$	N	Y	N	SD	Y (uniaxial compression)	Y	
Veitch et al. (1991b)	Dr+ThS	1 ridge 2 CS	whole	$h_k\ h_s\ h_{cl}\ h_i\ h_b$	Y	Y	N	T	N	N	

η: Macroporosity
V:Volume
T: Temperature; D: Density; S: Salinity
Y: Yes
N: No

D.8. Sea of Azov

References	Method	# ridges surveyed	Type of available data	Available dimensions	Block size	η	V	TDS	Mechanical tests	Micro structure	Comment
Kharitonov (2008)	Th Dr	2	avg	h_k h_s h_{cl} h_i	N	Y	N	N	N	N	

η: Macroporosity
V:Volume
T: Temperature; D: Density; S: Salinity
Y: Yes
N: No

D.9. Caspian Sea

References	Method	# ridges surveyed	Type of available data	Available dimensions	Block size	η	V	TDS	Mechanical tests	Micro structure	Comment
Kharitonov (2008)	Th Dr	9	avg	h_{cl} h_i	N	Y	N	N	N	N	summary of several investigations already published
Mironov and Porubayev (2005)	Th Dr	?	avg	h_s h_k h_{cl} w_r h_i	Y	Y	N	N	N	N	

η: Macroporosity
V:Volume
T: Temperature; D: Density; S: Salinity
Y: Yes
N: No

D.10. Offshore Sakhalin

References	Method	# ridges surveyed	Type of available data	Available dimensions	Block size	η	V	TDS	Mechanical tests	Micro structure	Comment
Beketsky et al. (1996)	Th Dr	3	avg, max	h_k h_s h_{cl} h_i	N	Y	N	N	N	N	
Mironov and Porubayev (2005)	Th Dr	?	avg	h_s h_k h_{cl} w_r h_i	Y	Y	N	N	N	N	
Mironov et al. (1998)	Th Dr	2	max	h_k h_s h_i	N	N	N	N	N	N	
Surkov and Truskov (1995)	Th Dr	18	max	h_k h_s h_i	N	N	N	N	N	N	
Kharitonov (2008)	Th Dr	14	avg	h_k h_s h_{cl} h_i	N	Y	N	N	N	N	summary of several investigations already published

η: Macroporosity
V:Volume
T: Temperature; D: Density; S: Salinity
Y: Yes
N: No

4.3 One season of a first-year sea ice ridge investigation – winter 2009

POAC'11
Montréal, Canada

Proceedings of the 21st International Conference on
Port and Ocean Engineering under Arctic Conditions
July 10-14, 2011
Montréal, Canada

POAC11-043

ONE SEASON OF A 1ST YEAR SEA ICE RIDGE INVESTIGATION - WINTER 2009

Lucie Strub-Klein[1,2] and Knut V. Høyland [2,1]

[1]The University Centre on Svalbard, UNIS, Longyearbyen, NORWAY

[2]The Norwegian University of Technology, NTNU, Trondheim, NORWAY

ABSTRACT

A small first-year ridge was investigated in the Van Mijen fjord, Svalbard, from 14 February to 14 May 2009. It was visited 6 times and the thickness of consolidated layer (h_c) was measured by drilling along two lines across the ridge. The average h_c grew from 1.17 to 1.54m in line 1 and from 1.04 to 1.37m in line 2 whereas the surrounding level ice grew from 1.0 to 1.25m. The block thicknesses in the sail were fairly constant and of 0.2m until May when they decreased due to solar radiation. TDS profiles were done 5 times and the average salinity of the consolidated layer was more or less constant. The micro-porosity increased during the season, mostly because of increasing temperatures. Uniaxial horizontal compressive strength was tested in field during 2 visits and the results fit reasonably well with the empirical formulas of Timco and Frederking (1990) and Moslet (2007). Two lines of four thermistor strings were installed and recorded temperatures from 4 March to 14 May. The rubble consistency was very soft and eroded, even more than in previous ridge studies in the Van Mijen fjord. We suggest that this is because the ridge was small and therefore the oceanic fluxes became more important.

INTRODUCTION

A sea ice ridge is formed when the ice is broken by the wind or the currents and piles up. It consists of water, ice blocks, consolidated ice, slush and air. The part above the waterline is defined as the sail and the part below the waterline is defined as the keel. The keel itself is divided into a consolidated layer and a lower unconsolidated part, the rubble. Ridges can be categorized by first-year and old ice features.

Sea ice ridges appear in most of cold offshore regions and are a major problem for winter navigation. From an engineering point of view, they can generate high loads against offshore structures (Blanchet, 1998) and in the absence of icebergs they often give the design ice action. However, models and codes describing the load they exert are still incomplete partly because of the lack of knowledge about temporal and spatial variability of both geometrical and mechanical properties of ice ridges. The consolidation of first-year ice ridges have been studied by e.g. Leppäranta et al. (1995) and Høyland (2002), and the spatial variation in both geometry and small-scale uniaxial compressive strength was studied by Shafrova and Høyland (2008), but little has been done on the combined spatial and temporal development and (to our knowledge) nobody has studied the temporal development of mechanical properties.

LOCATION AND EXPERIMENTAL SET-UP

The ridge was located on Van Mijenfjorden, Svalbard, 2km away from Kapp Amsterdam and 10km from the mining town Svea. It was situated 150m from the shore, slightly protected from the main currents coming from the outer basin. It was orientated almost along the main stream and seems to follow its change of direction (see Figure 1 for location and orientation). Water depth was measured at low tide to be 4.20m and the ridge was not grounded. The ridge was 4m wide and 7m long.

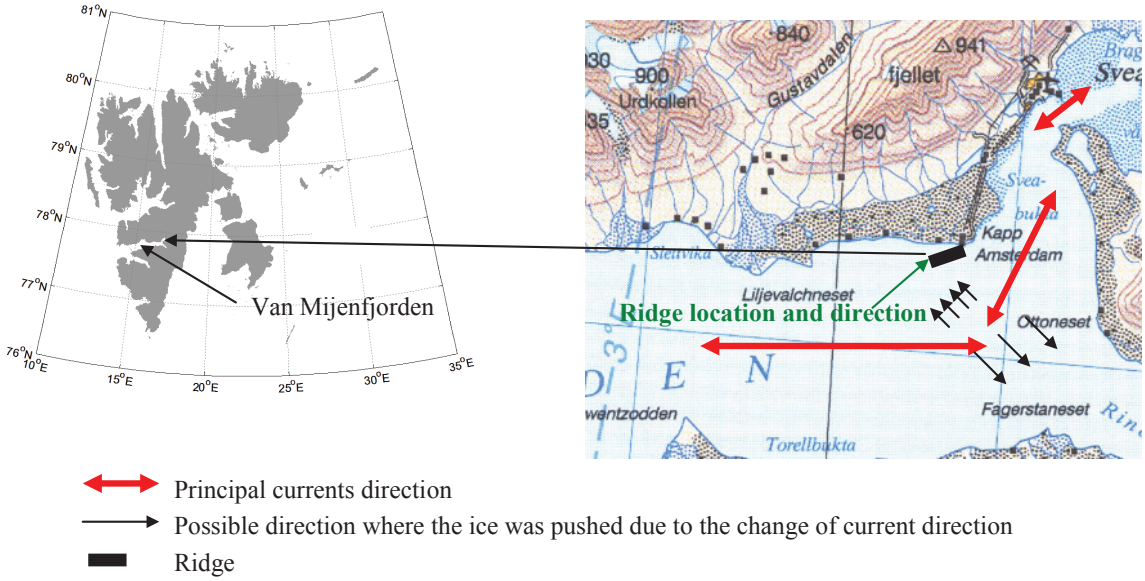

Figure 1: Location of the ridge on Svalbard

Different properties were investigated on site. First, two cross sections were drilled using 2'' augers at each visit along the thermistor strings line to determine the thickness of the ridge and some potential gaps. Any sudden drop of the drill was monitored. The consolidated layer was delimited by the transition from ice to slush or by any gap felt under the water line by drilling and can be related to the temperature measurements, as described by Høyland (2005). More details on the methodology used to study ice ridges are given in Strub-Klein et al (2010).

In most visits cores were taken and temperature, density and salinity (TDS) profiles established. The temperatures were measured every 5cm and density and salinity every 8cm. The relative air and brine volumes were calculated from the equations of Cox and Weeks (1983) for T<-2°C and Leppäranta and Manninen (1988) for T>-2°C. During two visits some cores were taken and uniaxial compression tests performed in field with the compression rig KOMPIS (see Moslet, 2007 for a description of the rig). The nominal strain-rate was 10^{-3} s^{-1}.

Table 1 gives an overview of the activities performed during fieldwork. Drillings and measurements of block thicknesses in the sail were done at every visit while the dates when TDS, uniaxial strength and level ice characterization were done are given in the table. Eight EBA thermistor strings were placed every meter in two lines crossing the ridge (Figure 2). Line 1 was

the westernmost line whereas line 2 was the easternmost line. These two lines were standing two meters apart from each other and recorded temperatures from 4 March to 14 May.

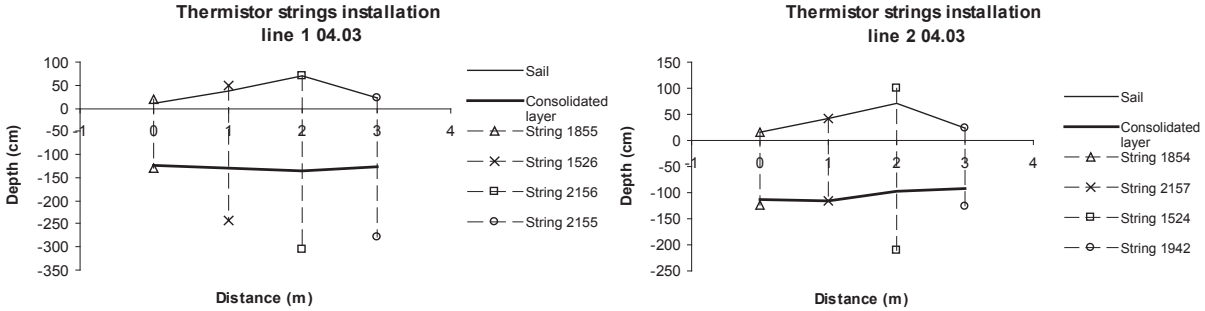

Figure 2. Ridge profiles and positions of the thermistor strings in both lines on 4 March.

Table 1. Field activities

	Morphological profile	TDS profile	Uniaxial tests	Level ice investigations	Thermistor strings
14.02.2009	x			x	
04.03.2009	x	x			installed
19.03.2009	x	x			
01.04.2009	x	x	9 samples	x	
16.04.2009	x	x[a]	12 samples		
14.05.2009	x	x			removed

[a]: no temperature measurements – no micorporosity calculations possible
T: Temperature, D: Density, S: Salinity

ICE GROWTH- STEFAN'S LAW

Stefan's law offers a simple way of estimating level ice thickness and growth. It assumes no snow, no oceanic flux, no solar radiation, a linear vertical temperature profile through the ice cover and (when using *FDD's*) that the ice surface temperature ($T_{i,surface}$) equals that of the air (T_a). The two assumptions about no snow and that $T_{i,surface} = T_a$ are often oversimplifications. An empirical coefficient ω can be introduced to account for this and Stefan's law then can be expressed (Leppäranta, 1993):

$$h_i^2 = h_{i,0}^2 + \omega \frac{2k_i}{\rho_i l_i} FDD \qquad (1)$$

where h_i and $h_{i,0}$ are the current and initial level ice thicknesses, ω the correction factor to account for the assumptions given above, l_i is the latent heat of ice, ρ_i is the density of ice, k_i is the thermal conductivity of ice and *FDD* are the freezing degree days. The thermal conductivity of sea ice is different from that of freshwater ice and varies with the state of the ice (mostly the size and shape of the brine channels/pockets). Schwerdtfeger (1963) derived an expression for sea ice where no brine movement is assumed so that the thermal conductivity of sea ice becomes less than that of freshwater ice. The question of brine movement with the sea ice matrix is not a trivial question. McGuiness et al. (1998) did field measurements and suggest that the conductivity

increases with increasing brine volume. This means that there are two unknown parameters in Eq.(1): ω and k, but they can be treated as one ($\omega \cdot k$). Høyland (2009) discusses level ice growth in the Van Mjien fjord. For a better comparison with his study, we will further use k = 2.1W/°Cm and find the factor ω that makes the model fit the measurements.
Finally the Stefan's law can also be used to predict the growth of the consolidated layer in first-year ice ridges (Leppäranta et al., 1995 and Høyland, 2002) by expressing the latent of the unconsolidated layer:

$$l_{ridge} = l_i \cdot \eta \tag{2}$$

where η is the macro-porosity of the ridge.

RESULTS

Met-Ocean data

Air temperature, air pressure, wind speed and direction are recorded every third hour by the airport of Svea, and figure 3 shows the air temperature (T_a) record of the 3 months period during which the ridge was surveyed. T_a fluctuated a lot and sometimes rapidly. It clearly increased at the end of April. The minimum temperature recorded was -33.1°C on 2 April.

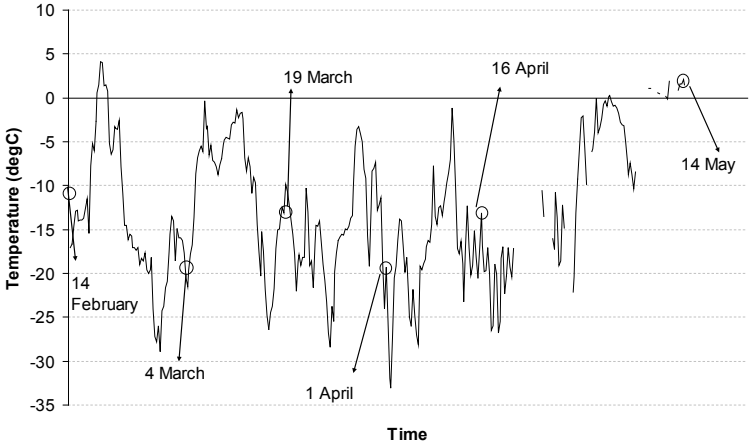

Figure 3. Air temperature evolution in Svea airport, Winter 2009.

The wind always follows a natural corridor formed by the fjord and the valley situated in the continuation of the fjord. It mostly came from the East, but the highest velocity was 16.8 m/s and came from the west.
Snow thickness has been measured close to each thermistor string, the loggers and the battery and at the eastern and western parts of the ridge. It was packed on the sides due to strong wind actions but soft close to the loggers and the battery. It varied between 0 and 35cm.
Water salinity in Van Mijenfjorden was measured inside Svea Bay early March 2009 by UNIS students and showed a variation between 30 and 35 ppt. We will assume a water salinity of 34 ppt which gives a freezing point of the water at T_f = -1.86°C according to the UNESCO formula given in Lepparänta and Manninen (1988).

Level ice thickness, ridge geometry and block thicknesses

The surrounding level ice grew from 1.0 to 1.25m between 14 February and 14 May. In the Svea Bay, about 5 km further in the Van Mijen fjord, the level ice grew from 0.75 to 0.98m.
When drilling through the ridge it was difficult or impossible to estimate the keel depth. The rubble was so eroded and soft that there was no clear evidence whether it existed at all. Figures 2, 4 and 5 give the sail and consolidated layer thicknesses (h_s and h_c) on 3 occasions. The profiles show that the lines were too short to include the full width of the consolidated layer / ridge. In this way the average h_c may have been somewhat underestimated. At the first visit a few small gaps were felt when drilling. However, on all later visits no voids could be detected anymore. Figure 9 presents the measured h_c, and between 19 March and 1 April little or no ice growth was measured in both lines. This corresponds to an increasing snow accumulation, which changed from 4.5 to 13.5cm (in average) between these dates.

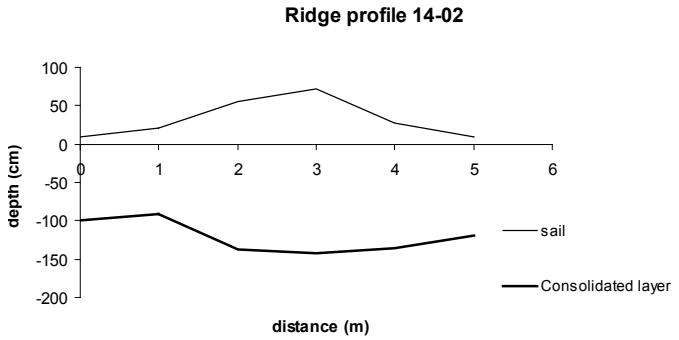

Figure 4. First cross-section on the ridge - 14 February

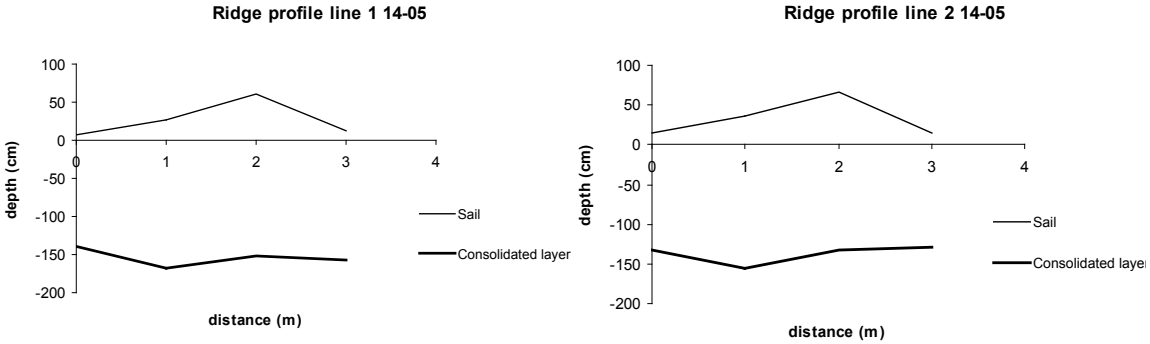

Figure 5. Ridge sail and consolidated layer thicknesses - 14 May.

The block thicknesses (h_b) of 9 pieces in the sail were measured each time the ridge was visited. At the first visit h_b ranged from 17 to 21cm with an average of 20cm. The average block thickness changed little (decreased to 18cm) until 16 April, but then it decreased to 13cm on 14 May. Figure 6 shows some pictures of the ridge. The distance between blocks 1 and 4 was zero at the two first visits, but then increased steadily up to 21cm on 14 May.

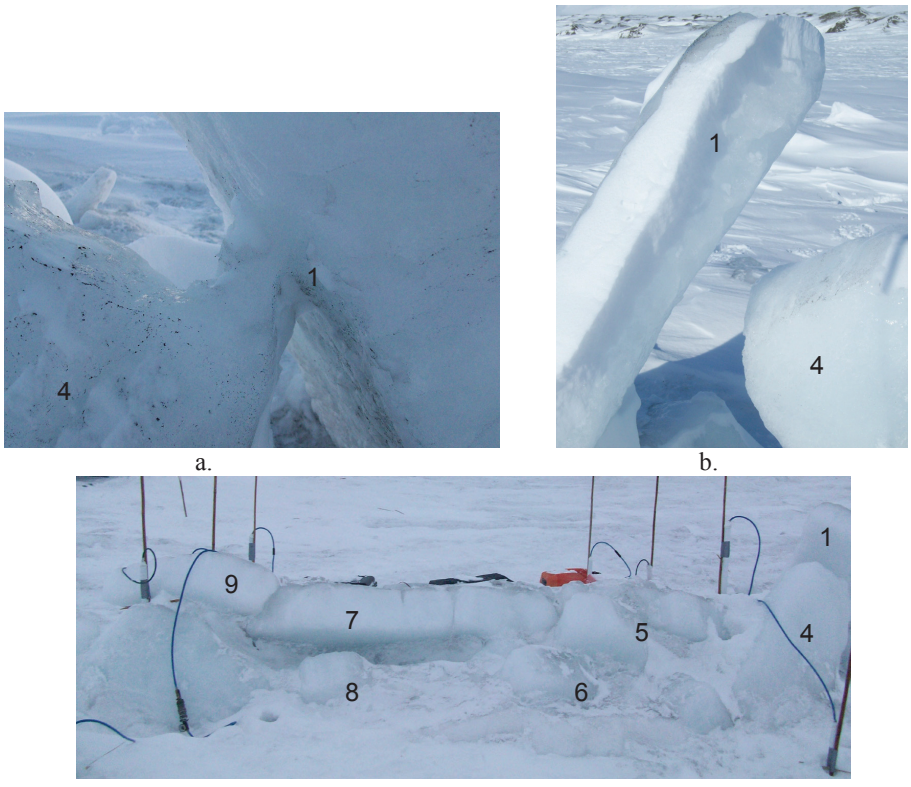

Figure 6. a) Space between blocks 1 and 4 on 4 March b) Space between blocks 1 and 4 on 16 April and c) Ridge on 4 March with numbered blocks.

Physico-mechanical properties

Both vertical profiles of TDS and uniaxial strength of vertical cores were measured as described in Table 1. Figure 7 shows salinity and porosity profiles from 1 April. The level ice salinity was less than that of the consolidated layer salinity and followed a typical c-profile whereas those of the consolidated layer were more random. The average salinity neither grew nor decreased throughout the season. It was typically 4-5psu, varying between 3.5 (16 April) and 5.5psu (14 May). The average micro-porosity of the consolidated layer varied between 9 and 15% from 4 March to 16 April and increased substantially up to 24.6% at the last visit.

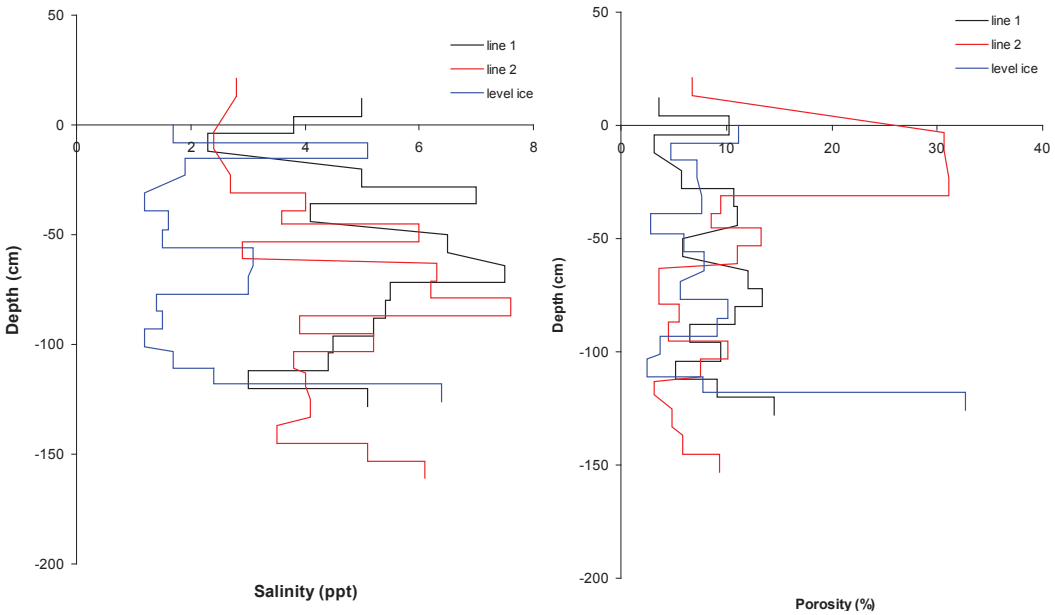

a) b)

Figure 7. a) Salinity and b) Porosity profiles from April 1.

The uniaxial compression tests were done on two visits, 1 and 16 of April, and respectively 9 and 12 samples were compressed. The average strength / porosity / temperature for the two dates were 3.0 MPa / 11% / -11.3°C and 2.6 MPa / 11% / -10.6°C. All the individual tests are plotted versus porosity in Figure 10.

Ridge temperatures

Figure 8 shows the weekly temperature profile of the thermistor string 1526, placed on line 1 in the ridge. According to the four thermistor strings in line 1, the consolidated layer grew from 1.27 to 1.53m between 4 March and 16 April. Around 1 May, warm water seems to have entered the fjord and could have penetrated up into the tube in which the string was placed (Figure 8). This made it impossible to predict h_c from the strings.

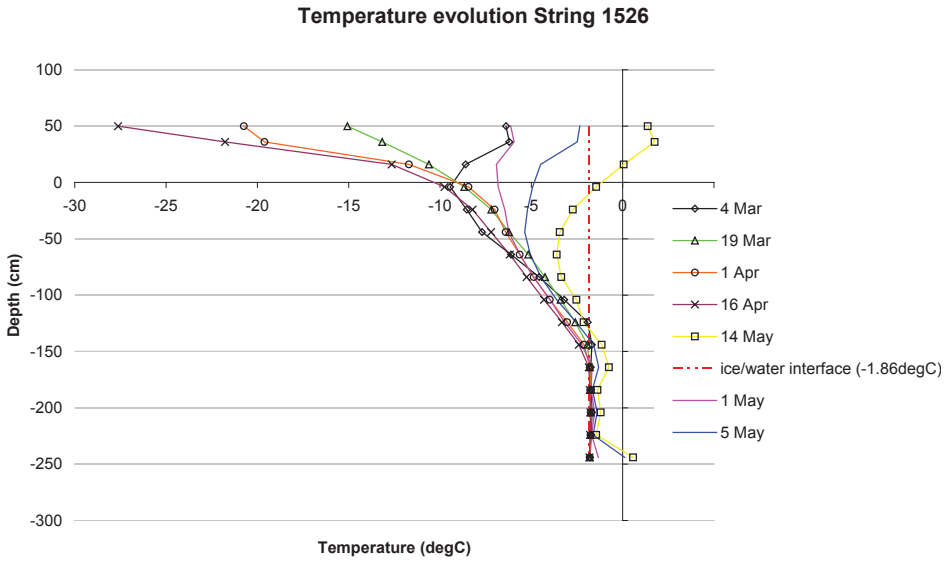

Figure 8. Temperature profiles for hole 2 in line 1 (string 1526)

Similar graphs have been plotted for all the thermistor strings. However, strings 1854 and 2157 appeared to be too short when the ridge grew up and thus its complete growth has not been recorded at these positions.

DISCUSSION

Ice growth and consolidation

We used the thicknesses of the level ice and the average thicknesses of the 4 first holes (0-3 in Figures 2, 4 and 5) in both lines in the ridge and fitted the parameters in Stefan's law. The level ice model (Eq.1) predicted the ridge surrounding level ice (*sli*) growth with ω_{sli} = 0.45 and the level ice growth in Svea bay (*SB*) with ω_{SB} = 0.33. Both are within the range estimated by Høyland (2009) for the years 1998-2006 in which the snow precipitation was modest. He also reports two different levels of level ice thickness and suggests that it is due to an early rafting event. We then combined Eqs.(1) and (2) to study the ridge consolidation and found that a combination of $\eta \cdot \omega = 0.25$ predicts the measurements for both lines. This gives a macro-porosity of 0.55 and 0.4 for respectively ω_{sli} and ω_{SB}. A combination based on the Svea Bay level ice thicknesses (ω_{SB} = 0.33 and η = 0.4) fits very well with earlier ridge consolidation measurements in the Van Mijen fjord reported by Høyland (2002). The ones derived from the surrounding level ice thicknesses may also be reasonable, but predict a relatively high rubble macro-porosity (0.55). The ratio of the consolidated layer thickness to the Svea Bay level ice thickness (*R*) varied between 1.4 and 1.57 for the two lines in the ridge. These values fit well what has been measured earlier in the Van Mijen fjord and other places (Høyland, 2002). When using the surrounding level ice thickness, the calculation of R gives then 1.2, which is somewhat lower. But if we include the date from all the holes in Figure 4, we get R = 1.33. This exercise demonstrates that

the simple version of Stefan's law (Eqs.1 and 2) is useful, but that one cannot expect an accurate prediction of the ice growth.
Figure 9 shows the measured thicknesses of the ridge and the level ice and the corresponding predictions by the Stefan's law.

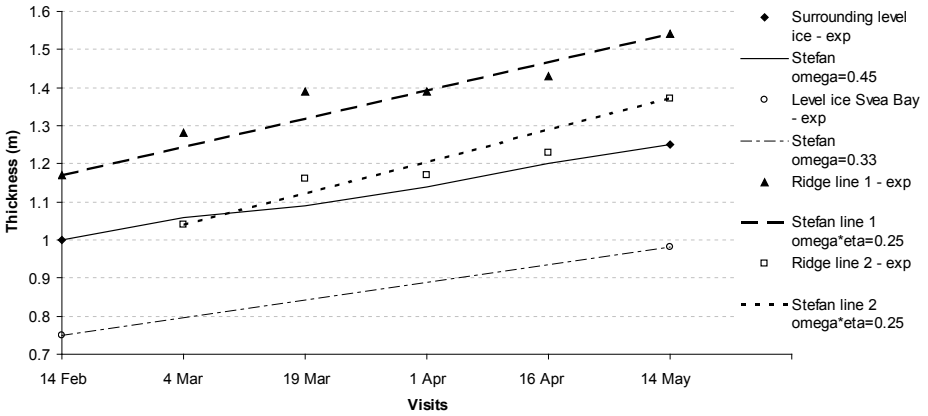

Figure 9. Measurements based on drillings and Stefan's law predictions. The thermal conductivity used in Stefan's law was k=2.1 W/°Cm.

The keel depth can crudely be estimated by empirical keel depth to sail height ratio (h_k / h_s). If we used the average value of Timco and Burden (1997) for first-year ridges (approximately 4.5) and the peak keel depth should have been about 2.2m. Using the average ratio for first-year ridges on Svalbard as reported by Strub-Klein (2011), the peak keel depth should have been around 2.3m.

Physico-mechanical properties

Very little data exists on salinities measured simultaneously in the consolidated layer and the level ice. Høyland (2007) states that the salinity of the consolidated layer was partly higher and partly lower than that of the level ice for first-year ridges in the Barents Sea investigated from 2002 to 2006. The same phenomenon was observed in further surveys of ridges (2007 and 2008) in the Barents Sea (student reports, unpublished data). In the present study, the average salinities in the consolidated layer were higher than those of level ice. Level ice salinities usually decrease through the season and are often 2-3psu in late spring. The mechanisms of desalination in first-year ice are not clear, but the different seasonal developments between level ice and the consolidated layer argue that the water below the level ice (accounting temperature, velocity and salinity) is an important factor.
The increase in micro-porosity in the final visit is basically due to increasing temperatures.

In Figure 10 the empirical formulas for level ice strength suggested by Timco and Frederking (1990) and Moslet (2007) are plotted together with our results. As the formulas gives some kind of upper limit, our ridge strengths lie as expected in between the predicted vertical and horizontal strengths of level ice, but closer to horizontal strength. This is of course due to the ice texture and argues that the consolidated layer has a more granular than columnar structure (see Høyland, 2007 for a deeper discussion and references about this). In addition to the porosity effect, it is

clear that cold ice is stronger than warm ice even for the same porosity (see e.g. Cox and Richter-Menge 1988), and our ice had been slightly cooled by the air temperatures before testing and had an average about -10°C when tested. Additional tests made on an artificial ridge in 2008 have been included in the following graph.

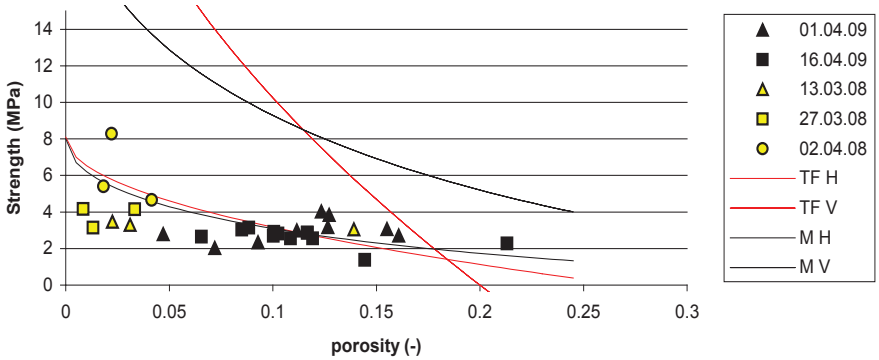

Figure 10. Comparison between the horizontal strengths measured in the field in 2009, unpublished data from 2008 (Strub-Klein 2008) and the empirical formulas for vertically and horizontally loaded samples of columnar ice developed by Timco and Frederking (1990) and Moslet (2007).

Rubble consistency

As explained earlier the rubble was so eroded and soft that it was difficult or impossible to determine the keel bottom. The calculations with the Stefan's law show that the consolidated layer grew more and faster than the level ice and this argues strongly that there was rubble beneath the consolidated layer. Earlier ridge investigations in the Van Mijen fjord (Høyland, 2002) have also reported soft and eroded rubble and in the Camp Morton case, it also became very difficult to determine the keel depth in the second half of the season. This was clearly different from the investigations done in the Northern Bay of Bothnia where the individual blocks could be easily felt throughout the season. There are important differences between these cases, with respect to both the oceanic conditions and the size and shape of the ridges. In the Van Mijen fjord there is a relatively strong tidal current, whereas there is almost no current where the ridge in the Baltic Sea was located. The second difference is that the Baltic ridge was a wide ridge field so that any oceanic flux would take more time to penetrate the ridge. It could also be that the permeability of brackish Baltic ridges is less than in saline ridges. Finally our 2009-ridge was substantially smaller than the ridges described by Høyland (2002) and thus the erosion should be much more efficient. The ratio of the oceanic flux to the conductive flux (the Biot number, see Høyland, 2007 for details) is a linear function of the size, so the effect of the oceanic flux increases with decreasing ridge size.

CONCLUSIONS

A small first-year ridge was investigated in the Van Mijen fjord, Svalbard, from 14 February to 14 May 2009. It was visited 6 times and the thickness of consolidated layer was measured by

drilling along two lines across the ridge. Two lines of four thermistor strings were installed and recorded temperatures from 4 March to 14 May.

The average consolidated layer grew from 1.17 to 1.54m in line 1 and from 1.04 to 1.37m in line 2 whereas the surrounding level ice grew from 1.0 to 1.25m. The measured consolidation and ice growth fit reasonably well with the Stefan's law, but show the importance of the spatial variation of the consolidated layer. The block thicknesses in the sail were fairly constant and of 0.2m until May when they decreased due to solar radiation.

TDS profiles were done 5 times and the average salinity in the consolidated layer laid between 3.5 and 5.5psu but remained more or less constant during the season. Level ice salinity usually decreases and this suggests that the effect of the water below the level ice is significant in the desalination process.
The micro-porosity increased during the season, mostly because of increasing temperatures.

Uniaxial horizontal compressive strength was tested in field during 2 visits and the results fit reasonably well with the empirical formulas of Timco and Frederking (1990) and Moslet (2007) for horizontal strength.

The rubble consistency was very soft and eroded, even more than in previous ridge studies in the Van Mijen fjord. We suggest that this is because the ridge was small and therefore the oceanic fluxes became more important. The consistency (and consequently the mechanical properties) of the unconsolidated layer in first-year ice ridges may vary considerably, depending on their size and the oceanic conditions. Small ridges in landfast ice with tidal current should erode faster than other ridges.

AKNOWLEDGEMENTS

We would like to thank Prof. Aleksey Marchenko for comments and explanations, Monica Votvik and Kåre Johansen for their help in the preparation of the fieldwork and in the field, Louis Delmas, Aleksey Shestov, Anatoly Sinitsyn, Serguey Sukhurukov, Simon Løvås, Professor Sveinung Løset and all the students from AT307F for their help in the field, The PetroArctic and PetroRisk projects funded by the Norwegian Research Council and DNV Research for providing the necessary funds (salaries and equipment).

REFERENCES

Blanchet, D. (1998). Ice loads from first-year ice ridges and rubble fields. Canadian Journal of Civil Engineering 25(1998) pp. 206-219.

Cox, G.F.N and Weeks, W.F (1983). Equations for determining the gas and brine volume in sea ice samples. Journal of Glaciology 29(102):306316

Cox, C.F.N. and Richter-Menge, J.A. (1988). Confined compressive strength of multi-year pressure ridge sea ice sample, Journal of Offshore Mechanics and Arctic Engineering, Vol. 110, pp. 295-301.

Høyland, K.V. (2002) Consolidation of first-year sea ice ridges, Journal of Geophysical Research, Vol. 107, C6, 10.1029/2000JC000526, 15,1-15,15.

Høyland, K.V. (2005). Ridges in the Barents Sea. Proceedings of the 18th Conference on Port and Ocean Engineering under Arctic Conditions (POAC). Vol.2 (2005) pp. 949-960.

Høyland, K.V. (2007). "Morphology and small scale strength of ridges in the North-Western Barents Sea." Cold Regions Science and Technology 48(2007): 169 - 187.

Høyland, K.V. (2009). Ice thickness, growth and salinity in Van Mijenfjorden, Svalbard, Norway. Submitted for publication in Polar Research. (2009).

Leppäranta, M. and Manninen, T. (1988). The brine and gas content of sea ice with attention to low salinities and high temperatures. Finnish Institute of Marine Research. Internal Report 2.

Leppäranta, M. (1993) A review of analytical models of sea-ice growth. Atmosphere Ocean, Vol. 31 (1), pp. 123-138.

Leppäranta, M. et al. (1995). The life story of a first-year sea ice ridge. Cold Regions Science and Technology. **23**(1995): p. 279-290.

McGuinness et al. (1998) Non-linear thermal transport and brine convection in first-year sea ice, Annals of Glaciology, Vol. 27, pp. 471-476.

Moslet, P.O. (2007). Field testing of uniaxial compression test of columnar ice. Cold Regions Science and Technology 48 (2007) pp.1-14.

Schwerdtfeger, P., (1963). The thermal properties of sea ice. Journal of glaciology, vol.4 October 1963, No 36. pp 789-807.

Shafrova, S. and Høyland, K.V. (2008). Morphology and 2D spatial strength distribution in two Arctic first-year sea ice ridges. Cold Regions Science and Technology **51**(2008) pp. 38-55.

Strub-Klein, L. et al. (2010). Physical and mechanical investigations of sea ice ridges in late summer in the Fram Strait. Proceedings of the 20th International Symposium on Ice (IAHR). Lahti, Finland.

Strub-Klein, L. (2011). A review of the morphological and mechanical properties of first-year sea ice ridges. Proceedings of the 21st International Conference on Port and Ocean Engineering under Arctic Conditions (POAC). Montreal, Canada.

Timco, G.W. and Frederking R. (1990). Compressive strength of sea ice sheets. Cold Regions Science and Technology 17 (1990) pp.227-240.

Timco, G.W. and Burden R.P. (1997). An analysis of the shape of sea ice ridges. Cold regions science and technology 25 (1997) pp.65-77.

4.4. Physical and mechanical properties of sea ice ridges in late summer in the Fram Strait

20th IAHR International Symposium on Ice
Lahti, Finland, June 14 to 18, 2010

Physical and mechanical investigations of sea ice ridges in late summer in the Fram Strait

Lucie Strub-Klein[1, 2], Nicolas Serré[2,3], Knut Høyland[2,1]
[1]*University Centre in Svalbard*
[2]*Norwegian University of Science and Technology, Trondheim, Norway*
[3]*Barlindhaug Consult, Tromsø, Norway*

Abstract

Six medium sized sea ice ridges have be investigated early September 2009 in the Fram Strait for the fourth year of a field study on multi-year ice ridges. Cross sectional drillings were made with 2'' augers in order to examine the geometry and the macro porosity of ridges. The largest depth recorded was 7.76m and the highest sail measured was 1.86m. In addition, a profile of the physical properties of each ridge has been established. Average density, salinity and porosity in the keel were found to be respectively 945kg/m^3, 2.05psu and 14.27%. For the first time in that area, uniaxial compression tests have been performed at three stations. The average strength in the keel was 1.75MPa. The strength in these ridges was in the same range as the ones measured by Cox and Weeks (1985) and lower than the strength of horizontally loaded samples of level ice predicted by Timco and Frederking (1990) and Moslet (2007).

1. Introduction

Sea ice ridges are formed by compression or shear in the ice cover. They consist of ice blocks partly refrozen together, water, salt and air. They are divided into 3 parts: the sail, above the waterline, the consolidated layer, below the waterline and a lower unconsolidated part, the rubble. At the ridge formation, water is trapped in between the blocks below the waterline in what is called water pockets. After the ridge has formed, cold air temperatures will induce the progressive freezing of the water pocket, starting from the water level and progressively towards the keel, thus contributing to the growth of the consolidated layer.

Ridges can be characterized according to their age. When a first-year ice ridge survives the summer melt season, it becomes a second-year ice ridge and a multi-year ice ridge if it survives at least two summers. During the melt season, the ice ridge is melting from the top and from the bottom. The angular ice blocks become gradually round off and the voids between them become filled with the refrozen melt of snow and ice. The required number of melt seasons for a complete refreezing of the voids depends on the thermal regime and the environment in which the ridge is travelling (Kovacs and Mellor, 1971; Johnston and Timco, 2008). Johnston and Timco (2008) explain that a new layer is growing each winter at the bottom of the ridge. Consequently, the ice that has survived a melt season presents a low salinity in comparison with the newly formed ice. Multi-year ice feature can comprise many ice layers, but it is usually not possible to distinguish them.

Due to the massive and continuous structure of the low saline ice composing multi-year ice ridges, Kovacs et al (1973) states that they represent a major problem in the design of potential offshore structures. The ice forces on conical structures are considered to be less than that for ice crushing against a vertical-sided structure. Therefore conical structures are often the first choice for designers in the development of an arctic oil field. In order to estimate multi-year ridge action, the standards propose different models. In all of them, the ridge is considered as a uniform body uniquely composed of ice. The standard API RP 2N 95 gives the most details on the estimation of multi-year ice ridge action. It indicates that forces on a ridge from bending can be determined by four different methods:

- Ice sheet approximation: it is valid when the ridge is wide or not much thicker than the level ice. The loads can be computed with three different theories: the elastic beam bending, the elastic wedge bending and the plastic wedge bending.
- Elastic beam on elastic foundation: the breaking forces are determined from the ridge breaking initially at the centre, and later at hinge cracks further away from the structure. The ridge breaks when its tensile stress reaches the tensile strength of the ice. The limiting force in the structure is determined from either the breaking of the ridge or the clearing of the last pieces.
- Plastic limit plate analysis: it is an upper bound plastic limit solution given by Wang (1984) for the forces on a conical structure due to a long pressure ridge. The hinges deform plastically and the geometry of the ridge and plastic hinges resemble a roof.
- Gravity forces from a ridge which rides onto a cone: Nordgren and Winkler (1989) have developed a method considering the rotation of the ridge as it is pushed up the cone. The gravity and buoyancy forces are considered and the ridge is analysed as a beam to determine the maximum length which will not break under flexure. The maximum force is determined as the maximum ride-up force.

The models mentioned above require information on the ridge geometry, density, elastic modulus and flexural or tensile strength. It is therefore needed to collect a large amount of data in the field to understand how these properties are linked and therefore to improve the accuracy of these models.
Very little information on the in-situ properties of multi-year ice ridges is available elsewhere than in the Northern Canada areas. Kovacs (1983) has investigated 11 ridges in Alaska and presents results on morphology, temperature, density, salinity, microporosity and strength. Hnatiuk and al (1978) presented 4 multi-year ridges, 1 first-year ridge and ice islands. They performed tensile Brazil tests and showed some morphological profiles established by drilling and diving. Kovacs et al (1973) investigated 1 multi-year ridge and presented its geometrical profile, made by drilling, and collected samples for density and salinity measurements. They also performed ice breaking experiments. Richter-Menge and Cox (1985a,b) had a special focus on the crystal orientation of the ice in multi-year ridges and its influence on the ice strength. They also reported values of salinity. Cox et al (1984), Cox and Richter-Menge (1985b, 1986) and Richter-Menge and Cox (1985b) focused more on the mechanical properties. In addition, Johnston and Timco (2008) published a guide which gathers observations (from airplane, boat or drilling) on old ridges geometry. Høyland et al (2008) and Strub-Klein et al. (2009) have been investigating the geometry and physical properties of second-year ridges in the Fram Strait.
In spite of the previous work on multi-year ridges there is still a lack of knowledge on their properties. The estimation of the mechanical properties is necessary for the ridge action computation, and understanding the link between their mechanical and physical properties would allow a better tuning of the models in function of the environmental parameters. In order to collect more data, six medium sized sea ice ridges were investigated early September 2009 in the Fram Strait for the fourth year of a field study on multi-year ice ridges.
This paper not only gathers information about some of the most important physical properties necessary to understand the ice behavior, but also geometrical and morphological data and presents the results for uniaxial compression field tests that have been performed in the Fram Strait for the first time.

2. Location and experimental set-up

UNIS and NTNU were given the opportunity to join the Norwegian Polar Institute (NPI) on board RV/Lance for the fourth time during their annual oceanographic cruise in the Fram Strait in September. The cruise lasted 16 days. Six ice stations were established. Each station lasted 4 to 6 hours. The ridges were selected first according to their accessibility from the ship, and if they were several on the same floe, according to their size. Since the working time on the ice was restrained, we chose ridges that did not present a too high sail. It was snowing and windy when working on station FS09-01b but there were good weather conditions for the other stations, with practically no wind. The air temperature was varying between -3 and 2°C during the day and -5 and 0°C during the night. Figure 1 is a map representing the different ice stations.

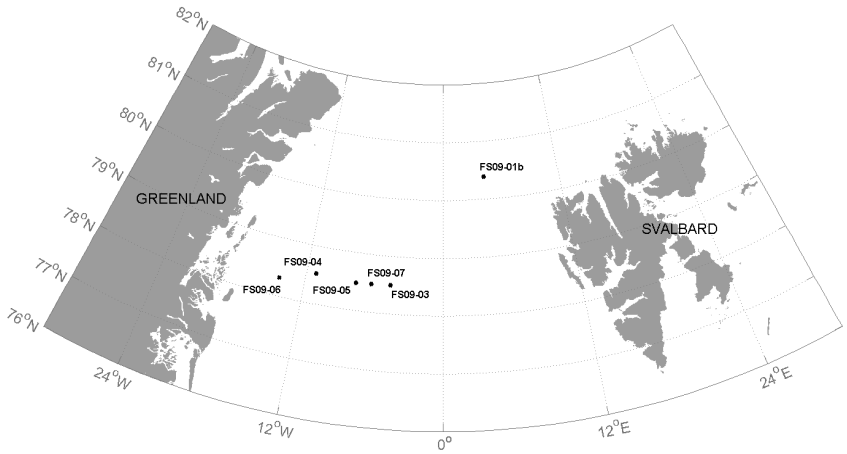

Figure 1. Location of the 6 ice stations

Several activities were performed on site:

- Cross section drilling with 2'' augers to detect some potential gaps and to establish a morphological profile of the ridge. The keel depth was measured with an ice thickness gauge fixed to a measuring tape. The water level (freeboard) was measured with a regular meter. The macroporosity was established by recording any sudden drop of the auger while drilling in the borehole and measuring the vertical extension of that drop. The consistency of the ice was considered for determining the macroporosity. Basically, any drop or slush was considered as a void whereas hard and soft ice were defined as ice. The total macroporosity of the ridge was then calculated by assuming that it is equal to the total length of the voids divided by the total length of the boreholes. The boundary between the consolidated layer and the rubble, if there was one, was defined by observing any water or slush coming up with the drill or by a transition from hard to very soft ice.
- Temperature, density and salinity (TDS) profile from core sampling. The core was taken with a 75mm diameter Kovacs core barrel and the temperature was measured from the bottom to the top of each core every 10cm. Then the core was sliced into 8cm long pieces that were weighed with a spring scale and placed to melt. The length of the specimen was measured at three different places and averaged. The density was then calculated. The ice porosity, which we will call microporosity throughout this paper to avoid any confusion with the ridge macroporosity, is calculated together with the air and brine volume from the formulas given by Leppäranta and Manninen (1988) for T_i>-2°C or from Cox and Weeks (1983) for T_i<-2°C. These formulas require temperature, density and salinity as input parameters.
- Uniaxial compression test. A second core was sampled for immediate strength tests with a portable uniaxial compression rig, Kompis. That device has been especially designed to be brought in the field and a description is given in Moslet (2007). Uniaxial compression tests were performed at stations FS09-04, FS09-06 and FS09-07. The diameter of the samples was 7.2cm with a testing length of 17.5cm. The strain rate at which the samples were compressed was fixed to$10^{-3}\,s^{-1}$. Table 1 shows the different stations and related activities.

Table 1. Ice stations

Name	Date	Position		Activities	Holes in morphological cross section
		latitude	longitude		
FS09-1b	01.09.2009	N 80 38,943	E 4 24,777	T,D,S, morph	8
FS09-03	03.09.2009	N 78 50,049	W 4 56,150	T,D,S, morph	8
FS09-04	05.09.2009	N 78 53,658	W 11 13,287	T,D,S, morph, σ	9
FS09-05	06.09.2009	N 78 48,055	W 7 59,044	T,D,S, morph	6
FS09-06	08.09.2009	N 78 32,482	W 14 2,660	T,D,S, morph, σ	8+longitudinal
FS09-07	12.09.2009	N78 49,100	W 6 27,208	T,D,S, morph, σ	6

T: Temperature, D: Density, S: Salinity morph: cross-section σ: strength tests

3. Results

Geometry and morphology

A thickness profile of 6-9 holes mostly with 2 m spacing was drilled in all 6 ridges. Table 2 gives the thicknesses and associated ratios. The maximum keel depths were between 2.7 and 7.2 m so the ridges were small to medium ridges. The degree of consolidation varied, the three first ridges (FS09-01b, 03 and 04) had a completely consolidated core, with some soft ice/slush in the bottom. In ridges 01b and 04 we also found partly refrozen surface meltponds. On the other hand, the two ridges FS09-05 and 07 were not completely consolidated as we found substantial amounts of slush/soft ice inside the keels. The macroporosity (ratio of slush/soft ice) was 23 % in both ridges. Ridge FS09-06 was mostly consolidated, but presented some very soft ice for about 3 m at 0.65m depth.

Table 2. Peak and average values of Sail and keel thicknesses and associated ratios

Table 2. Peak and average values of Sail and keel thicknesses and associated ratios

	Ice thickness				Ratios h_k/h_s		p [%]
	Sail (h_s)		Keel (h_k)				
	Average	Max	Average	Max	Max h_k / max h_s	Avg h_k / avg h_s	
FS09-01b	0,37	0,99	3,05	6,1	6,2	8,2	8,83
FS09-03	0,81	1,86	5,61	7,02	3,8	6,9	7,26
FS09-04	0,64	1,68	2,31	2,68	1,6	3,6	5,03
FS09-05	0,74	1,46	5,82	7,16	4,9	7,9	23,16
FS09-06	0,48	0,88	3,07	3,7	4,2	6,4	0
FS09-07	0,53	0,9	4,18	4,8	5,3	7,9	22,86
average	0,6	1,3	4,01	5,24	4,33	6,82	11,19
Δh	0,17	0,43	1,45	1,83	1,58	1,72	9,63

Δh is the standard deviation.

There was no snow covering the ridges at stations FS09-1b, FS09-03 and FS09-05, but the average snow thickness on the three other ridges was 6cm. It was more difficult to identify the blocks of the sail, either because they were covered by snow or because they were eroded and

melted together. Ridge 04 seemed to be the oldest ridge as the blocks were more weathered and we found sediments in the bottom ice layers.

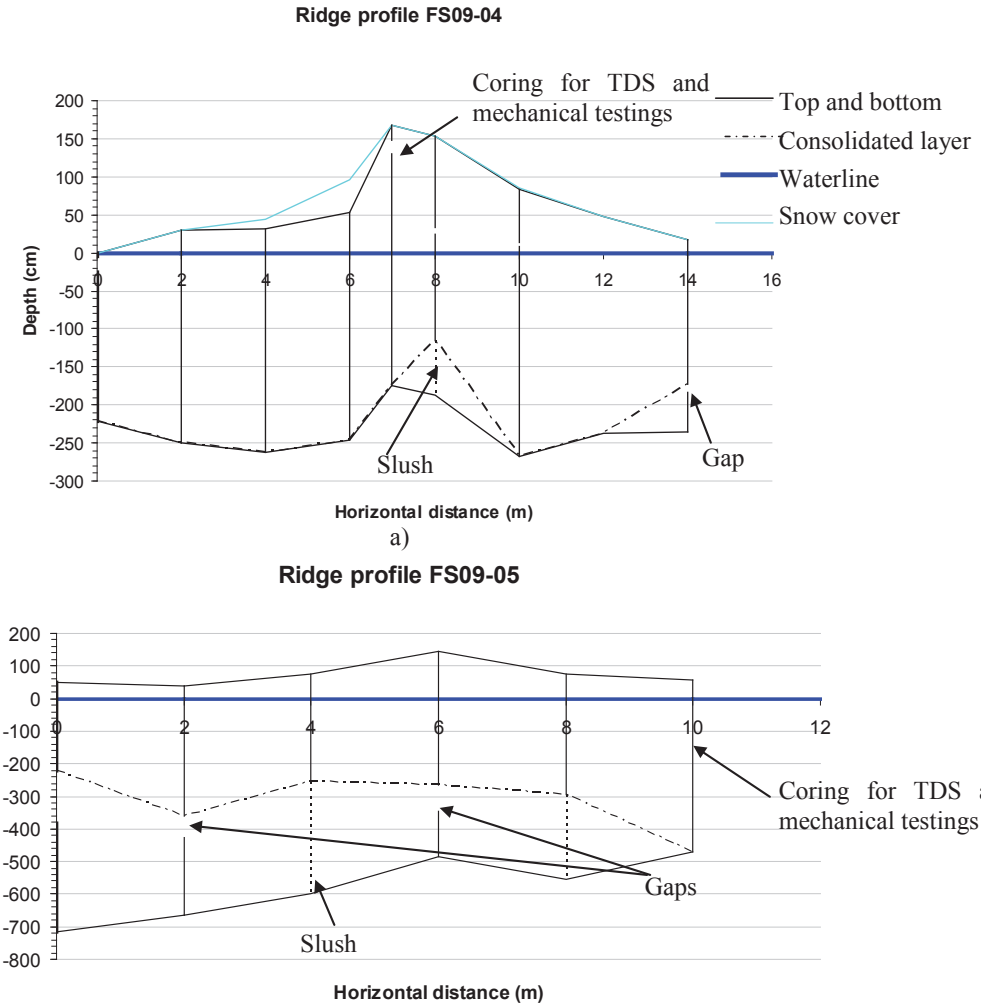

Figure 2. Morphology of FS09-04 (a) and FS09-05 (b).

Physical properties

Table 3 gives average values of temperature, density, salinity, air and brine volumes in the sail and the keel of each ridge. It can be observed that FS09-04 had lower keel salinity than the

others. Figures 2 and 3 shows the through-thickness profiles for ridges FS09-04 and 05. As expected the salinities in the sail were lower than in the keel.

Table 3. Physical properties of the six ridges, September 2009

	Temperature		Density		Salinity		Porosity					
							brine fraction		air fraction		total porosity	
	Sail	keel	Sail	Keel	sail	keel	sail	keel	sail	keel	sail	keel
	[°C]	[°C]	[kg/m^3]	[kg/m^3]	[psu]	[psu]	[--]	[--]	[--]	[--]	[--]	[--]
FS09-01b	-0,33	-0,95	819,22	906,12	0,21	2,69	0,02	0,20	0,11	0,05	0,13	0,25
FS09-03	-1,13	-1,64	831,41	927,48	0,16	2,09	0,09	0,08	0,12	0,01	0,22	0,09
FS09-04	-0,48	-1,24	719,78	868,52	0,66	1,29	0	0,07	0,21	0,07	0,21	0,14
FS09-05	-0,88	-1,07	649,51	907,28	0,17	1,83	0	0,06	0,29	0,07	0,29	0,14
FS09-06	-1,63	-1,25	863,69	852,05	0,45	2,71	0,02	0,10	0,06	0,09	0,08	0,20
FS09-07	-0,36	-0,69	892,34	954,47	0,23	1,73	0,06	0,13	0,05	0,01	0,12	0,14
Average	-0,80	-1,14	795,99	902,65	0,31	2,06	0,03	0,11	0,14	0,05	0,18	0,16
$\Delta\sigma$	0,51	0,32	92,65	37,58	0,20	0,56	0,04	0,05	0,09	0,03	0,08	0,05

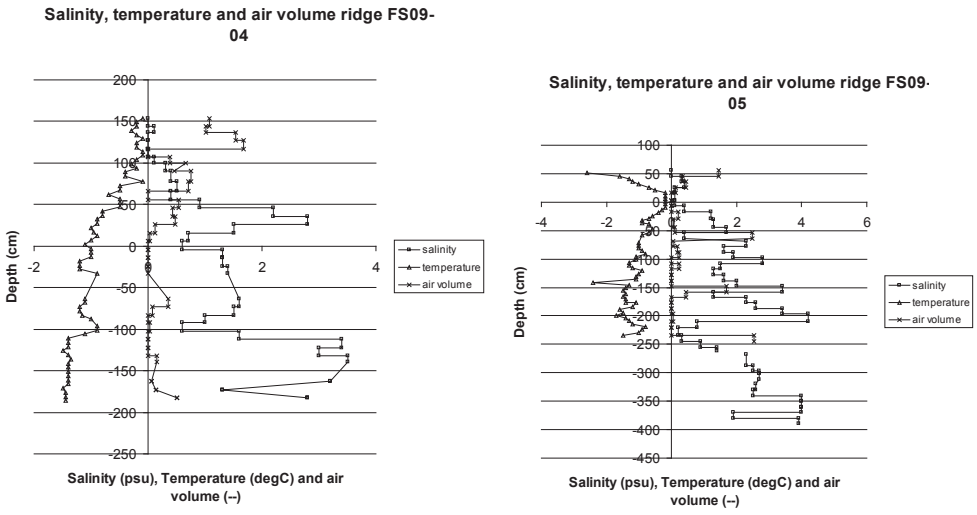

(a) (b)

Figure 3. The profile of temperature, relative air volume and salinity in ridge FS09-04 (a) and FS09-05 (b). The air fraction has been multiplied by a factor 5 to ease the reading of the plot

The temperature decreased with depth below the waterline and reached about -1.5°C in all the ridges but FS09-03 and 07 that were respectively -2°C and -0.5°C warm at the bottom. In ridges FS09-01b, 05 and 06 the sail had started to cool down.

Mechanical properties

Table 4 collects the average values of strength, density, salinity and microporosity for each additional core taken at ridges FS09-04, FS09-06 and FS09-07. Sometimes the core broke inside the core barrel while drilling and it was impossible to use the ice for uniaxial testing. Therefore there was no data collected in the sail for ridge FS09-07.

Table 4. Strengths and their related physical properties

	Strength				Temperature		Density		Salinity		brine volume		air volume		Porosity	
	sail		keel		sail	keel	sail	keel	sail	keel	sail	keel	sail	keel	sail	keel
	[MPa]	ds	[MPa]	ds	[°C]	[°C]	[kg/m^3]	[kg/m^3]	[psu]	[psu]	[--]	[--]	[--]	[--]	[--]	[--]
FS09-04*	1,3	0,87	2,5	2,07	-8,36	-9,4	---	---	1,3	2,5**	---	---	---	---	---	---
FS09-06	2,59	---	1,65	0,27	-1,1	-1,43	0,883	0,931	1,6	2,8	0,07	0,1	0,04	0,03	0,09	0,11
FS09-07	---	---	1,95	0,99	---	-0,94	---	1,004	---	1,85	---	0,1	---	0	---	0,103

* storage -30°C during 2 days
** only two cores measured : 0,7psu and 4,3 psu

For FS09-04, only two samples were tested in the keel. One specimen was 0.7psu and the other one was 4.3psu. The ice was stronger with lower temperature and higher salinity. The contrary can be observed for ridge FS09-06, where the ice strength was higher with higher temperature but lower salinity and density. However, the air fraction was calculated to be 0.015 in average.

4. Discussion

Geometry and morphology

The ridges had different ages, ridge FS09-04 was older than the others, it was the most eroded, had the lowest keel salinity and the lowest keel to sail ratio. The sediments at the bottom could mean that the ridge came from Siberia (S. Gerland, private communication). The important gaps at a constant depth in the morphological profiles of FS09-05 and 07 indicate either that these two ridges were still in the process of consolidating, or that the ice below the slush/soft ice layer could come from a second ridging event. Unfortunately no conclusion could be drawn since we do not have any physical properties from the lowest part of their keel.
The keel depths were in the range of what has been measured in the Fram Strait in the three previous autumns (Høyland et al., 2008 and Strub-Klein et al., 2009). Two of the keel depth to sail height ratio (5.3m and 6.2m) were higher than what Timco and Burden (1997) found in their review of 53 old ridges (3.2 in the Beaufort and 4.7 in the vicinity of Queens Islands). But this ratio strongly depends on the shape of the ridge, and if the surface is relatively flat, the ratio becomes lower that if a triangular sail exists. Furthermore, if only a part of the ridge/floe is examined it is difficult to know if the rest of the floe lifts or depresses the examined part. The h_k/h_s ratios of the two ridges from 2009 with a clearly distinguishable sail (FS09-03 and 04) were comparable with the results of Timco and Burden (1997).

Table 5. Summary of keel depths, sail heights and h_k/h_s for different regions

author	Location	sail height [m]	keel depth [m]	h_k/h_s [--]
Kovacs (1983)	Alaska	2,92	9,18	3,22[a]
Kovacs (1973)	Beaufort Sea	3,73	12,17	3,26[a]
Cox et al (1984)	Beaufort Sea	2,43	5,44	2,78[b]
Timco and Burden (1997)	Northern Canada			3,17[a]
Høyland et al (2008)	Fram Strait (2006)	0,6	3,82	6,87[a]
	Fram Strait (2007)	0,33	2,75	15,91[a]
Strub-Klein et al. (2009)	Fram Strait	0,52	4,33	8,21[b]
		0,6	4,01	6,82[b]
Present study	Fram Strait	1,29	5,24	4,33[a]

[a]: Maximum sail and keel
[b]: total average sail height and keel depth

There are three different ways to calculate those ratios. The first method (a) consists in taking the maximum keel and sail found by drilling. The second method (b) consists in calculating the total average sail height and keel depth and the third method (c) consists in calculating the ratio for each borehole that was drilled and then making a total average. For this study, methods (a) and (b) were used and the final results vary significantly. Care must then be taken when comparing ratios. The high value obtained from Strub-Klein et al (2008) can be explained by the fact that they used a different method of calculation.
Most authors that have examined old ridges report fully consolidated keels, sometimes with some softer first-year ice at the bottom in the spring (Kovacs, 1983; Hnatiuk et al, 1978). The ridges FS09-05 and 07 had about 7.4% slush and a macroporosity of 23% which is rather low, but still comparable to first-year ridges.
Hnatiuk et al (1978) did not measure any void extension, but felt cavities in only 2 boreholes out of the 25 they have been drilling. They also had divers examining the ice consistency. The observations revealed that the ice at the bottom of the ridges was deteriorated and shaped like long platelets. That layer was very thick and offered no resistance when the divers tried to get their arms through. This same layer was felt in all the ridges we investigated and explains why the macroporosities were so high.
The Canadian Ice Service define the graduation date of first year to second year ice on October 1 (Johnston and Timco, 2008). Our investigations took place the first half of September but there is no doubt that the ridges we studied would not melt before early October. We will then assume they were second-year sea ice ridges.

Physical properties

The temperatures and the salinities were correlated throughout the keels; the temperature generally decreased toward the bottom while the salinity generally increased. This was very clear for ridges FS09-1, 03 and 06, but also visible in ridges FS90-04 and 05. In addition the local changes in salinity were accompanied by corresponding temperature changes, e.g. at 1 m depth in FS09-04 and 1.5 m depth in FS09-05. The general trend is a result of the summer heating and corresponding desalination, but the local correspondence is more difficult to explain.

Our measured average keel salinities of about 2psu are somewhat higher than the 1.37 and 1.64 found by respectively Kovacs (1983) and Richter-Menge and Cox (1985) but well within the range presented by Johnston et al. (2003).
The relative air volume (η_a) is in addition to the salinity not dependent on the temperature so that measurements performed in ice of varying temperature can be compared. As the oldest and one of the younger ridges (FS09-04 and 05) had the same η_a it seems to be no relation to the age of the ridge. The average η_a for the keels in 2009 was 5 %, it was respectively 4.9, 2.1 and 6.8 % in 2006 to 2008 in the Fram Strait, and Kovacs (1983) and Richter-Menge and Cox (1985) measured respectively 7.47 and 2.7. First-year ridges in the Barents Sea had relative air volumes ranging from 3-7 % (Høyland et al., 2008). It supports the suggestion that summer consolidation only little affects the air volume.

The density is sometimes higher than 1. This particularity can be explained by the volume estimation method of each ice samples, which approximates each of them to a cylinder, without considering irregular broken edges. Furthermore, the weight was measured with a spring scale, very sensitive to any movement due to the wind or the operator holding it. The resolution of this scale was 10g. Finally, a high presence of brine pockets could have increased the density above the fresh water density. It was actually observed in some samples with a density slightly higher than 1 that the salinity was much higher than in the other samples.
Table 6 presents the average values for micoroporosity, air and brine volume, salinity and density for the past four years in ridge keels. In addition, it presents the difference between the results found the previous years and in 2009.

Table 6. Physical properties collected during 4 years in the Fram Strait

	η	difference with 2009	η_a	difference with 2009	η_b	difference with 2009	S	difference with 2009	ρ	difference with 2009
	[%]	[%]	[%]	[%]	[%]	[%]	[psu]	[%]	[g/cm3]	[%]
UNIS/NPI (2006)	13	+2,48	4,9	+48,48	8	-23,08	2	-9,50[a] +4,71[b]	0,88	-5,38
UNIS/NPI (2007)	10	-24,98	2,1	-36,36	6,9	-33,65	1,80	-18,55[a] -5,76[b]	0,91	-2,15
UNIS/NPI (2008)	18,40	+38,03	6,8	+106,06	11,6	+11,54	2,76	+24,89[a] +44,50[b]	0,86	-7,53
UNIS/NPI (2009)	13,33	--	3,30	--	10,4	--	2,21[a] 1,91[b]	--	0,93	--

[a]: with average keel salnity of 2,5psu for strength cores
[b] with average keel salinity of 0,7psu for strength cores

Mechanical properties

Strength results from the tests performed on ridge FS09-04 can not be considered as in-situ testing. In fact, due to some technical problems with the compression rig, the ice was stored in a freezer at -30°C for two days before testing. Consequently, the ice structure and properties had changed, the temperature was lower and therefore the ice was stronger.
The ice in ridge FS09-07 was stronger than in ridge FS09-06. The air present in the ice influences the strength of the ice that is tested. The more air there is in the ice, the weaker the sample will be.

A comparison between the field tests and the models established by Timco and Frederking (1990) and Moslet (2007) for first-year level ice is proposed. Those models were established by testing respectively 283 and 520 samples. They propose an estimation of the ice strength according to the direction the sample is loaded. Timco and Frederking propose formulaes with the strain rate and the porosity as variable whereas Moslet proposes a model with the porosity as only variable. The porosity is either calculated from Cox and Weeks (1983) or from Leppäranta and Maninen (1988).

Figure 4 shows the data collected on ridges FS09-06 and 07, the strength predicted by the models of Timco and Frederking (1990) and by Moslet (2007), as well as an area corresponding to the experimental data that Cox et al. (1985) collected for T=-5°C and T=-20°C.

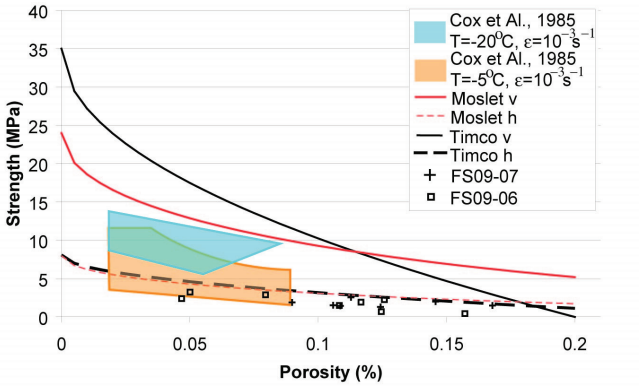

Figure 4. Strength as a function of the microporosity

There is a clear decrease of strength with increasing porosity. Some of the tests performed on ridge FS09-06 fit the data obtained by Cox et al. (1985) for samples at -5°C.
The model developed by and Frederking (1990) and Moslet (2007) for horizontally loaded samples of level ice slightly overestimates the strengths found on the ridges. Nevertheless, there is a very good agreement with both models. The underestimation might be due to the conditions the ice constituting the ridges grew as a contrast to level ice. The keel of the ridge is more submitted to ice pressure and oceanic fluxes, which contribute to lower its strength.
No thin sections were made to observe the ice texture, but it is believed it could have explained the difference in strength.

5. Conclusions

First-year to second year sea ice ridges have been investigated in late summer/early winter in the Fram Strait for the fourth year in continuation of Høyland et al (2008) and Strub-Klein et al (2009). Uniaxial compression tests have been performed for the first time in that region. Morphological profiles have been established and samples taken out for investigations on temperature, density and salinity.

The main conclusions of this study are:

- The average ice temperature was -0.8°C in the sail and -1.14°C in the keel, revealing that the ridge underwent a summer thermal regime
- The keels are more saline than the sails due to a drainage of the brine channels.
- A higher air volume in the sail confirms the ice is also formed from rain and refrozen snow
- Some high values of the density can be due to the inaccuracy of the measurement method or to the presence of brine pockets in the samples

The strength evaluated in the field has been compared to some existing models and other test results. The strength seems comparable to the data of Cox and Weeks (1985) for comparable porosities. The values agree with both models for horizontally loaded samples developed by Timco and Frederking (1990) and Moslet (2007) for level ice. Still, the models tend to slightly overestimate the strength in the Fram Strait. The reasons for that are still unclear but it is believed that the ice texture could have played a role.

Physical parameters, in particular the salinity and the microporosity, begin to be constant after four years of research. It is necessary to continue these annual investigations to be able to determine their trend more and more accurately. Stable parameters are actually better for the accuracy of the models and codes they will be used in. More strength tests are also required in order to get a clear tendency and adapt the existing analytical models to multi-year ridges.

Acknowledgements

The authors would like to thank the Norwegian Polar Institute for inviting UNIS and NTNU onboard RV/Lance, the crew of RV/Lance for their help and kindness, Sebastian Gerland for his advice, and Paul Dodd, Magnus Drivdal, Helene Erlandsen, Ole-Morten Olsen, Aleksey Pavlov and Johanne Rydsaa for their help on the ice.

References

API RP 2N 95 (1995). Recommended Practice for Planning, Designing, and Constructing Structures and Pipelines for Arctic Conditions. API recommended practice 2N second edition, December 1, 1995, American Petroleum Institute, 82p.

Cox, G.F.N and Weeks, W.F (1983). Equations for determining the gas and brine volume in sea ice samples. Journal of Glaciology 29(102):306316

Cox, G.F.N et al (1984). Mechanical properties of multi-year sea ice. Phase1: Tests results. CREEL Report 84-9.

Cox, G.F.N et al (1985). A summary of the strength and modulus of ice samples from multi-year pressure ridges; New York: American Society of Mechanical Engineers, 126-133

Cox, G.F.N and Richter-Menge, J.A (1985). A summary of the strength and modulus of ice samples from multi-year pressure ridges.

Hnatiuk, J. et al (1978). A study of several pressure ridges and ice islands in the Canadian Beaufort Sea. Journal of glaciology. Vol. 20. No 84.

Høyland, K.V et al. (2008). The consolidation in second and multiyear sea ice ridges Part 1:Measurements in early winter. 19th IAHR International Symposium on Ice. Vancouver. Canada.

Johnston, M. et al (2003). In-situ Borehole strength measurements on multi-year ice. Proceedings of the 13th International Offshore and Polar Engineering Conference (ISOPE), Hawai, 25-30 May 2003, pp. 445-452. ISBN 1-880653-60-5.

Johnston, M. and Timco, G.W (2008). Understanding and identifying old ice in summer. CHC-TR-055. December 2008

Kovacs, A. and Mellor, M. (1971). Sea ice pressure ridges and ice islands. Creare Inc. for Arctic petroleum Operators Association. Technical Note 122. Calgary. Alberta.

Kovacs, A. et al. (1973). Structure of a multiyear pressure ridge. Arctic 6(1): pp 2231

Kovacs, A. (1983). Characteristics of multiyear pressure ridges. Proceedings of the 8th International Conference on Port and Ocean Engineering under Arctic Conditions Helsinki. Finland. Vol 2. pp 173182

Leppäranta, M. and Manninen, T. (1988). The brine and gas content of sea ice with attention to low salinities and high temperatures. Finnish Institute of Marine Research. Internal Report 2.

Molset, P.O (2007) Field testing of uniaxial compression strength of columnar sea ice. Cold Regions Science & Technology, Vol. 48 Issue 1, pp.1-15

Nordgren, R.P and Winkler, M.M (1989). Dynamic ride up and crushing of short ice ridges on conical structures, proc 8th OMAE Conf., The Hague, Netherlands, Vol. 4, pp. 287-291.

Richter-Menge, J.A and Cox, G.F.N (1985a). Structure, salinity and density of multi-year sea ice pressure ridges. Journal of Energy Resources Technology; V.107, NO.4:493-497

Richter-Menge, J.A and Cox, G.F.N (1985b). The effect of sample orientation on the compressive strength of multi-year pressure ridge. Civil Engineering In The Arctic Offshore: Proceedings of the conference Arctic '85; p465

Strub-Klein, L. et al. (2009). Physical properties and comparison of first- and second-year sea ice ridges. Proceedings of the 20th International Conference on Port and Ocean Engineering under Arctic Conditions, Luleå, Sweden.

Timco, G.W and Frederking, R.M.W, (1990). Compressive strength of sea ice sheets. Cold Regions Science and Technology 17 (1990) pp.227-240

Timco, G.W and Burden, R.P (1997). An analysis of the shapes of sea ice ridges. Cold Regions Science and Technology 25(1997): pp. 6577.

Wang, Y.S (1984). Analysis and model tests of pressure ridges failing against conical structures. Proc. IAHR Symposium on Ice, Vol. 2, pp 67-76, Hamburg, Germany.

Chapter 5 – Conclusions and recommendations for further work

5. 1 Summary and conclusions

Field measurements and analysis of level ice properties

Several field campaigns were undertaken in the frozen fjords of Svalbard and the Barents Sea from 2003 to 2011 in which the ice thickness, temperature, density, salinity and strength were measured. From 2005, uniaxial compressive tests were conducted directly in the field using a transportable compressive rig (KOMPIS) designed for UNIS. During winter 2010, an intensive field study of level ice in Van Mijenfjorden was conducted, and the concept of strength variability has been introduced and analyzed. The main conclusions of the work on level ice are as follows:

- The variability of the uniaxial compressive strength is related to the localization of the brine (pockets and channels) in the sea ice. The coefficient of variation is lower for young ice, which has many small pockets, compared with older ice, which has fewer and larger brine channels. The spatial variation of the sea ice strength also depends on the distance between the samples.

- A statistical analysis of the uniaxial compressive strength for sea ice was performed, and the gamma, Weibull and lognormal distributions were compared to determine which of them would best describe the uniaxial compressive strength of sea ice. QQ-Plots combined with a least squares data fitting revealed that the gamma distribution is the best candidate for a statistical distribution for the sea ice strength.

- The spatial dissipation of stresses in ice subjected to borehole jack tests followed an exponential decay and the stresses decreased by 98% within the first 60 cm.

Morphology and physical and mechanical properties of first- and second-year sea ice ridges

Field investigations of sea ice ridges were conducted in Van Mijenfjorden on Svalbard and in the Fram Strait. An extensive analysis of floating first-year ice ridges catalogued and analyzed all their morphological characteristics. The main conclusions of the work on ice ridges are the following:

- Data from 45 sources and over 300 floating first-year ice ridges were extracted and analyzed. The best fit correlation between the keel depth and the sail height varied with the sampled region. For Arctic regions, a linear relationship $h_k = 3.84h_s$ fits best, whereas that for Subarctic regions, the data was better fit by a power relationship $h_k = 6.14h_s^{0.53}$. The maximum keel-to-sail ratio $h_k / h_s = 5.17$ was based on 308 values, and this ratio was logarithmically distributed. The cross-sectional geometry of the ridges

can vary greatly along the length of a ridge, even over a short distance. The sail height of individual ridges was more variable than the keel depth. The block thicknesses and the sail height were well represented by a square root model h_s=3.73$h_b^{0.5}$. The average consolidated layer of the ridge was 1.36 m based on 118 measurements, but this value varied strongly between different areas. The ratio of the consolidated layer thickness to the surrounding level ice thickness was in average h_{cl}/h_i=1.52. The variation of the consolidated layer did not change with time; hence the ridges developed evenly in width. Statistical analysis of 377 measurements of the consolidated layers of ridges in the Barents Sea showed that it is governed by a gamma distribution. Gaps of knowledge about sea ice ridges were identified from the compiled papers and reports.

- A small first-year ice ridge was found in Van Mijenfjorden in February 2009 and was visited 6 times between February 14 and May 14 the same year. The water below the level ice is involved in the desalination process. The rubble was soft and eroded because of the small size of the ridge (oceanic fluxes were more important). Small ridges of landfast ice should erode faster in tidal currents than larger ridges.

- Six first- to second-year sea ice ridges were investigated in late summer and early winter in the Fram Strait for the fourth time in 2009. Four were fully consolidated and two were in transition from first- to second-year. Average density, salinity and porosity in the keel were found to be respectively 945 kg/m^3, 2.05 psu and 14 %. The values for the salinity and the porosity were similar to those found in the previous years. The air fraction seemed to be independent from the age of the ridge. For the first time in that area, uniaxial compressive tests were performed at three stations and the average strength in the keel was 1.8 MPa. The results generally agreed with the existing models for horizontally loaded level ice.

5. 2 Recommendations for further work

Field measurements and analysis of level ice properties

- Further work could elucidate how to consolidate this information with existing load calculation methods.

- Numerous strength measurements have been reported for the frozen fjords in Svalbard. Further analysis could compare these strength measurements with those reported by others under similar conditions, e.g., temperature, salinity and strain rate.

- Further statistical analysis of ice strength could establish interval estimates of the Weibull parameters and increase the significance and confidence of the estimated parameters.

- Once the statistical distribution has been established for the sea ice strength, the methodology could be used for practical application and load calculations.

Morphology and physical and mechanical properties of first- and second-year sea ice ridges

- The following gaps of knowledge of first-year ridges were identified in the presented papers and reports:
    - The block dimensions are not sufficiently reported, although they are crucial for identifying the mechanism of formation of the ridge.
    - Keels widths are crucial in load determinations but are seldom reported.

- A better mapping of the ridge should include longitudinal cross sections.

- The spatial and temporal variation of the consolidated layer should be more closely examined with consistent and numerous measurements during several seasons.

- More expeditions in the Fram Strait are required to understand better the transition mechanism between first- and second-year ridges. They should also contribute to improve and widen the existing database on the ridges morphological, physical and mechanical properties in that region.

- More strength tests are required to observe a clear trend and to adapt the existing analytical models to multi-year ridges.